UNIVERSITY OF SOUTHAMPTON

FACULTY OF ENGINEERING AND THE ENVIRONMENT

Institute of Sound and Vibration Research

Brain connectivity measured from the EEG during auditory stimulation in normal hearing subjects and cochlear implant users

by

Pegah Tayaranian Hosseini

Thesis for the degree of Doctor of Philosophy

August 2015

UNIVERSITY OF SOUTHAMPTON

ABSTRACT

FACULTY OF ENGINEERING AND THE ENVIRONMENT
Institute of Sound and Vibration Research

Doctor of Philosophy

BRAIN CONNECTIVITY MEASURED FROM THE EEG DURING AUDITORY STIMULATION IN NORMAL HEARING SUBJECTS AND COCHLEAR IMPLANT USERS

by Pegah Tayaranian Hosseini

The human brain is regarded as an ensemble of dynamic systems in which communication between neural centres is very important. In order to perceive sounds many different cortical and subcortical brain areas have to coordinate their activity. After hearing loss, the connections and information pathways between these areas may rearrange and this may be one of the reasons for unsatisfactory speech perception after cochlear implantation (CI). It remains unclear how the brain connectivity and its re-organisation contribute to this, and this provides the motivation for the current study.

The brain organisation can be quantified by connectivity measures, which may give the strength, direction, and timing information on the connections between brain areas. This research project aims to assess different methods of brain connectivity and response detection in the Electroencephalogram (EEG) and use these to investigate brain responses during tone, word, and sentence perception in normal hearing adults and CI users.

The initial focus of this project was Dynamic Causal Modelling connectivity method, but early results raised questions regarding its reliability. DCM was then replaced by simpler and more established linear multi-variate auto regressive (MVAR) based models such as Coherence, Directed Transfer Function (DTF), and Partial Directed Coherence (PDC), as well as classical non-parametric power-spectral and coherence analysis. Both latter approaches could find changes in the brain activity in different time-frequency windows after the stimulus onset, which depended on the stimulus type and electrode positions. MVAR-based models were then employed and showed promising results when applied on synthetic data but on recorded data only model-based coherence (both pair-wise and multi-channel models) was able to detect connectivity changes in response to the stimuli presented to normal hearing participants; DTF and PDC appeared insufficiently sensitive.

Different artefact rejection methods were also employed to remove the CI artefact from the EEG, prior to performing connectivity analyses. While connectivity changes could

be identified, results need to be interpreted with caution, due to remaining uncertainty about the removal of all CI artefacts.

This work is original in analysing and detecting changes in connectivity following repeated stimulation with words and sentences. Finding these changes proved challenging, with many pitfalls with established methods, but the current results and methodological approaches are promising for the continuing study of higher level responses to speech stimulation.

Contents

List of Figures

List of Tables

Declaration of Authorship

I, Pegah Tayaranian Hosseini , declare that the thesis entitled *Brain connectivity measured from the EEG during auditory stimulation in normal hearing subjects and cochlear implant users* and the work presented in the thesis are both my own, and have been generated by me as the result of my own original research. I confirm that:

- this work was done wholly or mainly while in candidature for a research degree at this University;
- where any part of this thesis has previously been submitted for a degree or any other qualification at this University or any other institution, this has been clearly stated;
- where I have consulted the published work of others, this is always clearly attributed;
- where I have quoted from the work of others, the source is always given. With the exception of such quotations, this thesis is entirely my own work;
- I have acknowledged all main sources of help;
- where the thesis is based on work done by myself jointly with others, I have made clear exactly what was done by others and what I have contributed myself;
- parts of this work have been published as: (Hosseini et al., 2014b,c, 2015, 2014a, 2013b,a, 2011a,b)

Signed:.....

Date:.....

Acknowledgements

I wish to express my deepest gratitude to my supervisors Prof. David Simpson, Dr. Steven Bell, Mrs. Julie Brinton, and Dr. Shouyan Wang for their never-ending support and encouragement during the course of this research and if not for them, I would not be where I am today.

I would like to thank the Auditory Implant Service, the Institute of Sound and Vibration Research, and the University of Southampton for their financial support and specifically the Auditory Implant Service staff for their valuable consultations.

I would also like to thank the Psychology Department of the University of Southampton for providing me with their much needed data recording facilities.

I am so grateful to my husband for showing patience with me constantly when no one else would and for his unceasing words of motivation and confidence.

I am grateful to my parents and my sister for their continuous love and advice even when I was not lovable any more.

Last but not least, I am for ever thankful to all my friends, namely Newsha, Sara, Sanaz, Pegah, Atlas, Maryam, Reyhaneh, and Asieh, who helped me pull through at the hardest times of my work and lent me a shoulder to cry on without hesitance.

Abbreviations

AB	Arthur Boothroyd
ABR	Auditory Brainstem Response
ACF	Auto-Correlation Function
AEP	Auditory Evoked Potentials
AIC	Akaike Information Criterion
AIS	Auditory Implant Service
AL	Antero Lateral
ALR	Auditory Late Response
AM	Amplitude Modulated
ANOVA	Analysis of Variance
ANSD	Auditory Neuropathy Spectrum Disorder
AR	Auto Regressive
BIC	Bayesian Information Criterion
BKB	Bamford-Kowal-Bench
BP	Box-Pierce
BTE	Behind-The-Ear
CGC	Conditional Granger Causality
CI	Cochlear Implant
CL	Caudo Lateral
DCM	Dynamic Causal Modelling
dDTF	direct Directed Transfer Function
DFT	Discrete Fourier Transform
DL	Distributed Linear
DTF	Directed Transfer Function
ECD	Equivalent Current Dipole
ECoG	Electrocorticograph
EEG	Electroencephalograph
EM	Expectation-Maximisation
EP	Evoked Power
ERP	Event Related Potential
ffDTF	full frequency Directed Transfer Function
FFT	Fast Fourier Transform

FIR	Finite Impulse Response
fMRI	functional Magnetic Resonance Imaging
FPE	Final Prediction Error
GC	Granger Causality
GS	Generalised Synchronisation
ICA	Independent Component Analysis
IP	Induced Power
LB	Ljung-Box
LFP	Local Field Potential
LM	Li-Mcleod
MEG	Magnetoencephalograph
ML	Middle Lateral
MRI	Magnetic Resonance Imaging
MSC	Magnitude Squared Coherence
MSE	Mean Squared Error
MSP	Multiple Sparse Priors
MVAR	Multi Variate Auto Regressive
nDTF	normalised Directed Transfer Function
NGC	Nonlinear Granger Causality
NHS	National Health Service
NICE	National Institute for Health and Clinical Excellence
PC	Personal Computer
PCA	Principal Component Analysis
PCoh	Partial Coherence
PCT	Parallel Computing Toolbox
PDC	Partial Directed Coherence
PET	Photo-Emission Tomography
PMavg	Plus-Minus averaging
sLoreta	standardised Low Resolution brain Electromagnetic Tomography
SNR	Signal-to-Noise Ratio
sPDC	squared Partial Directed Coherence
SPL	Sound Pressure Level
SPM	Statistical Parametric Mapping
TDSEP	Temporal Decorrelation Source Separation
TF	Time-Frequency
TP	Total Power
WF	Wiener Filter
WMN	Weighted Minimum Norm
WSS	Wide-Sense-Stationary

To my husband, my parents, and my sister who were there for me every step of the way.

Chapter 1

Introduction

The human brain plays an important role in perception of different types of sounds (Hall, 2007). In a normal hearing human being, the sound is picked up by the external ear, transmitted through the middle and inner ear, and sent to the auditory nerve. This information is then processed and perceived in the brain. There are different brain areas which are responsible for perception of auditory stimuli (Hall, 2007).

The brain has a 'plastic' nature (Pascual-Leone et al., 2005) in that it has the ability to adapt itself to new conditions such as physiological changes and new experiences. Because of the plastic nature of the brain, the organisation of auditory areas and their interactions will change after hearing loss but they may rearrange towards that of normal hearing by using hearing aids or Cochlear Implants (CI) (Giraud et al., 2001). Brain plasticity after cochlear implantation has been studied in children and adults using different subjective and objective measurements (Limb et al., 2010; Sharma et al., 2009; Gilley et al., 2008). The objective measurements that are usually obtained from brain imaging techniques such as Electroencephalography (EEG) and Positron Emission Tomography (PET) show that the active areas of the brain tend to change toward normal condition over time after implantation (Gordon et al., 2005; Łukaszewicz et al., 2010; Kral and Sharma, 2012). Although there are many studies on the topic of brain plasticity in cochlear implant users and which areas are activated during speech perception, there is no research focused on the nature of interactions between these active areas. The interaction between brain areas is commonly called brain connectivity.

Brain connectivity measurement during auditory stimulation both in normal hearing and cochlear implanted subjects can improve our understanding of the brain activity during speech perception. Also, it may reveal which interactions are being affected most by hearing loss and which of them are retrieved after implantation. This information may be helpful for not only increasing our knowledge of speech perception pathways but also, in the long run, discovering new techniques in helping CI users to benefit more from their implants. Examples of potential methods might be new hearing and language

therapy techniques (Faulkner and Pisoni, 2013) or invasive or non-invasive brain stimulation targeting disrupted connections. The number of CI users in the UK was reported around 11,000 in the UK alone in the 2011-2012 annual report of the British Cochlear Implant Group (BCIG) with around 1,300 (half children, half adults) being new cases in that year (British Academy of Audiology (BAA), British Cochlear Implant Group (BCIG), and ENT-UK, 2007), which is almost twice the number of CI users reported in the year 2007 (British Cochlear Implant Group (BCIG), 2012). In the 2007 report, it is shown that the rate of CI implantation per year had an increasing trend since the year 1985. With the increasing number of CI users, some audiologists[1] comment that they prefer objective methods to the subjective ones to measure the performance and progress of cochlear implant patients. At the moment, speech perception tests, which count the number of correctly recognised words in a string of presented words or sentences, seem to be the most common available method. These tests are not very reliable and depend highly on the patient's physical and mental condition on the day of the test (Boothroyd, 2004). Also, with the higher demand on cochlear implantations, new questions arise from an audiologist's point of view that we think might be answered by connectivity analyses. These concerns include, but are not limited to: "the reason for different performances of patients with very similar conditions before and after implantation" (Faulkner and Pisoni, 2013), "the impact of neural plasticity on the outcome of cochlear implantation" (Faulkner and Pisoni, 2013), "the benefits of bilateral implantation" (Faulkner and Pisoni, 2013), "the effect of some specific brain areas such as the visual cortex on auditory related brain areas before and after implantation" (Dr. Carl Verschuur), and "the effect of two brain lobes on each other and the pathways of information flow between the two lobes in cochlear implant users" (Dr. Carl Verschuur).

The brain response to simple auditory stimuli has been studied in both normal hearing subjects and CI users (Sasaki et al., 2009; Sharma et al., 2005b, 2009). However, the brain response to more complex sounds such as words and sentences has not been approached as widely as simple stimuli. Existing research (Schack and Weiss, 2005; Obleser and Kotz, 2011) on this topic usually employs complicated presentation protocols targeting aspects such as attention, memory, or predictions abilities in a subject rather than their speech perception per se. The main focus of this research project is to investigate the brain response in EEG in response to these types of sounds and to use these responses to study the brain connectivity in normal hearing subjects. For the purpose of this study, EEG signal is targeted as it has a high temporal resolution, it does not have any interference with the implant, it is easy to be used in follow-up clinical settings, and it is a cheap procedure compared to other imaging techniques such as PET and functional Magnetic Resonance Imaging (fMRI) (Giraud et al., 2001).

[1] Personal communication with Dr. Carl Verschuur, Director of the Auditory Implant Service of the University of Southampton

There is a vast range of linear and nonlinear connectivity measures a few of which could be and has been employed in studying brain connectivity in this research including Dynamic Causal Modelling (DCM) (David et al., 2006a), pairwise coherence (Miranda de Sá et al., 2001), Partial Directed Coherence (PDC) (Baccala and Sameshima, 2001), and Directed Transfer Function (DTF) (Korzeniewska et al., 2003). DCM is a biologically informed nonlinear model that inherently estimates the relationships within and between the areas in the brain. PDC, and DTF are linear connectivity methods which are multivariate extensions of Granger Causality (GC) (Florin et al., 2011) with which the causality of the relations between different signals can be derived. These measures are calculated using estimated parameters of models based on Multi-Variate Auto-Regressive (MVAR) analyses. Linear methods are simpler to implement and because of the lower number of parameters and fewer required assumptions, they may be more reliable and more robust than nonlinear connectivity methods (Sakkalis, 2011).

The signals recorded from each EEG electrode (sensor) are mixed activities of signals in multiple brain regions (sources) (Sakkalis, 2011). The source level activity can be derived using different source reconstruction techniques such as Independent Component Analysis (ICA) (Hyvärinen and Oja, 2000) and standardised Low Resolution brain Electromagnetic Tomography (sLORETA) (Grech et al., 2008). Connectivity analyses can be applied to both sensor (surface electrode) and source space (cortex level) signals although in this exploratory study the focus is on the sensor level.

This study hypothesises that the brain response to different types of auditory stimuli does not arise from identical brain regions. Another hypothesis is that the brain perception process (thus, response observed in EEG) for more complex sounds such as words is different to that of simpler stimuli such as tone bursts. Thus, we also hypothesise that because of these differences between responses, the connectivity pattern may differ from one stimulus type to the other.

The objectives of the research can now be listed as follows:

- Detect the brain response to tones, words, and sentences in the EEG of normal hearing subjects.
- Determine if DCM and MVAR-based connectivity methods are robust means of detecting connectivity changes in response to auditory stimulation.
- Test if stimulation by tones, words and sentences produces measurable changes in connectivity, and to describe such changes.
- Assess the feasibility of measuring changes in brain connectivity with auditory stimulation in CI users.

To the best of our knowledge, there is no study on cochlear implant users that refers to the issue of which brain interactions may be responsible for the reduced level of speech

perception in this group. Other than one study (Castañeda-Villa et al., 2012) on the subject of connectivity in CI users, there is no other research on this topic. Even in normal hearing subjects, there are not many studies (Cooray et al., 2014; Weiss and Muller, 2013; Doesburg et al., 2012) investigating the effective connectivity in response to auditory stimuli and we have been unable to find any research in connectivity on the response to complex sounds such as words. The current thesis makes original contributions in these fields.

The outline of the current report is as follows. In chapter 2, the auditory pathway from the ear to the brain will be outlined and the brain areas involved in the perception of different types of auditory stimuli will be described along with the differences in brain activities of normal hearing people and CI users. Also, the issue of brain plasticity plus the methods that can quantify it will be discussed. In chapter 3, the experiment that has been performed to record data will be presented. In chapter 4, the existence of brain responses to different types of auditory stimuli are investigated in normal hearing subjects. Chapter 5 describes DCM as a method of effective connectivity measurement and it is applied on simulated data. In chapters 6 and 7, linear non-parametric and parametric connectivity approaches are explained and applied on both simulated and data recorded from normal hearing subjects. Chapter 8 explores different artefact rejection techniques for EEG data recorded from CI users and shows that it is a very challenging topic. The response detection and connectivity measures explained in previous chapters are then applied to the data in a feasibility study. Chapter 9 discusses the results achieved throughout this report, lays out the final conclusions, and elucidates the future plans of this study and how we hope to proceed to the next stage of this research.

Chapter 2

Literature Review

2.1 Introduction

As mentioned in the previous chapter, the main question in this study is how different brain regions interact in response to different types of auditory stimulation. To answer this question, some background information is required. In this chapter, the auditory pathway and areas of the brain responsible for perceiving different types of sound are explained and brain's event related potentials are discussed. In addition, an outline is given on how a CI works and who can benefit from it, how brain plasticity has been investigated previously in CI users, and if there are any objective measures of brain plasticity proposed in previous studies. The last section describes brain connectivity as a mathematical means of measuring brain plasticity and some techniques that can be used for the purpose of our study are presented.

2.2 The Auditory Pathway and Sound Perception

Hearing is carried out by the auditory system. Vibrations are detected by the ear and transduced into nerve impulses that are perceived by the brain.

The ear is divided into three anatomical regions: the external ear, the middle ear, and the inner ear (Figure 2.1.a). The external ear is the visible portion of the ear, and it collects and directs sound waves to the eardrum. The middle ear is a chamber called the tympanic cavity which is located within the temporal bone. It contains three ear bones named the incus, malleus, and stapes which collect and amplify the power of sound waves coming from the tympanic membrane and transmit them to the oval window (Martini and Bartholomew, 1997). The oval window is located at the base of the cochlea and is the interface between the middle and inner ear. The inner ear consists of two main functional parts: the vestibular system that consists of semi-circular canals

and is dedicated to balance and the cochlear system that is responsible for hearing. The cochlea consists of coiled chambers within the inner ear which is filled with fluid, partially protected by bone, and split along its length by a thin layer called the basilar membrane. The basilar membrane is covered with thousands of hair cells (Gelfand, 2004). The fluid inside the cochlea vibrates with the sound waves coming through the oval window and causes the vibration of the basilar membrane and the hair cells in turn. High-frequency sounds which have short wavelength vibrate the basilar membrane near the oval window (base of the cochlea) whereas the lower frequencies with longer wavelengths vibrate areas away from the oval window (towards the apex) (Figure 2.1.a). Displacement of hair cells transforms the mechanical waves of the fluid to electric signals in the cochlear nerve connected to the hair cells (Hackney, 1987). The neural activity of the cochlear nerve is further processed in the brainstem and middle brain nuclei, such as the cochlear nucleus, the superior olivary complex of the brainstem, and the inferior colliculus of the midbrain (Figure 2.1.b). The information eventually reaches the medial geniculate body of the thalamus and is then transferred to the primary auditory cortex which is located in the temporal lobe of the brain. The processing in subcortical nuclei includes sound localisation, frequency segregation, intensity coding, phase detection, and integration of all this information (Gelfand, 2004; Paxinos and Mai, 2004; Seikel et al., 1997).

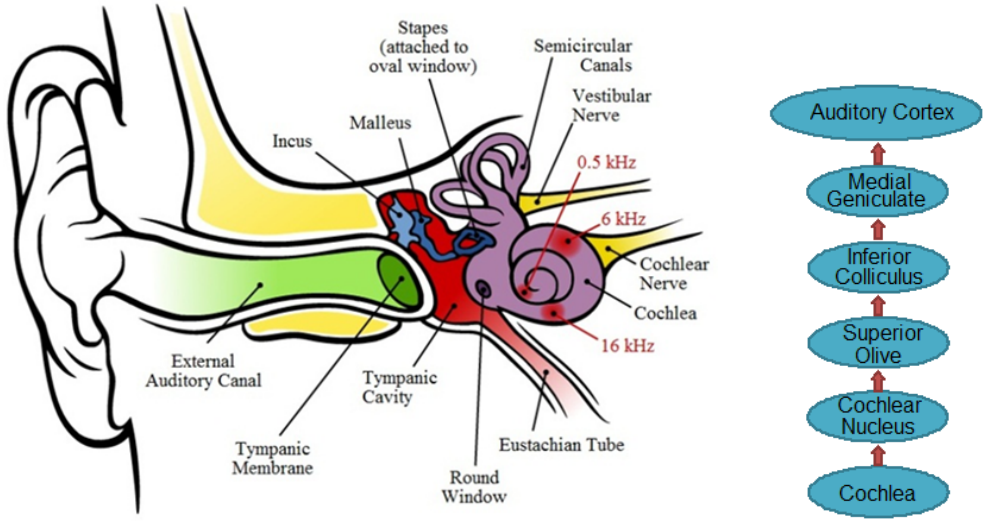

(a) (b)

Figure 2.1: a) Anatomy of the human ear (Chittka and Brockmann, 2005), b) Central auditory system

Auditory information is transferred from the thalamus to Brodmann areas[1] 41 and 42 in the temporal lobe of the brain (Webster, 1995), which comprise the primary and secondary auditory cortices, respectively (Figure 2.2.a). The primary auditory cortex

[1] In 1909, Brodmann defined and numbered different cortical areas according to cytoarchitectonics, or structure and organization of cells. Although Brodmann areas have been refined, and renamed for nearly a century, Brodmann's cortical map is still the most widely known and frequently cited cytoarchitectural organization of the human cortex.

(area 41) is half surrounded by the secondary auditory cortex (area 42), also called the auditory belt (Purves et al., 2001) as in Figure 2.2.b. The auditory cortex contains a frequency map of the cochlea. High frequency sounds activate one portion of the cortex, and low-frequency sounds affect another. This frequency map is called the tonotopic map of the auditory cortex (Figure 2.2.b); however, tonotopic preference is not limited to the auditory core or belt and extends to the higher-order auditory regions within the temporal lobe as far as the multisensory cortex (Striem-Amit et al., 2011). Auditory information is processed by areas 41 and 42 and passed on to area 22 (Figure 2.2.a). Area 22 is also located in the temporal region of the cerebral cortex. It is an important association auditory cortex and necessary for normal speech comprehension. This area is also known as Wernicke's area. In two thirds of human beings, Wernicke's area is larger on the left than the right which according to Webster (1995) can be the structural basis for the fact that speech perception and comprehension are dependent on the left area in over 90% of people. This includes all the right handed and most of the left handed people (Webster, 1995). Area 22 is then connected to areas 44 and 45 in the prefrontal cortex (Figure 2.2.a), also known as Broca's areas, where motor processing of speech information occurs. Broca's area is necessary for normal expressive speech. However, not all neuronal fibres go directly to the frontal cortex. Many make synaptic connections for further integration in areas 39 and 40 (Figure 2.2.a), in the parietal lobe, known to be involved in a number of processes related to language, mathematics and cognition (Webster, 1995).

Romanski et al. (1999) divided the auditory belt of rhesus monkeys into three parts (Figure 2.3), injected different fluorescent tracers to these three areas, and suggested that there are two pathways from the belt to different parts of the frontal lobe of the brain during pure tone and band-pass noise presentation (Romanski et al., 1999). One pathway, originating in the CaudoLateral (CL) part, projects to Brodmann areas 8a and 46 involved in uncertainty processing and attention; whereas, the other pathway, originating in the AnteroLateral (AL) part, projects to areas 10, 12, 45, and 46 which mostly involve memory retrieval and decision making. The Middle-Lateral (ML) projections were usually a combination of those from anterior and posterior fields.

The existence of three functionally defined areas in the auditory belt of rhesus monkey was further confirmed in Rauschecker and Tian (2004) and it was demonstrated that neurons in this belt respond vastly stronger to band-pass noise bursts than to pure tones (Rauschecker and Tian, 2004) showing that the brain responds to various types of auditory stimuli differently.

There are many studies that concentrate on the human brain rather than nonhuman primates to find which brain areas are more active during presentation of more meaningful sounds such as phonemes, words, and sentences, than pure tones. As a continuation to Rauschecker and Tian (2004), using fMRI, Wessinger et al. (2001) demonstrated that like the rhesus monkey, pure tones trigger mainly the primary auditory cortex in the

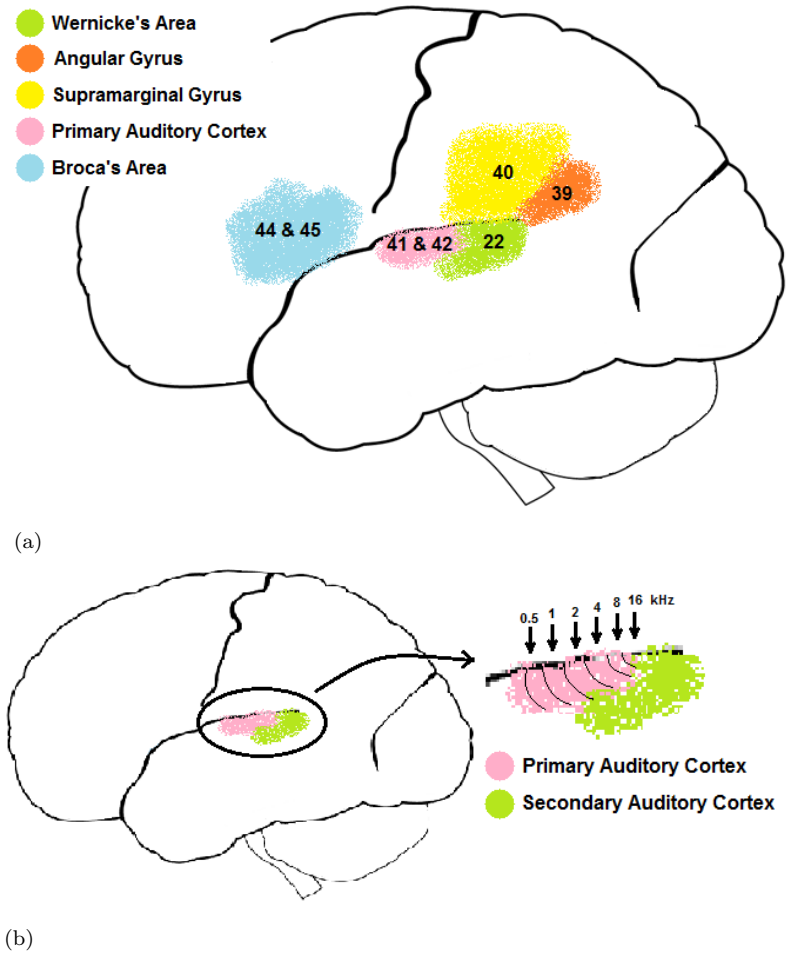

Figure 2.2: a) Brodmann areas associated with sound perception (reproduction of James.mcd.nz (2010)), b) Tonotopic map of the auditory cortex (reproduced from Fitzakerley (2007))

human brain; whereas, belt areas prefer complex sounds such as narrow band noise bursts (Wessinger et al., 2001). It was shown that there is a specialised region in the mid-portion of the superior temporal sulcus which responds to speech sounds rather than simple non-speech ones (Binder et al., 2000). The differences in phonetic and non-phonetic sound perception was investigated in another study by applying a method which gradually increased the presence of phonetic features in the auditory stimulus, creating a step-wise transition from a non-phonetic sound (music sound) into a phonetic sound (vowels) (Osnes et al., 2011). The results showed more and more activation in the superior temporal gyrus bilaterally when the subject was presented with higher-phonetic-included sounds compared to non-phonetic ones. Another study also exhibited involvement of the motor system in discrimination of speech signals, especially in noisy environments (D'Ausilio et al., 2012).

In summary, the areas of the brain involved in the perception of sound are still under investigation but there is evidence that the brain response to sound depends strongly on the type of sound that is presented (Osnes et al., 2011; Binder et al., 2000). This line

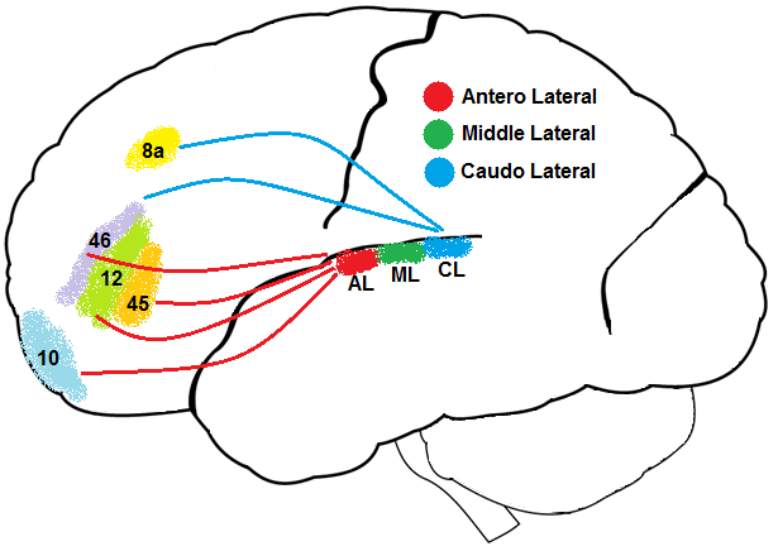

Figure 2.3: Lateral brain schematic showing colour coding of the auditory belt injections projections are summarized with arrows (reproduced from Romanski et al. (1999)).

of study will be investigated more closely in the current work both in normal hearing adults and CI users in particular by comparing responses to speech and tonal stimuli. In the next sections, cochlear implant and its effect on brain activation patterns (according to existing studies) will be discussed.

2.3 Cochlear Implantation

A CI is an electronic device which is implanted surgically and provides hearing for people who have severe to profound deafness. A CI as shown in Figure 2.4 consists of several parts which convert sound to the electrical stimulus that can be picked up by the auditory nerve. A CI bypasses the damaged hair cells of the cochlea and sends electrical signals directly to the auditory nerve. The auditory nerve then transfers these signals through subcortical nuclei to the brain. Engineering design of a CI is explained in more detail in section 2.3.1.

2.3.1 Engineering design of a CI

A cochlear implant in general (as in Figure 2.4) consists of the following parts (Bluestone et al., 2002):

- Microphone: receives sound and transduces it into an electrical signal. The microphone is placed in the speech processor which is located Behind-The-Ear (BTE).

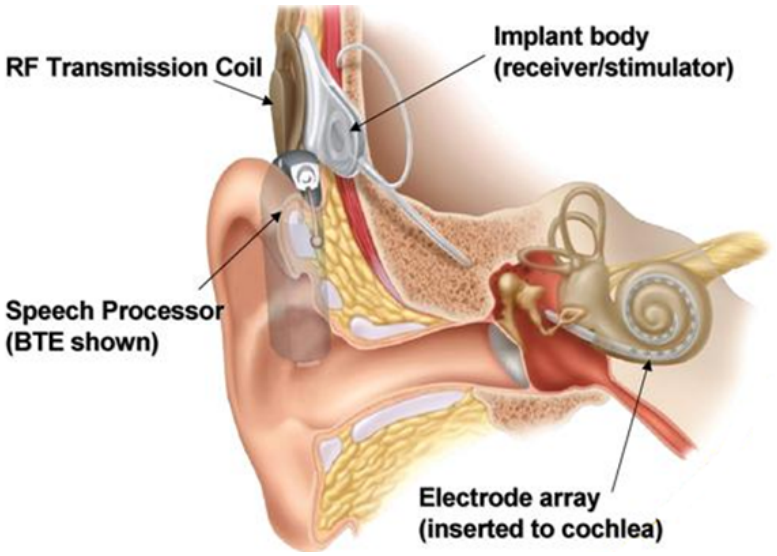

Figure 2.4: Components of the Nucleus® CI system (adapted from Hear & Say (2013))

A typical microphone does not pass very low frequencies so as to filter out the vibrations that might be produced by head movement or walking.

- External speech processor and signal-transfer component: transform the input signal of the microphone to a form that is perceivable by implant patients and have amplifying, filtering, compressing, and reshaping functions. Amplification increases the power of the signal and filtering divides the signal into different frequency bands. The bandwidths of the filters depend on the number of electrodes of the specific cochlear implant. The sound energy is then compressed to be in a useful range for the user in which the stimulus is being heard but it is not painful and then reshaped from an analogue to a digital signal for electrode stimulation.

- Transmitter (outer coil) and receiver (inner coil): the transmitter is placed on the mastoid (usually held in place adjacent to the inner coil by magnets) and sends the processed signal via a radio frequency link to the inner coil receiver, which is placed surgically inside the skull. The receiver sends electrical energy to one or more electrodes in the array. The electrode array which is placed inside the cochlea delivers the electric signal to different positions in the cochlea. The nerve then gathers, combines, and sends the stimuli to the brain which decodes and interprets the signal.

2.3.2 Who can benefit from a CI?

According to the UK's National Institute for Health and Clinical Excellence (NICE) (National Institute for Health and Clinical Excellence (NICE), 2009), there are some criteria that a patient should satisfy to be considered for cochlear implantation. After

considering many options such as clinical benefits and cost effectiveness of cochlear implantation, NICE committee recommends unilateral cochlear implantation for people with severe to profound sensorineural hearing loss who do not receive adequate benefit from acoustic hearing aids after a three-month trial of using valid hearing aids; for this case, only the sensorineural hearing loss with the malfunction of hair cells will be considered and the patient should have a functioning auditory nerve. Severe to profound deafness according to NICE guidelines and criteria is defined as hearing only sounds that are louder than 90 dB HL at frequencies of 2 and 4 kHz without acoustic hearing aids. Moreover, adequate benefit from acoustic hearing aids is defined for adults as a score of 50% or greater on Bamford-Kowal-Bench (BKB) sentence testing at a sound intensity of 70 dB Sound Pressure Level (SPL) and for children as speech, language, and listening skills appropriate to age, developmental stage, and cognitive ability.

If the patients satisfy all the above mentioned criteria and in addition, they are children, blind adults, or have other disabilities that increase their reliance on auditory stimuli as a primary sensory mechanism for spatial awareness, they can benefit from simultaneous bilateral cochlear implantation. Sequential bilateral cochlear implantation, i.e. receiving a second implant after they have used their first implant for a while, is not recommended in NICE guidance (National Institute for Health and Clinical Excellence (NICE), 2009).

The main decisions of the NICE committee are made according to the studies that have been carried out with the purpose of revealing the amount of life quality improvement after cochlear implantation. As the number of studies on bilateral adult implantees is too small due to small number of participants, the NICE committee states that the additional benefits of bilateral cochlear implantation are not certain enough for allowing bilateral implantation for all severe to profound deaf subjects. However, there are some results which show there is additional benefit in speech perception with the second implant in noisy environments (see next section). Considering cost effectiveness (the cost of a single CI is around £30,000 including the hospital procedure), allowing the second implant for adults based on uncertain reports has been a subject of debate for the NICE committee. In the end, they decided not to fund a second implant unless the spatial awareness of the adult is only possible through hearing, such as in blind people. The lack of clear knowledge on which to base difficult choices indicates the importance of more comprehensive investigations in the field of bilateral cochlear implantation for adults. The committee also expressed the need for more adequate evaluations on this subject (National Institute for Health and Clinical Excellence (NICE), 2009). The more this issue is studied, the more certain the committee can be in deciding about the necessity of the second implant for adults.

Investigating the effect of bilateral implantation was one of the primary purposes of this study.

2.4 Brain Plasticity and Hearing Impairment

Generally, the ability of the brain to adapt itself to new conditions is called brain plasticity. If the plasticity is towards increasing the functionality of an organ or higher perception of an input from the environment, it is called "adaptive" and if it leads to lower perception or less functionality, it is called "mal-adaptive" plasticity. Changes within the auditory system which lead to better perception of speech after cochlear implantation (Fallon et al., 2008; Kral and Tillein, 2006) are examples of positive plasticity, whereas spontaneous cellular, structural, and electrophysiological changes in the central nervous system after an injury to the spinal cord that have inhibitory effects on recovery can be considered as mal-adaptive plasticity (Lynskey et al., 2008; Blesch and Tuszynski, 2009). It has been shown that plasticity is a lifelong process although some types of plasticity are maximal in specific stages of life (May, 2011). For example, it has been established that the auditory cortex is most plastic during early stages of life (Fallon et al., 2008; Sharma et al., 2002, 2005a), but it has also been shown that plasticity in auditory cortex remains active even in adulthood (Ponton et al., 2001; Thiel et al., 2002; Nava et al., 2009a), both in humans and animals.

The development of the auditory system depends critically on auditory experience; thus, if it does not receive input for a while, its functionality will be altered intensely by this deprivation and sound perception levels will decrease proportionally (Kral et al., 2006). However, the auditory cortex may commence reorganising towards a normal hearing person's brain function if the patient starts to hear, e.g. after cochlear implantation (Giraud et al., 2001). Its success depends greatly on the age of implantation, the length of the time he/she has been deaf, the amount of auditory experience he/she had had before deafness and will have after implantation, etc most of which have been studied separately in the past years (Gilley et al., 2008; Sharma et al., 2009; Pantev et al., 2006; Fallon et al., 2008).

According to existing research, the activation of the brain during auditory perception is different in CI users compared to normal hearing adults (Limb et al., 2010). Because of the life-long plastic nature of the brain, both children and adults can benefit from cochlear implantation to some extent even if the implantation is just one-sided (Sharma et al., 2005b; Giraud et al., 2001). Children with bilateral implantation have higher levels of speech understanding and quality of life compared to unilateral implanted ones (Baumgartner et al., 2004) but this has not been demonstrated comprehensively for hearing impaired adults.

In the next sections, the studies performed on cochlear implant users to examine the plasticity of the auditory cortex after cochlear implantation will be discussed.

2.4.1 Normal hearing versus CI user

As was mentioned previously, the auditory cortex needs to be activated by auditory stimuli continuously else after some time, its functionality will be affected by the lack of input (Kral et al., 2006). However, it has also been shown by many researchers that it can gradually regain its capability of auditory processing when presented with sound even after a long period of deafness (Giraud et al., 2001; Limb et al., 2010).

Repeated Magneto-EncephaloGraphy (MEG) of postlingually deafened (i.e. deafness that occurs after the development of language) adults over two years post-implantation showed an increase in evoked brain activity over time. It also showed that after two years of CI utilisation, activation patterns resemble those of the normal group (Pantev et al., 2006). An EEG study on early- and late-implanted prelingually deafened (i.e. deafness that occurs before the development of language) children (Gilley et al., 2008) concluded that children with implantation before seven years of age have similar auditory cortex activation patterns to normal children in response to the vowel /ba/, whereas children with implantation after seven years of age have activation in the parietotemporal cortex which indicates that different pathways were employed in these children compared to normal subjects. PET scans of postlingually deafened adult CI-users and normal hearing adults during melody, rhythm, and language perception exhibited numerous differences between the two groups and three types of stimuli (Limb et al., 2010). Among these three conditions, language perception led to the greatest difference between the two groups. During language perception, CI-users had higher activation in the middle temporal gyrus and superior temporal gyrus bilaterally and a small cluster of activations in the right inferior frontal gyrus comparing to normal subjects. For all conditions, CI subjects showed greater activity in the temporal cortex compared to normal subjects; in contrast, normal subjects revealed elevated activity in the cingulate cortex, precuneus, parahippocampus, and hippocampus in comparison with CI users (Limb et al., 2010). One study using PET scans demonstrated that CI users and normal hearing adults even have differences in resting brain activity and such differences decrease over time after cochlear implantation (Strelnikov et al., 2010). The same study on resting brain activity revealed that CI users with higher activity of temporal and auditory cortex have better performance in word recognition (Strelnikov et al., 2010).

The research, in general, demonstrate that there are differences between utilising diverse brain areas by normal hearing subjects and CI-users both in the resting state and in sound perception condition. These studies considered levels of activation in individual channels or brain areas and there are only a few studies that focus on the connections between these areas generally.

2.4.2 Children versus adults

The age at which a patient is implanted is a significant factor with regard to the level of post operation speech perception. Different studies discussed the role of the age of implantation and the length of deafness before implantation in speech perception. It has been demonstrated in a subjective study that prelingually deaf children who are implanted under the age of three years have significantly higher levels of speech perception compared to late implanted ones (Baumgartner et al., 2002). However, these results show that even children who were implanted over the age of three will improve significantly after three years of experience with the CI. Thus, with more effort and over longer time, there is the hope of them gaining as much benefit from their implants as the younger implanted children. Also, these results show the existence of plasticity in the auditory system even after the age of seven. The age around six and seven is considered to be crucial for cochlear implantation (Manrique et al., 1999; Sharma et al., 2009, 2005b, 2002). EEG response to the vowel /ba/ in unilaterally implanted congenitally deaf children showed that the central auditory system is maximally plastic before the age of 3.5 years and it decreases significantly after the age of seven years (Sharma et al., 2002). Another speech perception study illustrated that the level of word recognition increases with decreasing age of implantation but this recognition does not change much if the implantation happens any time under the age of 2 years (Holt et al., 2004). Sharma et al. (2005b, 2009) further presented that late-implanted children (after the age of seven years), have different cortical auditory responses from early-implanted ones and both early- and late-implanted responses differ from the standard pattern of normal hearing children.

The plasticity of the adult auditory system has also been confirmed. Measures of sound localisation ability of pre and postlingual adult deaf subjects after cochlear implantation (Nava et al., 2009a) showed that the former were capable of localisation at a better than chance level if they had used their implants for more than six years. The postlingually deafened group were more successful even though they had less experience with their CIs compared to the prelingual group (Nava et al., 2009a). It has also been shown that the duration of deafness has a negative effect on speech perception after implantation (Fallon et al., 2008).

It is clear from the research that the plasticity of the auditory cortex is a life-long phenomenon and not only children but also hearing impaired adults can greatly benefit from cochlear implantation.

2.4.3 Unilateral versus bilateral implantation

The research on the differences between unilateral and bilateral cochlear implantation can lead to decisions of whether a second implant is necessary, recommended, or wasteful

both in children and adults.

There are many studies that confirm higher perception of sound in noise, increase in sound localisation, better speech understanding and production, and a superior quality of life for children with bilateral implants compared to unilaterally implanted children (Baumgartner et al., 2004; Kühn-Inacker et al., 2004; Peters et al., 2004; Wie, 2010; Godar and Litovsky, 2010). Most of these studies emphasise the necessity of intensive rehabilitation and extensive use of their second CI if one expects to gain more benefits from bilateral implantation (Kühn-Inacker et al., 2004; Wie, 2010; Sparreboom et al., 2011; Asp et al., 2011). It has been reported in some research that the gap between the two implantations is not an effective factor for higher speech understanding (Brademann et al., 2003; Sparreboom et al., 2011; Zeitler et al., 2008) but other research contradicts this claim and states that decreasing the time gap will increase the perception (Strom-Roum et al., 2012; Chadha et al., 2011; Kühn-Inacker et al., 2004). Overall, it has been shown that parents are more satisfied if their children have the second implant (Fitzpatrick et al., 2011).

Research on adults shows the positive effect of a second implant in increasing localisation ability and speech perception in noise (Au et al., 2003; Dunn et al., 2004; Das and Buchman, 2005) especially when the sources of noise and signal are separate (Van Hoesel et al., 2002; Van Hoesel and Tyler, 2003); however, some report higher speech perception rates even in quiet (Gantz et al., 2002) with the second implant. It is also stated that the patients who had auditory experience before deafness (Nava et al., 2009b) or the ones who used a hearing aid before their second implantation (Litovsky et al., 2004) will probably recover faster and benefit more from their second implant compared to non-experienced ones. Some other studies indicated that the second implant will be beneficial for adults, with respect to speech perception and localisation, even if there is a long gap between the two implantations (Tyler et al., 2007; Smulders et al., 2011). Sasaki et al. (2009) considered P3 (a positive deflection in the evoked response around 300 to 600 ms after the stimulus onset, see section 2.5.1) as an objective measure of level of speech perception and demonstrated that P3 latency increases with more difficult discrimination tasks in normal subjects. Then, they demonstrated that P3 latency decreases significantly in bilateral implanted subjects compared to unilateral ones suggesting that unilateral implanted subjects struggle more than bilateral implanted patients to understand speech (Sasaki et al., 2009).

In sum, implantation of a second CI appears beneficial in both children and adults, however, studies on adults are still limited.

2.5 EEG and Brain Studies

There are different imaging techniques available to study brain plasticity and connectivity. The ones currently available for studies on CI users are i) fMRI, ii) PET, and iii) EEG/MEG. Conventional CIs are not compatible with fMRI since it may damage electronic elements located within the skull, provoke local effects (heating, displacement of the device, etc.) because of high magnetic fields, and induce artefacts in the images by magnetisable elements (Giraud et al., 2001). PET, on the other hand, does not have any of these effects but its main disadvantage is that it offers poor temporal resolution. Also, because of injecting radioactive tracer to the subject, PET is not an appropriate technique in follow up studies either. EEG/MEG are non-invasive techniques that provide temporally accurate records of subcortical and cortical signals during spontaneous activity or after an auditory stimulus. Where MEG is a very expensive technique, EEG is relatively inexpensive and may therefore be used as often as required in follow-up studies (Giraud et al., 2001). That is why most imaging studies that target CI users use EEG as their data acquisition technique.

2.5.1 EEG activity

EEG is the electrical activity of the brain recorded from the scalp surface. This electrical activity originates from voltage fluctuations resulting from current flows in the ionic gates of neuronal cells of the brain. The activity that is recorded from the scalp is the summation of voltage fluctuations in thousands or millions of neurons (Tatum, 2007).

Two main types of EEG recordings can be used in clinical applications: 1) Event Related Potential (ERP) (see Figures 2.5.a and 2.5.b) which is the EEG recorded when the person is performing a specific task such as reading, listening, etc. and 2) Resting EEG which is the EEG recorded in the absence of any explicit task (often with eyes closed). The latter one is also called spontaneous EEG. The spontaneous activity of the brain has very low amplitude ($<100\mu$V) when recorded from the scalp and the response of the brain to an event is much lower than that (Tatum, 2007). ERP can either be both phase-locked and time-locked to the presented stimulus, i.e. peaks and troughs occur at fixed times (latencies) following the stimuli, (see Figure 2.5.a) in which case it is called an evoked potential or response (Wunderlich et al., 2006), or it can be time-locked but not phase-locked to the event (see Figure 2.5.b) which is then called the induced response (Sanderson, 2010). In the latter case, at a specific time following a stimulus, there may be an increase or decrease in the power of the signal, however, this increase or decrease in the amplitude does not consistently involve the same phase angle in all stimulus presentations. In Figures 2.5.a and 2.5.b, blue lines show the response to each stimulus with the vertical line being the onset of the stimulus and the black trace shows the average of all the blue lines. Note that in Figure 2.5.a there is a positive increase in

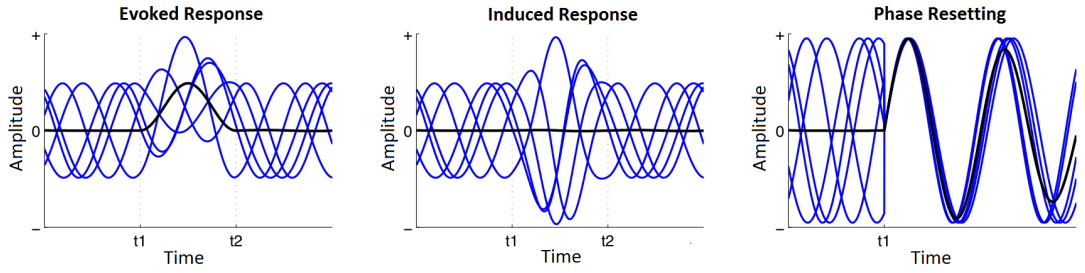

(a) (b) (c)

Figure 2.5: Schematic plots of a) an evoked response (TjeerdB, 2011a), b) an induced response (TjeerdB, 2011b), and c) phase synchronisation (TjeerdB, 2011c).

the magnitude of the signal at the same time (also known as latency) after each stimulus, but in Figure 2.5.b, it is the power of the signal that increases at a given latency after each stimulus. In the latter case, the increase in power reflects an increase in the signal magnitude which can have a positive or negative sign in successive stimuli, i.e. it is not phase-locked to the stimulus.

The common belief is that an evoked potential as illustrated in Figure 2.5.a is an additive signal to the resting EEG, time-locked to the stimulus (Makeig et al., 2002). However, in recent years, it has been suggested that it may not be simply an additive signal but a time-locked (with regard to the stimulus) synchronisation of neuronal activity (Makeig et al., 2002). If the response of the brain to a specific stimulus has an evoked nature and the same stimulus is applied repetitively, the same phase-locked response will be visible in the EEG at the same post-stimulus time in every repeat. This response can be extracted from the recorded EEG signal by averaging several EEG trials with respect to the onset of the stimulus (Wunderlich et al., 2006). The spontaneous EEG, which in this case is regarded as noise, will be averaged out and one will be left with only the phase-locked evoked response, if the Signal-to-Noise Ratio (SNR) is high enough. An example of evoked response is Auditory Late Response (ALR) which is the brain response to short bursts (less than 100 ms) of pure tones with inter stimulus intervals of around 1.5-2 seconds. Simple ensemble averaging on the EEG shows some significant peaks, the most important of which fall around 50 ms (called P1), 100 ms (called N1), and 200 ms (called P2) (Hall, 2007). Another example of an evoked response is the Auditory Brainstem Response (ABR) which occurs in response to very short (around 100 μs) clicks or tone bursts presented with inter stimulus intervals smaller than 50 ms. The major peaks of ABR are five positive peaks (numbered with Roman numerals I to V) that occur in the first 10 ms after the stimulus offset (Hall, 2007).

On the other hand, an induced response is a non-phase-locked synchronisation of the neuronal activity of the brain to specific types of stimuli. It is an increase of the power of the resting EEG in a particular frequency band after presentation of the stimulus as illustrated in Figure 2.5.b. This response cannot be extracted by averaging as the

response is non-phase-locked with respect to the onset of the stimulus and if averaged in the time domain (Sanderson, 2010), it will be averaged out. Thus, this response has to be investigated using power analyses, which usually takes the form of time-frequency analyses. Research has shown that specific frequency bands can be defined for the EEG and the power of each band shows different characteristics according to the stimulus (or event) the person is presented with. According to the literature, there are five main bands that can be investigated in EEG analyses (Palva and Palva, 2007; Kirmizi-Alsan et al., 2006). These bands are presented in Table 2.1 although the range of each band may change slightly from study to study.

Table 2.1: Commonly used frequency bands of EEG

Frequency Band	Delta	Theta	Alpha	Beta	Lower Gamma	Upper Gamma
Range (Hz)	0-4	4-8	8-13	13-30	30-60	60-90

One other hypothesis for the brain response to external stimuli is called phase resetting or phase synchronisation, in which neither the amplitude nor the power of the signal changes. Phase resetting refers to a time shift in background EEG activity in a specific frequency band (Makeig et al., 2002), and thus produces a phase-locked response to the stimulus without any increase in the power of that frequency band. An illustration of this type of response is presented in Figure 2.5.c. This type of response can be best detected using methods that extract phase information (Fuentemilla et al., 2006, 2008) from the EEG signal.

These types of responses will be investigated in the current study in response to different types of auditory stimuli.

2.6 Brain Connectivity

Our brain is an interconnected network and the interaction between regions is what makes a person perform a task (Daunizeau et al., 2011). This task can vary from movement control to speech perception. Brain connectivity usually refers to three basic terms: structural, functional, and effective connectivity (Daunizeau et al., 2011). Structural connectivity is about anatomical structure of the brain and the pattern of anatomical links inside the brain but functional and effective connectivity are related to the functionality of brain subsections. While functional connectivity refers to statistical dependencies of neural activities between distinct areas of the brain (i.e. if there is any link between two areas), effective connectivity measures the causality of brain interactions (i.e. which area drives the other). According to Friston et al. (2003), a definition of effective connectivity is the effect that one neuronal system has on another either at a synaptic or cortical level. Approaching neuroscientific questions from the connectivity point of view in recent years has helped researchers understand the mechanisms of

many functionalities of the brain in different conditions and in many cases even propose new techniques to enhance an adaptive plasticity or prevent a mal-adaptive plasticity (Rehme et al., 2011; Boly et al., 2011).

Functional connectivity can enlighten when there is a relation between the activities of two different brain areas but it can reveal neither the direction nor the strength of the connection with regard to other connections. Obtaining the latter information is achievable in addition to the former ones using effective connectivity analyses and that is why effective connectivity has attracted the attention of much research lately (Daunizeau et al., 2011).

Effective connectivity is not only useful in fundamental neuroscience research but also in clinical treatment for patients. Using effective connectivity measures, Rehme et al. (2011) reported that a shift in the role of the primary motor cortex after stroke might be the reason for mal-adaptive processes in these patients and indicated that this region could be a target for non-invasive brain stimulation (Rehme et al., 2011). A connectivity study on Parkinson's disease patients illustrated that their brain activity is abnormal during self-initiated movements and the interactions of motor networks are disrupted (Wu et al., 2011). Some findings (Boly et al., 2011) suggested that selective disruption of top-down processes in a cortical hierarchy can lead to the loss of consciousness in brain-damaged patients and measures of such disruption using effective connectivity can clearly differentiate a "vegetative state" from a "minimally conscious state" of the brain. This approach could provide a new diagnostic tool to quantify the level of consciousness of patients with brain damage, stroke, or even under anaesthesia. It is shown in Desseilles et al. (2011) that patients with major depression disorder present a counterproductive top-down recruitment of their attentional resources. Attentional training aiming at increasing the control of attention related connections could be helpful for these patients. This clearly shows the usefulness of studies on brain connectivity.

Despite the wide range of studies focusing on auditory brain plasticity (see section 2.4), the number of studies measuring brain connectivity in response to auditory stimuli is not very high. Most of these studies focus on simple stimuli such as tones and only some use more complex sounds such as vowels. The aim of the research is not generally sound perception abilities per se. Using auditory stimulation, functional connectivity measurements have been used for investigating auditory attention control (Doesburg et al., 2012), audio-visual interaction patterns in the brain (Marzetti et al., 2007), or diagnosing disorders such as tinnitus (Song et al., 2013) and Schizophrenia (Shim et al., 2014). There is also a group of researchers that have focused on functional connectivity in response to specifically selected abstract and concrete words and target the memory retrieval abilities in healthy participants by asking them to memorise the words and later remember them (Weiss and Mueller, 2003; Schack and Weiss, 2005; Weiss and Muller, 2013). Some studies use effective connectivity in response to auditory stimulation to investigate the connectivity in the ageing brain (Cooray et al., 2014), the brain of short

sleepers (Babajani-Feremi et al., 2012), patients with Alzheimer's disease (Zervakis et al., 2011), or brain interactions in response to simultaneous auditory, visual, somatosensory, and pain stimulation (Peng et al., 2012).

The number of connectivity studies that solely target sound perception is very limited and even these studies do not employ complex sounds such as words which is the purpose of the current report. Examples of such studies are functional connectivity for auditory selective attention (Huang et al., 2014) using dichotic (different sounds directed to different ears) pure tones, music perception (Wu et al., 2012) using Chinese music, or hemispheric couplings during dichotic stimuli presentation (Brancucci et al., 2005) again using pure tones. Some others investigate effective connectivity such as David et al. (2006a) who suggested bottom-up processes have a strong effect in perceiving tone bursts even in later components of ALR such as P300, Choi et al. (2013) who concluded that fronto-temporal connections are important in perceiving deviant sounds, or Hong and Tong (2012) who showed that parietal to prefrontal connections have key roles in maintaining high auditory attentional efforts.

To the best of our knowledge, there is almost no research aiming to uncover the effective brain connectivity in CI users with the exception of Marsella et al. (2014) that focuses on audiovisual perception rather than auditory perception alone, there are only a couple of studies on functional brain connectivity (Castañeda-Villa et al., 2012; Nash-Kille and Sharma, 2014). There appears to be no research on brain connectivity (either effective or functional) using speech stimuli rather than non-speech ones which is one of the purposes of this research.

In the following sections, existing methods for investigating the brain connectivity are mentioned briefly but more details on each method can be found in following chapters.

2.6.1 Functional connectivity

Functional connectivity is defined as temporal or spectral correlations or in other words statistical dependencies between activities of different neural assemblies (Daunizeau et al., 2011). It can provide us with information such as the existence of a connection between two areas of the brain but not its direction or strength. Different linear and nonlinear functional connectivity measurements have been introduced in the literature and used worldwide. Some of the most common techniques which have been applied to surface EEG will be explained briefly here but more details can be found in chapter 6.

The relationship between two time series can be quantified in the time or the frequency domain. Two commonly used linear functional connectivity measures are correlation (Jalili and Knyazeva, 2011) and coherence (Chan et al., 2013) that tell you about the

relationship between the two signals in temporal or spectral domain, respectively. Correlation refers to the similarity between two signals, allowing for time shift. Coherence is an extension of this, by being frequency specific in the analyses. If these measures are used in multi-channel systems, they can only be employed pairwise (only two time series analysed at a time) thus they can not eliminate the effect of a third signal. To surmount this problem, Partial Coherence (PCoh) (Sun et al., 2004) was introduced to determine if the observed relationship between two signals (say x and y) is due to a common input (say z) or if there is a genuine relationship between x and y. These methods have been used in diverse conditions to quantify the relationship between different brain areas in normal and disordered brain. The results of these studies have been used in diagnostic applications such as in schizophrenia and Alzheimer's disease (Chan et al., 2013; Jalili and Knyazeva, 2011; Sun et al., 2004).

Nonlinear measures were introduced to provide extra information on the relationship between two time series as the neural system inherently has nonlinear characteristics (Sakkalis, 2011). These methods are usually based on synchronisation of firing in neurons and some of them approach the connectivity question using chaotic characteristics in neurophysiological signals, examples of these methods are Phase Synchronisation and Generalised Synchronisation (Sakkalis, 2011). These methods have been widely used in EEG studies of epileptic patients (Lachaux et al., 1999; Sakkalis et al., 2009).

Overall, the mentioned functional connectivity methods are simple to implement and to understand. However, because of the high number of statistical analyses in multi-channel recordings thus increasing the probability of false positive rate, not being able to indicate the direction of information flow, and difficult interpretation of the results caused by pairwise analyses rather than the multi-channel ability, they are usually overseen by effective connectivity measurements.

2.6.2 Effective connectivity

Generally, causality refers to the relation of cause and effect. It can be defined as the directional relationship between two events or signals. In other words, causality indicates which event/signal is the consequence of the other. Causality and thus effective connectivity can be quantified according to different statistical measures based on characteristics of signals. These measures assess the causal relationship between different brain areas and specify the direction of receiving/sending signal based on statistical models (David et al., 2006a; Sakkalis, 2011). Some of these methods are explained briefly in the next subsections but are discussed more thoroughly in chapters 5 and 7.

2.6.2.1 Granger causality

Granger causality is a linear effective connectivity method which employs an AutoRegressive (AR) model to find the causal relationship between two signals (say x and y) (Granger, 1969). It forms the prediction model of 1) x from x and 2) x from x and y with errors of ϵ and ξ, respectively. The idea behind this method is if the signal x can be predicted from past samples of the signals x and y better than just from past samples of x only, then y is causally linked to x. This case is observed when ξ is significantly smaller than ϵ. If a third signal may be causally affecting the first two signals and this effect is not considered, the causality measure discussed above is not correct. Some modifications were thus proposed to classic Granger causality to embed the effect of the third signal, and the approach was called Conditional Granger Causality (CGC) (Geweke, 1984). Although this method was generalised to more than three channels, if the number of channels is very large such as in EEG systems, this generalisation becomes impractical as all 3-electrode combinations should be assessed separately and interpretation of results will become complicated (Florin et al., 2011). Other methods based on multivariate autoregressive modelling such as Diected Transfer Function (DTF) and Partial Directed Coherence (PDC) (Korzeniewska et al., 2003; Baccala and Sameshima, 2001) were developed from the original Granger Causality and tried to resolve some of the problems of CGC. In order to address the likely nonlinear characteristics in effective brain connectivity, Nonlinear Granger Causality (NGC) was developed (Hiemstra and Jones, 1994). Some of these techniques will be explained in more detail in chapter 7 along with their applications, advantages, and disadvantages.

2.6.2.2 Dynamic causal modelling

In contrast to the above approaches based on parametric multivariate modelling, dynamic causal modelling was developed on a neurobiological basis (Friston et al., 2003; David et al., 2006a). DCM is a biophysically informed model with a known input and EEG as the output. By introducing nonlinear state equations in the model, it can account for some nonlinearities of the system. The parameters of the model some of which are estimated and some of which are assumed include conduction delays, input parameters, and intrinsic and extrinsic coupling parameters which are the strength of connections within one area of the brain and between two different areas, respectively. DCM employs a Bayesian framework to estimate the parameters and produces a fitness value for the defined model. One can then compare these fitness values of different models to select the best-fitted model among them.

DCM has some advantages (such as encompassing some nonlinearities, having a known input, including biological information, etc) over other more conventional brain connectivity techniques. These are expanded further in chapter 5. As DCM was initially

the main focus of this research, chapter 5 focusses on DCM and Multiple Sparse Priors (MSP), one of its associated techniques.

2.7 Summary

As shown in this chapter, there are many studies on the subject of brain activity in both normal hearing and hearing impaired people during auditory stimulation but there is not much prior research in the area of brain connectivity in this field. Also, most previous research only employed simple sounds not speech. We plan to measure functional and effective brain connectivity in response to complex sounds such as words and sentences as well as simpler sounds such as tone bursts.

There is limited EEG studies on cochlear implant users that refers to the issue of brain connectivity in response to auditory stimuli and no research on complex sounds such as words. In the current report, the methodological foundations of brain connectivity will be laid using EEG from normal hearing subjects (in chapters 5 to 7) and a pilot study will be provided on CI users in chapter 8.

Investigating the brain connectivity is valuable in understanding the underlying activities of the brain during sound perception in both normal hearing subjects and CI users. It can also be beneficial, in discovering new procedures, from different therapy methods to invasive or non-invasive brain stimulation techniques, to help CI users gain more from their implants. They may also be useful as predictive measurements for the performance of the patient after second implantation or even their performance after the first implantation if combined with other experimental studies before implantation. However, these questions are outside the scope of the current report but this research can be considered as a base for further research in this field.

Chapter 3

Data Collection and Preprocessing

3.1 Introduction

One of the aims of this study is to investigate the brain connectivity in response to different types of auditory stimuli in normal hearing adults and CI users. This approach can provide an insight into the interactions between brain areas and the pathways of information flow in the brain.

To achieve this aim and as a first step to test the desired methods, EEG data were required from both groups of subjects according to a chosen protocol. The protocol was designed based on the objectives of this project and is explained thoroughly in the current chapter. Also, the data recorded in a linked project will be used in the current report, the protocol of which will also be explained in the next sections.

EEG data were recorded in response to simple stimuli such as tone bursts as well as more complex sounds such as words and sentences. To perceive speech, the brain will reach different areas than simpler stimuli such as tones (Limb et al., 2010). Measuring the connectivity of the brain in response to speech is one of the most important questions of this study.

Before starting any analysis (such as connectivity) on recorded EEG signal, one should test for the presence of a response in this signal to make sure what has been recorded is not all noise. The EEG signal is usually affected by different types of noise during recording such as movement artefacts, heart signals, eye blinks, and mains (50 Hz) noise (Repovš, 2010) (see section 3.3 for more details). In order to save time, it is more efficient to make sure there is a response in the data before any artefact rejection has been applied to the signal.

In the next section, the three experiment protocols are explained. The response detection steps (applied on normal hearing subjects) and the results achieved are presented next. The latter are only intended as a check on data quality, not as new results. In the discussion section, more details are presented on the reasons for including some of the criteria in the recording protocol.

3.2 Experiment Protocol

The data from three different protocols are used throughout this report and all protocols are explained in this section. Two experiments were conducted by the main researcher of this report which will be called Study#1 (S1) and Study#3 (S3) and another experiment was performed by a researcher (Dr. Siavash Mirahmadi) from a linked study which will be called Study#2 (S2) from this point on in this report.

3.2.1 Study # 1

The ethical approval from the University of Southampton was sought (reference number 1237) and the study was performed on normal hearing subjects. Written consent was sought from each participant before the start of the experiment.

3.2.1.1 Participants (S1)

Fifteen normal hearing right-handed native English speakers in the age range 18 to 45 years old participated voluntarily in this study as the control group and were paid £8 per hour for their participation. Their normal hearing, outer ear, and middle ear health were confirmed by pure tone audiometry ($\leq$20 dB HL in all frequencies), otoscopy (clear and clean ear canal), and tympanometry (tent shape and 0.3<Compliance<1.4 cc and -100<PeakPressure<100 daPa), respectively. The justification of selection criteria is presented in the discussion section of this chapter (section 3.5).

Subjects who had learning difficulties, took any neuroactive drugs which affected their consciousness, and/or had any psychiatric or neurological conditions, or troublesome tinnitus were excluded from the experiment. All these conditions might have had effects on the pattern of brain connectivity and would have been identified through a health questionnaire.

The proposed project is exploratory. It is therefore impossible to calculate the required sample size a priori. However, previous research using related methods have identified significant differences in the brain activity of adult subjects during presentation of other types of auditory stimuli with a sample size of 13-15 (David et al., 2006a). Thus, a sample of 15 subjects was considered sufficient for this study.

3.2.1.2 Stimuli (S1)

Stimuli were presented to the ear via Presentation® software (Neuro Behavioural Systems, California, USA) and Sennheiser HDA200 headphone (Sennheiser Electronic Corporation, Connecticut, USA). The room was not sound-proof (being a standard EEG lab) but Sennheiser HDA200 had excellent attenuation of passive noise which was 28.6 dB at 1 kHz as they were circumaural closed back headphones.

Sound files were saved with a sampling frequency of 22050 Hz with 16 bits per sample and were presented at 62 dB SPL which was targeted to represent a comfortable level for normal hearing adults. To set this level, a sound-level-meter and an artificial ear were used.

- Amplitude modulated (AM) tones: Two 2 kHz tone bursts (1 s long with 5 ms rise and fall times) modulated by 15 Hz and 80 Hz sine waves and 100% modulation rate were presented 50 times each with a stimulus interval of about 2.5 s. The inter stimulus interval changed randomly between 2 s and 2.5 s and the sequence of the presentation of the two tones was random. These tones aimed to induce phase-locked as well as non-phase-locked responses in the brain, i.e. increased power of the brain response around the modulation frequencies. The AM-induced response can be used for testing the algorithms before advancing to "word" and "sentence" stimuli.

- Words: 100 words were presented randomly from the Arthur Boothroyd (AB) word lists (Boothroyd, 1968) - recorded by the Institute of Hearing Research, UK Medical Research Council. The inter stimulus interval changed randomly between 2 s and 2.5 s. The average length of the words was 540±80 ms. The only controlled parameter in these words was that they were three-phoneme words in the shape of consonant-vowel-consonant such as "ship", "bone", "move", and "fan" and they were phonemically balanced, i.e. the phonemic composition was equivalent to that of everyday speech. The words were recorded by a male native English speaker.

- Sentences: 50 sentences were presented randomly from the BKB sentence list (Bench et al., 1979) every 5 s in a pseudo-random sequence - recorded by Institute of Hearing Research, UK Medical Research Council and University College of London. The average length of the sentences was 1630±175 ms. Sentences were initially developed for use with hearing impaired children and consisted of words used in everyday life. Examples of these sentences are "The clown had a funny face", "The shoes were very dirty", and "He frightened his sister".

3.2.1.3 EEG recording (S1)

After explaining the procedure of the experiment, a 66-channel customised EEG cap (Easycap, Falk Minow Services, Germany) pre-fitted with Ag/AgCl electrodes was placed on the subject's head. A 2D representation of electrode positions is presented in Figure 3.1.a which is called an equidistant map. Electrodes 67 and 68 were placed on the face under the eyes to record eye blinks which would be used for the noise reduction step and the reference electrode was placed on the nasion bone which is located at the bridge of the nose. The ground electrode was located just above the electrode 32, i.e. about 2-3 cm above the forehead. The impedance of the electrodes was reduced to less than 5 kΩ by cleaning the surface under each electrode using abrasive ABRALYT HiCl electrolyte gel (Falk Minow Services, Germany) which is a high-chloride abrasive electrolyte gel. The cap was connected to a Synamps^2 amplifier (Compumedics Neuroscan, Germany) and the signals were sent to a 32-bit SCAN4.3 acquisition software (Compumedics Neuroscan, Germany). The EEG signal was recorded while the subject was listening to different types of auditory stimuli. The signal was filtered in [0.05 200] Hz band at the time of recording and the sampling frequency was 1 kHz.

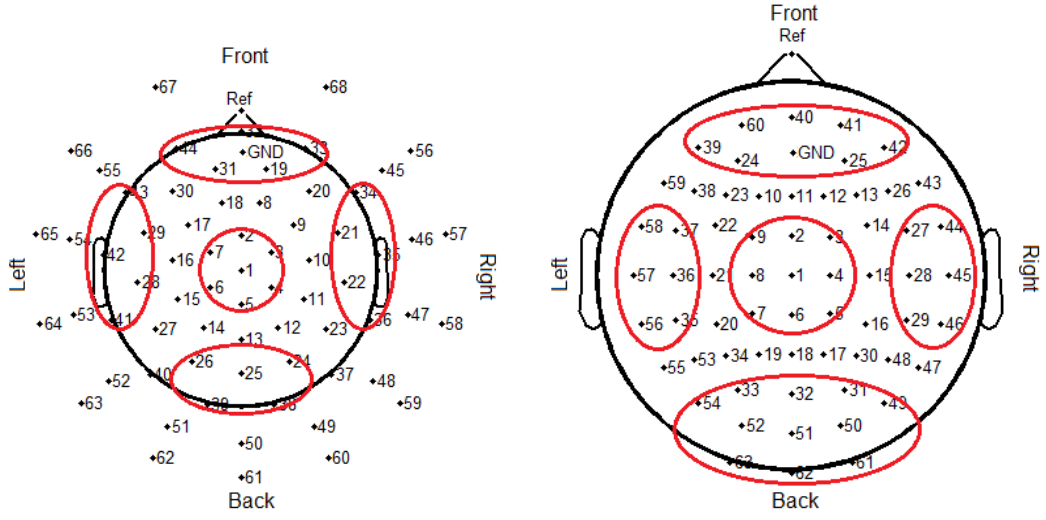

(a) (b)

Figure 3.1: Schematic of electrode locations in a) S1 (equidistant setup) and b) S2 (10-20 system) protocols. In a, the electrodes that fall outside the head circle fall below the ear. Red lines show the grouped electrodes that will be used in next chapters.

It is worth mentioning that the electrolyte gel made up of sodium chloride, was completely harmless, developed specifically for these types of investigations, and very widely used and sold by a reputable Europewide manufacturer. To be certain that the participant would not show any reaction to the gel, a tiny bit of paste was applied to the participant's hand at the very beginning of the testing session. The participant's skin would be checked for any redness or itching after the audimetry, tympanometry, and

explanations of the procedure and just before the experiment was started. In our study, no subject showed any reactions to this gel.

The subjects were sat in a comfortable armchair in a dimly lit room while looking at a small grey circle in the middle of a black screen placed about a metre in front of them and listened passively to presented stimuli. The data were recorded continuously and would be epoched offline. Every about 30 seconds, the auditory stimuli would stop and a count down was presented on the screen. The subjects were advised to try and keep their blinking, moving, frowning, etc for the count down period and refrain from doing so during the stimulations, to avoid artefacts. Each stimulus type was presented monaurally (first left ear then right ear) and then binaurally. After the presentation of each stimulus type, a 5-minute break would follow during which the participant could take water and biscuits.

3.2.2 Study # 2

As this protocol was not conducted by the researcher of the current project, the reasoning behind the flow of the protocol will not be presented here and only the aspect of the protocol relevant to this study will be described. The ethical approval from the University of Southampton had been granted (reference number 1204) to this protocol and written consent was obtained from each participant before the start of the experiment.

3.2.2.1 Participants (S2)

Ten normal hearing right-handed adults aged 18 to 30 years old participated voluntarily in this study.

3.2.2.2 Stimuli (S2)

Participants of this study were presented with different types and levels of sounds but the part that was used by our study was the EEG response to 70 ms-long tone bursts (1 kHz) with 10 ms linear rise/fall times which were presented monaurally to the right ear 160 times at 60 dB nHL every 1.4 s. The stimulus was presented using the Presentation® software through an Eartone 3-A insert earphone (E.A.R Tone, Indianapolis, USA). This whole stimulation sequence was repeated three times for each subject in the same session.

3.2.2.3 EEG recording (S2)

EEG was recorded using a 65-channel EEG cap pre-fitted with Ag/AgCl electrodes with the 10-20 setup (as in Figure 3.1.b). As can been seen in this figure, two of these electrodes were used as ground and nose-reference electrodes. Three more channels were used to record eye-blink, ECG, and the same sound stimulus presented to the ear. This last channel was used as a trigger for analyses. EEG was recorded with a sampling rate of 1000 Hz using the NeuroScan4.3 software (Compumedics Neuroscan, Germany) filtered from 0.05 Hz to 100 Hz at the time of recording.

3.2.3 Study # 3

This study was performed on CI users for which National Health Service (NHS) ethical approval was granted (Reference number 12/SC/0477) before the beginning of data collection. Written consent was sought from each participant before the start of the experiment.

3.2.3.1 Participants (S3)

According to the explanation offered in section 3.2.1.1, initially, a group of 15 unilaterally implanted patients was considered to be sufficient for this study for which the Ethics approval was granted; however, the number of eligible patients who consented to take part in the experiment did not pass four, within the time period available for data collection - following the initial and preparatory work on normal hearing subjects. The ethics approval was also obtained for bilateral implanted subjects but no such subjects could be recruited during the course of this research.

Four CI users in the age range 18 to 70 participated voluntarily and were paid £25 for each session they attended. Participants were included if they were healthy adults and were postlingually deaf patients i.e. they had become deaf after the acquisition of speech and language, usually after the age of six. See section 3.5 for the justification behind the participant selection criteria.

A similar health questionnaire to the one mentioned in section 3.2.1.1 for normal hearing subjects would be sent to patients along with their information pack. Patients having any of the mentioned conditions in this questionnaire would be excluded from the experiment.

Cochlear implant patients were approached by invitation letters along with an information sheet and a consent form sent by the audiology staff at the Auditory Implant Service (AIS) of the University of Southampton and they responded by email, telephone, or mail to the researcher directly if they were happy to take part in the study. They were assumed to be unwilling to participate if there was no response from them within one

month from sending the invitation letter. CI users participated in two different sessions. Usually, the implant is activated about 4-6 weeks after the surgery (implantation), when wound-healing is deemed to be fairly complete. The first session of recording was in the first week after activation of their implant (between the first and second tuning sessions) so that their brain is expected to have experienced limited reorganisation to auditory stimulation. The second session was about 3 to 6 months after activation of their implant at which point their speech perception was typically much better than in the first session.

3.2.3.2 Stimuli (S3)

Stimuli were presented to CI users through the direct input of the cochlear implant processor. The direct input is connected to the output of the sound presentation device by a direct lead (cable) and there would be no sound input from the environment when the direct input lead was connected to the processor.

The stimuli were presented to CI users at a comfortable level according to their own assessment. According to the design of the CI, if the stimulus is too loud it will be attenuated automatically by the processor so that the stimulus falls into the comfortable range of patient's hearing. Still, to make sure that a set level was comfortable for the patient and also they could hear it without struggle, before the start of the experiment, the patient would be presented with some sample stimuli to make sure that they were comfortable with the level of the sound.

The specification of sound files and patient preparation was similar to study S1 (see section 3.2.1.2). Sounds were only played to the implanted ear while the hearing aid on the other ear (if any) was turned off. The presentation protocol of AM tones, words and sentences were similar to normal hearing subjects as explained in section 3.2.1.2.

- Pure tones: Tones of 2 kHz with 5 ms rise and fall times and 80 ms duration were presented every about 2 s to the implanted ear for a total of 150 stimuli. The inter stimulus interval changed randomly between 2 s and 2.5 s. This aimed to decrease the possibility of habituation which is defined as a decrease in response to a stimulus after repeated presentations. This simple tone is expected to produce auditory late response in the brain. As there are many studies on ALR and it is a recognised signal (see section 2.5.1), it was included in this study as a means of testing the applied methods before proceeding to more complicated stimuli that produce less well-known responses in the brain.
- AM tones: Refer to section 3.2.1.2.
- Words: Refer to section 3.2.1.2.
- Sentences: Refer to section 3.2.1.2.

3.2.3.3 EEG recording (S3)

Hardware, software, and data acquisition steps were identical to study S1 (see section 3.2.1.3).

3.3 Quality Control of Data

There are many biological and environmental sources of noise that affect the EEG such as movement artefacts, heart signals (ECG), eye blinks, and mains (50 Hz) noise causing a low SNR in the recorded signal (Repovš, 2010). If the electrodes are not connected properly to the scalp or the impedance of the skin at the location of the electrode is not low enough, what is recorded by the electrodes may be predominantly noise and does not include a meaningful signal. When measuring the brain response to a designed stimulus, even background/spontaneous EEG activity is an unwanted signal and is also regarded as noise (Repovš, 2010). The low-amplitude response is buried in the high-amplitude noise. In some cases, the SNR is so low that it becomes impossible to extract a meaningful stimulus-related EEG signal out of the recorded data even after artefact rejection. Thus, it is essential to check for the existence of the brain response to a presented stimulus in recorded EEG before proceeding in the analysis any further.

Therefore, following the conventional methods of response detection in EEG (Wunderlich et al., 2006; Pfurtscheller and da Silva, 1999; Allen and MacKinnon, 2010), we tested the quality of data recorded using the S1 protocol in normal hearing adults. This quality test was performed before applying any artefact rejection or noise cancellation techniques or employing any pre-processing procedures other than the ones actually required to detect the response in the data. For the sake of confirming that the signal contains a stimulus response, we checked for the presence of the more established evoked responses first and the results are presented in section 3.3.1. We then proceeded to test for induced responses, however, the procedure that was initially employed to detect the induced response was not very successful, probably, because of the low level of SNR, the results of which are presented in appendix A. It soon became clear that to detect the induced response, we need to clean the data first (as in section 3.4) and then employ the response detection algorithms. This task is performed and explained more comprehensively in chapter 4.

It is shown in the literature that the electrode placed on the vertex (in this study electrode number 1 in both S1 and S2 protocols) is one of the electrodes that shows a significant response to auditory stimulation for different types of stimuli (Friederici, 2002; Wunderlich et al., 2006). Thus, for response detection in this study, we focused on this electrode along with some other electrodes placed around auditory perception areas such as the Primary Auditory Cortex (like electrodes 41 and 36).

3.3.1 Evoked response detection

Similar to other studies on auditory brain responses and specifically ALRs, we expected to detect a response in the [1 30] Hz frequency band in response to AM tones and speech as well. Thus the data from the protocol S1 were filtered in the [1 30] Hz band, and the ensemble average was calculated for different stimuli types (AM tones, words, and sentences) recorded from normal hearing subjects. For this purpose, EEG signals were epoched (sectioned) around the stimulus onset time for each stimulus type. The pre-stimulus time which can also be called the baseline was 1000 ms and the post-stimulus time was 2 s/2 s/4 s for AM tones/words/sentences, respectively. No response could be found in the ensemble average of data in this frequency band by visual inspection. The data in S2 had been checked by the relevant researcher and their results are not presented here.

In Sanderson (2010), it is shown that the most affected frequency band when listening to BKB sentences is the theta frequency band. Thus, we filtered the data to a lower frequency band, namely [4 8] Hz, and then applied ensemble averaging for each stimulus type. This time, three peaks similar to ALR response emerged after the stimulus onset in all stimulus types and subjects. This result impelled us to look at ensemble averaging in other frequency bands mentioned in Table 2.1 as well and again, in some of these bands an evoked response was detected.

To verify the significance of these peaks in each recording, a bootstrap method was employed (Lv et al., 2007) to estimate the statistics of non-event-related averages for comparison with the event related ensemble average. The aim was to compare the peaks in the original ensemble average (containing an evoked response) to the statistics of the non-event-related data in which the evoked response was absent. To obtain this non-event-related data, it was important to eliminate the response in any of the frequency bands without changing the statistics of the data such as its mean and standard deviation. Thus, all epochs of each stimulus type were put together for one channel generating a concatenated signal. Data points were selected randomly from this signal and were considered as the starting point of new sets of epochs. The number of these randomly selected starting points was the same as the number of epochs in each condition, e.g. 100 in words or 50 in sentences. The length of epochs was the same as those in the original dataset, e.g. 3 s in words and 5 s in sentences. The selected epochs were then filtered to different frequency bands and ensemble average was calculated for each band, i.e. at each time point an average was calculated over all epochs. This random selection, filtering and ensemble averaging was repeated 1000 times, i.e. a pool of 1000 random ensemble averages was generated. Then, at each time point along the epoch, the values of 1000 ensemble averages were sorted and the highest and lowest 2.5% values were selected. These values mark the 95% confidence interval of the probability distribution for that time point. In each frequency band, a peak in the original ensemble average of

the signal was considered significant if it fell outside this 95% confidence interval at that time point.

For group analyses, a similar approach was employed but instead of ensemble averaging on single subjects, the ensemble average on all subjects were computed for each stimulus type. Also, in group bootstrap analyses, the confidence interval was identified on the average signals of all subjects.

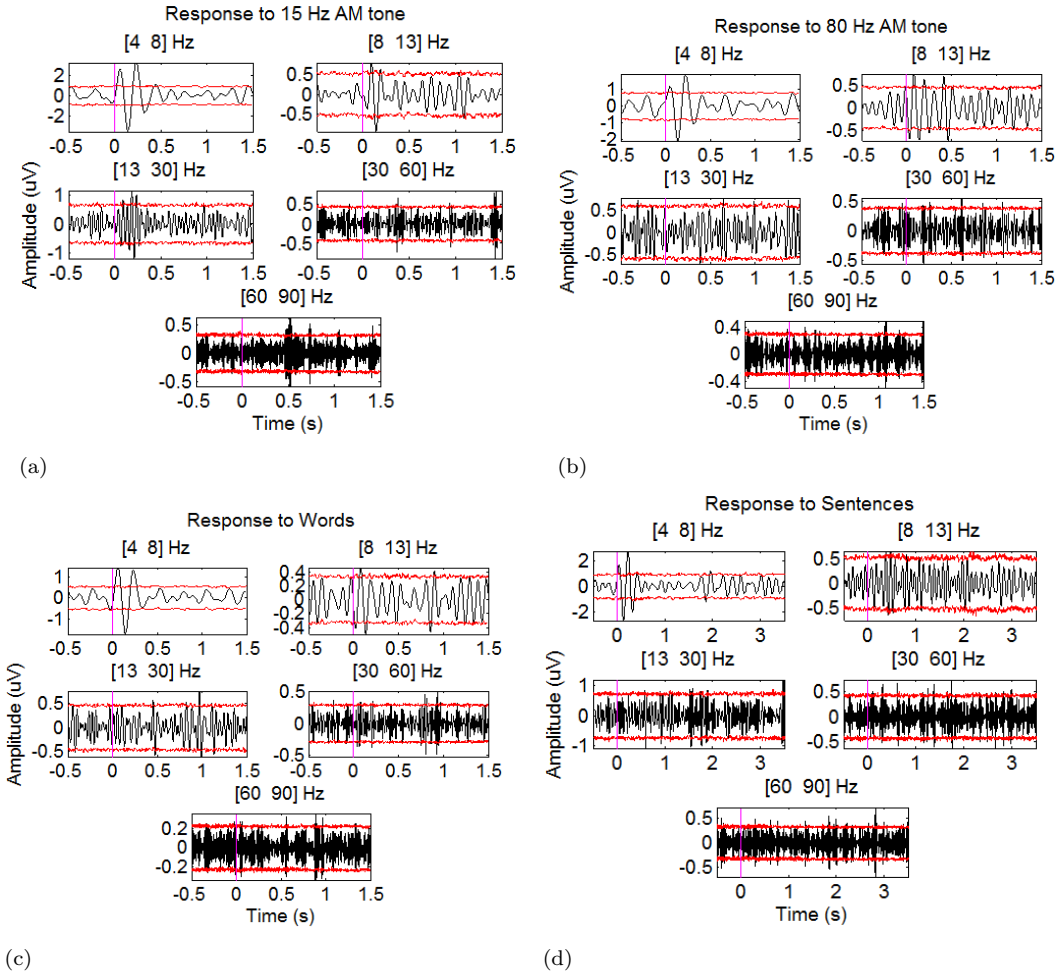

Figure 3.2: Ensemble averaging and bootstrap analyses for various frequency bands in channel 1 (vertex) of one subject in response to a) 15 Hz AM-tone, b) 80 Hz AM-tone, c) word, and d) sentence stimulus types presented to the right ear. Red lines indicate the 5% confidence intervals for each frequency band along time. The vertical magenta line shows the stimulus onset.

Figure 3.2 shows an example of ensemble averaging in different frequency bands for four different stimulus types presented to the right ear in only one subject along with the 95% confidence interval obtained from bootstrap analyses for that frequency band. These are the results of bootstrapping in channel 1 on a single subject. Note that in these figures, 500 ms of the beginning and end of each epoch has been removed. This was done to eliminate the filter effect. There are three (around 50 ms, 150 ms, and 200 ms) significant peaks present in the theta band ([4 8] Hz) in response to all stimulus

types. These peaks were observed in almost all subjects and in response to all stimulus types. In some subjects, a peak around 300 ms was also observed. Similar peaks to the theta band, though with different delays, were observed in the [8 13] Hz frequency band in many but not all subjects. These peaks in the alpha band along with a peak just before the onset of the stimulus in the theta band were marked as significant in group analyses in response to all stimulus types.

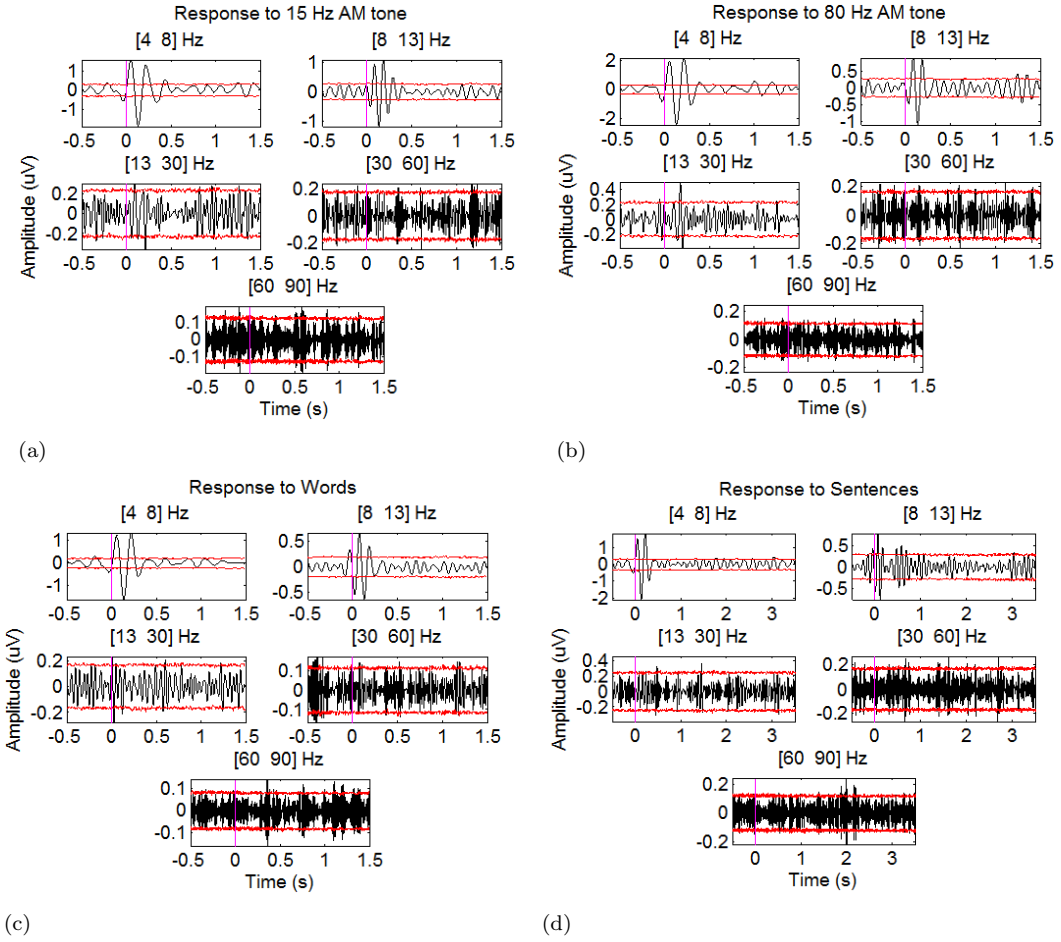

Figure 3.3: Ensemble averaging and bootstrap analyses for various frequency bands in channel 1 (vertex) of ALL subjects over a) 15 Hz AM-tone, b) 80 Hz AM-tone, c) word, and d) sentence stimulus types presented to the right ear. Red lines indicate the 5% confidence intervals for each frequency band along time. The vertical magenta line shows the stimulus onset.

Figure 3.3 presents the results of bootstrapping on the ensemble average over all subjects for different stimulus types presented to the right ear. The peaks that fall outside the confidence intervals are regarded as significant ones. As the results of the left ear and binaural presentation are very similar to Figure 3.3, they are not presented here.

Finding these peaks helped us specify that there was significant evoked response in our data at both single subject and group level analyses. The existence of the evoked response confirmed that the recorded data were not all noise and we could then confidently

use the data for further investigations of brain activity such as connectivity.

3.4 Pre-processing

After it was determined that the recorded data included some meaningful response in it, the data were preprocessed as described in following paragraphs.

Before epoching, the data were first filtered in the [1 120] Hz frequency band for protocol S1 and S3 and the [1 100] Hz for protocol S2, it was mentioned in section 3.2.2.3 that data from S2 were low-pass filtered to 100 Hz at the time of recording. Data were then epoched around the onset of each stimulus. In protocol S1 and S3, data in response to tone bursts were epoched to [-0.5 1] s, AM tones and words to [-1 2] s, and sentences to [-1 4] s. In protocol S2, data were epoched to [-0.5 1] s as for tone bursts in study S3. Note that the time course before the onset of the stimulus is considered the baseline condition in our analysis. Epochs were then zero-meaned by subtracting the average from each epoch.

The extended Infomax ICA (Makeig et al., 1997) was applied to each dataset using EEGLAB software (Delorme and Makeig, 2004). Components representing stereotypical artefacts such as ECG and eye-blinks were detected visually using the time-domain representation of components and were removed and data were reconstructed. In data recorded from CI users (study S3), artefactual components were selected differently, the procedure of which is presented in chapter 8. After reconstructing the data, epochs with amplitude values outside ± 100 μV in any channel were removed from further analysis. The data were again visually inspected and epochs with obvious artefacts were removed from the data. An example of an epoch before and after de-noising is presented in Figure 3.4. This epoch was contaminated with 50 Hz noise and eye-blink artefact (Figure 3.4.a) which were removed using ICA (Figure 3.4.b).

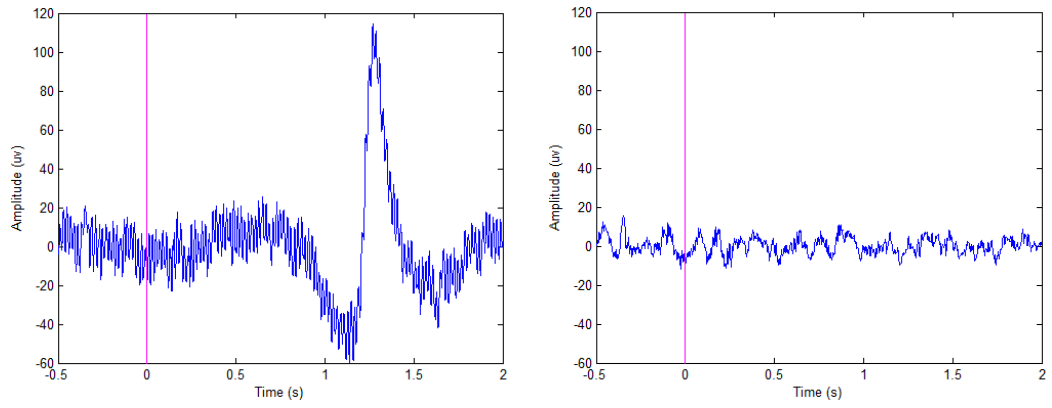

(a) (b)

Figure 3.4: An example of a noisy epoch (contaminated with 50 Hz noise and eye-blink artefact) a) before and b) after artefact rejection.

When the number of epochs is too small, the SNR will not be high enough for the stimulus effect to be detectable in the recorded EEG and this result will affect our significance analyses. That is why data with too few epochs (i.e. less than 70%) compared to the rest of the data had to be removed from further analyses. Thus, for each stimulus type and presentation ear in protocol S1, one or two subjects had to be eliminated as the number of their remaining good quality epochs was too small compared to the rest of datasets, i.e. less than 70%. Also, two subjects from protocol S2 were omitted from computations for the same reason.

3.5 Discussion

In this chapter, the protocols of EEG recording for the data used in this report were presented and the quality of EEG recorded from normal hearing subjects was checked.

In studies S1 (section 3.2.1) and S3 (section 3.2.3), adult right-handed English speakers were recruited. As right- or left-handedness might affect activation patterns in the brain (see section 2.2), to decrease variability among subjects, only right-handed people were recruited.

As participants were presented with English words and sentences as one part of the experiment and there was the possibility of different brain activation patterns when people were subjected to a language other than their mother tongue (Reiterer et al., 2005), to decrease the variability of brain connectivity patterns, the participants were chosen to be native English speakers.

Because this was a new line of research, it would be more convenient to work with adult subjects rather than children. For example, one of the biggest complications in working with children was their tendency to move during EEG recording which would cause higher noise levels in the signal. Also, getting an Ethics approval for children was more demanding than for adults.

Research has shown that postlingually deaf patients have better performance after implantation compared to prelingually deaf patients (Nava et al., 2009a). This is the main reason for selecting a postlingual patient group rather than a prelingual group in study S3 (section 3.2.3). We assume the brain connectivity of the former group would be more similar to normal hearing participants when they reach their initial optimum speech perception point. Although in the long run, it might be useful to compare the brain activity for pre and postlingually deafened groups.

Considering all the inclusion and exclusion criteria, normal hearing adults and CI users were recruited and their EEG were recorded. Bootstrap analyses showed that there was indeed response in our normal hearing data and the data could then be used for other

analyses explained in following chapters. Analysis of CI data was not presented in this chapter and can be accessed in chapter 8.

3.6 Summary

In this chapter, three protocols of the experiments that were performed on normal hearing adults and cochlear implant users for recording EEG were explained. Surface EEG was recorded from these two groups of participants while they sat silently in a comfortable chair and listened to auditory stimuli of amplitude modulated tones, words, and sentences.

As sometimes the signal to noise ratio is too low in EEG recordings that no meaningful response can be extracted from the recorded data, it was necessary to check for the presence of response in the EEG before proceeding to data analysis and feature extraction.

Data validation using ensemble averaging in some known frequency bands over the peristimulus time range revealed some significant peaks after the stimulus onset in theta and sometimes alpha and beta frequency bands using bootstrap analyses. These significant peaks were indicative of the presence of responses in the data after the onset and thus suitable for further analysis.

Basic pre-processing steps common for all recorded signals were described in this chapter. Further pre-processing steps are required for each analysis method used in following chapters. Those steps are presented for each method in their related chapters.

Chapter 4

Detection of Induced Responses

4.1 Introduction

The evoked response is phase-locked to a stimulus such that peaks and troughs occur at fixed times (latencies) following the stimuli. Coherent (ensemble) averaging can be used to enhance these responses and suppress the usually overwhelming background EEG activity which hides the response in the raw signals (David et al., 2006b). On the other hand, induced responses are defined as time-locked but not phase-locked brain responses to the presented stimuli. Thus, at a specific time following a stimulus, there may be an increase or decrease in the power of the signal. This increase or decrease in the amplitude does not consistently involve the same phase angle in all stimulus presentations and that is why it may be cancelled out using time domain ensemble averaging. The induced response is best investigated in the frequency domain using time-frequency analysis of the signal (David et al., 2006b).

An evoked response is believed to be the result of coherent firing of neurons in response to the stimulus, whereas an induced response is thought to be related to higher order processes of the brain which are not directly related to the stimulus but are caused indirectly by nonlinear interactions of neurons following the stimulus (David et al., 2006b). The induced response can be linked to cognitive functions of the brain such as perception, attention, and learning (Gruber et al., 2001; Gurtubay et al., 2004; Graichen et al., 2009) which can be considered to be higher-order processes. Different frequency bands can be affected depending on the task being performed. The gamma band, for example, has been associated with recalling information in learning tasks (Gruber et al., 2001) and was also observed in response to auditory mismatch negativity stimuli (Gurtubay et al., 2004) while participants counted the deviant tones. Alpha band power has been found to increase in response to flicker stimuli (Graichen et al., 2009) and beta power has been related to visual attention (Gola et al., 2013).

The auditory induced response of the brain has been studied with specific stimulus types such as perturbed and unperturbed sequences of pure tones (Zanto et al., 2005; Fuentemilla et al., 2006, 2008; Haenschel et al., 2000), repeated identical words (Krause et al., 1998), targeted words in specifically designed sentences (Obleser and Kotz, 2011), and repeating modified and unmodified sentences (Howard and Poeppel, 2010, 2012). The gamma band was activated in response to pure tones with temporal perturbations (changing the pitch of the last word) (Zanto et al., 2005), an increase in 40 Hz power was observed in response to standard but not deviant repeating words (Krause et al., 1998), and the gamma band was affected when subjects were presented with different types of keywords in sentences (Obleser and Kotz, 2011). In all these studies, specific presentation protocols were used that aimed to generate an attention or a cognition related response, e.g. by presenting pure tones in randomly changing inter-stimulus intervals (Zanto et al., 2005) or including keywords with high or low prediction probability in sentences (Obleser and Kotz, 2011). These protocols all aim to test quite specific hearing tasks and are not usually easy to reproduce. Whether such sophistication is necessary to find induced responses, has remained an open question. To the best of our knowledge, none of these studies has ever targeted the brain's induced response to a group of words or sentences with little restriction on their frequency or lexical content, or to repeating tone bursts, as commonly used in evoking the ALRs.

The brain's response to repeating pure tones has attracted much attention in audiology and has been shown to be beneficial for objective estimation of the hearing threshold (Lightfoot and Kennedy, 2006; Carter et al., 2010; Golding et al., 2009). For the purpose of finding hearing threshold, the brain response is typically analysed in the time domain focusing on the evoked response (Lightfoot and Kennedy, 2006) to different sound levels of pure tones and considerable research effort has gone into improving the detection rate of this response (Ikeda et al., 2010) for different conditions, such as in children with Auditory Neuropathy Spectrum Disorder (ANSD) (He et al., 2013). However, to the best of our knowledge, little research has focused on the presence of induced response to pure tones (Zanto et al., 2005; Fuentemilla et al., 2006, 2008; Haenschel et al., 2000) and none on induced responses to repeating pure tones without manipulating the presentation protocol. This may be due to the assumption that a simple tone burst stimulus may not provide any higher order perception cues that would lead to the induced response, or because it is presumed that habituation of the brain to a repetitive sound may cause existing induced responses to vanish rapidly in repetitive stimulus presentations. Because the tone is simple and commonly used in clinical recordings, it may produce some insight into perception abilities of the participant rather than their hearing ability only, which presents itself primarily as an evoked activity. This simple stimulus can also provide baseline data for the subsequent analysis of words and sentences. It may also provide a baseline for the clinical assessment of ANSD and auditory processing disorder, but such studies are beyond the scope of the current

project. A comparison of induced responses to tone bursts and speech stimuli also provides additional insights into the specific effect of speech.

There are limited number of studies with EEG on the brain's response to normal speech such as words and sentences (Krause et al., 1998; Howard and Poeppel, 2010, 2012; Obleser and Kotz, 2011; Schack and Weiss, 2005; Weiss and Muller, 2013; Peelle et al., 2013) and even those studies present the stimulus with quite restricted protocols. In addition, not all of these studies target the induced response but focus on the evoked response to these stimuli. There are some studies with patients such as cochlear implant and hearing aid users (Ching and Dillon, 2013), children with ANSD (He et al., 2013), patients who have had a stroke (Maiorova et al., 2014), and hidden hearing loss in people who have been subjected to loud noise for too long (Tyler and Tye-Murray, 1986), who show normal hearing thresholds when listening to pure tones but still report hearing problems in response to more complicated sounds such as words in quiet or noisy environments, i.e. they can hear the word but they do not understand it. It has been suggested (Gruber et al., 2001; Gurtubay et al., 2004; Graichen et al., 2009) that induced responses may provide additional insight into higher level processing disorders, and this path is pursued in the current work.

Recent publications have utilised different methods to investigate the existence and the significance of the induced response in the brain in response to various types of passive or active tasks. For example, time-frequency analyses have been carried out using Fourier transform (Vialatte et al., 2009) or Wavelet transforms (Obleser and Kotz, 2011; Gurtubay et al., 2004), normalisations have been performed using the baseline power (Hannemann et al., 2007; Sanderson, 2010; Friedrich et al., 2013; Gurtubay et al., 2004) or the power of the whole time window being investigated (Zanto et al., 2005), and statistical methods such as non-parametric Wilcoxon test (Karrasch et al., 1998), Analysis of Variance (ANOVA) tests (Krause et al., 1999), and bootstrapping (Telenczuk et al., 2011) have been used to test the significance of the observed response. An induced response is not usually easy to detect and our preliminary analyses for detecting the induced response using the envelope of the signal (see appendix A) is a confirmation of this statement as they failed to detect the induced response in our data. Therefore, more in depth analyses were required to assess the presence of the induced response in our data. In addition to providing new insights into brain responses to auditory stimuli, this work also addresses some of the methodological issues evident in previous works in induced response detection. As the data will be further used for measuring connectivity in future chapters and the induced response plays an important role in connectivity measurement (see section 7.4.1.2), in this chapter, specific attention is given to different approaches of detecting induced responses. These methods were first tested on simulated data (see appendix B). Those deemed most suitable, were then applied on the EEG and are described in this chapter. The results of response detection on EEG are presented in section 4.3 followed by a summary of the conclusions in section 4.4.

In sum, using simulated data, appendix B identifies the most appropriate response detection methods for the purpose of this study. These methods are then used in this chapter to assess the brain response to tone bursts, AM tones, words, and sentences using recorded EEG. Not only will this chapter provide more insight into brain's activity in response to these sounds, it will establish that the recorded EEG data are good enough for future connectivity analyses.[1]

4.2 Methods

Following on from the preliminary work (appendix B), the methods deemed most appropriate were applied to the recorded signals. These methods are described in the following sections.

4.2.1 Time-Frequency (TF) analyses

Trautner et al. (2006) showed that by averaging the Fourier transform of EEG over all epochs and then calculating the power of the Fourier transform, the phase-locked activity of the brain will be enhanced and any activity that is non-phase-locked to the stimulus will be averaged out. Indeed, it can readily be shown that due to the linear properties of averaging and Fourier transformations, the order of the processes can be reversed without affecting the results. On the other hand, by first calculating the power of the Fourier transform of each epoch and then averaging the power spectra over all epochs, one will be left with a linear combination of both the phase-locked (evoked) and non-phase-locked (induced) power of the brain, see Equations 4.1 to 4.3 in which the Total Power (TP), the Evoked Power (EP), and the Induced Power (IP) are calculated. The phase-locked power can thus be subtracted from this spectrum so that the non-phase-locked power is retained. If the non-phase-locked activity is time-locked to the stimulus, it will stand out in the averaged spectrum and can be regarded as an induced response. Equation 4.1:

$$TP(t,f) = EP(t,f) + IP(t,f) + \epsilon(t,f) = \frac{1}{K}\Sigma_{i=1}^{K}(Re_i(t,f)^2 + Im_i(t,f)^2) + \epsilon(t,f), \quad (4.1)$$

is a representation of the total power of the signal in the time-frequency domain in which K is the number of epochs and Re and Im indicate the real and imaginary parts of the Discrete Fourier Transform (DFT) of each epoch at each time-frequency point. ϵ is the background EEG power at each time-frequency point. As can be seen, the total power

[1] Parts of the results of this chapter are presented in Hosseini et al. (2013a, 2015, 2014a).

is the power averaged over all epochs plus a background noise factor. In this equation, EP is:

$$EP(t,f) = (\frac{1}{K}\Sigma_{i=1}^{K} Re_i(t,f))^2 + (\frac{1}{K}\Sigma_{i=1}^{K} Im_i(t,f))^2, \tag{4.2}$$

which calculates the average of DFT values at each time-frequency point before calculating the power so IP can be calculated as:

$$IP(t,f) = TP(t,f) - EP(t,f) - \epsilon(t,f). \tag{4.3}$$

In our analyses, after removing EP from the total power before and after the onset, we are left with both IP and background power. However, as significance analyses will compare the power before and after the onset (see section 4.2.2) and background power has the same distribution before and after the onset, the background noise power will be neutralised in significance analyses. From this point on in this report, TP - EP will be called IP although it includes the background power as well.

Data were first pre-processed according to steps in section 3.4. Then, the 256-point short time DFT of each epoch was performed over the whole epoch for each subject, stimulus type, channel, and monaural or binaural condition with 256ms windows (multiplied by a Hamming window) and 245ms overlap. Hamming window was used because of its wide peak and low side lobes. The 256 ms window is centred around each time point. As the DFT values were calculated using Fast Fourier Transform (FFT) techniques, DFT will be called FFT from this point on in this thesis. Using these FFT values, following Trautner et al. (2006), the evoked and induced power spectra were estimated. In this chapter, the power of the evoked response was also estimated for comparison with induced power. If one's purpose is evoked response detection only, coherent averaging in time domain is a simpler choice (Simpson et al., 2000) as employed in Figures 3.2 and 3.3.

Because the power in the EEG spectrum generally decreases with increasing frequency, normalisation was required to facilitate visualization. It is very common to normalise the power at each time-frequency point in the spectrogram to the averaged power before the stimulus onset in that specific frequency (Hannemann et al., 2007). However, this type of baseline normalisation proved inappropriate in simulated data (see section B.4.1 in the appendix). Baseline normalisation would introduce a bias to the normalised power after the stimulus onset causing significance analyses to report significant power change after the onset compared to the baseline in almost all time-frequency points even when there was no response present in the simulated data. The reason is discussed in section B.5 of appendix B. Therefore, power values in each frequency were normalised to the average power of the whole epoch in that frequency instead. This normalisation brings

all frequency bands to a similar range and enhances the visibility of peaks (Zanto et al., 2005). To enhance the SNR, the normalised spectra were averaged over a few electrodes (5 or 7 depending on the area) over adjacent areas of the brain as marked by red lines in Figure 3.1.a and 3.1.b for studies S1 and S2, respectively.

After that, power was averaged in specific time-frequency regions in the spectrogram of the evoked or the induced response to be used for significance analyses. Averaging into regions decreases the number of significance tests required and increases the chance of finding a response if the timing of the response is different in different subjects. These regions were selected as in Figure 4.1 for different types of stimuli with different time widths depending on the type of the stimulus. According to the average evoked and induced responses observed for each specific stimulus and bootstrap analyses (see section 4.2.2), 100/200/200/500 ms and 200/500/500/1000 ms windows were selected for the evoked and induced power for tone burst/AM tone/word/sentence stimuli, respectively. Note that the windows do not overlap and that the onset is always the starting point of the first window after the onset and the ending point of the window before the onset. Obviously, the number of windows over time was different depending on the selected time width and the length of the epoch in each stimulus type, however, the frequency bands were kept constant.

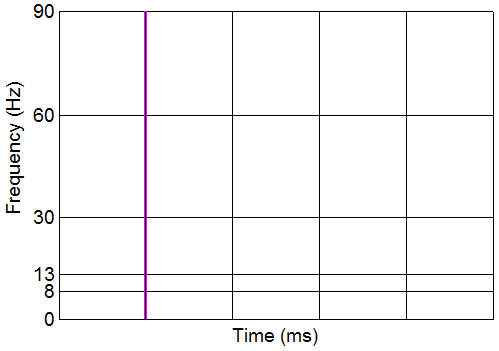

Figure 4.1: Areas in the power spectrum in which an average power was calculated. The magenta line indicates the stimulus onset. The width of windows over time were selected according to the stimulus type, e.g. 100/200/200/500 ms and 200/500/500/1000 ms for the evoked and induced power for tone burst/AM tone/word/sentence stimuli, respectively.

4.2.2 Significance analyses

Significance tests were required to identify if a power change in a specific time-frequency window after the stimulus onset was truly different from the baseline power, indicating an event related change in the power. For this purpose, both single-subject and group tests could be used.

In appendix B, commonly used approaches in related studies of this field were tested by simulated data to find the most appropriate significance test for the purpose of

this study. Tests that could be applied on single subjects or a group of subjects were employed (see section B.4.2) and Friedman's test (as a group analysis) was proved the most appropriate among those tested. Most of the significance tests examined produced higher false positive rates than expected. Different factors may affect each significance test. Let us first clarify that a group of power values consists of power values in all subjects in a specific time-frequency window. Detailed reasons for high false positive rates observed are presented in sections B.4.2 and B.5. In short, dependency between different pairwise tests (different groups after the onset against the same group, i.e. baseline) would affect pairwise tests (as used in related work (Karrasch et al., 1998; Gurtubay et al., 2004)) and dependency between the values in different groups (all groups come from the same subject) would affect one-way ANOVA (as used in related work (Fuentemilla et al., 2006)). In group bootstrap analyses that were used in appendix B, dependency between FFT values over time would affect the false-positive rate and in repeated measures ANOVA, outliers would affect the results (as used in related work by (Krause et al., 1999; Gruber et al., 2001; Fuentemilla et al., 2008)). Friedman's test was the only method which had the correct number of false positives when applied on simulated data, was sensitive enough to detect the simulated response in the data, and was not susceptible to outliers (see appendix B for more details). Therefore, it was selected as the most appropriate method for applying on recorded EEG data.

Although Friedman's test could detect the response in the recorded EEG, bootstrap (slightly different from appendix B.2.2 and explained below) was also employed to find the best length for windows in Figure 4.1 for each stimulus type. As the induced response is assumed to be related to cognition, it should also be assumed that the induced response occurs with different delays in different subjects. Thus, depending on the stimulus type being presented, a range of delays should be expected and the time-length of windows of Figure 4.1 should cover all these delays so that the response can be detected in statistical analyses. However, as this is an exploratory study, this range was not known a priori from the existing literature. For this reason, bootstrap analyses were applied on individual subjects (as explained below) for each stimulus type to find a proper time-length for averaging. Note that this approach was not tested in appendix B as it was just used for some preliminary analyses and testing it would be a very time consuming process.

The following describes the protocol for Friedman's and bootstrap analyses, bear in mind that single subject bootstrap analyses was not strong enough to detect induced activity in the data that is why the following group analyses were approached:

1. Bootstrap: Used as an extra step to determine a proper window length for averaging. For bootstrap analysis, the distribution of the data with no *event*-related activity is first required for significance comparisons. Then, the *event*-related spectra (induced and evoked response) should be compared with the *non-event*-related

spectrum distribution to find out if the increase or decrease seen in the calculated power spectra rejects the null hypothesis of no response present. For this reason, first, the normalised induced and evoked power spectra were calculated as *event*-related response and averaged over groups of electrodes (as marked in Figure 3.1) for each stimulus type (as described in section 4.2.1).

The bootstrap process has been presented in a block diagram in Figure 4.2. To produce a non-event-related distribution of the spectrum, first the time-varying FFTs of all epochs of the original data were calculated. Then, new epochs were generated by randomly (with replacement) selecting FFT values from the baseline of all epochs and placing them in all time-frequency points of the FFT matrix (a 3D matrix in the form of "Frequency x Time x epochs"). The randomly selected FFT values will be placed in the same frequency band as it was selected from. For example, assume that after FFT calculations, a 50 x 60 x 100 matrix of FFT values is obtained. After randomisation, again, a 50 x 60 x 100 matrix is generated but this time all the values in this matrix come only from the baseline FFT values. After the randomised spectrum was generated, the evoked and induced powers were calculated for this new set of epochs and averaged over a few electrodes, the same as before (see section 4.2.1). This procedure was repeated 200 times. The lower/upper 5% value of the 200 bootstrap samples were identified for each time-frequency point. If the *event*-related power values (induced or evoked) in a time-frequency point were lower/higher than this 5% value, that time-frequency point was assumed to have a significant power decrease/increase compared to the baseline, thus having a significant *event*-related change of power. This bootstrap analysis was applied on each subject and each stimulus type separately. Then, for each time-frequency point, the number of subjects showing significance was counted and plotted in a colour coded map. Note that we expected a high false positive rate for each subject individually but also expected to see a difference between the response and non-response time-frequency areas when all subjects were considered. Using the results of these analyses and finding the areas in which most subjects showed significant change of power, the length of windows in Figure 4.1 were identified for each stimulus type. The same window size was then used for all subjects.

2. Friedman's test: To find if any time-frequency window after the stimulus onset showed significant power change compared to the baseline, thus consisting a brain response. After the average power of evoked and induced spectra was calculated in each window of Figure 4.1, Friedman's test was applied to groups of powers (each group consisted of power values of all subjects in that time-frequency window) over time in each frequency band separately at the 5% significant level, i.e. Friedman's test was applied five times (five frequency bands). For example, for induced response in tone bursts, Friedman's test was applied over these five groups

[-200 0] ms, [0 200] ms, [200 400] ms, [400 600] ms, and [600 800] ms on each frequency band separately. The number of observations in each group was the same as the number of subjects for that stimulus type. If the p-value was smaller than 5% in a frequency band, post-hoc analysis (Tukey's test) were performed at the 5% significance level to find the time windows after the stimulus onset that had significant power change compared to the baseline in that frequency band.

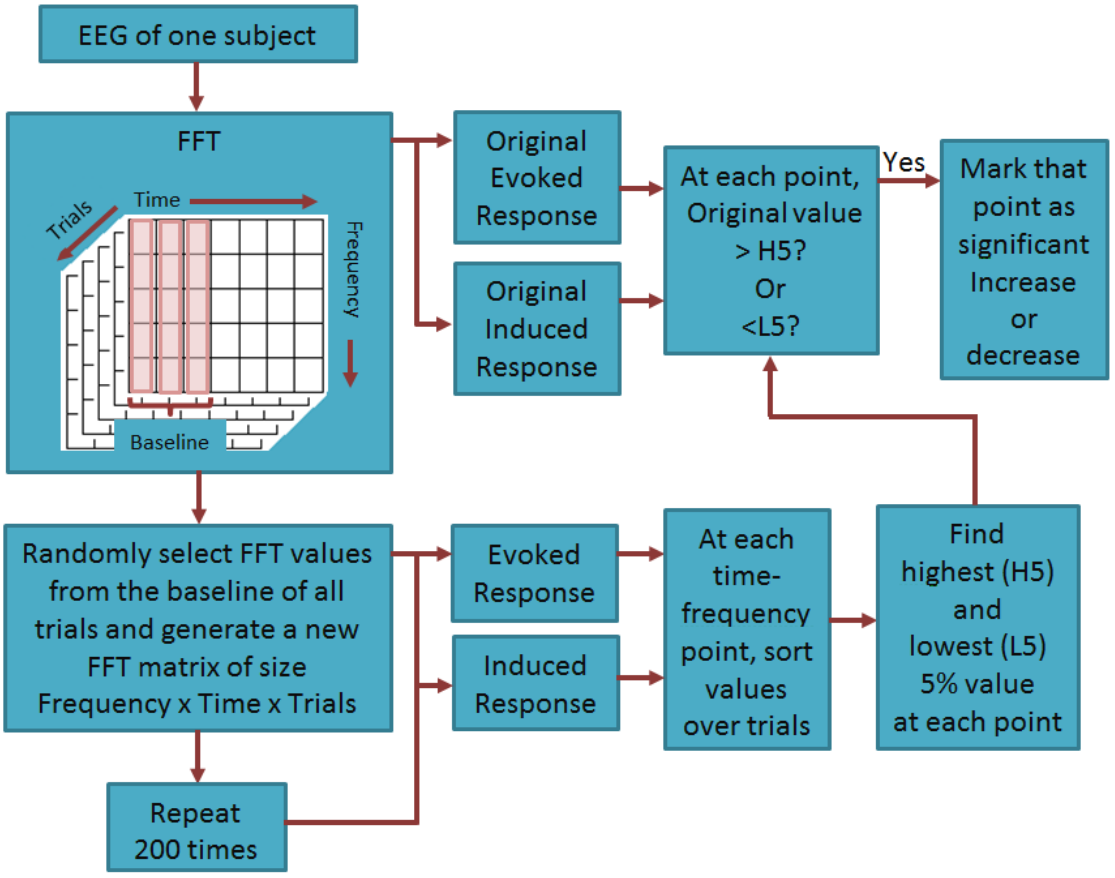

Figure 4.2: Block diagram of bootstrap procedure.

4.3 Results

The methods described above were applied on recorded EEG data to find out if any evoked or induced response is present in response to different types of auditory stimuli. In this chapter, the time-frequency analysis of the evoked response is used to compare it to the time-frequency analysis of the induced response and not for response detection purposes.

4.3.1 EEG in response to tone bursts

This dataset was recorded according to section 3.2.2, was preprocessed as in section 3.4, and two subjects were removed from further analyses because of low number of epochs after the pre-processing step (see section 3.4). The induced and evoked spectra were estimated and averaged in different channels by following the steps in section 4.2.1.

It was mentioned in section 4.2.1 that to find the best time length for windows of Figure 4.1 for averaging power over, bootstrap analyses (as in section 4.2.2) were employed. For this stimulus, bootstrap was applied on each subject as in section 4.2.2. The number of subjects showed a significant ($p<0.05$) decrease or increase at each time-frequency point compared to the baseline was counted for the evoked and induced power separately. The results of the number of subjects showing significant increase in evoked and induced power in response to tone bursts are presented in Figures 4.3 and 4.4, respectively. The number of subjects is colour coded in these figures. Note that after artefact rejection for this stimulus, eight subjects remained for further analyses (see section 3.4).

According to these figures, most of the subjects show significant ($p<0.05$) increase in the evoked power just after the stimulus onset but different areas of the brain seem to engage different frequencies in response to tone bursts. Also, as expected (Picton et al., 1974; Knight et al., 1980), more subjects show significant evoked activity in fronto-cental areas than occipital areas. There does not seem to be much consistent activity in the induced response over all subjects, see Figure 4.4. Similar figures were also obtained for significant decrease in evoked and induced spectra but they did not show any consistent response either and their results are not presented here. From these results, it seems that the evoked response mainly happens in the first 400 ms after the onset and it visually appears to change in 100ms windows according to the changing number of subjects showing significance over time. Thus, it was decided that for evoked response to tone bursts, the time-frequency windows of Figure 4.1 could be selected as 100ms windows. For the induced response, although no area appears to be affected consistently over all subjects, a 200ms window was decided upon.

To find the areas in the spectra with significant change compared to the baseline over all subjects, the power in induced and evoked response spectra were averaged over time-frequency areas defined in Figure 4.1 with 100ms windows for the evoked and 200ms windows for the induced spectrum. For each subject, there were three recordings. The power values were averaged over the three recordings in each subject. Then, Friedman's test and post-hoc analyses were applied to power values according to section 4.2.2 to find the time-frequency areas after the onset significantly ($p<0.05$) different from the baseline.

Figures 4.5 and 4.6 respectively show the average of the evoked and induced power over groups of channels (as shown in Figure 3.1.b) and over all subjects. The averaged evoked

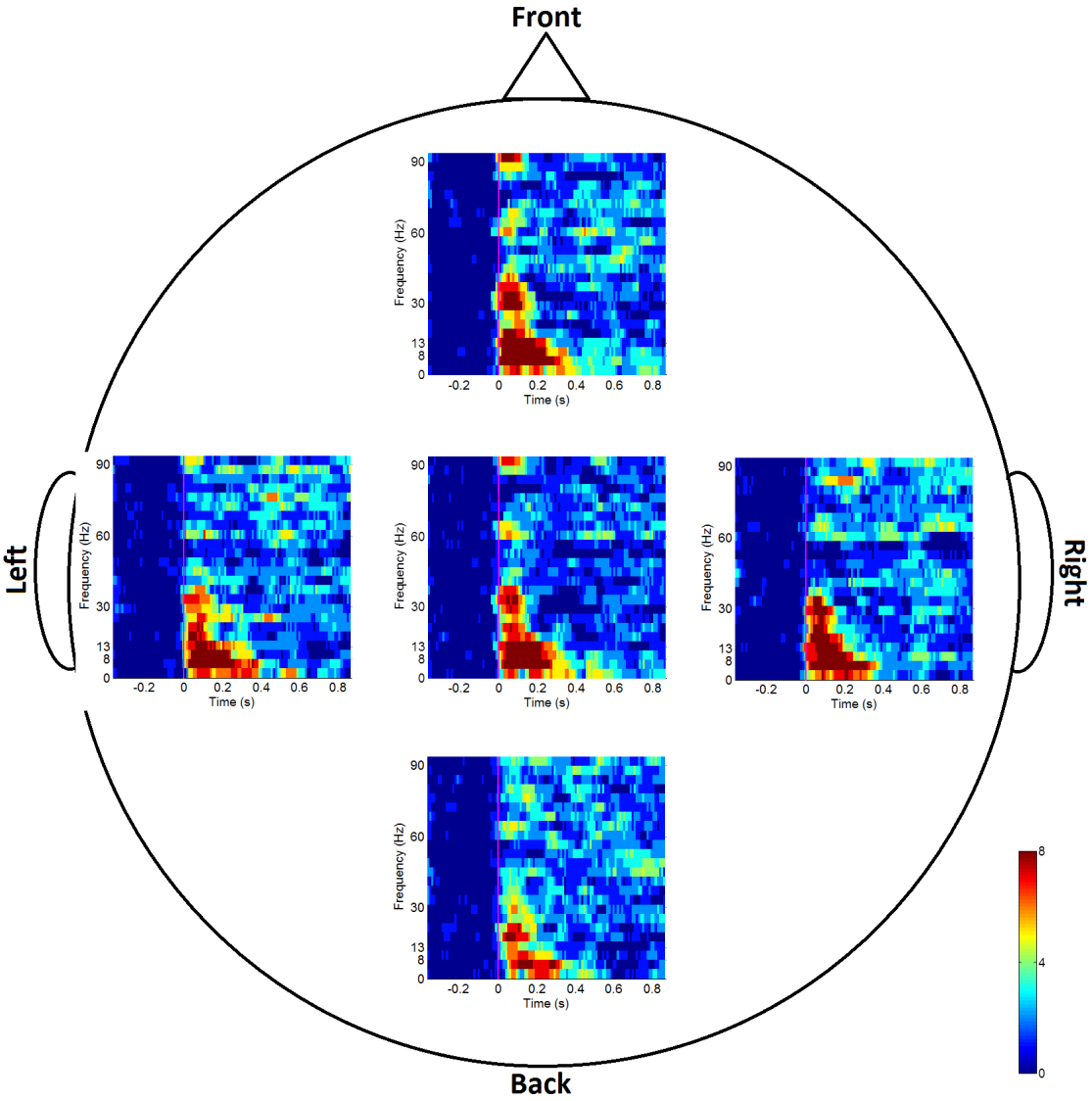

Figure 4.3: Number of subjects showing significant (bootstrap, $p<0.05$) increase in the evoked power at each time-frequency point over groups of electrodes shown in Figure 3.1.b in response to tone bursts presented to the right ear. The magenta line indicates the stimulus onset. The colour bar on the bottom right hand side shows the number of subjects.

power in Figure 4.5 looks similar to the results obtained by bootstrap analyses in Figure 4.4. Areas indicated by black windows show significant ($p<0.05$) increase of the power compared to the baseline. Figure 4.5 demonstrates that the evoked response in fronto-central areas consist of higher frequencies than other brain areas and that the occipital lobe has the lowest frequency contributions. Also, the evoked response appears to have a delay in occipital electrodes compared to other brain areas, or maybe it is missing the first peak. On the other hand, in Figure 4.6 it is clear that no induced response could be detected for tone burst stimulation using the employed methods.

It can be concluded that a simple repeating tone burst causes evoked activity but does

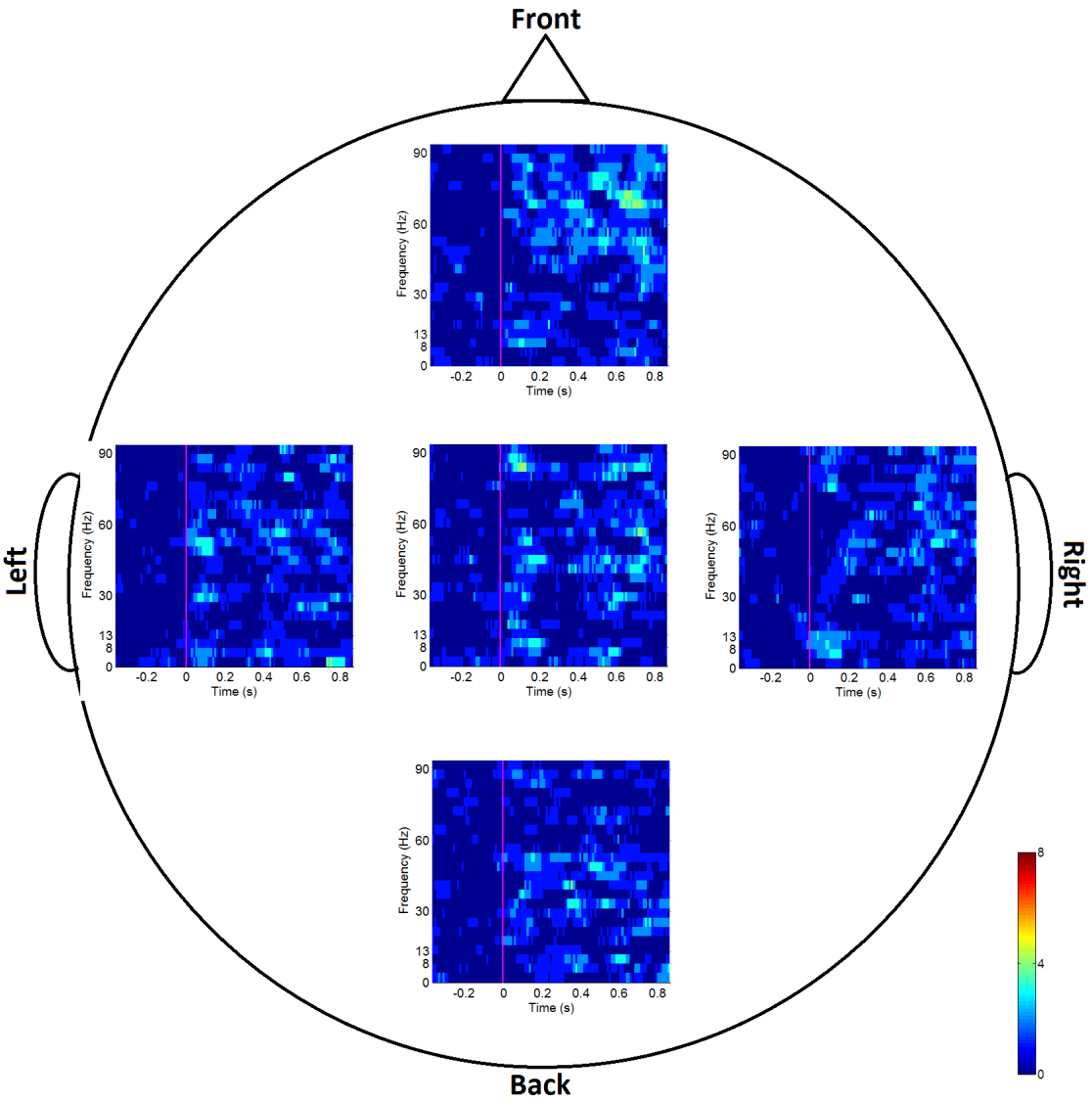

Figure 4.4: Number of subjects showing significant (bootstrap, $p<0.05$) increase in the induced power at each time-frequency point over groups of electrodes shown in Figure 3.1.b in response to tone bursts presented to the right ear. The magenta line indicates the stimulus onset. The colour bar on the bottom right hand side shows the number of subjects.

not cause any induced response in the brain or the induced response is not big enough to be detected by approaches taken in this chapter.

4.3.2 EEG in response to AM tones

This type of data were recorded according to protocol S1 (see section 3.2.1), preprocessed as in section 3.4 and two subjects were removed from further analyses in each AM tone type and presented ear because of the low number of epochs after artefact rejection (see section 3.4). Then, the induced and evoked powers were estimated in the frequency

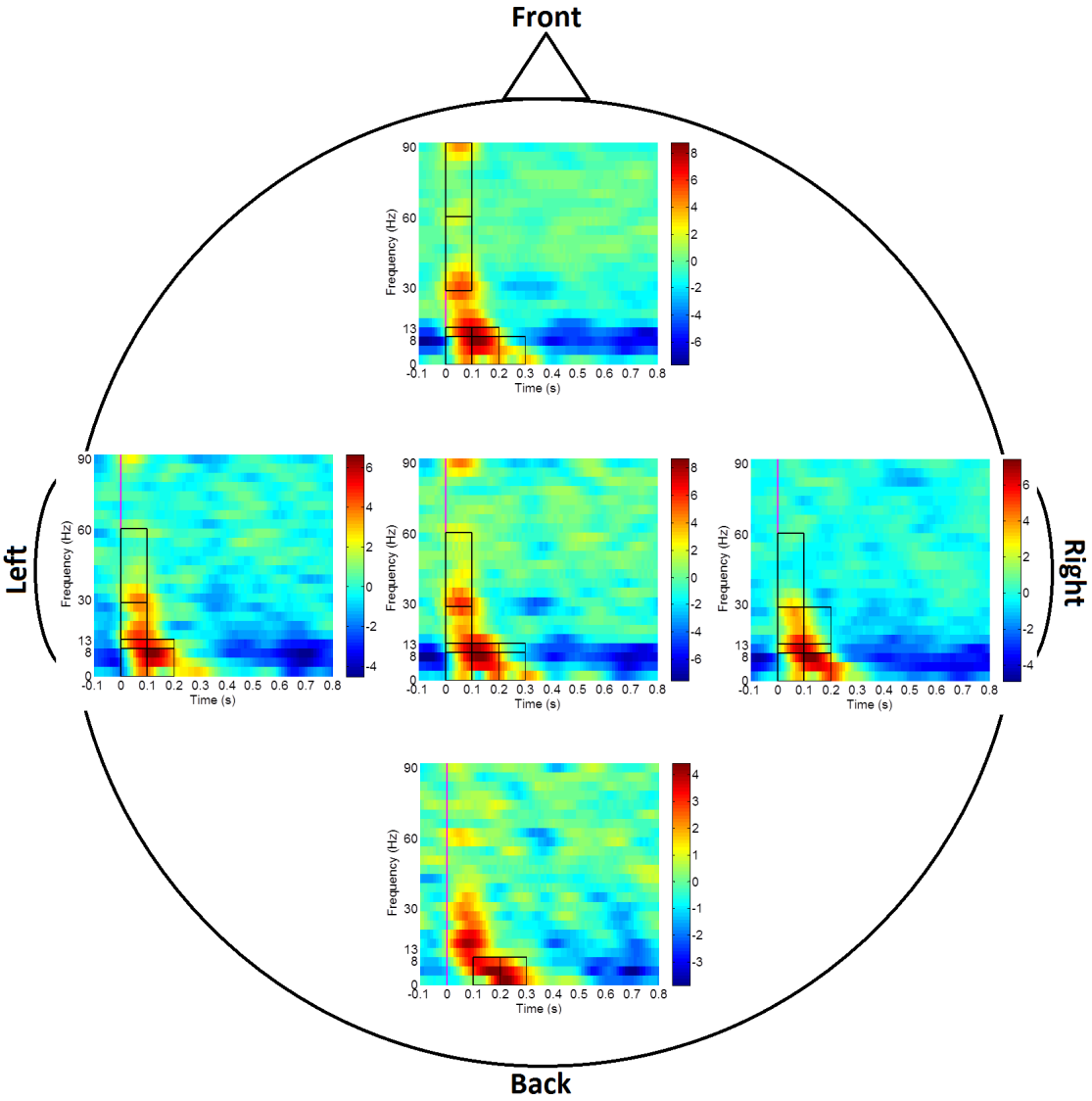

Figure 4.5: Average of evoked power in response to tone bursts presented to the right ear over subjects and groups of electrodes shown by Figure 3.1.b plotted in dB. The black windows show significant (Friedman's test, $p<0.05$ - Tukey's test, $p<0.05$) increase compared to the baseline.

domain and averaged over different groups of electrodes as indicated in Figure 3.1.a for each AM tone and each presented ear for statistical analysis using the Friedman's test.

Amplitude modulated tones are expected to provoke an increase in the power of the frequency of modulation (Hall, 2007). Therefore, for 15 Hz and 80 Hz modulated tones, instead of averaging in time-frequency areas of Figure 4.1, power was averaged in frequencies around the two modulation frequencies in different time ranges. However, in none of the AM tones to right ear or binaural presentation were any significant changes of power, compared to the baseline, observed. We thus did not proceed to the left ear presentation.

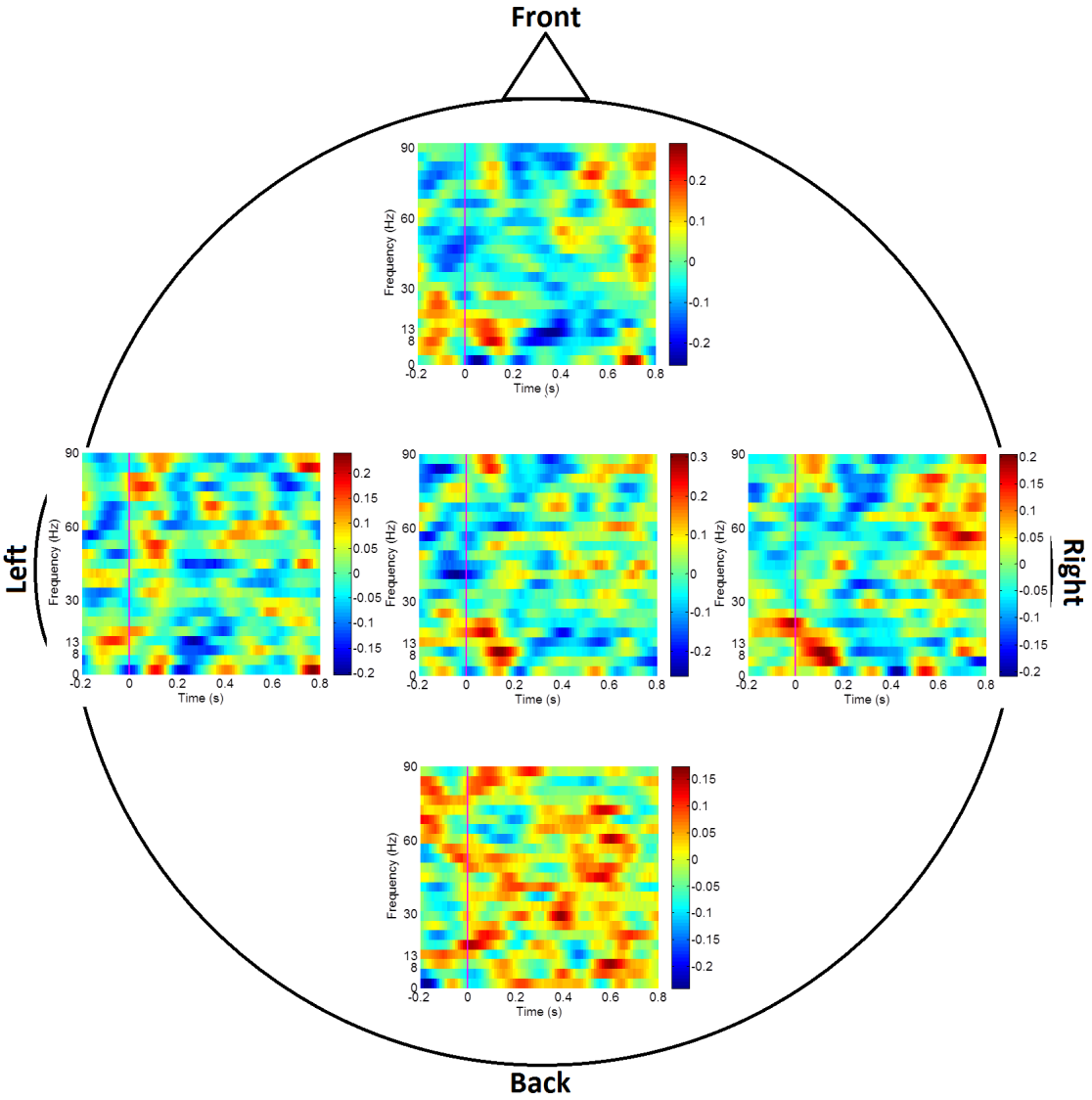

Figure 4.6: Average of induced power in response to tone bursts presented to the right ear over subjects and groups of electrodes shown by Figure 3.1.b plotted in dB. There is no significant (Friedman's test, $p<0.05$ - Tukey's test, $p<0.05$) change of power after the stimulus onset compared to the baseline.

Bootstrap analyses were performed according to section 4.2.2, to find the EEG frequency bands that had been affected in most subjects after presentation of these AM tones. From the results of these analyses on right ear presentation, in most subjects, only evoked power showed significant ($p<0.05$) increase in lower frequency bands and the first 200-300 ms time range after the stimulus onset (the length of AM tones was 1000 ms), confirming our findings in chapter 3 using bootstrap analyses in the time domain, see Figure 3.3. Similar results were achieved from both AM tones in response to binaural presentation. As no induced response was observed in these cases, left ear presentation was not tested.

To explore whether there was any change of power which would present itself more

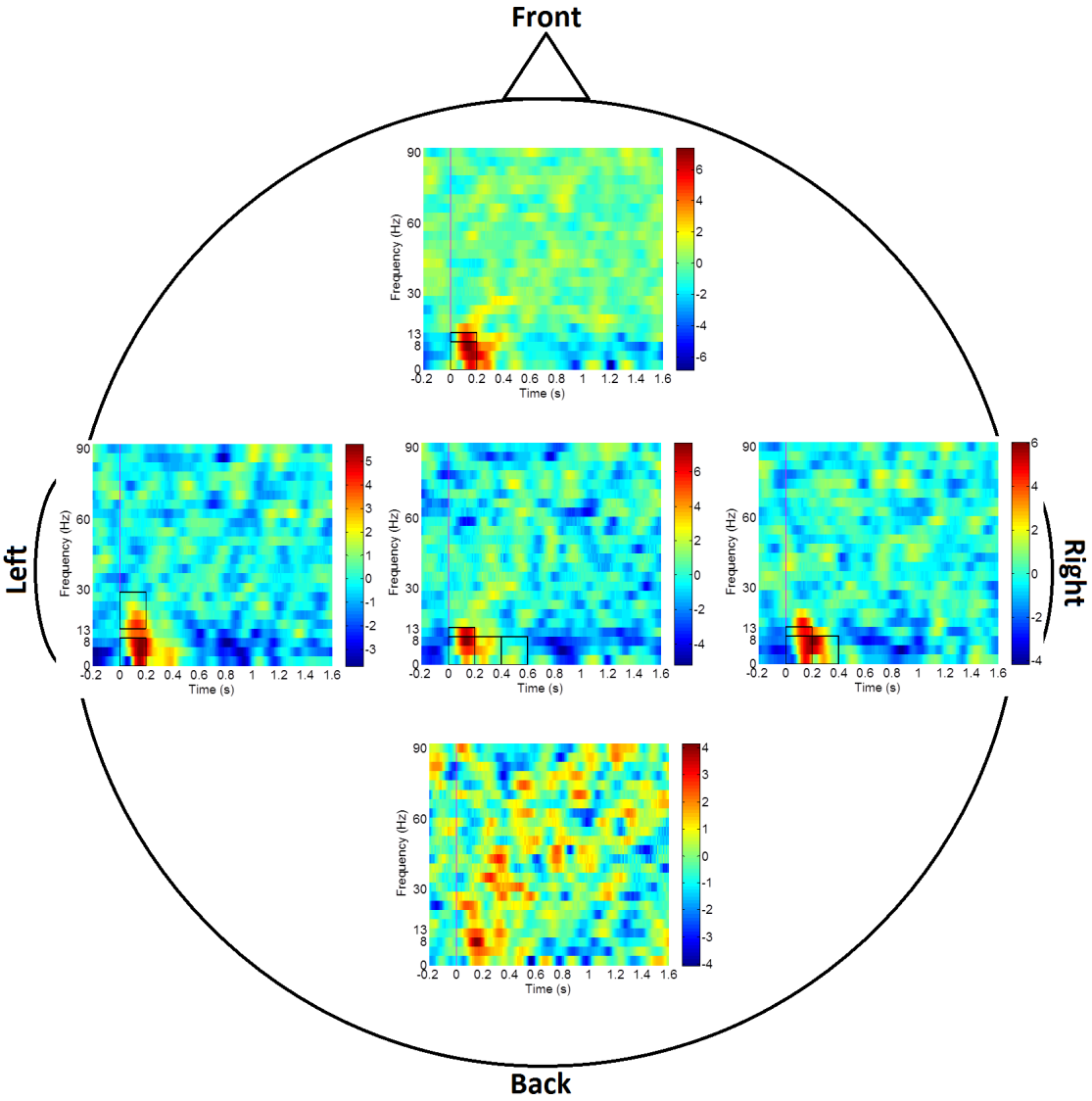

Figure 4.7: Average of evoked power over subjects and groups of electrodes shown by Figure 3.1.a in response to 15 Hz AM tones played to the right ear, plotted in dB. Black windows show significant (Friedman's test, $p<0.05$ - Tukey's test, $p<0.05$) increase in the power compared to the baseline. The magenta line indicates the stimulus onset. The unit of the colour bars is dB.

clearly in the average power instead of separate time-frequency points, the evoked and induced power spectra were averaged in areas of Figure 4.1 with the areas being 200ms or 500ms long and Friedman's test and post-hoc analyses (section 4.2.2) were applied on these average powers. But again, no consistent significant change was observed other than an increase in the evoked power. Similar results were observed for both AM tones and different presentation ears thus only an example is presented here. Figures 4.7 and 4.8, respectively, show the average of the evoked power for EEG response to 15 Hz and 80 Hz AM tones when presented to the right ear. These spectra are averaged over groups of channels presented by Figure 3.1.a and over all subjects. Areas indicated by black windows show significant ($p<0.05$) increase of the power compared to the baseline. In

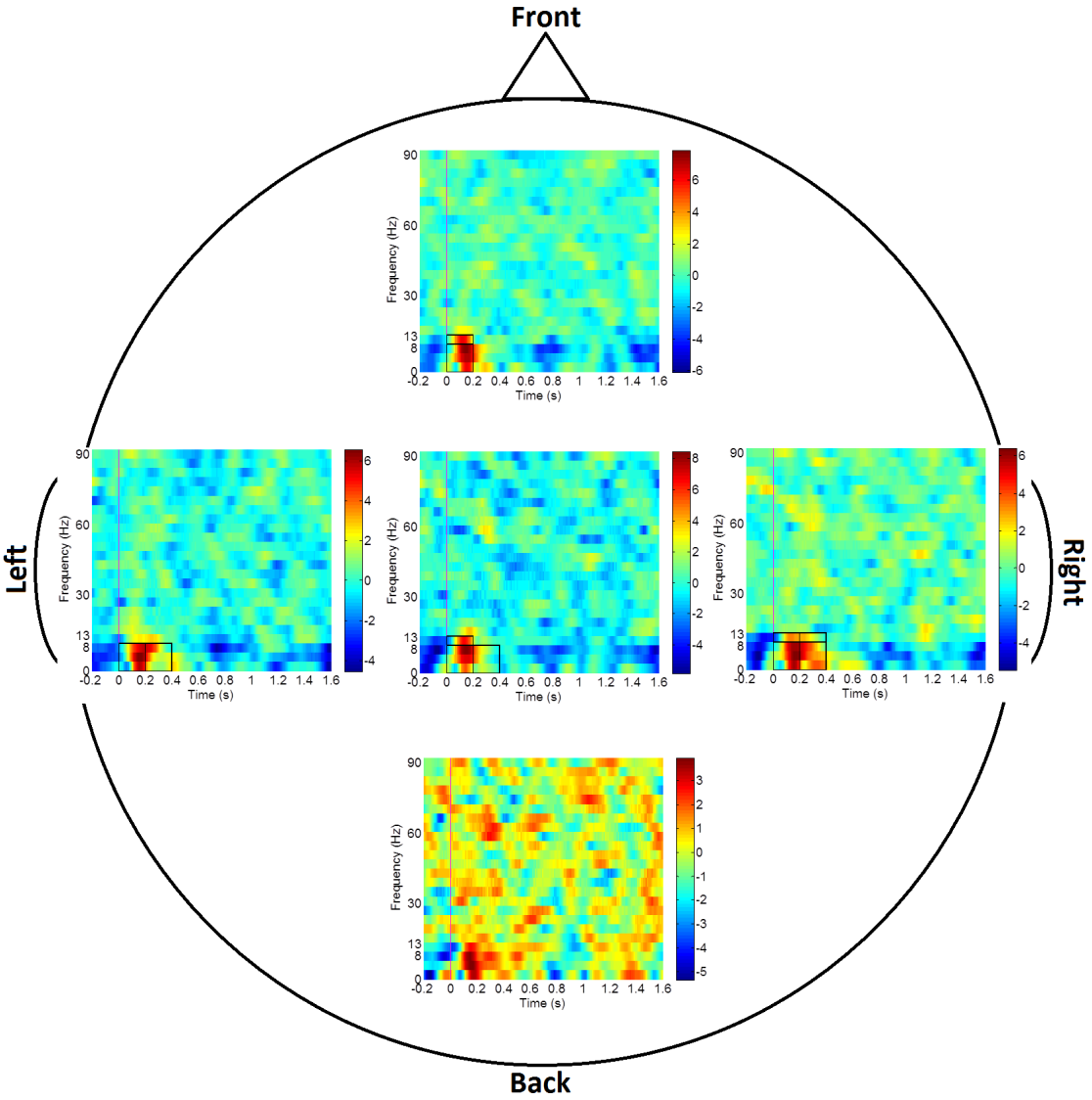

Figure 4.8: Average of evoked power over subjects, and groups of electrodes shown by Figure 3.1.a in response to 80 Hz AM tones played to the right ear, plotted in dB. Black windows show significant (Friedman's test, $p<0.05$ - Tukey's test, $p<0.05$) increase in the power compared to the baseline. The magenta line indicates the stimulus onset.

both types of the AM tone, an increase in the evoked power was observed in frequencies lower that alpha in almost all areas of the brain and shortly after the stimulus onset for about 200-400 ms. In the induced spectrum, a few time-frequency areas (in alpha or beta range) were marked to have significant decrease in the power compared to the baseline but as these time-frequency areas were not consistent over different groups of electrodes or presentation ears, they were considered to be false positives and their results are not presented here. The number of positives was consistent with an α value smaller than 5%.

Both pure tones and AM tones showed clear evoked responses but no consistent induced

responses. Although a response around 15 Hz or 80 Hz was expected in AM tones, no response could be detected.

4.3.3 EEG in response to words

EEG was recorded according to protocol S1 (see section 3.2.1) in response to words, pre-processed as in section 3.4 and a couple of subjects were removed from further analyses because of the low number of epochs after artefact rejection (see section 3.4). Induced and evoked powers were estimated and averaged over different groups of electrodes as marked in Figure 3.1.a.

Bootstrap analyses were performed according to section 4.2.2, to find the EEG frequency bands that had been affected after presentation of words. Both evoked and induced responses were observed and most subjects showed significant ($p<0.05$) increase (and not decrease) compared to the baseline in both the evoked and induced power. This increase occurred in lower frequency bands than alpha but the timings were different between the evoked and the induced power. The number of subjects showing significant increase in the evoked and induced power at each time-frequency point is colour coded in Figures 4.9 and 4.10, respectively. These figures show the results of playing words to the right ear. Left ear and binaural presentations also produced very similar maps, i.e. significant evoked and induced activity in low frequency bands with similar time ranges as in the right ear presentation (they are not shown here).

For group analyses and to apply Friedman's and post-hoc tests to the calculated powers, induced and evoked powers in each subject were averaged over time-frequency areas marked by Figure 4.1. According to the results obtained from Figures 4.9 and 4.10 and the dispersion patterns of significance observed in the evoked and induced spectra, the length of these averaging areas were chosen as 200 ms and 500 ms for the evoked and induced power, respectively, to cover the activity in all subjects.

Figures 4.11 and 4.12, respectively, show the average evoked and induced powers (in response to words played to the right ear) over groups of electrodes presented in Figure 3.1.a and over all subjects when words were played to the right ear (average length of words was 540 ± 80 ms). Areas indicated by black windows show significant ($p<0.05$) power increase compared to the baseline power of the same frequency band. The presence of evoked activity is consistent with the results observed in chapter 3, Figure 3.3. These figures show that the evoked and induced response occur in lower frequency bands (delta, theta, and alpha). The evoked response lasts longer (about 600 ms) than the ones from AM tones and tone bursts and it starts with a delay in back and right electrodes (about 200 ms) compared to other areas of the brain. Moreover, the induced response starts much later than the evoked response and starts around the average end time of the words. As induced response is considered to be related to cognitive functions of the

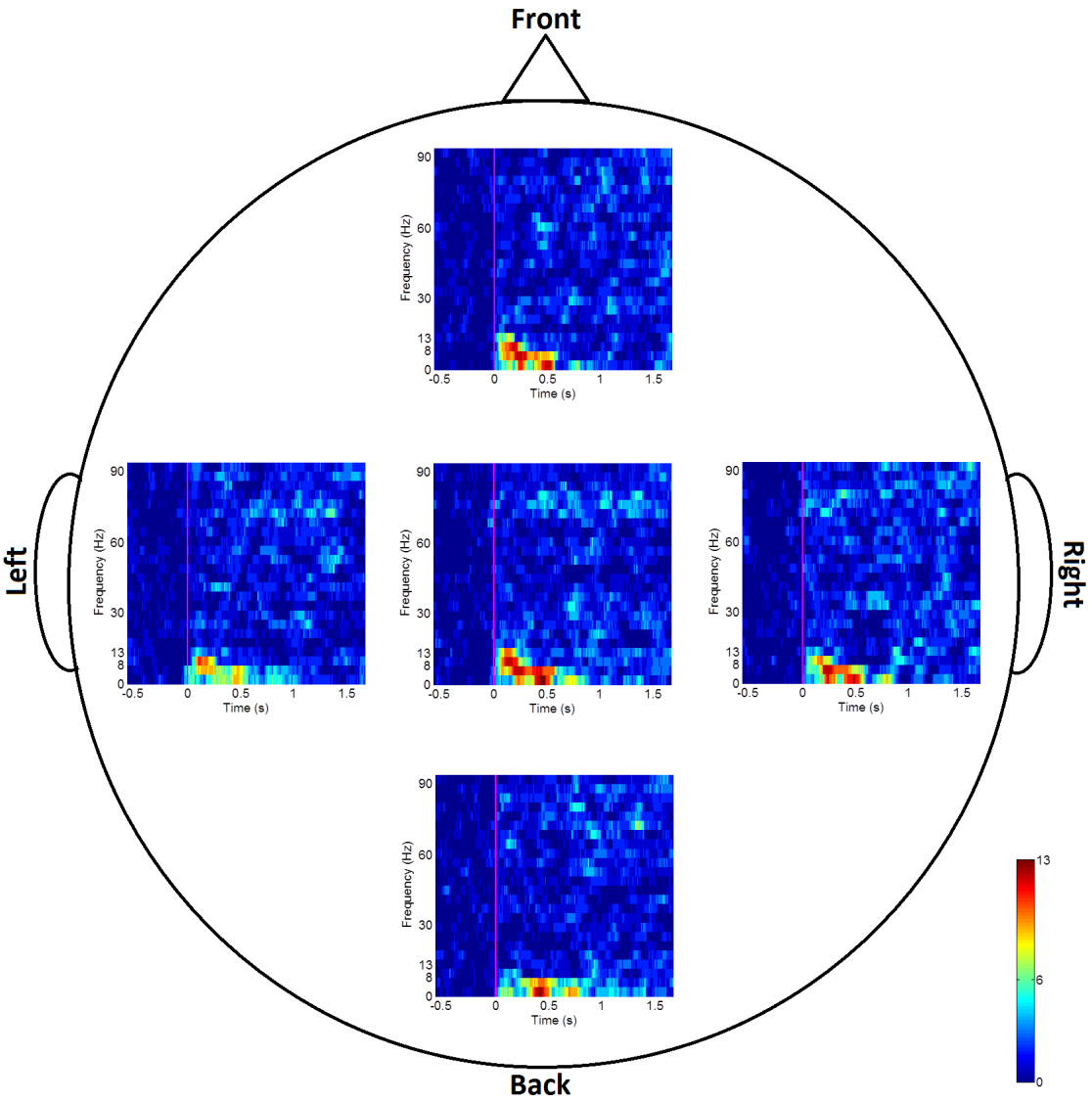

Figure 4.9: Number of subjects showing significant (bootstrap, $p<0.05$) increase in the evoked power at each time-frequency point over groups of electrodes marked by Figure 3.1.a in response to words presented to the right ear. The magenta line indicates the stimulus onset.

brain, it may be concluded that near the end of a word, the brain starts to analyse what it means and that is when induced response is observed in the EEG. It is worth mentioning that in the areas that show significant change, 10-13 subjects out of 13 have an increase in the power compared to the baseline, depending on the time window and electrode group being analysed. Besides, in these figures, a decrease in beta power around 500 ms post-stimulus is visible and when the averaging was focused to a time frequency area from 400-600 ms in the beta band, this decrease was also marked as significant ($p<0.05$).

When similar analyses were performed on EEG in response to left ear or binaural word presentation, similar results were obtained, i.e. in the average power spectrograms

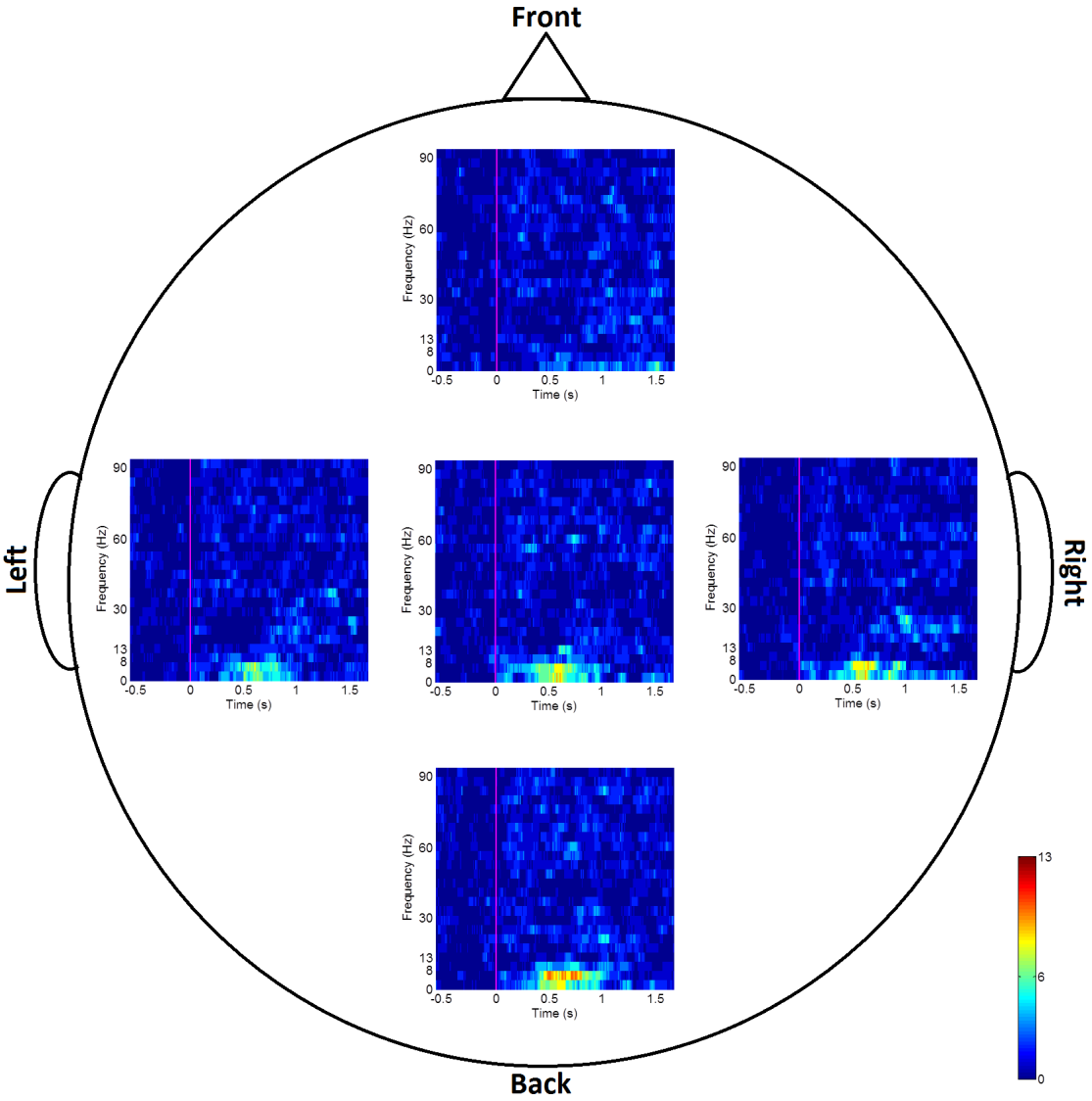

Figure 4.10: Number of subjects showing significant (bootstrap, $p<0.05$) increase in the induced power at each time-frequency point over groups of electrodes marked by Figure 3.1.a in response to words presented to the right ear. The magenta line indicates the stimulus onset.

evoked and induced power increase was observed in frequency bands lower than alpha but induced response arose later than the evoked response. Also, a decrease in beta power around the average end time of the words was observed in the induced power. In left ear and binaural presentation, the significant windows in the evoked spectrogram were almost identical to the right ear presentation. In response to left ear presentation, only central electrodes and in binaural presentation, temporal and central electrodes showed significant induced power increase.

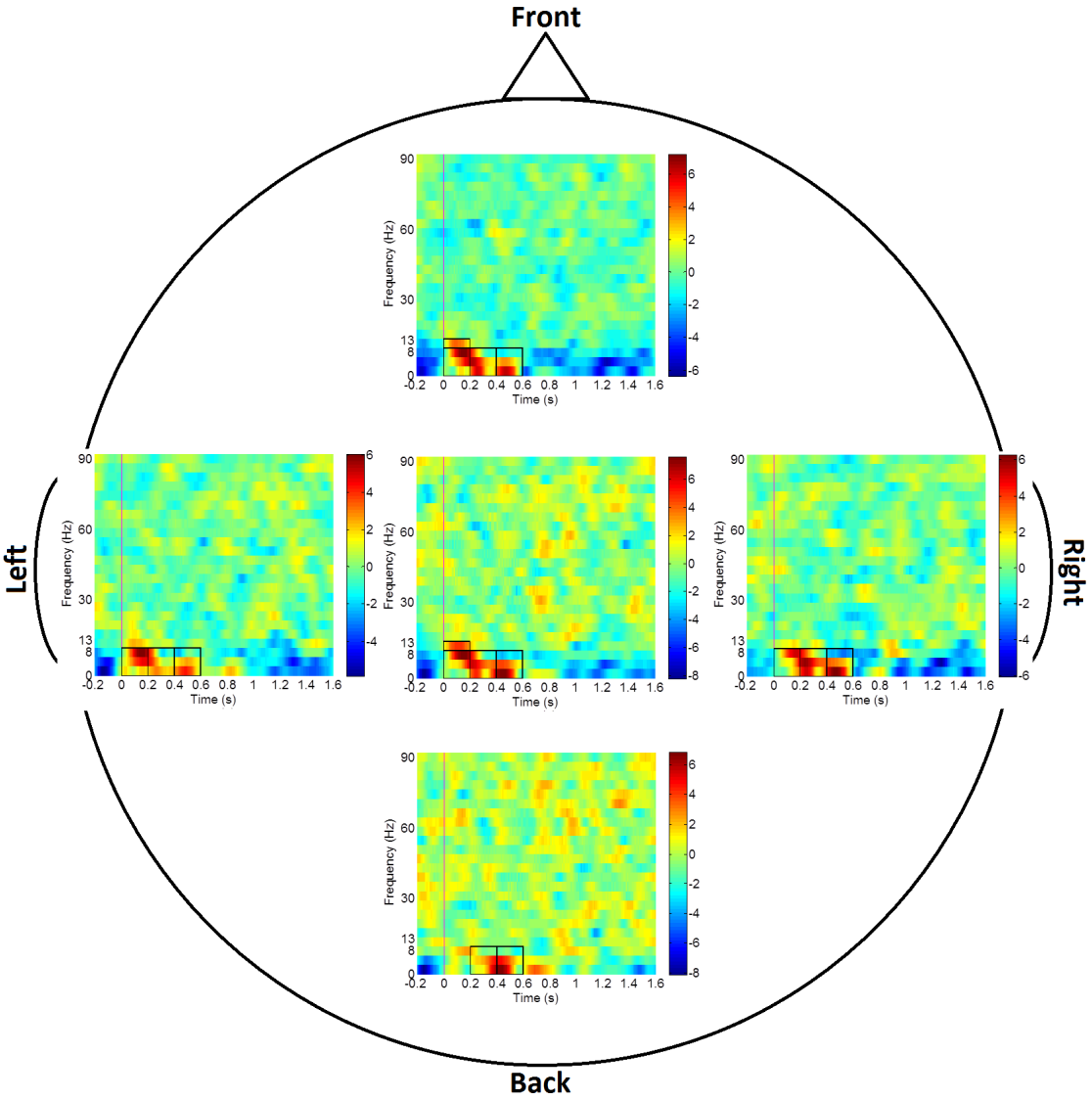

Figure 4.11: Average of evoked power over subjects and groups of electrodes shown by Figure 3.1.a in response to words played to the right ear, plotted in dB. Black windows show significant (Friedman's test, $p<0.05$ - Tukey's test, $p<0.05$) increase in the power compared to the baseline. The magenta line indicates the stimulus onset.

4.3.4 EEG in response to sentences

EEG was recorded according to protocol S1 (see section 3.2.1) in response to sentences, preprocessed as in section 3.4 and a couple of subjects were removed from further analyses because of the low number of epochs after artefact rejection (see section 3.4). Induced and evoked powers were estimated and averaged over different groups of electrodes as marked in Figure 3.1.a for each ear separately.

Bootstrap analyses were performed according to section 4.2.2, to find the EEG frequency bands that had been affected after presentation of sentences. Subjects showed significant ($p<0.05$) increase (but no decrease) compared to the baseline in the evoked power and

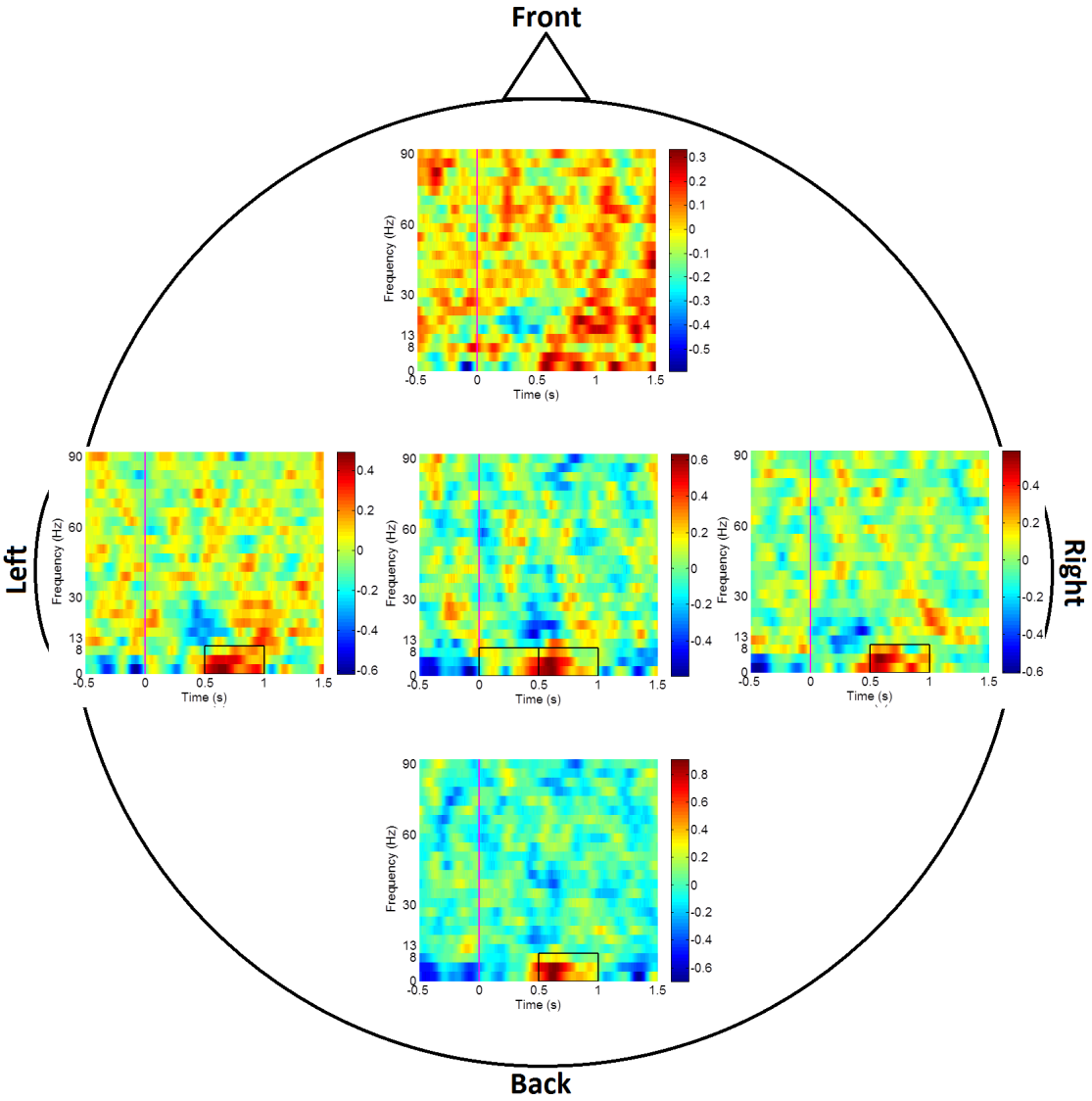

Figure 4.12: Average of induced power over subjects and groups of electrodes shown by Figure 3.1.a in response to words played to the right ear, plotted in dB. Black windows show significant (Friedman's test, $p<0.05$ - Tukey's test, $p<0.05$) increase in the power compared to the baseline. The magenta line indicates the stimulus onset. The unit of the colour bars is dB.

many of them showed an increase in the induced power as well. However, the induced power is scattered over time between subjects and does not seem as focused as the evoked power. This increase occurred in the [0 8] Hz frequency band for both evoked and induced responses but the timings were different between the two responses. The number of subjects showing significant increase in the evoked and induced power at each time-frequency point is colour coded in Figures 4.13 and 4.14, respectively. Note that the average length of sentences was 1630±175 ms. These figures show the results of playing sentences to the right ear. Left ear and binaural presentations also produced very similar maps so they are not shown here.

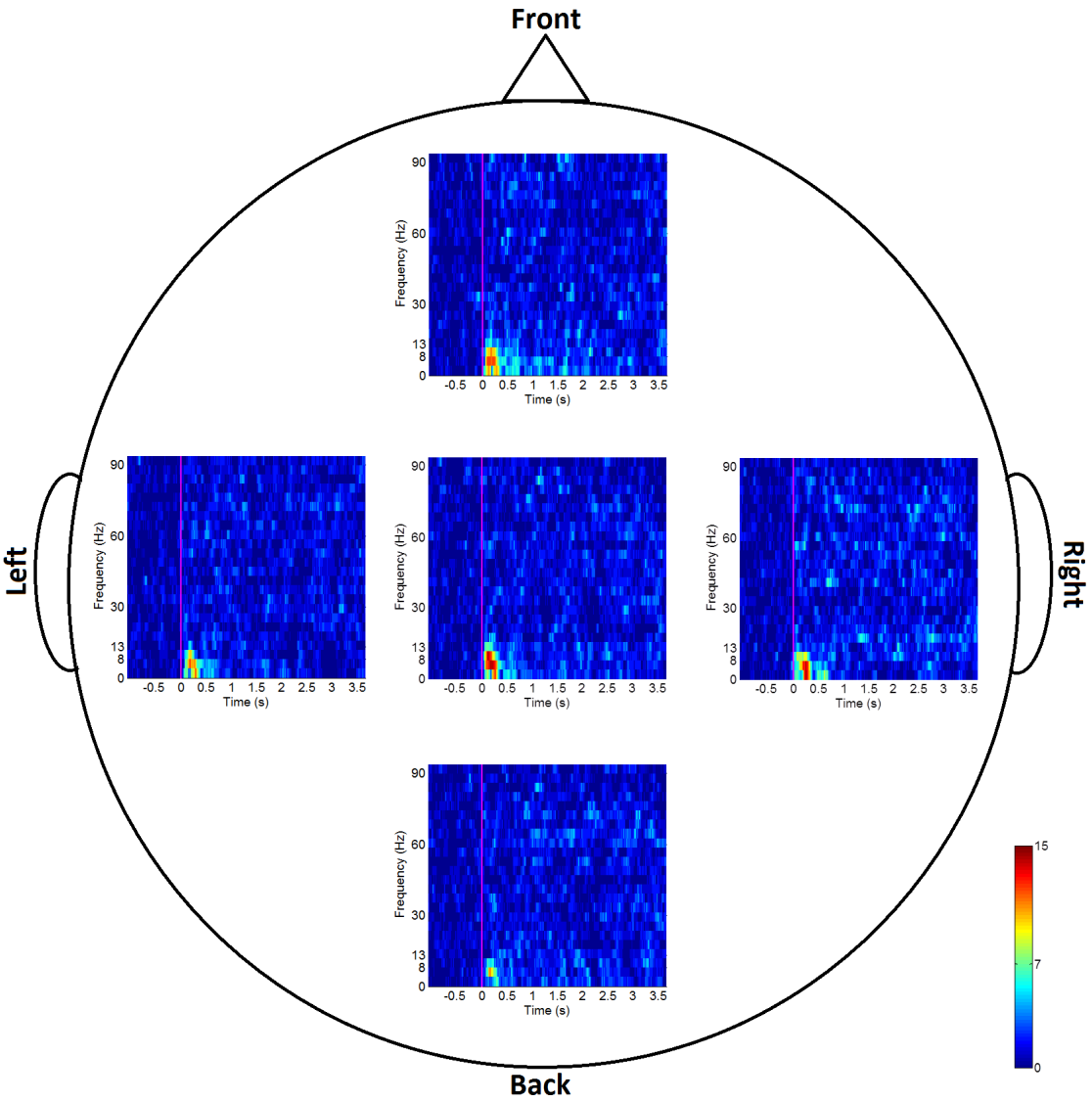

Figure 4.13: Number of subjects showing significant (bootstrap, $p<0.05$) increase in the evoked power at each time-frequency point over groups of electrodes marked by Figure 3.1.a in response to sentences presented to the right ear. The magenta line indicates the stimulus onset.

For group analyses and to apply Friedman's and post-hoc tests to the calculated powers, induced and evoked powers in each subject were averaged over time-frequency regions shown in Figure 4.1. According to the results obtained from Figures 4.13 and 4.14 as well as the dispersion patterns of significance observed in the evoked and induced spectra, the length of these averaging areas were decided to be 500 ms and 1000 ms for the evoked and induced power, respectively.

Figures 4.15 and 4.16, respectively, show the average evoked and induced powers (in response to sentences played to the right ear) over groups of electrodes presented in Figure 3.1.a and over all subjects. Areas indicated by black/white windows show significant ($p<0.05$) power increase/decrease compared to the baseline power of the same frequency

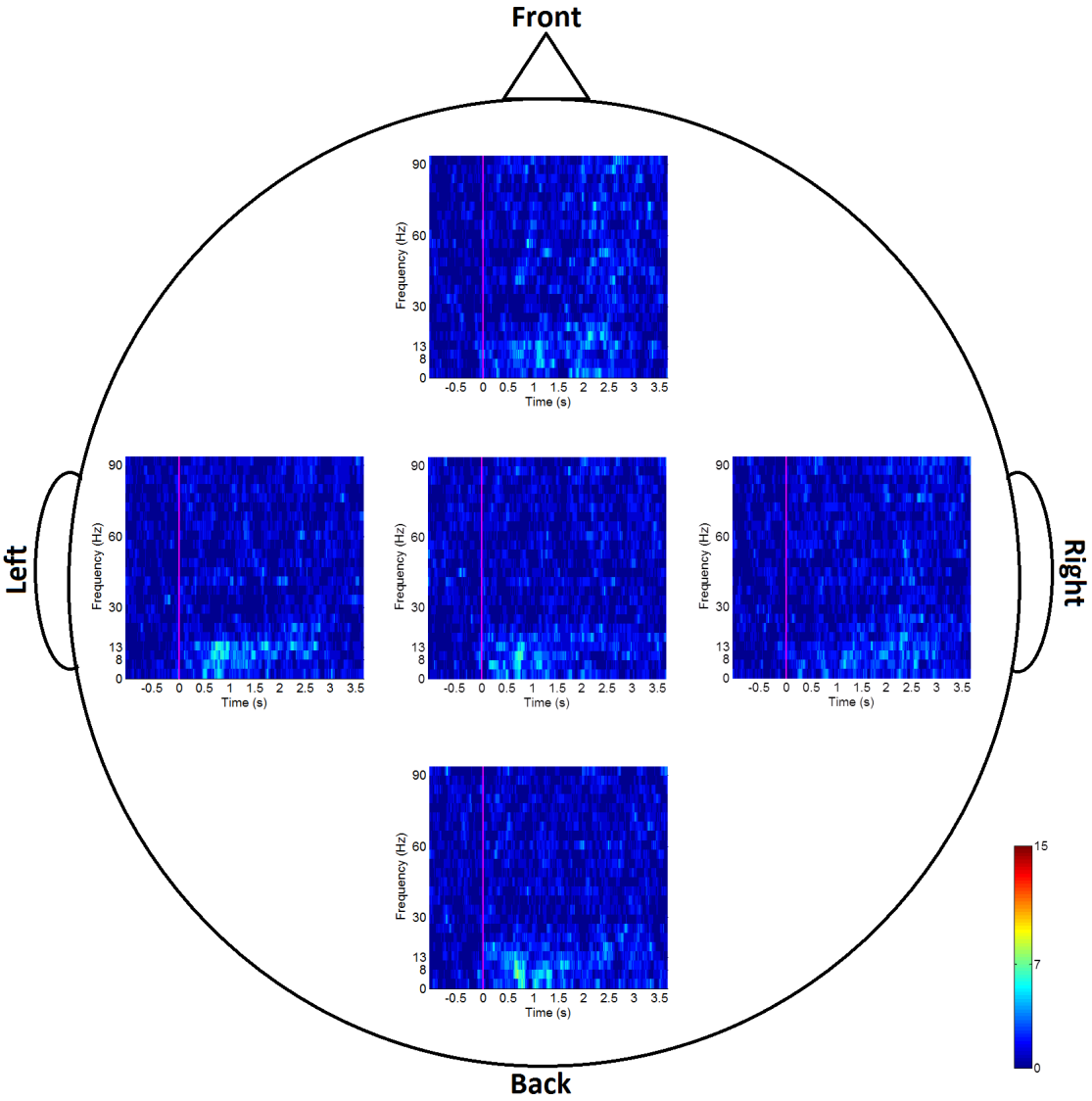

Figure 4.14: Number of subjects showing significant (bootstrap, $p<0.05$) increase in the induced power at each time-frequency point over groups of electrodes marked by Figure 3.1.a in response to sentences presented to the right ear. The magenta line indicates the stimulus onset.

band. These figures show that like words (and consistent with time domain analyses shown in Figure 3.3), there is a significant increase in the evoked power in delta and theta bands just after the stimulus onset. Following the results obtained from words, it was expected to see an induced response in lower frequency bands which starts shortly after the onset and ends a couple of hundred milliseconds after the average end time of sentences. Although the induced response occurs in lower frequency bands and it seems that it starts with a delay compared to the evoked response, it does not continue past the average length of sentences (1630±175 ms). With wide dispersion of sentence lengths, one would expect the response to be disperse also, and this may contribute to the statistically weak results. Long averaging (1000 ms) will mean that in all cases there will probably be some epochs with a response and some without a response present. No

significant induced power change is observed in posterior electrodes but 13 out of 15 subjects show an increase in the first 1 s area after the onset in the [0 8] Hz band. So, although the power change is not large enough to be marked as significant, it can be said that there is definitely a repeating trend in that window. Again, similar to words, there appears (visually) to be a decrease in the power of the beta band which is not selected as significant but is worth pointing out.

Results obtained from sentence presentation binaurally also demonstrated similar results although the induced response lasts longer almost up to 2 s post stimulus and it is marked as significant even in occipital electrodes. However, the results obtained from the left ear presentation do not show any significant induced response except in the occipital electrodes in the [0 8] Hz frequency band and in the first 1 s window after the onset.

4.4 Discussion

The main purpose of this chapter was to investigate if there was any induced response present in the EEG following different types of auditory stimuli when methods based on power analyses were employed. This was done both to get an insight into sound perception processes of the brain and to make sure the recorded data can be used by selected connectivity methods (see chapter 7), as they mainly work with the induced and not the evoked response. Given the variety of statistical analysis methods used in related work in the literature and concern about some of their underpinning assumptions, to make sure that the methods used were appropriate, they were examined with simulated data first (appendix B) before being applied on recorded EEG data.

As expected, the EEG obtained in response to tone bursts showed significant increase in the evoked response in the first few hundred milliseconds after the onset in all electrodes (see Figure 4.5). The evoked power included higher frequency components in central and frontal areas of the brain and the posterior electrodes showed the lowest frequency components. This result confirms the previous findings that the tone burst usually activates fronto-central areas (Picton et al., 1974; Knight et al., 1980) of the brain more than other areas. Moreover, posterior electrodes appear to be missing the early components (earlier than 100 ms) that can be observed in other areas. It may be concluded that either the induced activity was not present in response to simple repeating tone bursts or it was not strong enough to be detected with power analyses and subsequent statistical methods. The induced response is more difficult to detect than the evoked response, as observed in appendix B.

In AM tone stimuli (section 4.3.2), an increase in the evoked response was observed in lower frequency bands in the first 200 ms after the onset of the stimulus and sometimes this increase was extended to the analysis window up to 400 ms post-stimulus in some of the frequency bands. The evoked response was more evident in fronto-central areas

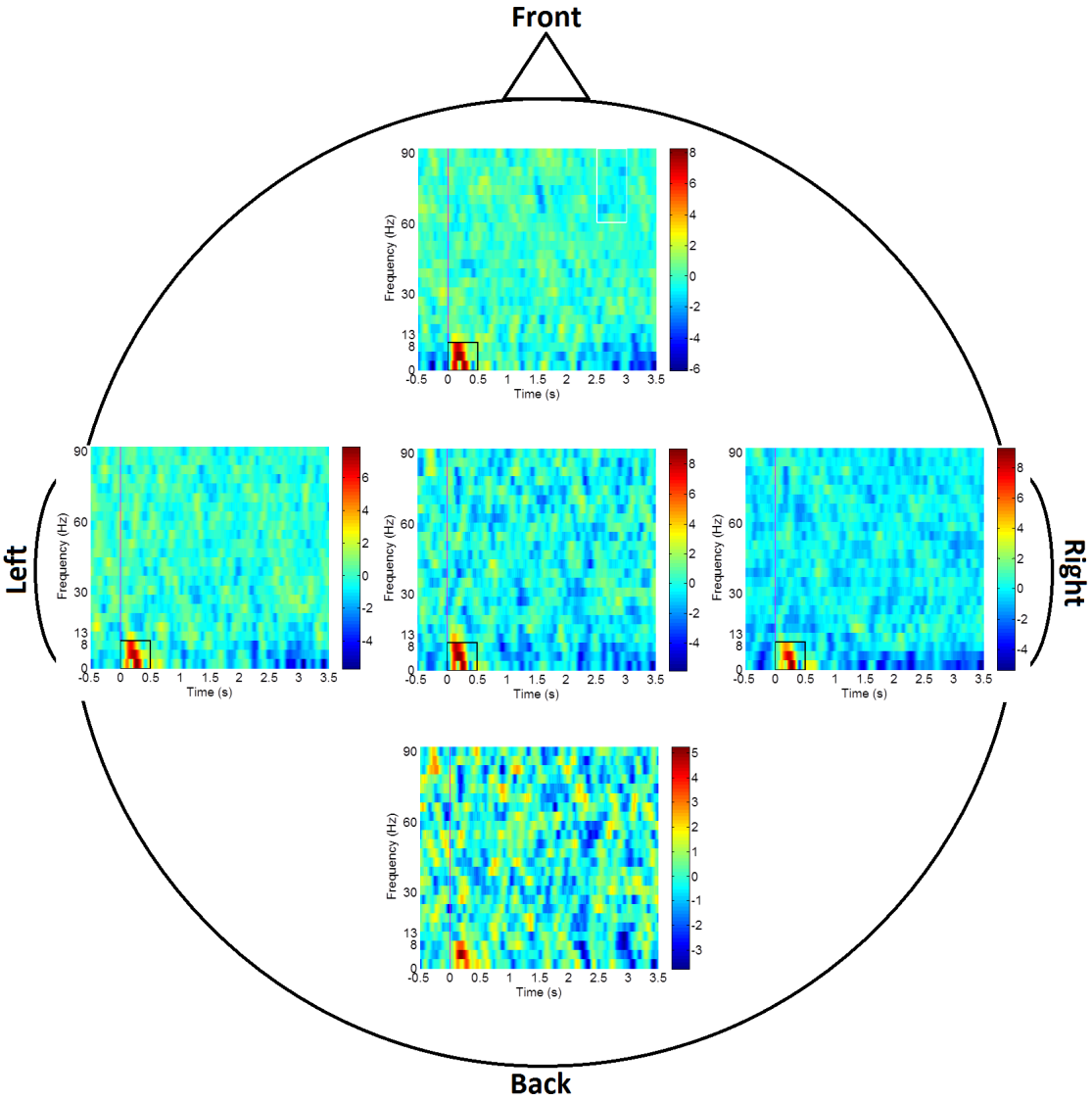

Figure 4.15: Average of evoked power over subjects and groups of electrodes shown by Figure 3.1.a in response to sentences played to the right ear, plotted in dB. Black/white windows show significant (Friedman's test, $p<0.05$ - Tukey's test, $p<0.05$) increase/decrease in the power compared to the baseline. The magenta line indicates the stimulus onset. The unit of the colour bars is dB.

similar to the results obtained from tone bursts. An increase in the power was expected at the modulation frequency for each AM tone (Hall, 2007) but such an increase was not achieved for these stimuli with the current protocol of repeated AM tone bursts. The reason might be the low number of presented stimuli thus a low SNR, or low presentation level of sounds compared to the number of epochs recorded. The repeated presentation of 1 s AM tones instead of playing it continuously, as used in most previous work in this area with stimulus durations of a few minutes, might be another reason for not inducing a strong modulation frequency in the EEG signal. The response at the modulation frequency was not marked significant and thus not shown in this chapter but a power decrease in the beta band was observed in both stimuli around the offset of

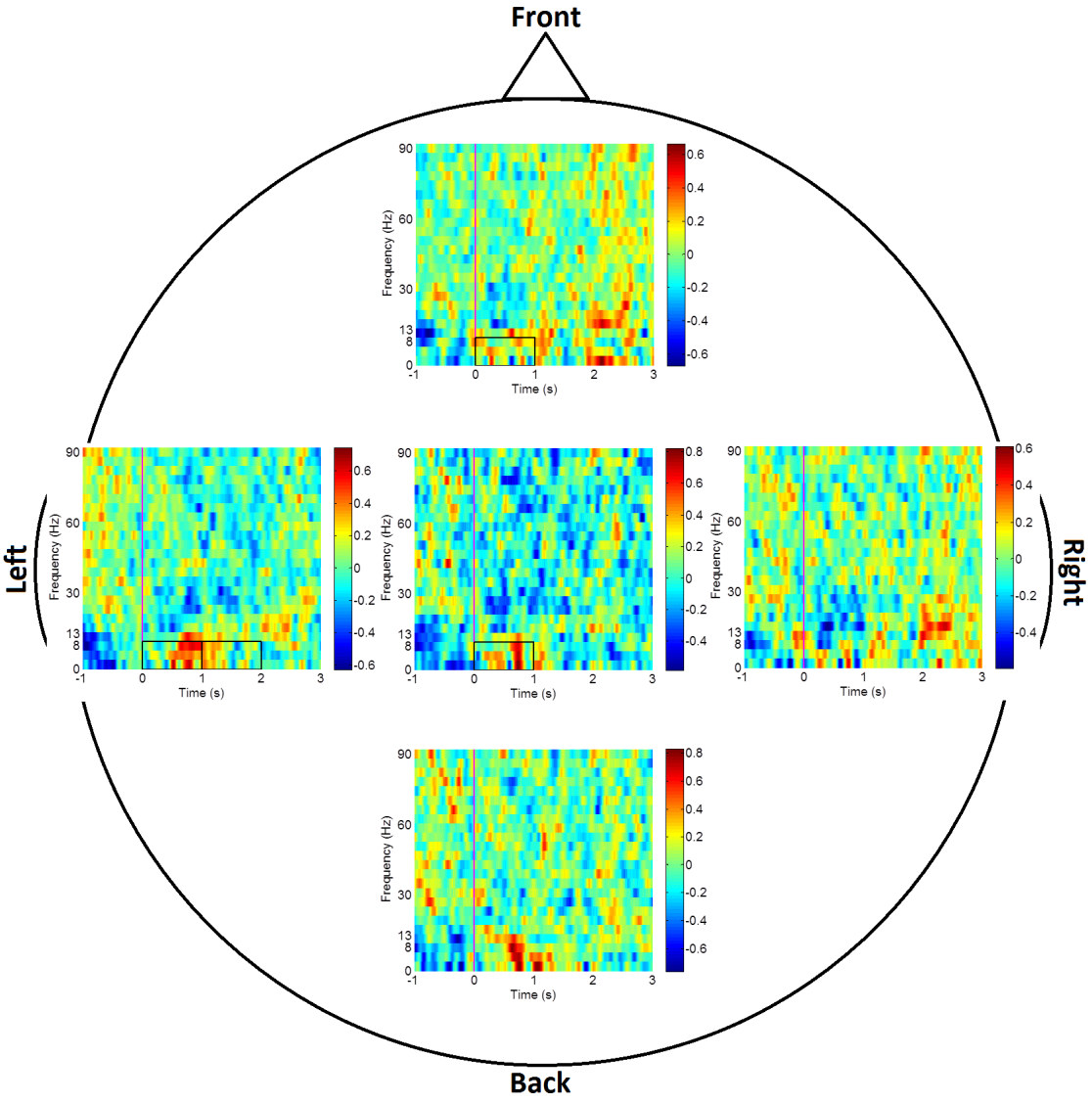

Figure 4.16: Average of induced power over subjects and groups of electrodes shown by Figure 3.1.a in response to sentences played to the right ear, plotted in dB. Black windows show significant (Friedman's test, $p<0.05$ - Tukey's test, $p<0.05$) increase in the power compared to the baseline. The magenta line indicates the stimulus onset. The unit of the colour bars is dB.

the stimulus in the induced power though the time range of this decrease was different between the two stimuli. Although the role of the beta activity is not clear in auditory tasks, beta de-synchronisation has been shown to be present in some auditory oddball and language perception studies (Kim and Chung, 2008; Hirata et al., 2007). The nature of the auditory task here is different from these studies, however, observing beta de-synchronisation in AM tones is of interest and deserves further exploration.

EEG in response to words played to the right ear showed a long-lasting (600 ms post-onset) increase in the evoked response in lower frequency bands (lower than alpha) in all electrodes (see Figure 4.11). The evoked power consisted of lower frequency components

and missed earlier peaks in posterior electrodes compared to other brain areas, similar to tone bursts. The spectra for the evoked response showed a power decrease in delta and theta bands after about 300 ms and again an increase at around 500 ms. As the lengths of the words were around 540 ms (±80 ms), the increase around 500 ms occured around the average length of the words. It may be speculated that the response at this time point was due to the offset response of the brain to words. Moreover, the induced activity in lower frequency bands started much later than the evoked response around the average end time of the words (540±80 ms) and continued for a few hundred milliseconds afterwards (see Figure 4.12). Left ear and binaural presentation showed almost identical results in the evoked spectra but there were some windows missing in the induced spectra in these cases, i.e. the induced response was not as strong as the right ear presentation. This might be due to lower SNR, different words that were played in each case, or different brain reaction depending on the presentation ear. As the induced response is considered to be related to cognitive tasks of the brain (Gruber et al., 2001; Gurtubay et al., 2004; Graichen et al., 2009), it was expected to start with a delay compared to the evoked response. It can be concluded that when the word is about to finish, the brain starts the perception process and it takes some time for it to perceive the whole word. That is when an induced response was observed in the EEG. Other studies have shown increase in the theta power (Bastiaansen et al., 2002; Bastiaansen and Hagoort, 2006) after the target word onset in speech perception studies though with different auditory stimulus presentation approaches. Weiss and Rappelsberger (2000) and Schack and Weiss (2005) also reported an increase in theta power in response to recalled versus non-recalled German nouns although they do not seem to have subtracted the evoked power from the whole power. In this chapter, a pairwise signrank test showed that there was a significant decrease in the beta power for about 200-300 ms starting around 400 ms after the onset in the [13 30] Hz frequency band. As explained before, this frequency band has been associated with language perception in previous studies (Kim and Chung, 2008; Hirata et al., 2007; Weiss and Mueller, 2012).

Sentences (section 4.3.4) seem to evoke low frequencies for a short period of time (300 ms) in all electrodes except the occipital ones. An increase in theta and delta powers can be seen in induced response in centre, front, and left electrodes starting a little after the onset and continuing about up to 1.5 s. Thus, it is safe to say that the brain starts to process the sentences slightly after the beginning of the first word and stops processing slightly after the end of the sentence. From the results obtained from words, it was expected that the induced response continues to a couple hundred milliseconds after the average length of the sentences (1630±175 ms). The reason this was not the case was probably because of the averaging of shorter sentences with longer ones. However, the results from binaural presentation, which are not presented in this chapter, showed an induced response that lasted longer than the one obtained from monaural presentation. It should be mentioned that although the induced response was not marked significant in the occipital electrodes when the stimulus was played to the right ear, 13 out of 15

subjects showed an increase in the first window after the onset compared to the baseline power in the [0 8] Hz band. Thus, there seems to be a trend even if the change is not large enough to be detected as significant. Furthermore, again, a decrease in the beta band is observed while the sentences are being presented. This decrease was not marked as significant but as it was observed in almost all stimulus types and with unilateral and bilateral presentation, this should be considered as an important finding. All in all, these results are similar to previous publications on speech perception (Bastiaansen et al., 2002; Bastiaansen and Hagoort, 2006) where they show that there is an increase in the power of theta band after auditory presentation of sentences though the experimental protocol differs.

4.5 Summary

In this chapter, the presence of evoked and induced responses was investigated in recorded EEG data obtained in response to different types of auditory stimuli. The research on induced responses provides insight into the higher order processing of the brain in response to auditory stimuli, particularly speech, and may be useful for understanding the access to speech processes of the brain. However, for the purpose of the current project, investigating the presence of induced responses was even more important because the selected connectivity methods (see chapter 7) target the induced response of the brain rather than its evoked responses.

Different methods were first tested on simulated data (see appendix B) and the most appropriate ones were employed on recorded data. Recorded data in response to all types of stimuli (tone bursts, AM tones, words, and sentences) show a short- or long-lasting evoked response. The results also confirm the presence of induced response in the brain of normal hearing subjects in response to words, and sentences but not simple tone bursts and AM tones. The areas of the brain that show the induced response and the timing of the response is very different between stimuli. Some results are in agreement with previous studies but some differ.

Although it looks like power analyses can detect induced responses, some of the results in this chapter did not turn out as expected. It has been shown (Simpson et al., 2000) that power analyses are less sensitive in response detection than the methods that included phase information such as coherence, so in the next step the existence of induced activity will be investigated using coherence analyses. Chapter 6 focuses on studying the recorded EEG with coherence analyses as both a response detection and connectivity analysis technique.

Chapter 5

EEG Analyses Based on Physiological Modelling: Multiple Sparse Priors and Dynamic Causal Modelling

5.1 Introduction

There are different methods available for measuring functional and effective connectivity of the brain as was explained in chapter 2. Among these methods, DCM (Friston et al., 2003; David et al., 2006a; Kiebel et al., 2006) appeared, initially, to have more advantages for the purpose of our project. This method will be explained more in this chapter along with its advantages and some initial results obtained. DCM proved unreliable for the purpose of our work.

The first step in using DCM is to feed the model with the location of areas inside the brain that are assumed to be responsible for the observed response (e.g. EEG). To detect the position of these areas, one can either search in previous neuroimaging (e.g. fMRI and PET) studies that investigate the brain response to auditory stimulation (Binder et al., 2000; Wessinger et al., 2001; Meyer et al., 2005; Strelnikov et al., 2010; Limb et al., 2010; Osnes et al., 2011) or try mathematical source localisation methods (Friston et al., 2008; Grech et al., 2008). A reasonable conclusion could not be obtained from the former as the results in the literature are not consistent probably due to different experimental procedures, variable patient selection criteria, and/or various scanning approaches. Therefore, MSP as a source reconstruction method (Friston et al., 2008) was primarily used for finding source locations. MSP can be applied to individual subjects in order to produce more acceptable source locations. Further explanations are

presented in this chapter together with some results on MSP. MSP appeared unsound for source reconstruction and for our preliminary analyses using DCM, we used source locations obtained from the literature (David et al., 2006a).

In sections 5.2 and 5.3, MSP and DCM are explained. The validity of MSP and DCM are tested using methods explained in section 5.4. The results are shown in section 5.5 and followed by a discussion and summary of the chapter.[1]

5.2 Source Localisation using MSP

In recent years, many scientists have become interested in the notion of source reconstruction or source localisation of EEG (Friston et al., 2008; Grech et al., 2008). Source localisation methods try to find the current sources inside the brain responsible for a set of observed EEG data and reconstruct the signals in these sources using the recorded EEG data. As was explained before, one of the basic bits of information that DCM needs is the approximate location of brain areas causing the observed data to estimate connectivity parameters (David et al., 2006a). The locations of active sources reported in the literature with fMRI and PET scans in response to speech signal is controversial probably due to the large number of variables in different studies such as the speech presentation protocol, patient selection criteria, and scanning approaches. For this reason, we had to proceed with a source reconstruction method to localise the recorded EEG and feed the source locations to the DCM algorithm.

There are a large number of source reconstruction techniques that are used worldwide. sLORETA is one of the mostly used source localisation methods and is shown in the literature to have more accurate results among the many employed techniques (Grech et al., 2008). In Friston et al. (2008) it is shown that MSP produces more focal sources than sLORETA with lower estimation error than sLORETA so it was assumed to be a reasonable method for the purpose of our project. Also, it is implemented in the Statistical Parametric Mapping (SPM8) toolbox which is the same toolbox that contains DCM and to reduce the possibility of variations from toolbox to toolbox, it was decided to use MSP as the source localisation method in this study.

5.2.1 Forward model

The brain's source signals are electrical activities of the brain which are modelled as current dipoles located in the grey matter of the cortex (Mattout et al., 2007). These current dipoles are actually the postsynaptic potentials of pyramidal cells the dendrites of which are situated in the grey matter of the cortex. The location of these dipoles can

[1] The results of this chapter are presented in Hosseini et al. (2014c,b, 2013b).

be modelled as voxels. A voxel is a very small cubic volume and is a similar concept as a pixel in a two dimensional environment.

In some source reconstruction techniques such as MSP, it is assumed that the brain consists of a very large number of voxels (each including a dipole) and that the recorded EEG on the surface of the scalp is a linear combination of signals in all these voxels. Source reconstruction approaches aim to find the signal in these voxels by solving the following equation (Equation 5.1) where Y is the observed EEG signal, J is the source signal (in all these voxels), L is the combination matrix which is also called the lead-field matrix and transforms the activity in voxels to the surface EEG, and ϵ is the additive noise. c, s, and t indicate the number of channels, sources, and time points, respectively (Mattout et al., 2007):

$$Y_{c\times t} = L_{c\times s} J_{s\times t} + \epsilon_{c\times t}, \tag{5.1}$$

Before solving the inverse problem to find the source signals in each voxel inside the brain, the forward matrix L should be computed which is independent of the observed data. This process is called forward modelling. L is calculated by assuming that the head consists of three homogeneous concentric spheres namely the cortex, the skull, and the scalp with different electrical conductivity. The cortex is divided into a large number of voxels, and then using electromagnetic equations, the effect of each voxel on each EEG channel is computed (Mattout et al., 2007). It should be noted that the recorded data do not have any role in the process of forward modelling. The only effective factors are channel locations and their distance from each dipole.

After the forward matrix is shaped, it is time to solve the inverse problem to find the signal at the source level (voxels).

5.2.2 Inverse solution

As the problem of inverse solution is intrinsically ill-posed (i.e. lacking a unique solution) because of the high number of brain sources and the low number of EEG channels, there should be some assumptions about the solutions (source signals). There are two main approaches to solve the inverse problem depending on these assumptions. Equivalent Current Dipole (ECD) methods that assume the observed data are generated by a small number of sources and Distributed Linear (DL) techniques which consider all possible source locations but apply constraints on the relationship between these sources (Mattout et al., 2007). Different DL methods apply different constraints on the sources and employ various estimation approaches. One of the widely used estimation approaches to solve the inversion problem is the Bayesian framework (Mattout et al., 2007).

Generally, Bayesian inversion models assume a zero mean normal distribution for the source and sensor activity (Friston et al., 2008) and the constraints on these activities are based on anatomical and physiological knowledge of the brain structure. Brain activities are considered to have an spatial covariance at each level (source and sensor) which is a mixture of different components of the source. A component comprises of some prior knowledge that is known from experience or the literature and exerts some constraint on the relationship between the sources, e.g. neighbouring sources have higher correlations to each other, specific areas of the brain are more probable to produce the observed response, or bilateral connections among some sources. These components are prior assumptions of the model and the model tries to estimate and optimise the weight of each component on the probability of the observed data. These weights are assumed to have a normal distribution with mean μ and covariance C and Bayesian inversion methods try to estimate and optimise these hyperparameters (μ and C) from which an inversion matrix is formed and used to compute the source signals which are the parameters of the model (Mattout et al., 2007; Friston et al., 2008).

The distribution of the parameters (source signals) are being optimised by assuming a prior distribution for the parameters and hyperparameters of the model and knowing the distribution of the output (Mattout et al., 2007; Friston et al., 2008). A fitness value, called the free energy, which is a combination of the accuracy (how close the estimated output is to the true output) and the complexity (the number of components contributing to the output) of the model is defined. The aim of the Bayesian framework is to maximise this fitness value by increasing the accuracy and decreasing the complexity of the model. This aim is usually pursued through an iterative Expectation-Maximisation (EM) algorithm by first keeping the hyperparameters constant in the E-step and optimising the parameters and then optimising the hyperparameters in the M-step while holding the parameters constant. As this free energy depends on the log-evidence of the model, the above mentioned mean and variances play important roles in this EM algorithm. In each iteration, the mean and covariance of hyperparameters are updated and fed to the parameter estimation equations until convergence of the fitness value. Note that if the mean value of the weight of a component goes to zero, its variance goes to zero as well and the component is switched off meaning that the prior assumption of it being responsible for the observed data was wrong (Mattout et al., 2007; Friston et al., 2008). When the fitness value converges, the estimated hyperparameters are used to calculate the inversion matrix which is multiplied by the observed data to produce the signal at the source level.

It has been shown that MSP produces more focal sources (less dispersed over the cortex) which are closer to the true sources (distance-wise) compared to the similar Bayesian inversion methods such as sLORETA and Weighted Minimum Norm (WMN) (Friston et al., 2008).

5.3 Connectivity Analyses using Dynamic Causal Modelling

DCM was first introduced by Friston et al. (2003) for fMRI data as a brain effective connectivity measure but was further developed to be used for EEG data as well by David et al. (2006a). DCM is a biophysically informed model whose computations result in not only the strength of connection between two areas but also the effect of one area on itself. As opposed to other techniques with unknown inputs, the couplings in a DCM model are estimated by perturbing the system with designed inputs and measuring the response (David et al., 2006a), e.g EEG. DCM accounts for the non-linearities of the neural system by introducing nonlinear voltage transform functions to the model which lead to derive nonlinear state equations. The true effect of a third signal on two other signals or the indirect effect of a third signal on the causality of these two signals, which can be considered as shortcomings of some other models (see section 7.2), is not an issue and can actually be tested by comparing the fitness values of different defined models. Moreover, it can be used as a source reconstruction technique as it inherently estimates the interactions at source level (cortical areas) not sensor signals (recorded EEG) (Kiebel et al., 2006). DCM has been used in many studies for various purposes such as diagnostics (Boly et al., 2011), understanding the neural interactions in healthy brain (David et al., 2006a; Kiebel et al., 2006), or in psychological disorders (Dima et al., 2009) given auditory or visual stimulation.

DCM first considers a neuronal mass model for the brain regions of interest. The mass model that is used for DCM-EEG (David et al., 2005; David and Friston, 2003) is an extension of Jansen and Rit (1995) model (see section 5.3.1). Then, using the output response measured by EEG and some prior biological knowledge about the parameters of the model, DCM identifies the parameters so that the model can best fit the output (see section 5.3.2). For this purpose, a Bayesian framework is employed in which the prior is the distribution of the parameters and the posterior is the distribution of the measured output (EEG) (David et al., 2006a). The prior hyperparameters are set according to biological knowledge about the architecture and the behavioural characteristics of brain's neural networks (David et al., 2005). The parameters are identified iteratively by minimising the free energy of the system, which can be regarded as the estimation error, using an EM algorithm. In each iteration, first a posterior distribution is calculated according to minimum free energy (E-step) and then a new set of parameters are computed according to the updated posterior distribution (M-step). The EM procedure iterates the E and M steps till the decrease of free energy stops. The important point is that various models can be defined and compared according to the fitness value calculated from the model and the best fitted model is selected from the candidates as the one with the highest fitness value (see section 5.4.2).

5.3.1 Neural mass model

Jansen and Rit (1995) introduced a basic mathematical model to generate EEG from any arbitrary signal as the model input. He considered a block diagram such as Figure 5.1.a as forward excitatory potentials of cortex pyramidal cells in one brain area. It is presumed that the EEG signal recorded from the scalp is a summation of the electrical activity in pyramidal cells of the brain (Jansen and Rit, 1995; David et al., 2006a). In Jansen's model, these cells are affected by inhibitory and excitatory interactions of neurons inside this area (known as interneurons), neighbouring areas, or even some areas further away from this target area. In this diagram (Figure 5.1.a), e/i stands for excitatory/inhibitory, P represents excitatory input from other brain areas and can be any arbitrary signal including white noise, h function models the transformation of average pre- to average post-synaptic potentials either for excitatory or inhibitory neurons (represented by Equation 5.2), S models the transformation of average post synaptic potentials to average pulse density of action potentials fired by the neurons (presented by Equation 5.3), and γ_1-γ_4 model the number of inhibitory and excitatory inter-area synapses which affect pyramidal cells. Using the results from experimental research on mice, γ_1-γ_4 were assumed to be constants with the relationship $\gamma_1 = \gamma$, $\gamma_2 = 0.8\gamma$, $\gamma_3 = 0.25\gamma$, and $\gamma_4 = 0.25\gamma$.

$$h_{e/i}(t) = \begin{cases} \frac{H_{e/i}}{\tau_{e/i}} t \exp(-\frac{t}{\tau_{e/i}}) & t \geq 0 \\ 0 & t < 0 \end{cases}, \tag{5.2}$$

$$S(\nu) = \frac{2e_0}{1 + e^{r(\nu_0 - \nu)}}, \tag{5.3}$$

in which $H_{e/i}$ represents maximum post synaptic potentials and $\tau_{e/i}$ demonstrates the lump sum of membrane and dendritic network delays for excitatory/inhibitory interactions. Furthermore, e_0 determines the maximum firing rate, ν_0 represents the voltage for which 50% of the firing rate is achieved, and r controls how steep the sigmoid function is.

This one-area diagram (Figure 5.1.a) was then extended to model the interactions between two areas as in Figure 5.1.b where k and δ are gain and delay between two areas (Jansen and Rit, 1995). Changing different parameters of the model, Jansen and Rit (1995) suggested that their model could describe some of the characteristics of the EEG and that this model was able to produce different types of EEG such as evoked potentials. They showed that by changing different parameters of a single area model given a white noise as the model input, various classes of output signals such as alpha-like activity and spike-wave complexes could be obtained. Using a two-area model, they further demonstrated that if the parameters of the two areas were set similarly, even small amounts of k_1 or k_2 would synchronise the outputs of the two areas. By changing k_1

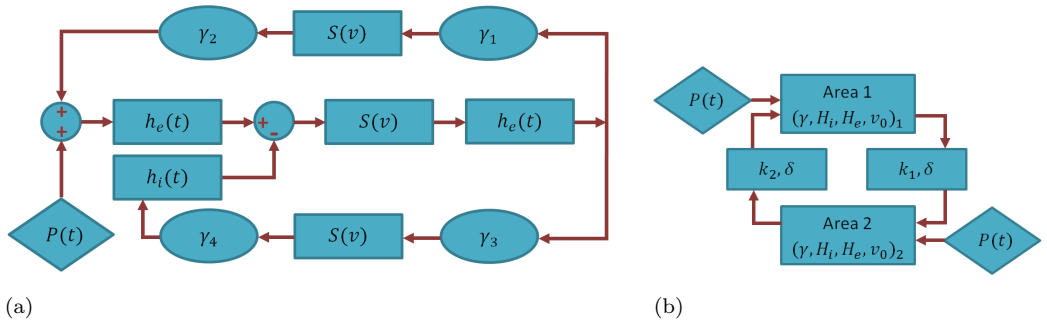

(a) (b)

Figure 5.1: a) Block diagram of Jansen's model for one area of the brain (Jansen and Rit, 1995), b) the Jansen's model for interactions between two areas of the brain (Jansen and Rit, 1995)

and k_2 from very small amounts to very large values, they obtained outputs that showed more and more characteristics of the EEG signal. They also illustrated the response of each area to a transient input for different parameter values in a two-area model and showed that there was a set of parameters which could produce outputs similar to visual evoked potentials.

Jansen's model was then extended by David et al. (2005) to model more characteristics of the EEG signal. They assumed that one brain area consisted of two types of excitatory neurons namely pyramidal cells and excitatory interneurons (as opposed to Jansen's model with only pyramidal cells) and one type of inhibitory interneurons (see Figure 5.2.a). They extended the model to more than one brain area and showed that the new model can cover a larger range of biological behaviours than Jansen's model (David and Friston, 2003; David et al., 2005). For example, depending on the values of model parameters, phase-locking, phase-resetting, evoked, and induced response characteristics could be observed. Connections between two separate areas were named extrinsic connections and the ones between different populations inside one area of the brain were named intrinsic connections. Using the connectivity rules which had been achieved in experimental studies and the subpopulation being excited, three types of extrinsic connections were defined (David et al., 2005) (see Figure 5.2.a): 1) forward or bottom-up, 2) backward or top-down, and 3) lateral. In all areas, the same rules as Jansen's model were used for γ parameters, h function as in Equation 5.2, and S function as in Equation 5.3. Transmembrane voltages and currents of different subpopulations in each brain area were computed as differential equations using these rules (see David et al. (2006a) for current and voltage equations), the parameters of which should be estimated, refer to the next section. The voltage of the transmembrane potential of pyramidal cells is considered as the voltage being picked up by scalp electrodes, see section 5.3.2.

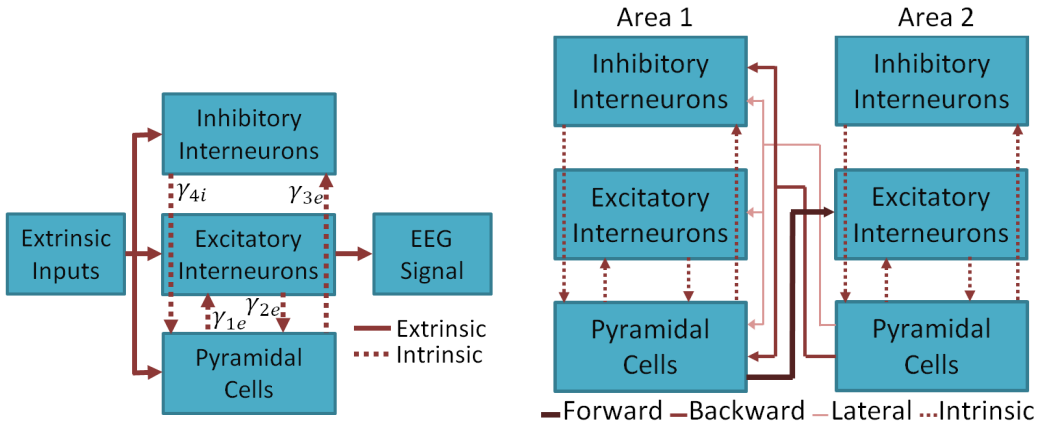

Figure 5.2: a) Configuration of different subpopulations in one area of the brain in David's model (David et al., 2005). i/e stands for an inhibitory/excitatory effect. b) Types of connections between two areas in David's model (David et al., 2005).

5.3.2 DCM specification and estimation

DCM is specified by its state equations (see section 5.3.1) which are based on neurobiological characteristics and an output equation which is based on an electromagnetic forward model (David et al., 2006a):

$$\dot{x} = f(x, u, \theta), \tag{5.4}$$

$$h = g(x, \theta) = LKx_0, \tag{5.5}$$

in which, u's are model inputs defined as Gaussian pulses with a bit of a jitter, the parameters of which such as the pulse shape and delay can also be computed during model estimation. h is the estimated output of the system, and θ are model parameters which include intrinsic and extrinsic coupling parameters (C^F, C^B, C^L, γ), conduction delays (Δ), synaptic parameters (T and H), and parameters of the model input. The state equations (f) are a set of differential equations of the current and voltage in different subpopulations of neurons in each brain area and x_0 is the difference between excitatory and inhibitory currents in pyramidal cells. L is the forward matrix and K is a leading diagonal matrix which encodes the effect of each source over itself. The recorded data y can then be described by:

$$\begin{aligned} y &= h(\theta) + X\theta^X + \epsilon \\ p(y|\theta, \lambda) &= N(h(\theta) + X\theta^X, diag(\lambda) \otimes V) \end{aligned}, \tag{5.6}$$

where ϵ is the error which is zero mean and independent over channels with λ as channel-specific variances. Also, its temporal autocorrelation is assumed to be an identity matrix V so its fluctuations can be defined by $Cov(\epsilon) = diag(\lambda) \otimes V$. X represents low frequency noise or drift components which is a block diagonal matrix containing information for each channel and each epoch.

The parameters of the model would then be estimated employing a Bayesian framework in which the posterior density was defined as $p(\theta \mid y, \lambda) \propto p(y \mid \theta, \lambda)p(\theta)$. $p(y \mid \theta, \lambda)$ and $p(\theta)$ are the likelihood of the measured output and the prior density of the model parameters, respectively. The probability of each parameter was defined as $p(\theta) = N(\mu, \nu)$ in which N indicates normal distribution and μ and ν are expectation and variance of θ. There were both informative (small variance) and uninformative (large variance) priors on different θ according to biological knowledge and some parameters were set as known parameters from the beginning. For example, coupling parameters were set with relatively uninformative distributions ($\nu = 1/2$) whereas synaptic parameters were appointed with tight distributions ($\nu = 1/16$), and intrinsic coupling parameters were set as known parameters ($\nu = 0$).

Similar to inverse solution in MSP, a parameter called free energy was defined according to conditional moments (hyper-parameters) of θ. The free energy was the difference between two amounts, the first being the discrepancy between the true and approximate posterior density (the probability of a parameter given a specific set of data and hyperparameters) and the second being the log-likelihood of data, i.e. the model evidence. The free energy would be minimised by applying an iterative EM algorithm during which the hyper-parameters and thus the parameters were optimised. In the E-step, the hyperparameters of the posterior density and in the M-step, the channel specific variances would be updated while minimising the free energy. The estimated conditional moments (mean and covariance) of each parameter and the log-evidence (the probability of the output given a specific model) is used to describe the connectivity and the goodness-of-fit of the model.

The inference on the connectivity can be obtained with two approaches: 1) in a specific model, by considering each connection and the probability of this connection being greater than zero (or a baseline value) thus being responsible for generating this specific output and 2) between models, by considering each with their various sets of parameters and comparing their log-evidences and selecting the best model accordingly. This best model is considered significantly better than other models if its log-evidence is at least 3 units larger than the log-evidence of other models (David et al., 2006a). It is worth noting that in DCM, there is no right or wrong model. Any model can be simulated and estimated with DCM but among the models defined and estimated, the best model can be selected according to the 3-unit rule.

5.4 Methods

5.4.1 MSP validation

Although the method has been reported to have promising results (Friston et al., 2008), there was still some uncertainties regarding MSP and its accuracy. The previously presented validity tests were not comprehensive. To find out how accurate this method was in reconstructing the sources, simulated data were generated with different number of sources and levels of SNR. MSP was employed for reconstructing the sources to confirm the accuracy of this method before proceeding any further with our analysis.

To generate simulated EEG data Y according to Equation 5.1, a matrix of source signals J, a forward matrix L, and some noise ϵ were required. For this purpose, a 5124-voxel model was selected, simple Gaussian-like source signals were generated as in Figure 5.3 with a 1000 Hz sampling frequency, and template head models available in SPM8 MATLAB toolbox were used to place these signals at desired voxel positions, which were selected almost randomly (see Figure 5.3). Thus in the $J_{5124\times500}$ matrix, all rows are zero except the ones related to those specific voxels. As explained in section 5.2.1, L is only dependent on the position and number of voxels and channels and not the observed EEG. Thus, to find the L matrix for a 66-channel EEG data, one of the recorded EEG signals (see section 3.2.1) that was prepared to be compatible with SPM8 and was loaded in the source reconstruction subroutine of the SPM8 toolbox, was co-registered to the template Magnetic Resonance Imaging (MRI) map using the nasion and right and left auricular fiducials, the number of desired voxels (5124) were defined, and then the forward model was estimated for this dataset to generate the $L_{66\times5124}$ matrix. This matrix was multiplied by the simulated J matrix to simulate EEG outputs. Different levels of noise ϵ were then added to the simulated data at the sensor level 100 times to obtain a 66-channel evoked-like EEG signal with 100 epochs. Figure 5.3 shows an example of different steps of producing synthetic EEG data for a single-source signal and a 10 dB noise level. It should be noted that the maximum level of SNR in all channels is 10 dB in this figure and that the noise is generated by convolving a noise that has a Gaussian distribution with a Gaussian window to simulate a 20ms correlation in noise over time. The simulated EEG signals were then fed to the MSP algorithm in the SPM8 toolbox to reconstruct the sources and to compare them with the original source locations.

5.4.2 DCM validation

Since its introduction for EEG analysis, DCM has been used for a range of purposes such as understanding the neural interactions in psychological disorders (Dima et al., 2009; Kempton et al., 2010), in the vegetative state (Boly et al., 2011), and in response

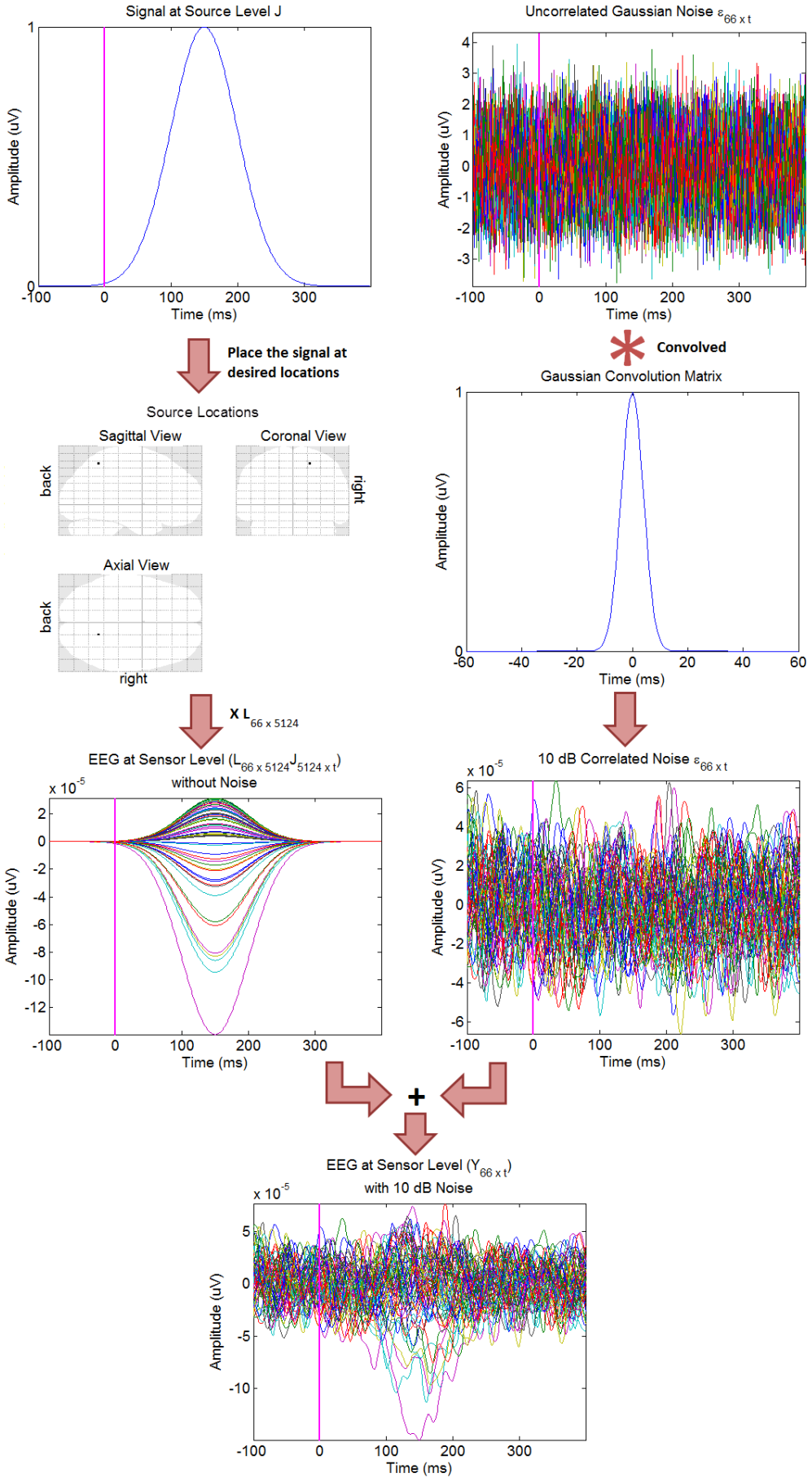

Figure 5.3: Different steps of generating synthetic EEG. In this signal time zero is assumed to be the onset of the stimulus.

to various types of stimulation (Brown and Friston, 2012; David et al., 2006a; Garrido et al., 2009; Marreiros et al., 2010). Precisely because of all the attention it has been attracting, it is very important to test its reliability, considering aspects of within and between subject repeatability, the physiological plausibility of inferences and also the implementation of the algorithm in the toolbox that all current research uses.

DCM has been available for about a decade now but there are not many critical comments on its validity or reliability other than the ones presented by the developers of the algorithm (Daunizeau et al., 2011; David et al., 2006a; Garrido et al., 2007; Kiebel et al., 2007). Using simulated data, it was shown that DCM was sensitive and specific to changes in parameters of the model but not too sensitive to the level of initial variances of the parameters (David et al., 2006a) by changing the mean and standard deviation of initial prior distributions. It was also demonstrated that DCM could generate realistic evoked responses (Kiebel et al., 2007) and that it produced similar results for different subjects under similar conditions (Garrido et al., 2007). In the latter, the reproducibility of DCM was tested using the data from 13 different subjects, giving consistent (but of course not identical) results. There does not appear to have been much investigation of repeatability of the analysis in the same subjects over multiple sessions.

To the best of our knowledge, the only major questions regarding implementation of DCM have been raised by Lohmann et al. (2012), who argued that comparing different estimated DCM models and selecting the best model according to its fitness value might not be the best approach. They showed that even defining a 3-area model could lead to a huge pool of possible models, not all of them plausible. They went on to discuss that it was quite possible that the winning model, even among very carefully defined set of models, might turn out to be an implausible one. It was also showed that a high fitness value might be obtained because of a good fit in one area but not in the other one. Lohmann et al. (2012) discusses that this might be the ramification of assuming a Gaussian distribution for both data and parameters of the model which is mainly selected for computational simplification purposes and not based on real observations. This comment started a debate (Breakspear, 2013; Friston et al., 2013) about the credibility of DCM ending with Lohmann et al. (2013) claiming that the counterarguments were not quite convincing.

Therefore, there were still many questions about the reliability and robustness of DCM that needed to be answered before employing it on recorded EEG data in response to speech. These questions included the 1) DCM's reproducibility for each subject in one session, 2) DCM's repeatability for each subject over different sessions, 3) the minimum SNR tolerable by DCM, and 4) the effect of different electrode placements on DCM. For this purpose, a sample EEG was recorded from one subject in two different sessions (see section 5.4.2.1). If we could verify any of these questions on one subject, more subjects could be recruited so that a more comprehensive conclusion could be obtained. However, as can be seen in the next sections, the software package implementing DCM

was shown to be unreliable for the application of this project in the first stage of testing so there was no need to record more data or to move on to our next questions which targeted the reliability of the DCM algorithm. SPM8 is the toolbox used in (to the best of our knowledge) all recent studies involving DCM and its robustness are addressed in this chapter (see section 5.5.2).

In sections 5.4.2.1 through 5.4.2.3, the process of recording and preprocessing of EEG data is explained. Note that these data are only used in this chapter and not the rest of this thesis and are not the same data that were explained in chapter 3. The DCM models implemented, their specification in SPM8, and the software versions used for estimating the models are also given. The DCM method was tested on two sets of data. The first was recorded by our group from a 30-year-old male subject and is referred to as "Pilot data" throughout this chapter and the second set of data were the EEG from an adult normal hearing subject downloaded from the SPM website and will be referred to as "SPM data" in this chapter (accessible at `http://www.fil.ion.ucl.ac.uk/spm/data/eeg_mmn`).

5.4.2.1 Materials

Pilot data: Two pure tones were presented binaurally at 62 dB SPL approximately every 2 seconds at random intervals. The tones were 80 ms long, and either 1 kHz (120 stimulus repetitions) or 2 kHz (480 stimulus repetitions) with 5 ms rise and fall times. These tones were presented in a random sequence.

Data acquisition was performed using the same equipment and with the same procedure as in study S1 explained in section 3.2.1.3.

EEG was filtered in the [0 30] Hz band and epoched around the onset of the 2 kHz stimulus (200 ms pre- and 500 ms post-stimulus). Data were visually checked and showed the expected evoked potential. Fifteen different sets of data were generated by randomly selecting 240 epochs out of 480 epochs of the 2 kHz stimulus and averaging them. DCM analysis was carried out using this dataset to assess robustness to relatively small changes in the data (within sample variability). Then one of these datasets was used for more extensive analyses using the different combinations of software systems, as well as repeatedly analysed using the same systems, on the same computer. Electrode positions were co-registered to the template MRI map available in the SPM8 toolbox with nasion, right, and left auricular points being the fiducial points which were defined manually.

SPM data: Two pure tones were presented binaurally every 2 seconds at random intervals. The tones were 70 ms long tones at 2 kHz (120 stimulus repetitions) or 1 kHz (480 stimulus repetitions) with 5 ms rise and fall times. These tones were presented in a random sequence and the subject was asked to count the 2 kHz tones Garrido et al. (2007).

A 128-channel EEG dataset was recorded with a Biosemi system at a sampling frequency of 512 Hz. Two extra electrodes were used to monitor eye movements Garrido et al. (2007).

This dataset was already preprocessed when it was downloaded from the website. A brief summary of the preprocessing procedure is: EEG was referenced to average activity in all channels, band-pass filtered in the [0.5 30] Hz frequency band, downsampled to 200 Hz, and then epoched around the onset of the auditory stimulus with a -100 ms pre- and a 400 ms post-stimulus window. Epochs with amplitudes exceeding the [-80 80] μV range were removed and the remaining epochs were averaged. The data already consisted of channel locations (more details can be found in the SPM8 manual accessible from http://www.fil.ion.ucl.ac.uk/spm/doc/).

5.4.2.2 DCM analyses and inference

Pilot data: The graphical user interface of SPM8 DCM was used and the five different models shown in Figure 5.4.a were defined with all forward, backward, and lateral connections present (David et al., 2006a). In the models, Left and Right Primary Auditory Cortices (LA and RA), Left and Right Superior Temporal Gyri (LS and RS), and Left and Right Inferior Frontal Gyri (LI and RI) were included. These areas have been shown to be related to sound perception in the brain (David et al., 2006a). The positions of these areas were taken from Garrido et al. (2007) and RI was assigned a symmetrical position to LI with respect to the sagittal line. Furthermore, the delay of the input of the system was defined to occur around 40 ms after the stimulus onset and to affect both LA and RA. The distributed spatial model was set to ECD and other parameters of DCM GUI were left as default values set in the toolbox.

SPM data: The model in Figure 5.4.b was defined for this set of data to be consistent with the simulations in the SPM8 manual and the publications based on this dataset (David et al., 2006a; Garrido et al., 2007). A time window from zero to 200 ms and only the 1 kHz tone was considered for DCM estimations. Positions of these areas were the same as in Figure 5.4.a and the input of the system was defined to occur around 60 ms after the stimulus onset and affect both LA and RA. The distributed spatial model was set to ECD and other parameters in the DCM GUI were left at default values, as above.

As was mentioned earlier, there are two approaches for determining the best model after DCM estimation. In this chapter we employ both approaches.

First, model parameters were estimated using DCM and a probability value was reported for each parameter being greater than zero (or a baseline value). Parameters with probabilities higher than a set value were considered responsible for the differences between the observed output and the baseline condition. Here, the probability threshold was set to 90%.

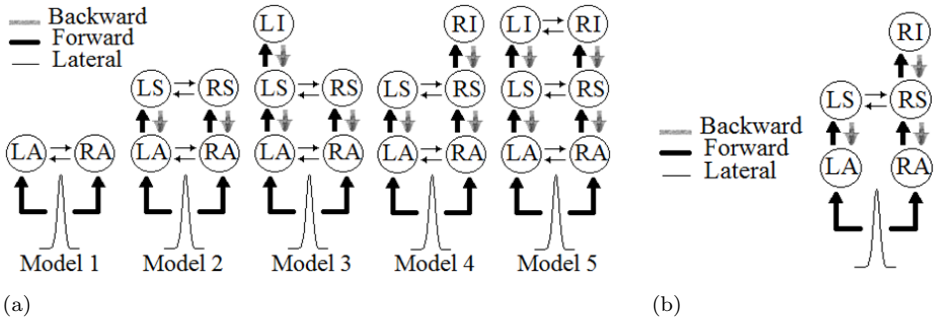

Figure 5.4: a) The five different models analysed in DCM using the Pilot data. b) The DCM model studied on the SPM data. LA/RA: Left/Right Primary Auditory Cortex, LS/RS: Left/Right Superior Temporal Gyrus, and LI/RI: Left/Right Inferior Frontal Gyrus.

Second, for each estimated model, a "fitness value" was calculated which depended on the goodness-of-fit and the complexity of the model. Among different models estimated for a specific set of data, the significantly better model was defined to be the one with fitness values at least three units larger than other models. This second approach was employed because, it has been argued (K.J. Friston, personal communication) that a single connection should not be dealt with individually to decide if it is or is not responsible for the observed data. It was suggested that two separate models that do or do not contain an individual connection should be compared via their log-evidence and the best model should be selected using the 3-unit rule. If this best model contains a specific connection, this suggests that this connection is responsible for the specific output.

5.4.2.3 Software systems

Parameter estimations were performed using versions 4290, 4667 and 5236 of SPM8 (denoted as sv.4290, sv.4667, and sv.5236), two versions of MATLAB 64-bit (denoted as mv.2011a and mv.2012a), and three Personal Computers (PC), with two using Windows 7 64-bit and one with Red Hat Enterprise Linux 64-bit as their operating systems. Note that sv.5236 is a newer version of SPM8 than sv.4667, which in turn is newer than sv.4290, and that DCM GUI default values were the same in all the versions of SPM8 used.

5.5 Results

5.5.1 Implementations using MSP

As mentioned before (section 5.4.1), the reliability of MSP needed testing before it could be used on our data.

As explained in section 5.4.1, different datasets were simulated by changing the number of source signals, changing their locations, and adding different levels of noise to the simulated EEG using the algorithm in Figure 5.3. Note that the forward matrix was extracted from the SPM8 package. MSP was then applied to these simulated data to find out if it was capable of detecting source positions correctly. Figures 5.5 to Figure 5.8 show the simulated and estimated source locations for different number of simulated sources and different noise levels. In each figure, subfigure (a) shows the true locations and subfigures (b), (c), and (d) show estimated source locations for 5 dB, 10 dB, and 20 dB SNRs, respectively. In each subfigure, the source locations are presented using three different views (saggital, coronal, and axial) for better understanding. In these figures, one main difference between the true source locations and the estimated ones is that the true locations only affect one voxel at that position but in the estimated sources, a group of voxels are being affected. It may be more reliable to simulate EEG data as a source that has activity over a few neighbouring voxels as this is what probably happens in reality, and this fact (a distributed source) is what the MSP algorithm relies on. One of the prior hypotheses of MSP is the correlation between neighbouring voxels. However, as the focus of these tests at the time was the accuracy of location detection rather than how the signal is distributed around that source, we continued to simulate a one-voxel source.

According to these figures, it can be concluded that MSP does not work well (with regards to detecting an accurate source location) in lower than 20 dB SNRs even for only one source location. It would be acceptable if we assumed that the Pilot data would have higher than 20 dB SNR which is debatable on its own, however, SNR was not the only problem in these simulations. As can be seen in Figure 5.8, when the number of sources increases, even with 20 dB SNR, the sources cannot be located accurately or even approximately.

At this point just to be able to move on to DCM simulations, it was decided to use auditory related source locations (David et al., 2006a) that were used in the literature and if the need arose, come back to source localisation techniques.

It is worth mentioning that before MSP was dropped, another study was carried out. As MSP had been used on a 128-channel EEG data with a 10-20 system electrode placement (Friston et al., 2008) where the lowest electrode was not placed lower than the ear, it was decided to test if the lower electrodes in our equidistant electrode placement (see Figure 3.1.a) could have any effect on the source reconstruction results. For this purpose, the lower channels (channels 45-66) in the simulated data used for MSP evaluation were eliminated from the data and MSP was employed to reconstruct the sources again. It was observed that the estimated source positions were not much different from their full-channel peers.

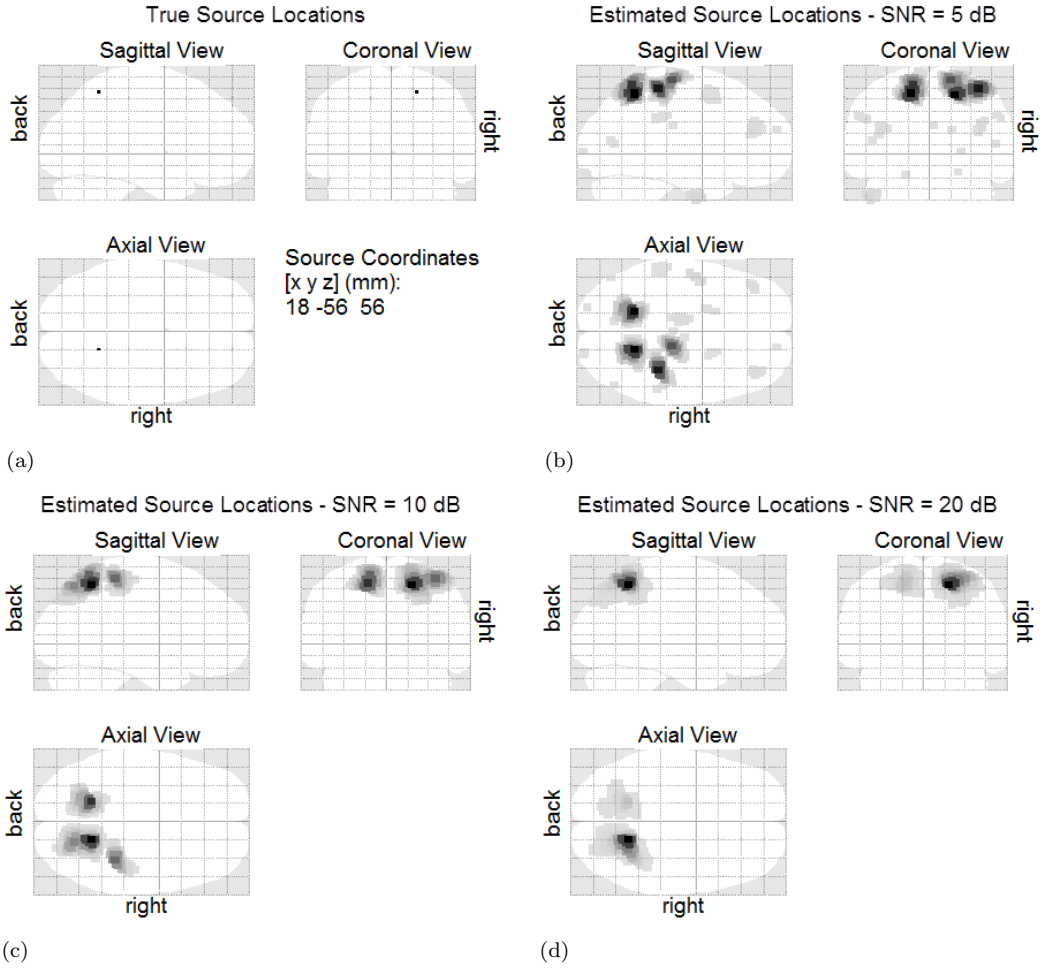

Figure 5.5: Source localisation performance with MSP for a single simulated source at different SNRs. a) The true positions and the estimated ones for b) 5 dB, c) 10 dB, and d) 20 dB SNR are presented using three different views of the brain. Only 20 dB SNR gives a proper estimate of a single source.

5.5.2 Implementations using DCM

In this section, the results of applying DCM on the data introduced in section 5.4.2.1 are presented. While these are not exhaustive results, inconsistencies between different versions of the same software uncovered in just a few cases are sufficient to raise concern regarding the robustness of the toolbox.

5.5.2.1 Reproducibility of DCM

The first question about DCM was if it was reproducible meaning that it would produce similar results in the same subject if different epochs were selected from the original EEG signal. For this purpose, fifteen datasets were generated from the Pilot data as in section 5.4.2.1 by randomly selecting 240 epochs from the 480 epochs in response to the 2 kHz tone.

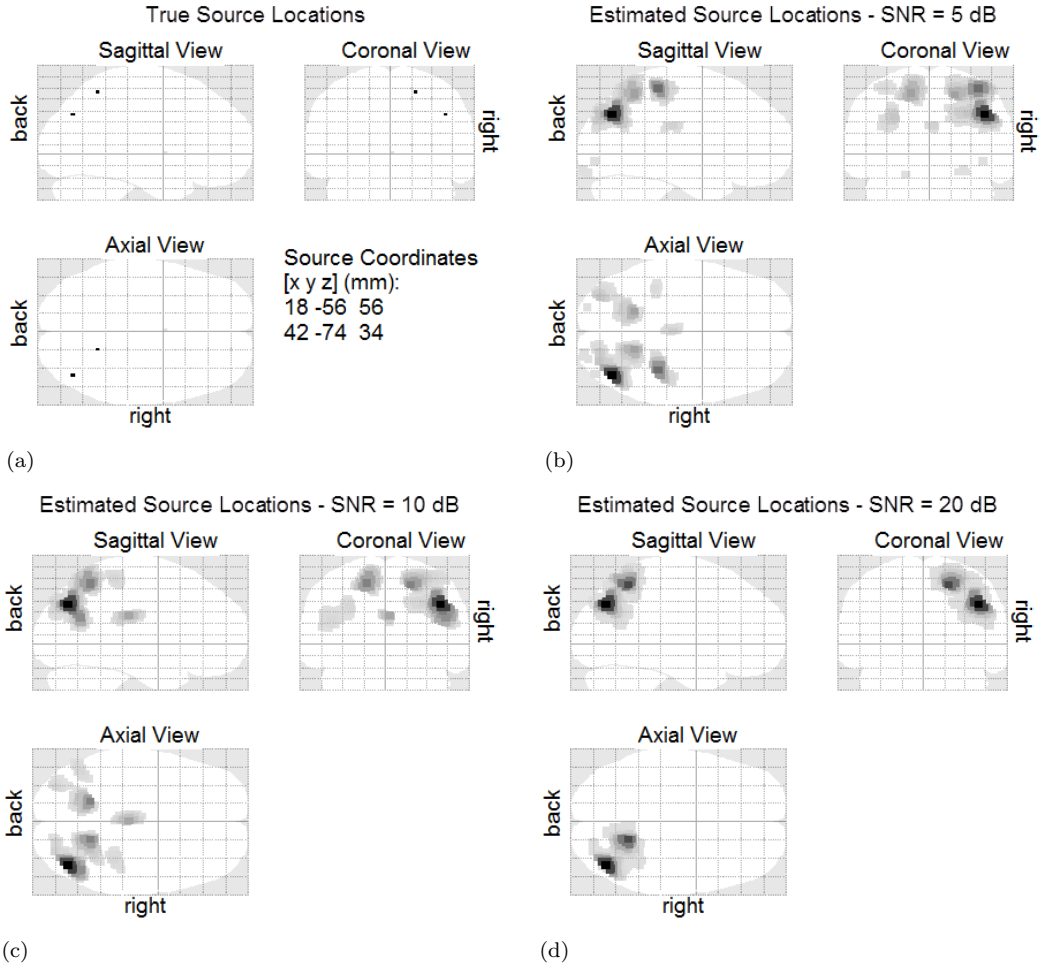

Figure 5.6: Source localisation performance with MSP for two simulated sources at different SNRs. a) The true positions and the estimated ones for b) 5 dB, c) 10 dB, and d) 20 dB SNR are presented using three different views of the brain.

Models 1 to 5 of Figure 5.4.a were estimated by DCM (specifications presented in section 5.4.2.2) for each dataset in the same combination of the software (sv.4290, mv.2011a, and Windows 7). Source locations corresponded to those used by David et al. (2006a). The fitness values of these models are presented in Figure 5.9. Model one was consistently the poorest. Using the 3-unit rule (see end of section 5.3.2), it is clear that in all except 2 datasets (5 and 14), model 5 was significantly better than other models. This result would suggest fairly good reproducibility regarding the choices between models. However, closer investigation of the estimated strengths of connections of model 5 showed that for each dataset, different connections were held responsible for the output (probability>90%). Thus, even though model 5 was selected as the best model most of the time, not much could be inferred about the individual parameters of the model, raising some concern regarding inferences on connectivity patterns. However, assuming the reproducibility on a single session, there was still the question of its reproducibility over different sessions.

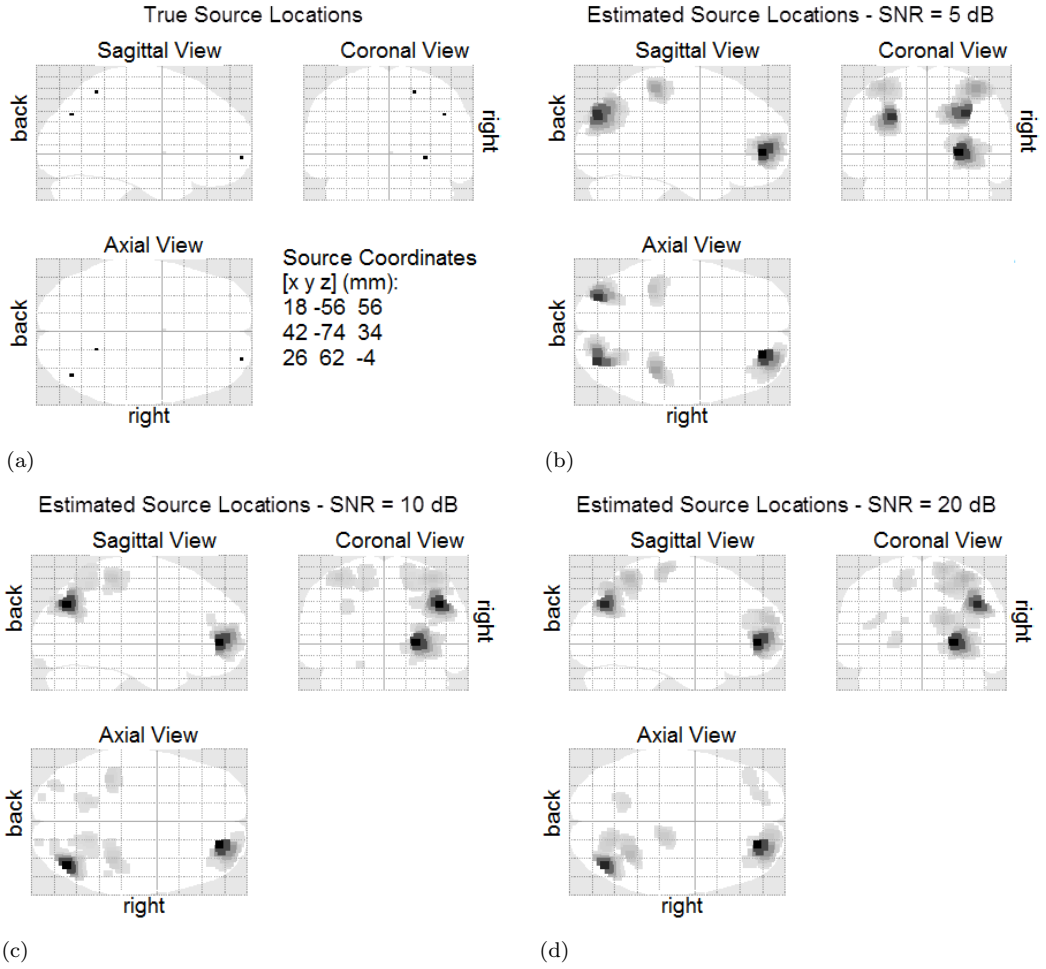

Figure 5.7: Source localisation performance with MSP for three simulated sources at different SNRs. a) The true positions and the estimated ones for b) 5 dB, c) 10 dB, and d) 20 dB SNR are presented using three different views of the brain.

To check the model further for its reproducibility over different recording sessions, we decided to analyse the second session of Pilot data. Also, the initial plan was to select fewer epochs for averaging to increase the noise level (reduce SNR) and find a breaking point for DCM with regards to SNR. However, as DCM proved unreliable (see section 5.5.2.2), these tests were not pursued.

5.5.2.2 Reliability of DCM

As was discussed in section 5.4.2.2, one can derive inferences from the results of DCM using firstly, the confidence intervals and probability of individual parameters or, secondly, comparing a set of models using their fitness values (log-evidence of the model). Both procedures are approached in the following subsections.

Individual Parameters:

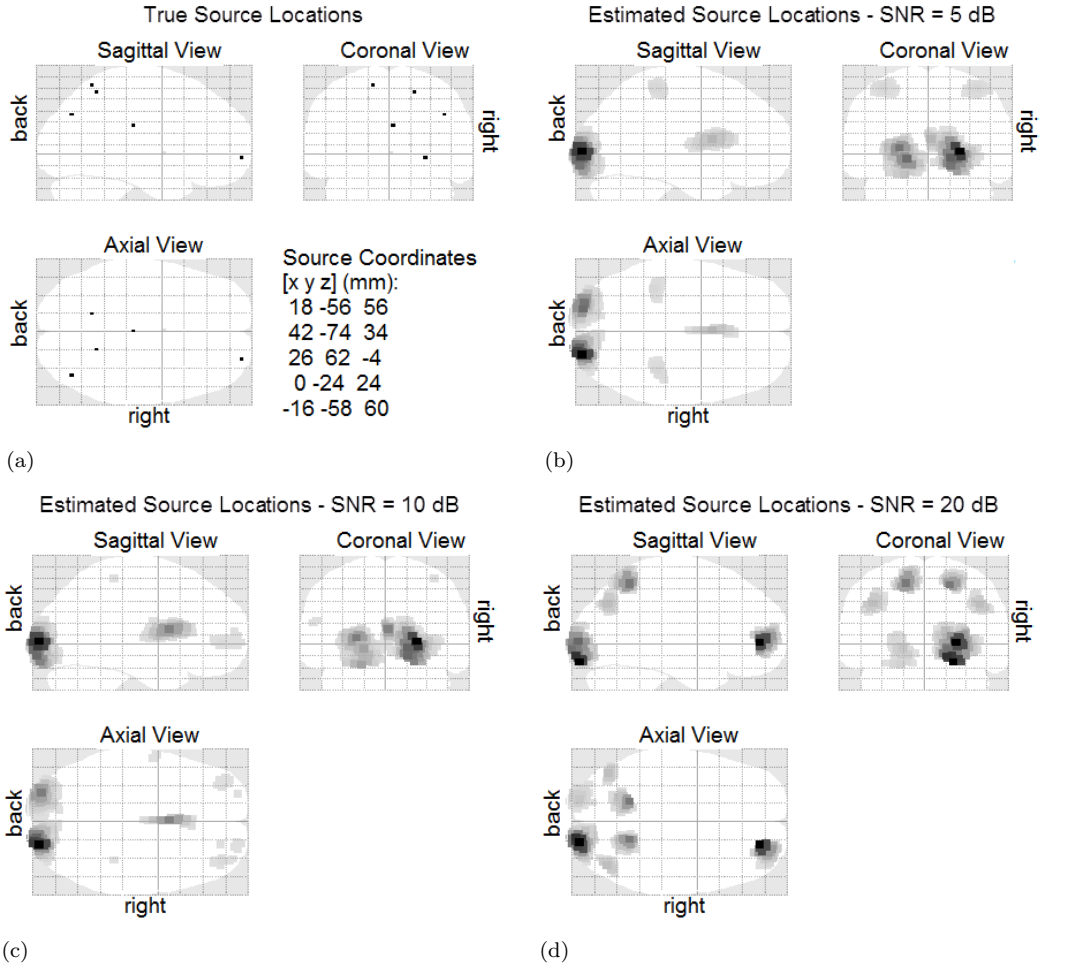

Figure 5.8: Source localisation performance with MSP for five simulated sources at different SNRs. a) The true positions and the estimated ones for b) 5 dB, c) 10 dB, and d) 20 dB SNR are presented using three different views of the brain.

As DCM is a very computationally intensive method and each model takes about 45 to 60 minutes to converge, the time required for all the different hypotheses mentioned above to be tested was very long. Thus, Parallel Computing Toolbox (PCT) of MATLAB was used to speed up the analyses. PCT would engage all computer cores for analyses thus decreasing the computation time.

To make sure that the results from serial computing were the same as parallel computing, before moving to the second session of Pilot data (see section 5.4.2.1), model 5 was again applied to all generated datasets of the first session using PCT. However, the fitness value (log-evidence of the model) and model parameters were different in PCT than the ones obtained from serial computing in all datasets. An example of the two estimations in one of the datasets is presented in Figures 5.10.a and 5.10.b. For the results to be more intelligible, only the connections with probability higher than 90% are plotted in these figures. It is clear that connections reported responsible for the observed output are very different between serial and parallel computing. For example, where serial

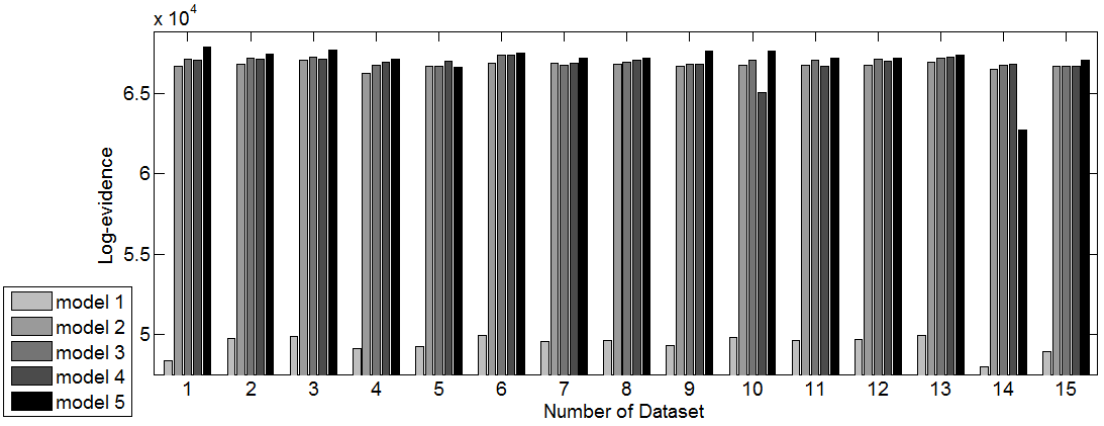

Figure 5.9: Fitness values of models 1-5 when applied on 15 generated datasets with sv.4290, mv.2011a, and Windows 7.

computing takes connections between RI and RS accountable for the observed output, parallel computing reports these connections to not be responsible.

As it was very important to decrease the computation time, toolbox codes were closely examined for the two conditions but the factor causing the discrepancies could not be found. Therefore, we contacted the group that developed SPM8 toolbox and after examining the toolbox themselves, they confirmed that there probably is a problem in the interaction between the two toolboxes SPM8 and PCT and they would try to solve the issue in the future versions; this problem was solved in the next version by thanking the author of this report but by that time DCM had been discarded.

As the results of PCT were not consistent with serial computing, we submitted our codes and datasets to the cluster computer system of the University of Southampton. The results that were obtained from cluster computers were again different from the results of both serial and parallel computing (Figure 5.10.c). In cluster computing, no connection seems responsible for the observed evoked response, nor does the input information seem to have been affecting the EEG.

As the version of the SPM8 on cluster nodes was a newer version than the SPM8 on the PC that was running the serial and parallel computing, SPM8 on this PC (PC1) was updated to the latest version which was sv.4667 (27th of February 2012). In PC1, after updating the SPM8 version, model 5 (see Figure 5.4.a) was estimated using serial computing and the result was again different from all previous outcomes presented in Figure 5.10. That made us contact the SPM8 developers again and they stated that for getting consistent and comparable results it is advisable to stick with one version of MATLAB and SPM8 and the same operating system through the whole project (and by this time we had already updated the version of our SPM8) and that this discrepancy may be due to the precision of different software. Figure 5.11 shows an example of the effect of different software versions on the outcome of DCM for model 2 and model 5 (see

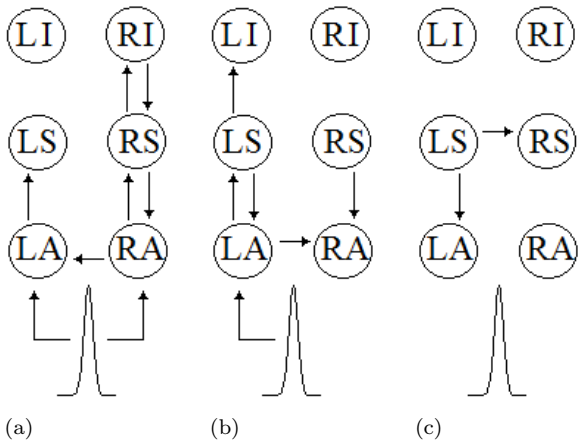

Figure 5.10: DCM estimation (model 5 of Figure 5.4.a) on the same dataset (dataset 1) using a) serial computing, b) parallel computing, and c) cluster computing. Only connections with probability higher than 90% are plotted. A pulse acts as the input to the model. The patterns of connections found using the three approaches are clearly different.

Figure 5.4.a) and Figure 5.12 shows the outcome of estimating model 2 in two different operating systems when the version of SMP8 and MATLAB were kept unchanged.

As a last quick inspection over the effect of software version on the outcome of DCM, the model of Figure 5.4.b was estimated for SPM data (see section 5.4.2.1) on two different PCs with the help of Wasifa Jamal, PhD student at the Electronic and Computer Science faculty of the University of Southampton. The operating system on both PCs was Windows 7. The processor on the first PC (PC1) was Intel(R) Xeon(R) and the MATLAB used on this computer was MATLAB R2011a (win 64). The second PC (PC2) had MATLB R2012a (win 64) and Intel(R) Core(TM) i7-2600 as its processor. It was verified that the combination of these two variables (MATLAB and operating system) has obvious effect on the outcome of DCM results (Figure 5.13); not only the fitness value but also the significant connections were different. PC2 produced much higher fitness values than PC1.

It should be noted that when the same model was estimated more than once in the same combination of software versions and on the same set of data, results were identical. Also, when the software combination (SPM8/MATLAB/operating system) was kept consistent on different computers, the results were again identical. This was observed for both Pilot data and SPM data.

Model Comparison:

The second approach in comparing different models is by considering the total fitness value instead of the probability of individual parameters. This approach was suggested to us in reply to our conference paper on DCM (Hosseini et al., 2014b) by K. J. Friston, the founder of DCM.

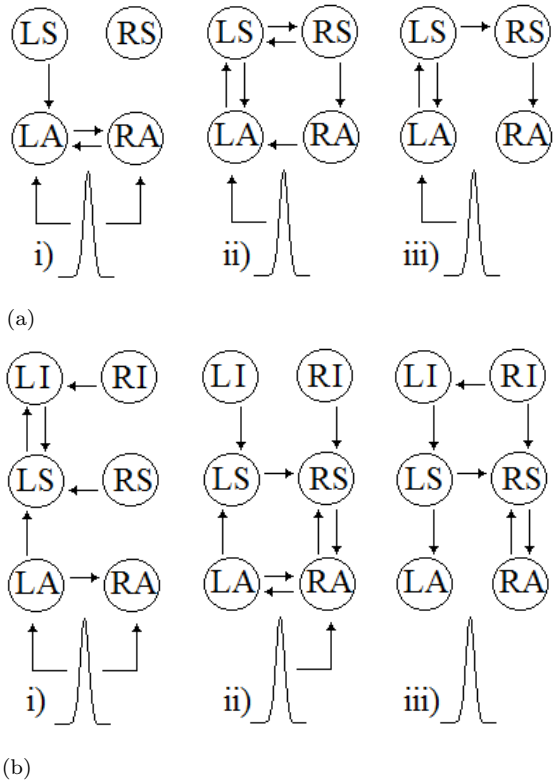

Figure 5.11: Responsible connections in generating the evoked response (probability>90%) in a) model 2 and b) model 5 for the same set of data. i) mv.2012a & sv.4667, ii) mv.2012a & sv.5236, iii) mv.2011a & sv.5236. A pulse acts as the input to the model. The patterns of connections found using the three combinations of MATLAB and SPM8 combinations are clearly different for both models.

This approach was also tested with the 5 models of Figure 5.4 on the same set of data (dataset 1) generated from the Pilot data, with two combinations of the software. In Figure 5.14, the log-evidence of these estimated models are presented when the estimation was performed in two different combinations of MATLAB and SPM8 software. Note that in this figure, the scale is not the same, but for both, a 3-unit difference should be considered significant (see end of section 5.3.2). It is clear that the log-evidence of the estimated models did not vary in a consistent way across software versions. Although model 5 (the most complex model) was identified as the best model in both combinations, the ranking of the remaining models is not consistent. According to Figure 5.14.a, the model order will be $5 \rightarrow 4 \rightarrow 2 \rightarrow 3 \rightarrow 1$ but in Figure 5.14.b, it will be $5 \rightarrow 3 \rightarrow 4 \rightarrow 2 \rightarrow 1$. Thus, if model 5 is excluded, within the remaining ones, model 4 would be selected in one software combination and model 3 in the other. Therefore it cannot be said if the connection to the right or the left Inferior Frontal Gyrus is responsible for the output EEG if the estimations are performed in these two software combinations. The inferences are thus quite different but in both cases deemed significant (greater than 3-unit difference).

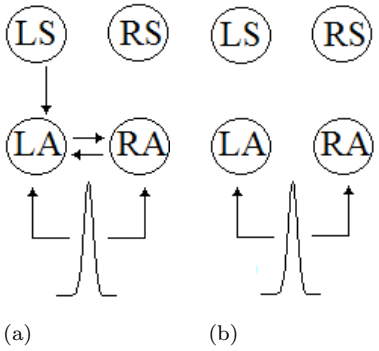

Figure 5.12: Responsible connections in generating the evoked response (probability>90%) in model 2 (see Figure 5.4.a). In both a and b, sv.4667 and mv.2011a were used for the same set of data but the operating system was different: a) Windows 7 and b) Linux. A pulse acts as the input to the model. The patterns of connections found using different operating systems are clearly different.

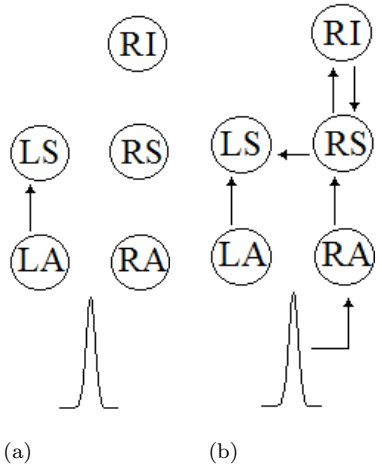

Figure 5.13: Responsible connections in generating the evoked response in the model of Figure 5.4.b for SPM data. In both a and b, sv.4667 and Windows 7 were used but the MATLAB version was different: i) mv.2011a and ii) mv.2012a. A pulse acts as the model input.

5.6 Discussion

In this chapter, some preliminary results obtained from MSP were presented. Applying MSP on simulated data reported unreliable results on low SNRs and high number of sources. Further analyses were required before any verdict could be issued on the reliability of MSP. However, we were more concerned with DCM rather than source reconstruction techniques in our project and we had planned to test the reliability of DCM as well. As the latter could be achieved using the recorded EEG data in response to tone bursts (see 5.4.2.1) and there were already some predefined source locations in response to tone bursts in the literature (David et al., 2006a), we decided to drop MSP at this point of the work and move on to testing DCM using already available source

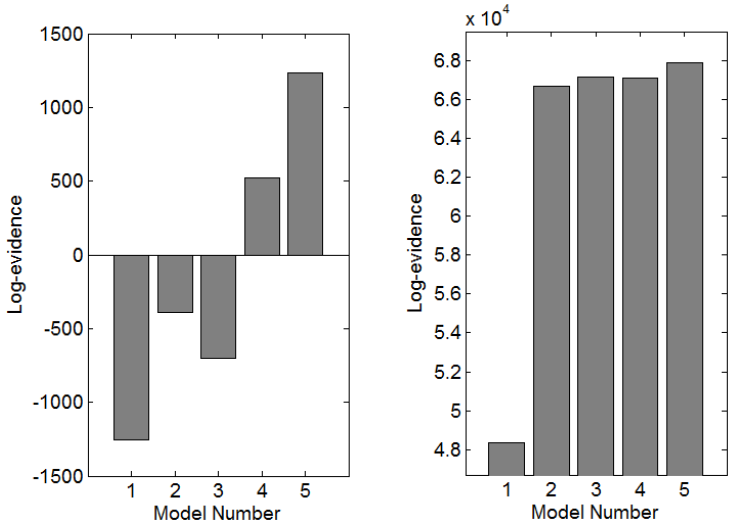

(a) (b)

Figure 5.14: Fitness values of models 1-5 for the same set of data and operating system (Windows 7) but different version of the software: a) mv.2012a & sv.5236 and b) mv.2011a & sv.4290

locations. If we were able to achieve reliable results for using this dataset (see 5.4.2.1), we would come back to testing MSP further in the hopes of employing it for source reconstruction of EEG in response to more complicated stimuli such as AM tones, words, and sentences. As DCM proved to be an inappropriate method for the purpose of this study (the results of which are presented in section 5.5.2), research on the topic of source reconstruction was also dropped at that stage.

Estimating DCM for the same set of models over different datasets from the same subject and with the same software systems showed some inconsistencies. The fact that 13 out of 15 datasets reported the same model (model 5) as the best model was both promising and worrying. It was promising because one might expect some variability within a biological sample, but worrying because it may indicate that DCM can give inconsistent results. Discrepant results in 2 out of 15 datasets randomly selected from within the same recording acquired over a period of a few minutes in the same subject would seem rather high. Furthermore, if model 5 is eliminated from the comparison, the inconsistency continues, with almost half of the datasets reporting model 3 as the best model and the remainder favoring model 4. These exploratory results on reproducibility of DCM analysis within the same session were insightful, but highlighted the need for further investigation which should consider multiple subjects, and larger datasets acquired within the same session and then also on different days.

The key result of this study was that DCM/SPM8 showed discrepancies when using different combination of the software (SPM8, MATLAB, and operating system). These discrepancies were observed both in the estimates of the strength of individual connections and in model comparisons using the log-evidence. Within the same model,

depending on the software combination used, different connections showed higher probability of affecting the output. Likewise, when comparing models according to fitness values, the order of preference for model selection was not the same for the various combinations of the software, even on identical datasets.

The current results clearly do not prove that connectivity measures derived from DCM are always unreliable. However, the examples presented show clear evidence of lack of robustness and raise concern that results can be misleading. Possible reasons behind the variation in results could include different numerical precision of the MATLAB versions used with different operating systems, or perhaps different numbers of computational loops in iterative estimates, or slightly different estimation algorithms in various versions of SPM8. The obvious question is whether there is a random component in the estimation process and the seeds of the random number generator is the same in the same software combination, but different for different systems. However, as confirmed by Karl Friston (through personal communication), the algorithm does not use a random process. Though it is not clear what the exact reasons are, it does raise questions regarding the robustness of the DCM algorithm or the SPM8 software implementation when applied to the EEG and caution should be employed in the interpretation of results of DCM using the SPM8 toolbox.

One of the long term goals of this study was to investigate brain plasticity in cochlear implant users over time by measuring brain connectivity. Although it is an exploratory study at the moment, it is hoped that it may have applications specifying a specific therapy method for individual patients. The measurement technique could also be used as a diagnostic tool for identifying the probability of positive aftermath of cochlear implantation. If DCM is selected as the connectivity measurement method, according to the results presented in this section, it then necessitates the use of a specific set of operating system/MATLAB/SPM8 forever for the mentioned applications which is not practically possible.

5.7 Summary

In this chapter one of the popular effective connectivity measurement techniques (DCM) was discussed. An EEG source reconstruction method was required for studying DCM as DCM needs the location of sources in its analyses. MSP technique was selected for this purpose but it was shown to be a poor technique in preliminary studies as it performed poorly with increasing the number of sources or decreasing the SNR of the simulated data. Thus, source locations to be fed to DCM were selected from the literature.

Because of its many reported advantages over other connectivity methods such as being biophysically informed, comprising a designed input in the model, and considering the nonlinearities of the neuronal system, DCM initially became the focus of this study.

However, it was discarded after simulations were performed on EEG data using this approach and showed poor reliability. When estimating the parameters of a specific model using a constant set of EEG data in different Operating Systems and with various versions of MATLAB and SPM8, it was noticed that the existing implementation of DCM in the SPM8 toolbox may produce different results depending on the combination of operating system, MATLAB, and the SPM8 version. This issue makes it impractical for the purpose of this thesis to utilise DCM, and thus we were compelled to turn to other connectivity measurement methods that are explained in more detail in chapter 7 along with their simulations on synthetic data and results on recorded EEG.

Chapter 6

Measuring Responses using Non-parametric Pairwise Coherence

6.1 Introduction

As shown in chapter 4 and appendix B, induced response is not a very strong response and it may be undetectable using power analyses. It has been shown that the evoked response to rhythmic stimulation is easier to detect with coherence analyses (coherence with the stimulus) rather than power analyses (Simpson et al., 2000; Miranda de Sá et al., 2001, 2002). This is tested in this chapter for induced activity and in response to both rhythmic (repeating pure tones) and not rhythmic (different words) stimuli. Also, in this chapter we establish a basis with which the results of the future model-based connectivity methods will be compared.

Coherence is a statistic that measures the similarity of two signals in the frequency domain and specifies the amount of linear power coupling between the two signals (Faes et al., 2004). It is calculated by normalising the cross-spectral density between two signals by the auto-spectral density of each signal.

As mentioned before, it has been shown that coherence is a stronger measure than power alone in finding an evoked response in EEG data (Simpson et al., 2000). In chapter 4, it was shown that with power analyses alone, induced activity can be detected in lower frequency bands in response to words and sentences. One of the aims of this chapter is to investigate if coherence analysis is a more sensitive tool than power analyses in detecting induced responses in EEG data. While there is considerable analysis of EEG coherence in the literature, the novelty here is to do this in the context of stimulation

by words and sentences and investigation of induced activity, starting from a foundation of more conventional stimuli such as tones.

The ultimate aim of this thesis is to assess connectivity among different EEG channels. For the reasons explained in chapter 7, using too many channels in Multi-Variate Auto-Regressive (MVAR) connectivity measures can lead to misleading results as there may not be enough data points to estimate the parameters of the model reliably. It is thus important to decrease the number of channels for connectivity analyses and one way to do so is to analyse only the channels with the most power transfer among them. This can be achieved by calculating the pairwise coherence between all combinations of channels and finding the ones which have the strongest event-related connections.

Moreover, as the analyses in this chapter are based on non-parametric calculations and our intended effective connectivity methods (refer to chapter 7) are parametric model-based ones, the results of this chapter would work as a test of reliability for the employed effective connectivity methods (refer to chapter 7). Coherence is also a functional connectivity method which will show which channels are connected to each other.

Thus, the objectives of this chapter are to determine if coherence is more sensitive in detecting induced stimulus responses than power, to identify the channels most tightly connected, and to provide baseline measurement for the analysis using MVAR models in the next chapter, to which those more sophisticated measures can be compared.

In the next section, coherence will be defined and the approaches taken in the literature and in this report for investigating its significance will be explained. These methods are then employed on EEG data in response to different types of auditory stimuli and the results are presented in section 6.4. The results are then followed by a discussion and a summary of results and inferences.[1]

6.2 Method

6.2.1 Definition of Coherence

The coherence between two discrete signals $x[k]$ and $y[k]$ is a measure of linear inter-dependence between two signals and can be estimated as Equation (6.1) (Carter et al., 1973):

$$Coh_{xy}(f) = \frac{\sum_{i=1}^{K} X_i^*(f) Y_i(f)}{\sqrt{\sum_{i=1}^{K} |X_i(f)|^2 . \sum_{i=1}^{K} |Y_i(f)|^2}}, \tag{6.1}$$

[1] Parts of the results of this chapter are presented in Hosseini et al. (2015).

where $X_i(f)$ and $Y_i(f)$ are, respectively, the Fourier transforms of x_i and y_i where i is the index of an epoch, * denotes the complex conjugate, and K is the number of windows the signal has been divided into, which in the case of this study is the same as the number of epochs. Coherence is a complex value and it is more common to talk about its modulus (or modulus squared) rather than the complex value (Miranda de Sá et al., 2001). The modulus of the coherence is a value between zero and one where zero indicates no correlation and one indicates perfect correlation between the two signals. Magnitude Squared Coherence (MSC), presented in Equation (6.2), is a more conventional measure than the magnitude coherence so in this report we will proceed with MSC and for simplicity, it will be called coherence from this point on.

$$|Coh_{xy}|^2(f) = \frac{|\sum_{i=1}^{K} X_i^*(f)Y_i(f)|^2}{\sum_{i=1}^{K} |X_i(f)|^2 . \sum_{i=1}^{K} |Y_i(f)|^2}. \tag{6.2}$$

6.2.2 Statistical significance of coherence estimates

In principle, if MSC is greater than zero, one may reason that there is some relation between the two signals. However, because of the random effect of noise and random estimation errors, in practice, values greater than zero will almost always be found, even if there is no coherence between the signals (null hypothesis). To identify if the MSC value calculated is significantly greater than zero, a critical value should be defined. If the coherence is larger than this critical value, then it can be considered as a significant correlation. There are a few parametric (Thompson, 1979; Miranda de Sá et al., 2001; Faes et al., 2004) and non-parametric (Faes et al., 2004) methods presented in different publications for estimating this critical value but not all of them are appropriate in the presence of electrical conduction between electrodes, i.e. when electrodes are too close, there is a chance of linear relationship between them because of the spread of electrical activity.

In event related EEG analyses, because of the existence of background EEG activity and its highly correlated structure in neighbouring electrodes, usually a large coherence between close pairs of electrodes is observed but this large value is not necessarily related to the stimulus. Note that in the current study, the focus is not on detecting the significance of a coherence value per se but rather the significance of this value changing over time compared to the baseline. Most of the currently available methods for measuring the statistical significance of coherence, focus on the coherence value rather than its significance change from the baseline.

One parametric formula (Thompson, 1979) that exists for calculating the critical value only depends on the desired significance level and the number of epochs being used. Thus, they do not correct for the closeness of EEG electrodes and the always present large coherence value in neighbouring electrodes, and are not applicable to our analyses.

Another study (Miranda de Sá et al., 2001), tries to eliminate the effect of neighbouring electrodes by directly calculating the coherence between the stimulus and the response rather than calculating the coherence between two electrodes. However, as in the future chapters, the relationship between two electrodes is of interest and one aim of this chapter is to provide a baseline for future connectivity analyses, this method is not suitable for the purpose of this study either.

Most common non-parametric methods for assessing statistical significance of coherence are based on time randomisation and phase randomisation (Faes et al., 2004) using FFT analyses. However, they also focus on the value of the coherence and not its event-related change. In each of these two approaches, the first step is to find the coherence between the two original signals and the second step is to find the coherence between two randomly generated uncorrelated signals (following the null hypothesis of absence of coherence) from the original signal. The second step is repeated many times (usually a couple of hundred times) and the distribution of the coherence is estimated. The confidence intervals of this distribution is identified for a specific significance level α and the significance of the original coherence is decided according to this interval. To obtain the randomly generated signals, in time randomisation, the data points of the two signals in the time domain are shuffled around randomly. In phase randomisation, usually the FFT of the signal is estimated, the power of FFT is kept unchanged but the phases are selected randomly from the $[0\ 2\pi]$ rad range, and then the inverse FFT is calculated. These methods were tested but proved inefficient in the application of this project as they would ascribe significance to almost all coherence estimates given the high inherent coherence in neighbouring electrodes due to electrical conduction effects. Therefore, all neighbouring electrodes would always report significant coherence and it would not be possible to find the event-related coherence among these connections.

Thus, a new approach for measuring the significance of coherence was employed. In this approach, the focus is on the significance of coherence change from the baseline to different time windows after the onset. For this purpose, similar to induced response analyses (see section 4.2.2), a time varying coherence was calculated for all channel pairs and the significance of their change from the baseline was tested using Friedman's test and post-hoc analyses. This approach will be explained more thoroughly in section 6.3.3.

6.3 Materials

6.3.1 Pre-processing

For the purpose of coherence analyses, the data (both S1 and S2) that were explained in section 3.2 were used, epoched, and artefact rejected according to section 3.4. However, more pre-processing was required before coherence was estimated.

Data were further filtered in the forward and reverse direction (to give zero phase) with a 5-th order low-pass Butterworth filter with a 100-Hz cut-off frequency acting as an anti-alias filter and downsampled to 250 Hz to decrease the number of samples and therefore the computation time. For each stimulus type and presentation ear, the mean value was subtracted from each epoch and all values in each epoch were divided by the standard deviation of that epoch. This step would ensure that all epochs have equal weight in the analyses of coherence. Then the ensemble average of all epochs was subtracted from each epoch to eliminate the phase-locked activity and ensure stationarity of the mean in the signal and zero-mean value at all samples. Then all epochs were divided by the ensemble standard deviation over all epochs to make the results comparable over time and to ensure stationarity of the variance in the signal. In model-based analyses of the next chapter, the latter step is mandatory and because one purpose of the analyses in this chapter is to have a baseline with which to compare the results of that chapter, this step was performed in this chapter as well.

For each stimulus type and presentation ear, the data in each epoch were then divided into 200 ms or 500 ms non-overlapping windows (same windows as Figure 4.1 depending on the stimulus type). One window before the onset and multiple windows (with the same length) after the onset were selected for each stimulus type. For consistency and for the results to be comparable with power analyses, the length of windows were selected similar to those obtained from induced analyses in chapter 4, i.e. 200 ms for tones bursts, 500 ms for AM tones and words, and 1000 ms for sentences.

6.3.2 Coherence estimation

In each set of data, the pairwaise coherence was estimated over all pairs of channels for each time window by calculating the FFT of each segment (the number of points for FFT analyses was the same as the length of the segment) and using the Equation (6.2). The value of M in this equation equals the number of epochs for that stimulus. The average coherence over different frequency bands of Figure 4.1 was then estimated for each time window, note that 0 Hz was excluded. This procedure was repeated for all subjects.

6.3.3 Significance test

Similar to power analyses (see section 4.2.2), Friedman's test with 5% significance level was applied to coherence values of each channel pair and each frequency band separately. Note that this analysis was done across the cohort of subjects and not on individual subjects, i.e. in Friedman's test, the number of observations in each group of coherence values was the same as the number of subjects.

If a significant change over time was detected in a frequency band, post-hoc (Tukey's test) analyses was applied to find the time windows that had significantly different coherence values compared to the baseline, i.e. the time window before the onset of stimulation. The post-hoc analysis was used to identify changes in connectivity over time rather than individually significant connections. In order to reduce the number of potentially spurious connections identified, a 1% α-value was used at this stage. There were a large number of hypotheses that were tested, but because this was an exploratory study the p-value was not corrected any further for the fear of losing sensitivity. Given that multiple tests were carried out between the results from the window before stimulus onset and all remaining windows, conventional Bonferroni correction of the p-value would not be appropriate, since these are not independent tests. Future work with more data will be required to confirm a smaller number of more targeted hypotheses. Significant coherence changes from the baseline to different segments of data after the stimulus onset would show the existence of event-related activity in those windows after the onset. As the evoked activity had been removed from the data, if a significant change was observed in any segment after the onset, it could be related to the induced activity. As neighbouring electrodes in EEG data show high coherence values (close to one) even without stimulus related activity in the data, we focused on the change in the coherence over time rather than the actual coherence values between two electrodes.

6.4 Results

6.4.1 Coherence in response to tone bursts

EEG data in response to tone bursts were preprocessed according to section 6.3.1 and the coherence was calculated as in section 6.3.2 for all channel pairs and different time windows. Coherence was then averaged in different frequency bands of Figure 4.1.

A time-frequency representation of these coherence values is shown in Figure 6.1. In this figure, x and y axes show the channel numbers and the coherence is colour coded where dark blue indicates zero coherence and dark red shows maximal coherence. The rows of this figure show the average coherence in different frequency bands and the columns show the coherence over time. In this figure, no change in the coherence values can be seen over time as the coherence is high in neighbouring electrodes (refer to Figure 3.1.b for electrode positions) and the event-related changes in the coherence are rather small in comparison. The diagonal values in each subfigure is the coherence of the electrode with itself and the upper and lower triangles are identical because the coherence between x and y is the same as coherence between y and x. For the change in coherence to be clearer, the coherence value between each electrode pair in the baseline was subtracted from all coherence values of the same pair after the onset. The result is presented in Figure 6.2. In this figure, each subfigure shows the change in coherence from the

baseline coherence in all electrode pairs in different time and frequency windows after the stimulus onset. Rows and columns of each subfigure are marked by channel numbers between which the coherence is computed (refer to Figure 3.1.b for electrode positions). Although the changes are very small, it can be seen that main coherence changes occur in the [0.2 0.4] s time window in the [0 8] Hz frequency band (as dark blue) and in the [13 30] Hz frequency band in the [0.2 0.4] s and [0.4 0.6] s time windows (as dark red). To find if these changes are significant or random, significance analyses were then applied to coherence values.

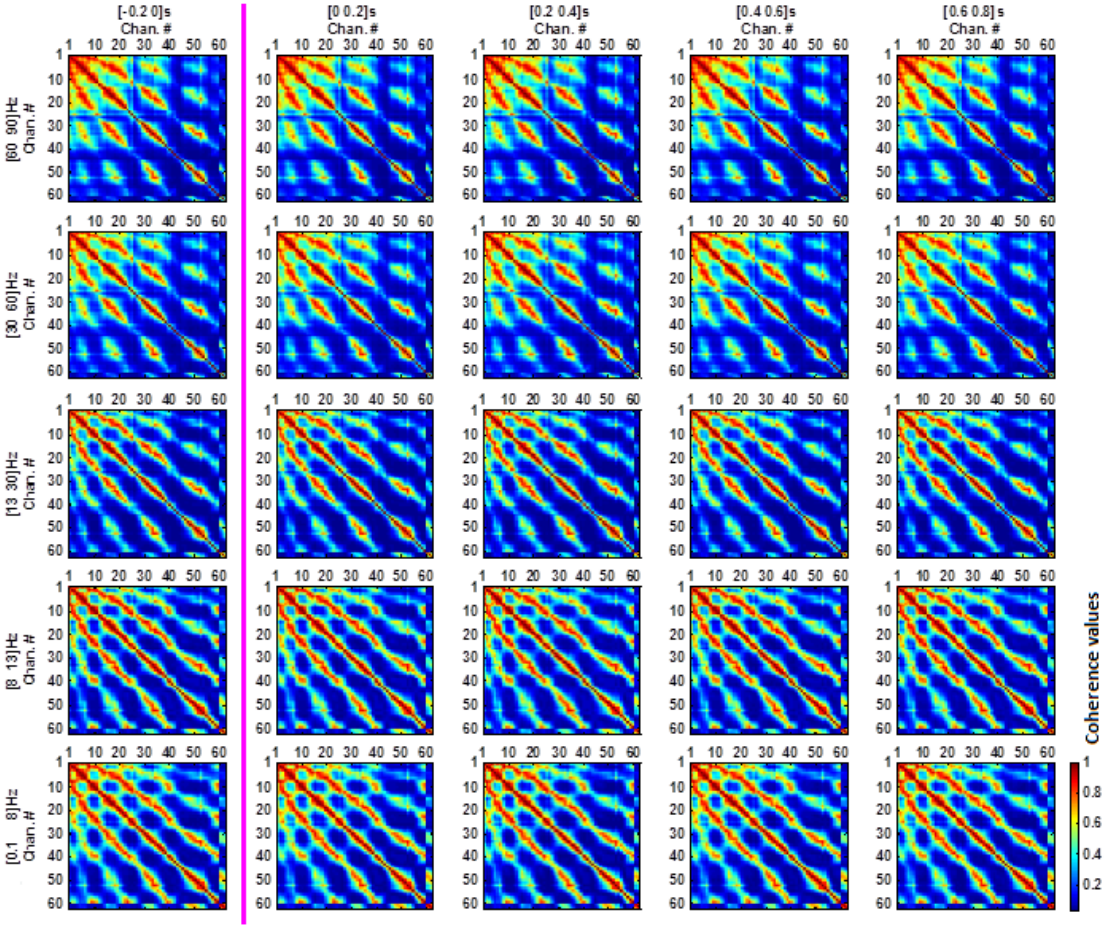

Figure 6.1: Tone bursts: Pairwise coherence values along time (columns) and over different frequency bands (rows). In each subfigure, rows and columns show channel numbers between which the coherence is computed. Dark red/blue shows 1/0, i.e. complete/zero coherence. The stimulus onset occurs at zero seconds and is indicated by the magenta line.

Significance analyses were performed according to section 6.3.3 on each channel pair in each frequency band and the ones with significant coherence ($p<0.05$) change over time were identified. Among these selected pairs, channel pairs with significant ($p<0.01$) coherence change after the onset (compared to the baseline) were identified employing post-hoc analyses. Figure 6.3 shows the results of each of these steps. Note that in each subfigure, rows and columns are marked by channel numbers. In this figure, the left

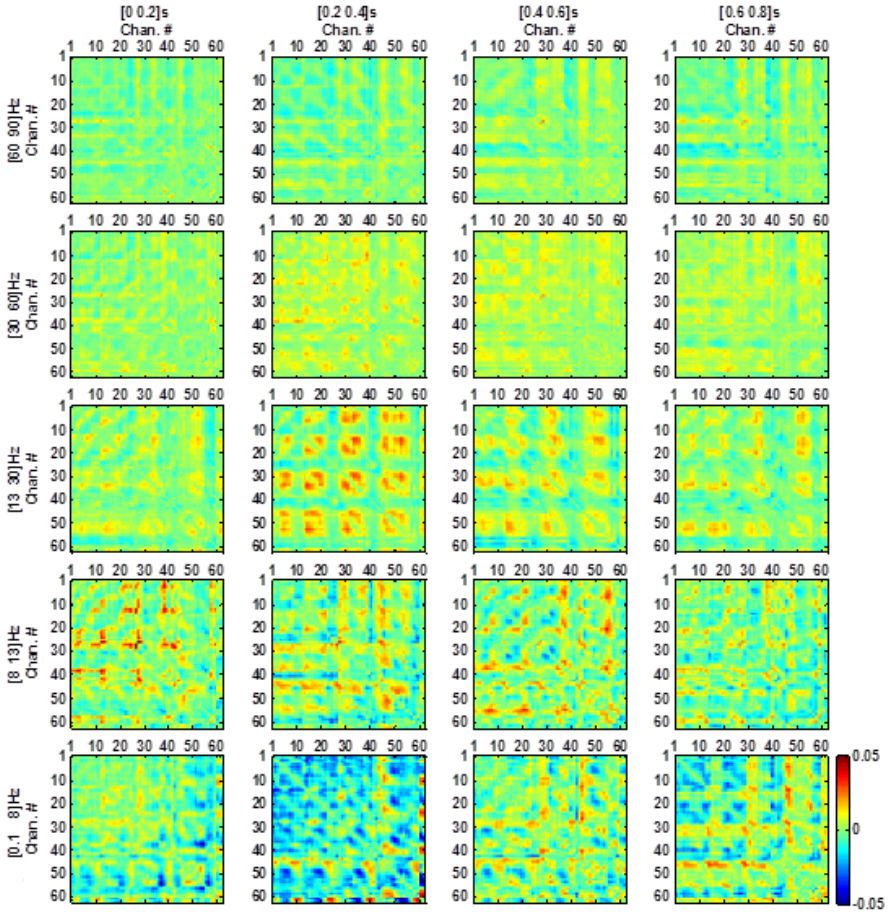

Figure 6.2: Tone bursts: Pairwise coherence after subtraction of baseline values along time (columns) and over different frequency bands (rows). In each subfigure, rows and columns show channel numbers between which the coherence is computed. Blue/red indicates decreased/increased coherence compared to the baseline. The stimulus onset occurs at zero seconds.

column shows p-values of Friedman's test (rescaled and recalculated as $log_{10}(1-pvalue)$ for clearer visualisation) in a colour coded format for different frequency bands and the middle column identifies the p-values that are smaller than 0.05. Frequency bands are matched with those of Figure 6.2. Using post-hoc analyses, the right column shows channel pairs that have at least one window with a significant change ($p<0.01$) after the onset compared to the baseline. From the right column of this figure, it can be seen that there is a significant coherence change in the [13 30] Hz band but the changes in other frequencies seem to be very random.

As can be seen, Figure 6.3 does not clearly demonstrate the channel locations or the exact time windows in which the coherence change occurred. Therefore, another presentation approach was employed using the *arrow.m* file by Johnson, Erik (2009) with which arrows can be plotted at exactly specified locations on a map. In Figure 6.4, arrows show connections between channel pairs that were marked in post-hoc analyses as significant. Red/blue arrows indicate increase/decrease in the coherence compared to the baseline.

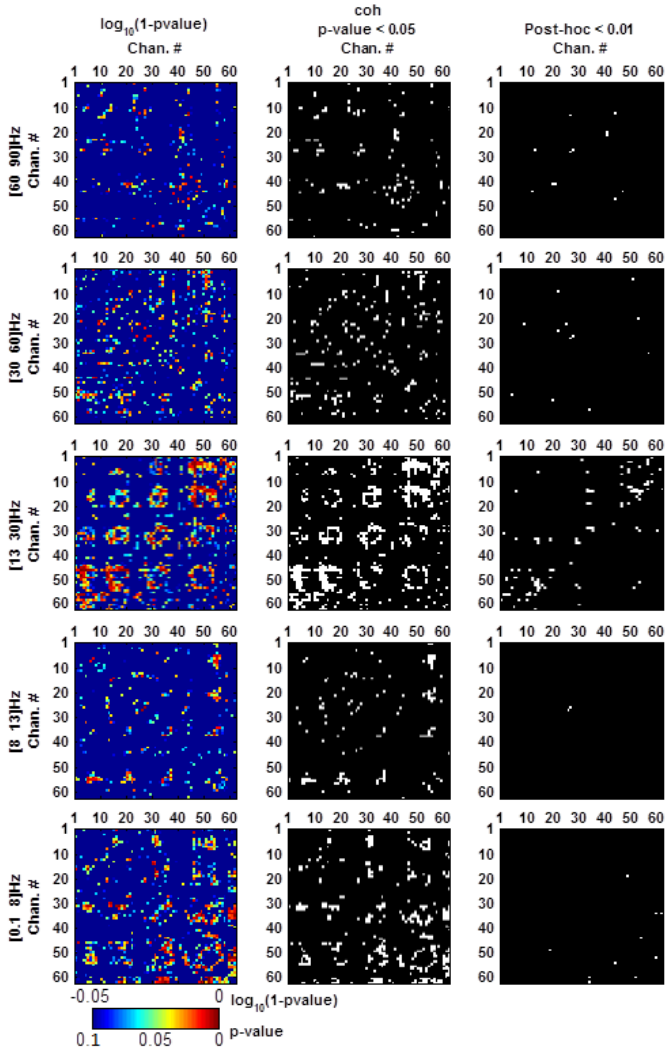

Figure 6.3: Tone bursts: Results of Friedman's test. In each subfigure, rows and columns are marked by channel numbers. Left column: p-values of Friedman's rescaled to $log_{10}(1 - pvalue)$, for clearer visualisation, and colour coded. Zero (dark red), -0.0223, and -0.05 (dark blue) correspond to p-values of 0, 0.05, and 0.1, respectively. Middle column: channel pairs with significant coherence change ($p<0.05$) are marked by white dots. Right column: channel pairs with significant ($p<0.01$) coherence change (in at least one window after the onset) from the baseline are marked by white dots.

Rows and columns are the same time-frequency windows as in Figure 6.2. Each subfigure is an axial view of the head. Although it was expected that there would be false-positives in each time-frequency window of Figure 6.4, the number of significant arrows in [13 30] Hz and [0.2 0.6] s windows are notable (especially when compared to other time-frequency windows), i.e. they cannot be attributed simply as false positives. Therefore, there appears to be a clear increase in the coherence in posterior areas (towards the left side) and a decrease in coherence in frontal areas when listening to pure tones. This can be linked to induced response, as the evoked activity has been removed from the signal prior to coherence estimation.

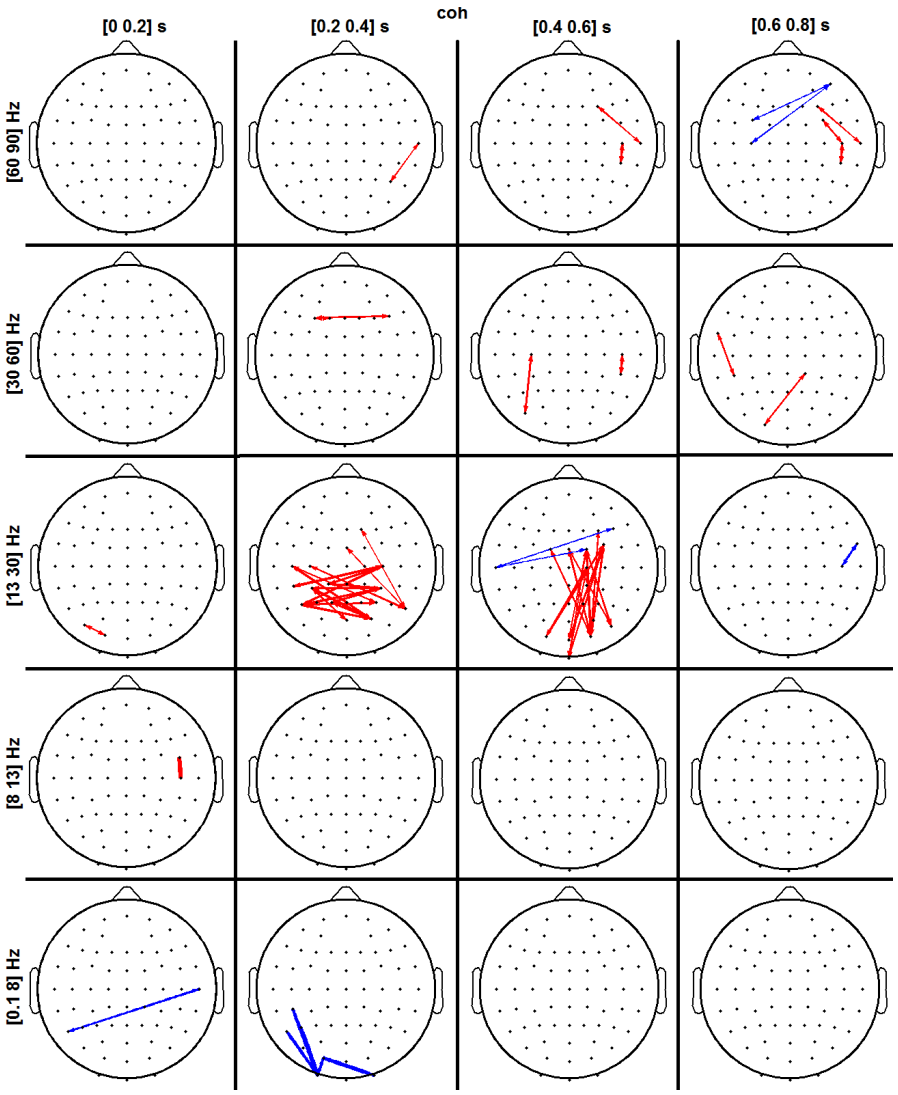

Figure 6.4: Tone bursts: Significant coherence changes from the baseline (Friedman's test, $p<0.05$ - Tukey's test, $p<0.01$) in pairs of electrodes in different time-frequency windows are marked by arrows. Red/blue arrows indicate increase/decrease in the coherence compared to the baseline. The stimulus onset occurs at zero seconds.

6.4.2 Coherence in response to words

Similar to tone bursts (section 6.4.1), pre-processed epoched data in response to words when played to the right ear were divided into 500 ms windows without overlapping, starting from 500 ms before the onset and ending at 1.5 s after the onset. Longer time-windows were used here because the stimulus and the responses are longer and stimuli are not all of the same duration. Longer time windows thus aim to smooth out some of the variability between stimuli.

The coherence was calculated for each time window for all channel pairs and then the average of the coherence was computed for each frequency band in each time window

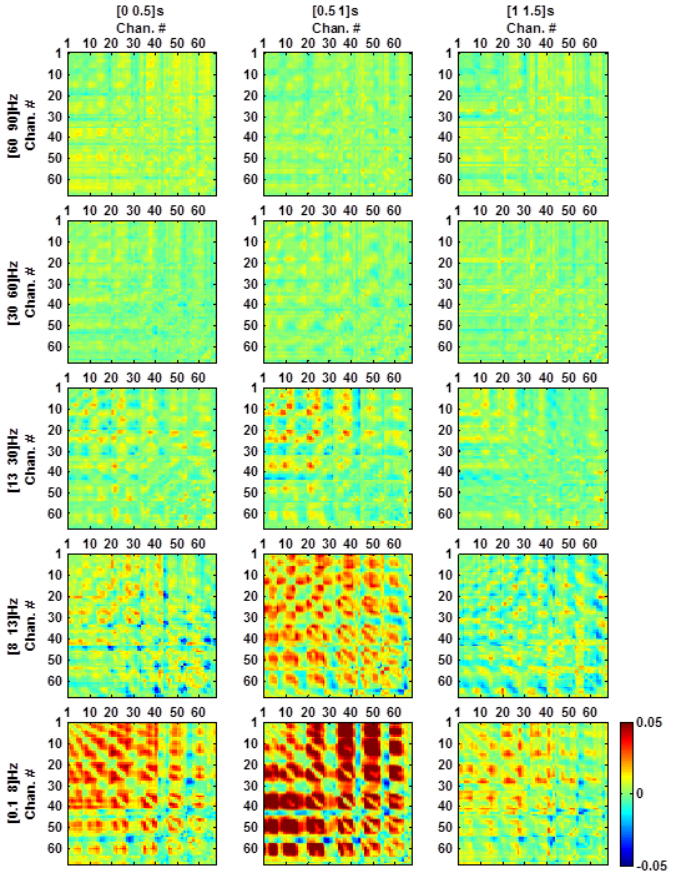

Figure 6.5: Words played to the right ear: Pairwise coherence after subtraction of baseline values along time (columns) and over different frequency bands (rows). In each subfigure, rows and columns show channel numbers between which the coherence is computed. Blue/red indicates decreased/increased coherence compared to the baseline.

(according to Figure 4.1) and channel pair. As in Figure 6.1, the actual coherence values over time did not show any clear changes over time.

Therefore, the coherence values of each channel pair in the baseline were subtracted from coherence values of the same channel pair in all time-windows after the onset (in the same frequency band) and then the baseline corrected coherence values were plotted in Figure 6.5. In this figure, x and y axes show the channel numbers and the coherence change is colour coded where blue/red indicates decrease/increase in coherence compared to the baseline. Rows/columns show the coherence difference in different frequency/time windows. It is now clear that main coherence changes occur in the [0 8] Hz frequency band in all time windows and in the [8 13] Hz band in the [0.5 1] s time window. Significant analyses were applied to find out if these changes are significant or random.

Fridman's test was then applied to the coherence value of each channel pair in each frequency band over time on the whole cohort of subjects. If Friedman's test showed a significant coherence change ($p<0.05$) between two channels, post-hoc analyses (Tukey's test) was applied to find which (or if any) time window after the onset is significantly

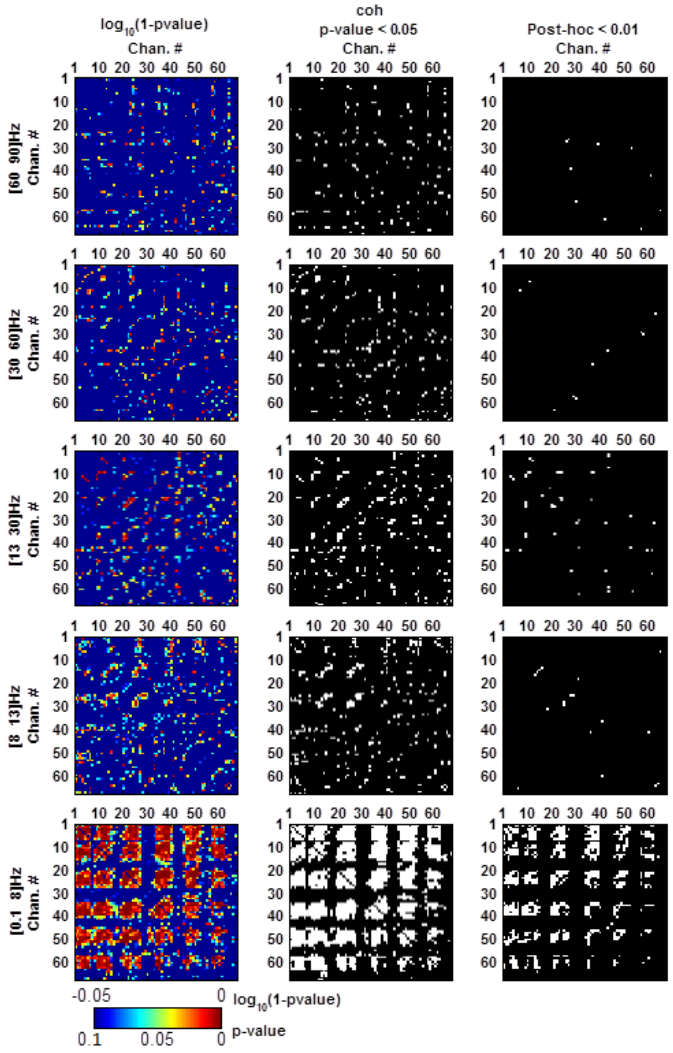

Figure 6.6: Words played to the right ear: Results of Friedman's test. In each subfigure, rows and columns are marked by channel numbers. Left column: p-values of Friedman's rescaled to $log_{10}(1 - pvalue)$, for clearer visualisation, and colour coded. Zero (dark red), -0.0223, and -0.05 (dark blue) correspond to p-values of 0, 0.05, and 0.1, respectively. Middle column: channel pairs with significant coherence change ($p<0.05$) are marked by white dots. Right column: channel pairs with significant ($p<0.01$) coherence change (in at least one window after the onset) from the baseline are marked by white dots.

($p<0.01$) different from the baseline. Figure 6.6 shows the results of these steps. In this figure, x and y axes show channel numbers. Left column shows p-values of Friedman's test rescaled to $log_{10}(1 - pvalue)$ for clearer visualisation. Red/blue indicate a small-/large p-value. The middle column specifies channel pairs with Friedman's p-value<0.05 (i.e. significant coherence difference among all time windows). After post-hoc analyses, the right column identifies channel pairs that show significant ($p<0.01$) coherence change after the onset (in at least one time window) compared to the baseline. It can be seen that there is a significant coherence change in the [0 8] Hz band compared to the baseline but the changes in other frequency bands seem to be rather random.

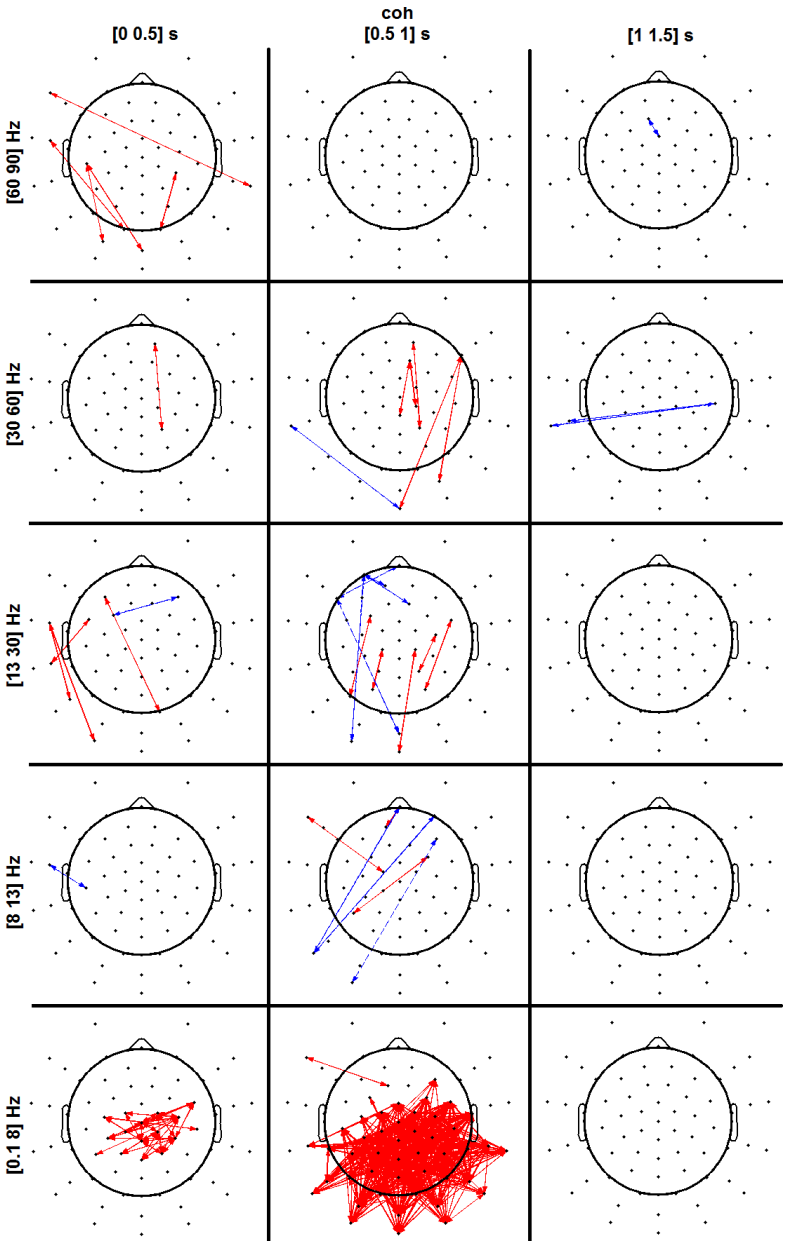

Figure 6.7: Words played to the right ear: Significant coherence changes from the baseline (Friedman's test, $p<0.05$ - Tukey's test, $p<0.01$) in pairs of electrodes in different time-frequency windows are marked by arrows. Red/blue arrows indicate increase/decrease in the coherence compared to the baseline. The stimulus onset occurs at zero seconds.

For the results to be clearer, i.e. to indicate which time windows and brain areas show the most coherence change or if the change is an increase or a decrease, the results were plotted over time using arrows as in Figure 6.7. This figure shows the same time-frequency windows as in Figure 6.5. Only pairs that show a significant change in the coherence from the baseline (as indicated by the post-hoc tests) are identified using arrows. Red/blue indicates an increase/decrease compared to the baseline value. The onset of the stimulus occurs at zero seconds. Each subfigure is an axial view of the head.

Although it was expected that there would be a few false-positives in each time-frequency window, the number of significant arrows in the [0 8] Hz and the [0 1] s windows is again notable. Therefore, there seems to be an increase in the coherence at first in central areas and then in posterior areas (concentrated towards the right side). These results thus agree with those from induced response power analyses.

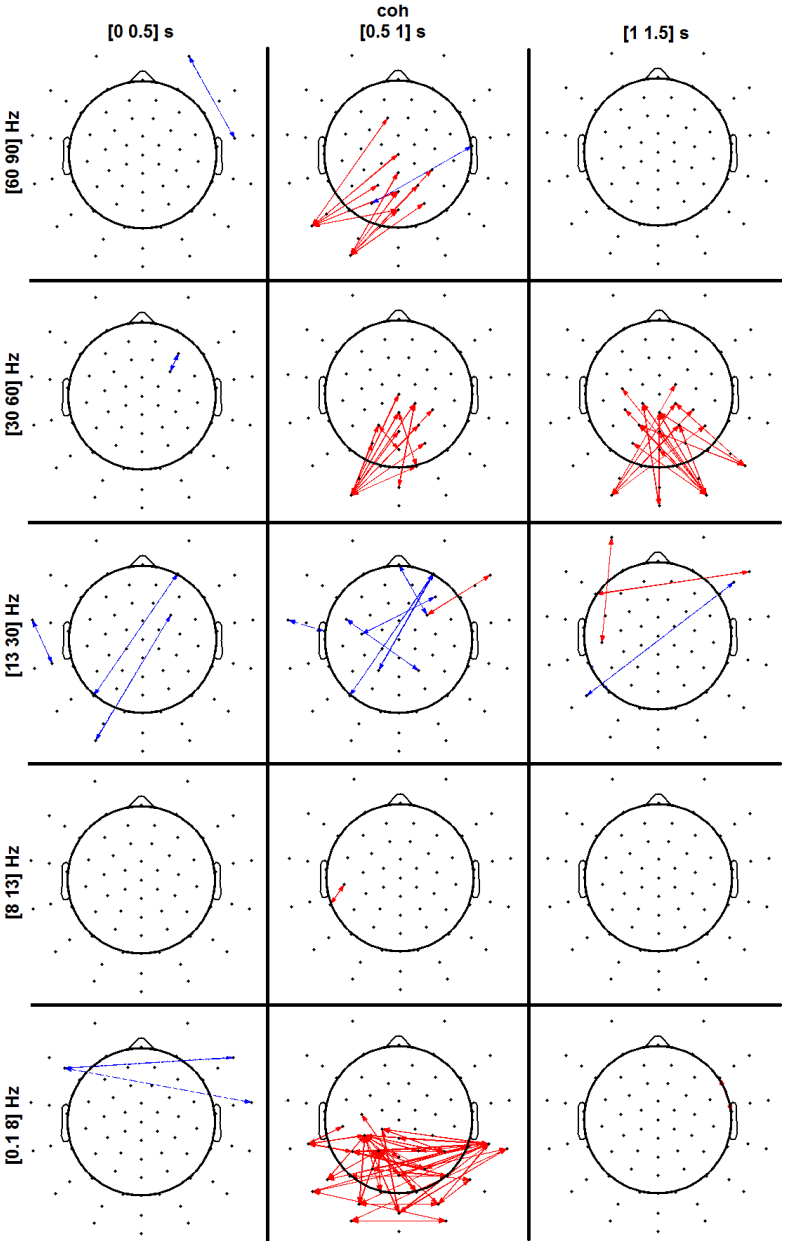

Figure 6.8: Words played to the left ear: Significant coherence changes from the baseline (Friedman's test, $p<0.05$ - Tukey's test, $p<0.01$) in pairs of electrodes in different time-frequency windows are marked by arrows. Red/blue arrows indicate increase/decrease in the coherence compared to the baseline. The stimulus onset occurs at zero seconds.

To check the reliability of the results, three datasets were generated by randomly selecting 50 epochs out of the set of 100 epochs of each subject (with words played to the right

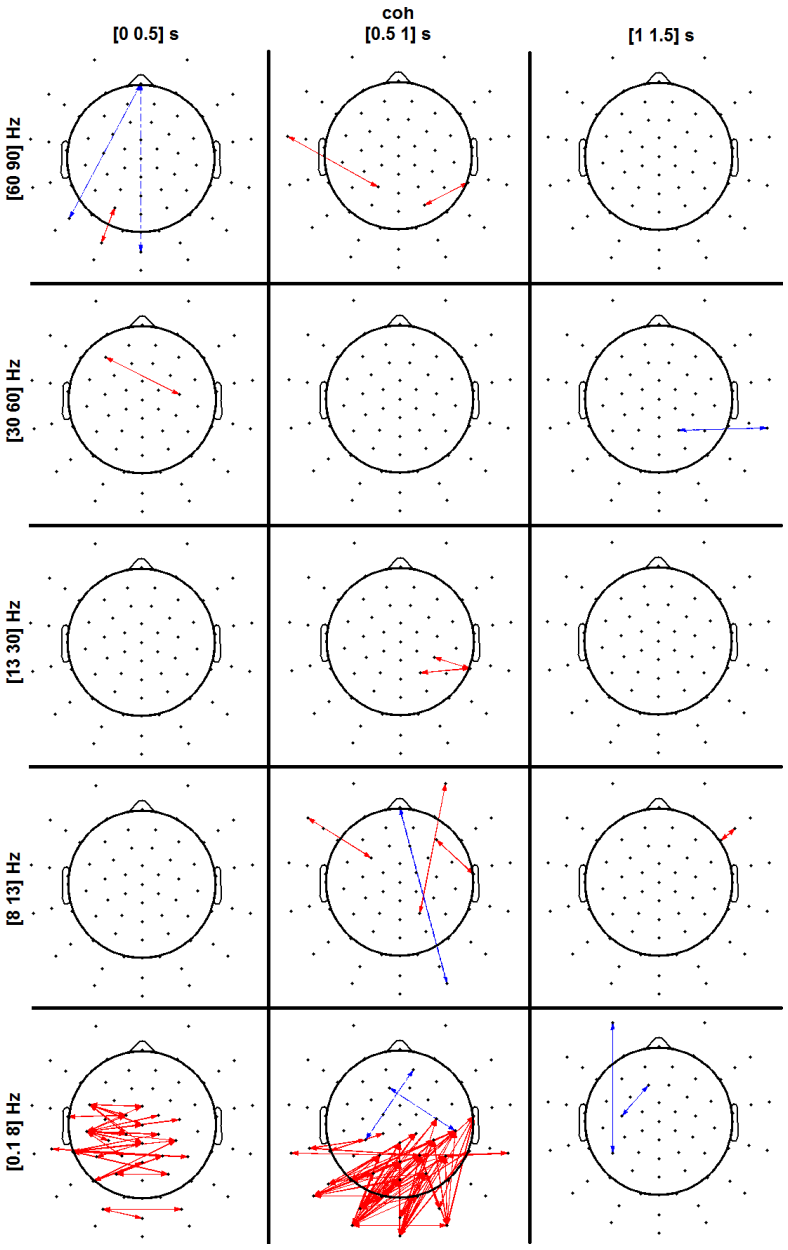

Figure 6.9: Words played binaurally: Significant coherence changes from the baseline (Friedman's test, $p<0.05$ - Tukey's test, $p<0.01$) in pairs of electrodes in different time-frequency windows are marked by arrows. Red/blue arrows indicate increase/decrease in the coherence compared to the baseline. The stimulus onset occurs at zero seconds.

ear) and the same coherence procedure was repeated on these datasets. Every time, the same result was obtained: there was a significant increase in the coherence in the [0 8] Hz band in the [0.5 1] s window compared to the baseline coherence.

Also, similar results were obtained by applying the same procedure on EEG data recorded in response to words played to the left ear or binaurally. The results of these experiments are plotted in Figures 6.8 and 6.9. Although the number of channel pairs showing significant coherence changes is different in these figures and the change is not

as clear as in Figure 6.7, it is still clear that there is a notable change in the [0 8] Hz and the [0 1] s windows. These results are all in line with those obtained with power analyses, i.e. strong induced activity for words played to the right ear and a decrease in this activity when played binaurally and another decrease when played to the left ear. This result along with the results obtained from random selection of epochs confirms the repeatability of results.

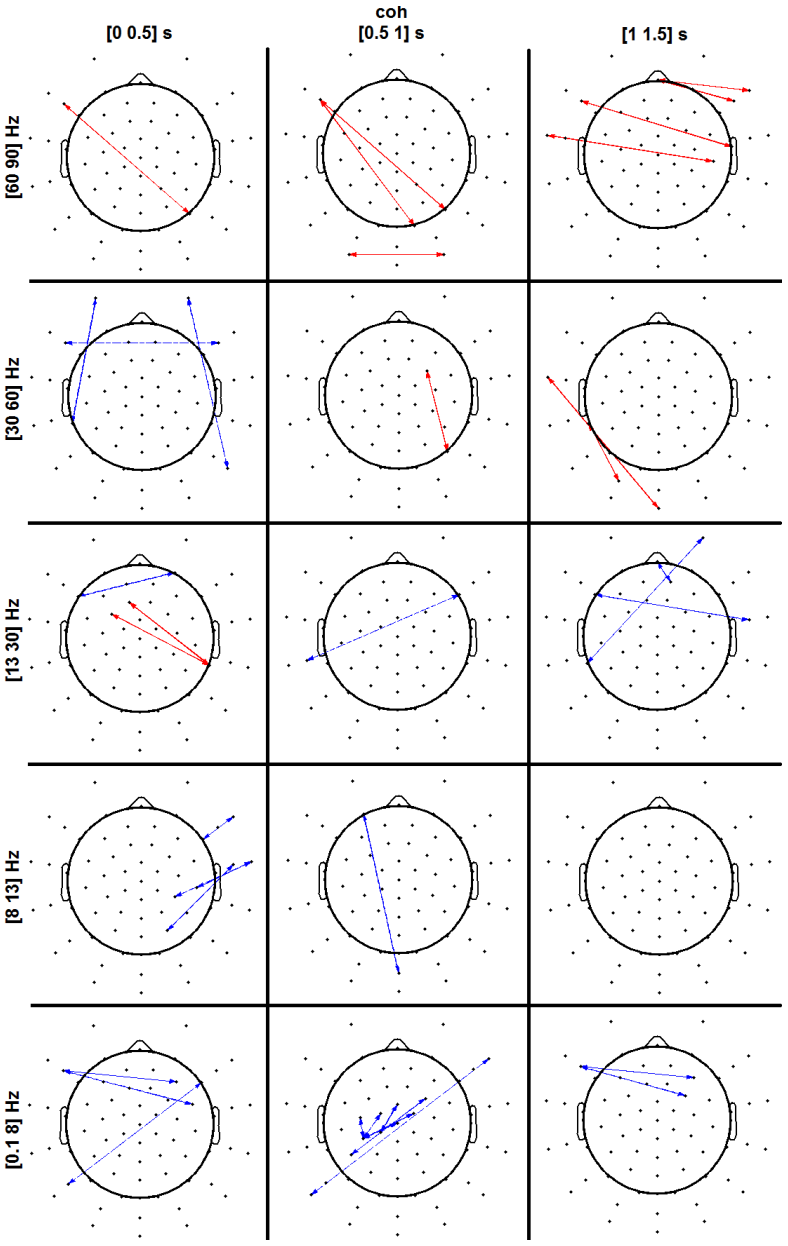

Figure 6.10: 80 Hz modulated tone played to the right ear: Significant coherence changes from the baseline (Friedman's test, $p<0.05$ - Tukey's test, $p<0.01$) in pairs of electrodes in different time-frequency windows are marked by arrows. Red/blue arrows indicate increase/decrease in the coherence compared to the baseline. The stimulus onset occurs at zero seconds.

6.4.3 Coherence in response to AM tones

The same procedure as in word and tone burst stimuli were employed for calculating the coherence (in 500 ms non-overlapping windows starting from 500 ms before the onset and ending at 1.5 s after the onset) and investigating the significance of its change over time for amplitude modulated tones when played to the right ear. Amplitude modulated tones are believed to induce an increase in the power of the EEG at the modulation frequency (Hall, 2007). Therefore, at first, the frequency bands of [10 20] Hz and [75 85] Hz were selected for coherence averaging for 15 Hz and 80 Hz modulated tones, respectively. However, no significant change of coherence was observed in these frequency bands in time windows after the onset compared to the baseline.

Thus, the set frequencies of Figure 4.1 were used for averaging the coherence and similar significance analyses as used in sections 6.4.1 and 6.4.2 were applied on these averaged coherence values. Still, in both 15 Hz and 80 Hz modulated tones when played to the right ear or binaurally, only a few connections showed significant change of coherence in each time-frequency window. These connections could not be easily considered as a response as they did for word stimulus because they are rather scattered and are not consistent between the right ear and binaural presentation. An example of these results is presented in Figure 6.10 for the 80 Hz AM tone when played to the right ear. As the rest of the results obtained from AM tones are very similar to this figure, they have not been presented here.

6.4.4 Coherence in response to sentences

The same steps as in previous stimuli were followed to calculate the coherence in response to sentences and find out the significant coherence changes after the onset compared to the baseline in response to this stimulus. The coherence was calculated in 1 s non-overlapping windows starting from 1 s before the onset and ending at 3 s after the onset.

Significance analyses were then applied using Friedman's test and post-hoc analyses. Figures 6.11, 6.12, and 6.13 show the significant coherence changes for the right and left ear and binaural presentation, respectively, using arrows. Red/blue arrows show significant increase/decrease in the coherence compared to the baseline. These figures show that when sentences are played binaurally, there is a clear increase in the coherence in lower frequency bands, i.e. [0 8] Hz and [8 13] Hz respectively, lasting for about 2 s after the onset. However, no clear significant change was observed when sentences were played to the left ear. The results from coherence analyses are very similar to those obtained from power analyses for EEG in response to sentences (see section 4.3.4) and demonstrate a consistent pattern of brain activity following stimulation with sentences.

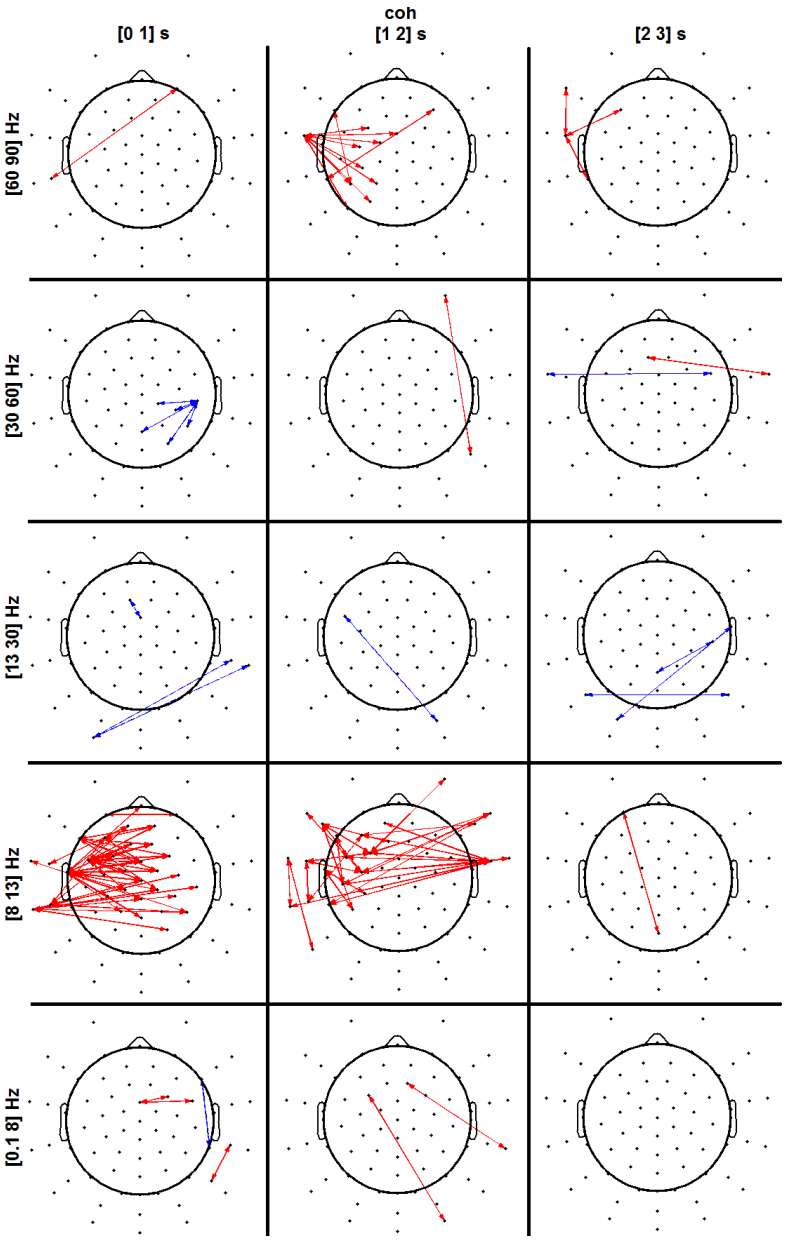

Figure 6.11: Sentences played to the right ear: Significant coherence changes from the baseline (Friedman's test, $p<0.05$ - Tukey's test, $p<0.01$) in pairs of electrodes in different time-frequency windows are marked by arrows. Red/blue arrows indicate increase/decrease in the coherence compared to the baseline. Thicker arrows indicate larger difference from the baseline. The stimulus onset occurs at zero seconds.

6.5 Discussion

In this chapter, the coherence between all pairs of EEG channels was calculated for different time windows before and after the onset of different types of acoustic stimulation. The significance of coherence change over time across the cohort of subjects was then investigated. These analyses were performed for various stimulus types separately and it

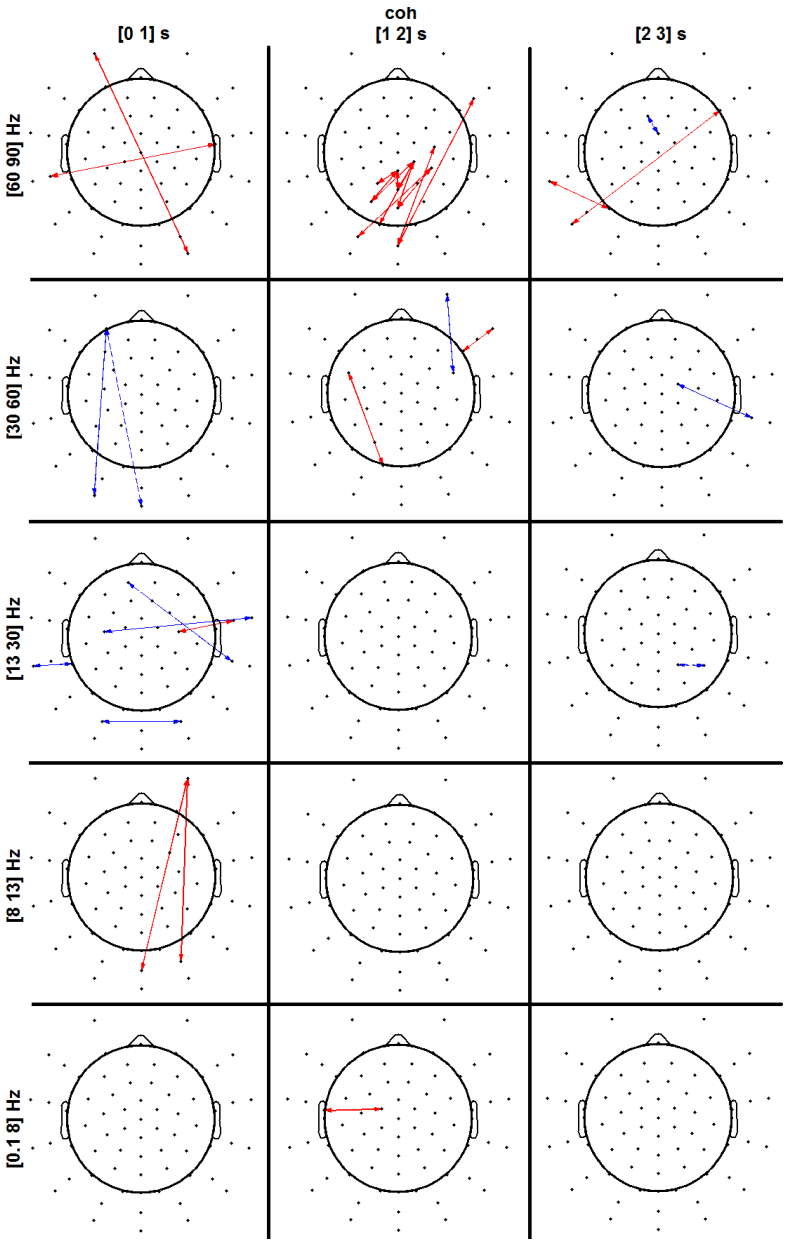

Figure 6.12: Sentences played to the left ear: Significant coherence changes from the baseline (Friedman's test, $p<0.05$ - Tukey's test, $p<0.01$) in pairs of electrodes in different time-frequency windows are marked by arrows. Red/blue arrows indicate increase/decrease in the coherence compared to the baseline. Thicker arrows indicate larger difference from the baseline. The stimulus onset occurs at zero seconds.

should be noted that before estimating the coherence, the evoked activity was subtracted from each epoch thus we were left with only the induced responses. The phase-locked activity was removed as we were primarily interested in the non-phase-locked activity. Also, for the results to be comparable to those achieved using model-based connectivity analyses (see chapter 7), the evoked response had to be removed as the first step to make the mean of the signal stationary.

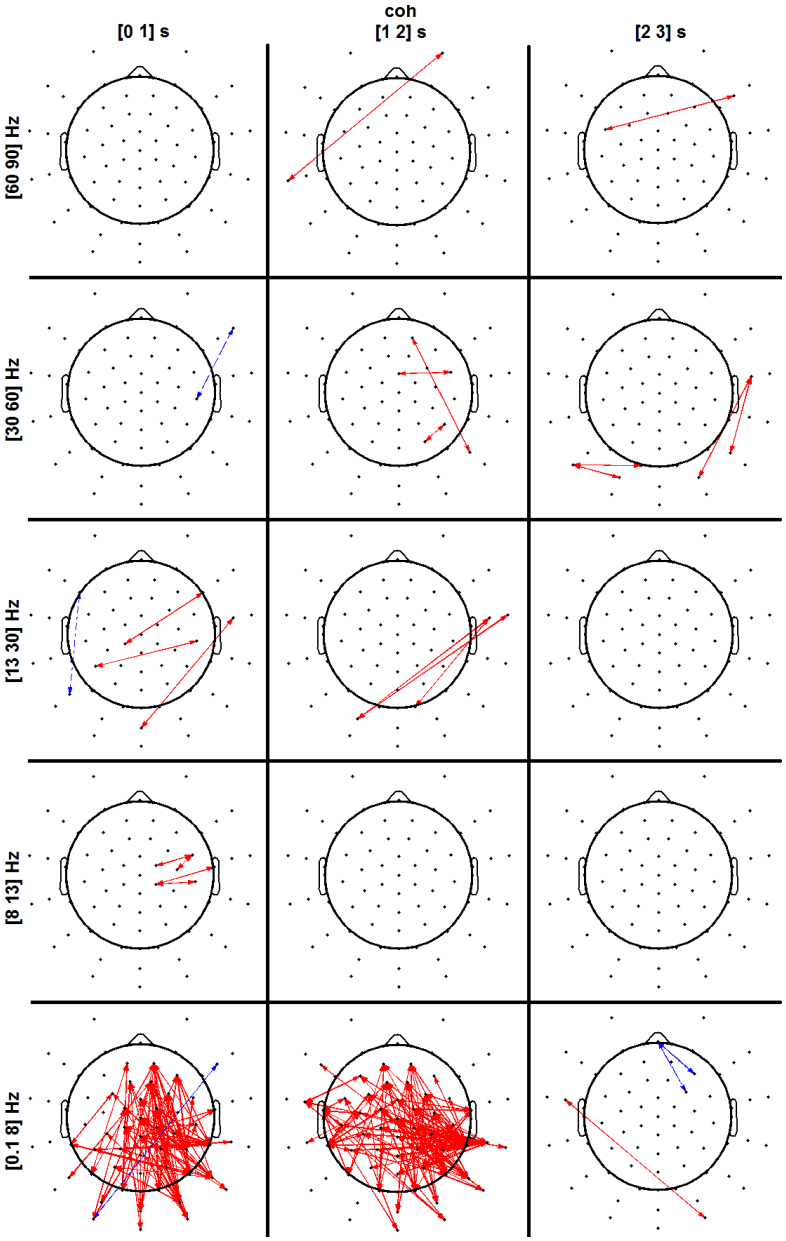

Figure 6.13: Sentences played binaurally: Significant coherence changes from the baseline (Friedman's test, $p<0.05$ - Tukey's test, $p<0.01$) in pairs of electrodes in different time-frequency windows are marked by arrows. Red/blue arrows indicate increase/decrease in the coherence compared to the baseline. Thicker arrows indicate larger difference from the baseline. The stimulus onset occurs at zero seconds.

There were three main reasons for employing pairwise coherence: 1) as a dimension reduction approach, to find the most correlated electrodes and select them for analyses of connectivity (in chapter 7), 2) to lay out a basis for comparing the results obtained from model-based connectivity analyses and determine which of the methods is more appropriate, and 3) to investigate if coherence analyses are stronger techniques than power analyses in detecting event related changes in EEG signals.

Unlike power analyses that could not detect any induced activity in response to tone bursts (see Figure 4.6), pairwise coherence reported a clear change of activity in the beta band in the [0.2 0.6] s time range (see Figure 6.4), where an increase in posterior and a decrease in frontal areas was observed. The role of beta activity is not clear in auditory tasks, however, beta de-synchronisation has been shown to be present in some auditory oddball and language perception studies (Kim and Chung, 2008; Hirata et al., 2007; Weiss and Rappelsberger, 2000). Although the nature of the auditory task here is different from these studies, observing a significant change in beta bands in response to tone bursts does not seem unreasonable. The difference between the results from the two methods (power and coherence) may imply either/or that the coherence is a more sensitive method than power analyses (as Simpson et al. (2000) also claims) for detecting induced activity in the signal, or that there really was no increase/decrease in the power in the beta frequency band but rather only a phase resetting in the [0.2 0.6] s time range which could be picked by coherence analyses but not power analyses. Phase resetting leads to a time shift in background EEG activity in a specific frequency band (Makeig et al., 2002), and thus produces a phase-locked response to the stimulus without any increase in the power of that frequency band (refer to Figure 2.5.c). This type of response, is not detectable by power analyses but reflected only in phase information (Fuentemilla et al., 2006, 2008). It is thus possible that the observed change in the coherence is caused by phase resetting in background EEG in response to the stimulus. However, in appendix B, sections B.3.4 and B.4.2.5, phase synchronisation to the stimulus onset was simulated and it was shown that if there was any phase synchronisation to the stimulus at a given time, it would present itself as an increase in the evoked power and at the same time a decrease in the induced power at that time. As no change was observed in either the evoked or the induced power in response to tone bursts (section 4.3.1) in the beta band in the [0.2 0.6] s time range, it is quite possible that the change in coherence does not occur because of phase synchronisation. Another explanation might be that there is slight time shift, causing phase shift, between stimuli (Tallon-Baudry and Bertrand, 1999; David et al., 2006b; Gruber et al., 2006), but such shift is coherent between different channels. Whatever the reason for this coherence increase in the beta frequency band, the results of this chapter show that some response other than just the evoked response occurs in the brain in response to simple tone bursts.

Coherence estimates from the EEG in response to words showed that there is an increase in the coherence in the [0 8] Hz frequency band in the [0 1] s time range which is a confirmation of the results obtained from power analyses. These changes were seen in electrode pairs falling behind the coronal pane tending towards the right hemisphere when words were played to the right ear and tending towards the left hemisphere when words were played to the left ear (refer to Figures 6.7, 6.8, and 6.9). The main speech and language related areas close to these electrodes are right and left superior temporal gyri that encompass auditory cortices and Wernicke's area. The reason that fewer number

of connections are selected in the left ear and binaural presentation cases compared to the right ear might be due to numerous reasons such as different combinations of words played, lower SNR, or in fact different reaction of the brain to speech depending on which ear the sound is being presented to. It was discussed in chapter 4 that other EEG studies (Bastiaansen et al., 2002; Bastiaansen and Hagoort, 2006) have shown the existence of induced response in lower frequency bands in response to speech stimuli such as targeted words in specifically designed sentences. In a review paper, Weiss and Mueller (2003) also showed that low frequency bands such as delta, theta, and alpha respond to German names, nouns, and verb presentations and show higher coherence values compared to the resting EEG although the procedure of word presentation is not explained in the paper. However, they concluded that the categorical differences between different words, such as verbs versus nouns or concrete versus abstract nouns, present themselves in higher frequency bands whereas lower frequency bands, i.e. [1 10] Hz, reflect only non-specific components of words such as attentional and basic semantic parts of the task (Weiss and Mueller, 2003). In this chapter, similar analyses were also applied to data generated by randomly selecting epochs from EEG data in response to words presented to the right ear, the results are not presented. The results were consistent with those obtained from the original EEG, i.e. significant coherence changes in the [0 8] Hz frequency band in the first second after the stimulus. Although it is not possible to say which electrodes are mostly affected by word presentation in our study, it is reasonable to say that a few of these electrodes can be representative of all of them. For this reason, instead of using all electrodes for connectivity analyses, a few of them will be selected in a symmetrical manner and used in the next chapter.

No clear change was observed in the coherence in response to AM tones. Whilst we can not reject the null hypothesis of no response, we cannot be sure that there is no small response that our methods were not sensitive enough to detect.

No clear significant change in coherence was observed when sentences were played to the left ear but the first two 1 s windows after the onset showed significant increase in the coherence in lower frequency bands when sentences were presented to the right ear and binaurally. This appears consistent with the results from words. In right ear presentation, the significant frequency band is different to that of power analyses which can be caused because of the difference in frequency resolution between the two methods. So there is some indication of asymmetry in the brain response (at least as regards the EEG) having different reactions depending on the presentation ear. The results from coherence analyses are in line with the results obtained from power analyses. Lower frequency bands (specially theta) have been shown to be associated with language related tasks in specific sentence presentation protocols (Bastiaansen et al., 2002; Schack and Weiss, 2005; Bastiaansen and Hagoort, 2006) which agrees with the current work. However, the reason behind the difference observed when sentences were played to different ears is not clear.

Overall from the results in this chapter, we can not conclude that coherence is a more sensitive measure than power analyses in detecting induced activity, however, it is clear that coherence can present more information about the response, like in tone bursts, than power analyses. Also, coherence analyses could give a better understanding of the event-related relationships between different electrodes which could help us decide how to select fewer electrodes from the whole dataset for further connectivity analyses.

6.6 Summary

In this chapter, pairwise coherence was estimated in different time-frequency windows between all channel pairs of EEG datasets to explore induced activity following auditory stimulation. It was shown that an increase in the coherence occurs in the [0 1] s post-stimulus window in the [0 8] Hz frequency band in response to words and in the [0.2 0.6] s post-stimulus window in beta band in response to tone bursts. Both these responses were more concentrated in the posterior areas rather than frontal ones and the results from different ear presentations were consistent for words. No obvious change of coherence pattern was observed in AM tones and some inconsistent (depending on the presentation ear and in comparison to power analyses) coherence patterns were observed in response to sentences. In summary, it was concluded that coherence analysis can act as a complementary approach to power analyses in studies that target the response in the data.

The results of this chapter can now be used as a comparison basis for the results of model based connectivity analyses which will be presented in chapter 7. Also, pairwise coherence analyses can help in understanding the relationships between different electrodes in response to various types of stimuli and may be beneficial in selecting which electrodes to include for subsequent connectivity analyses because (as it will be shown in the next chapter) model based connectivity analyses can only work on a limited number of electrodes.

Chapter 7

Connectivity and Multivariate Autoregressive Modelling

7.1 Introduction

As explained in chapter 2, there are many linear and nonlinear causality methods that are being applied to EEG signals with the purpose of detecting the direction of information flow in the brain while performing a specific task. The current research focuses on applying these methods on the brain signal recorded during auditory stimulation.

The initial connectivity method selected in this project was DCM which was shown in chapter 5 to be unreliable for the purpose of the current research. This was dropped and replaced with Multi-Variate Auto-Regressive (MVAR) based measures which are discussed in this chapter. The key difference between the methods and those in the previous chapter is that those only considered connectivity, without taking the direction of information flow into account.

It was discussed in chapter 2 that one of the most widely used approaches to multi-channel causality analyses is based on GC (Granger, 1969) and the fact that if one signal can be predicted from past values of a second signal better than it is predicted from its own past values, then it can be inferred that the first signal is (Granger) caused by the second signal. GC was extended to multi-channel methods (Korzeniewska et al., 2003; Baccala and Sameshima, 2001) that inspect the causality of signals in multiple channels and does so in the frequency domain. The main assumption behind these methods is that the signals in all the channels form an MVAR model in which the present value of each channel signal can be predicted from the past values of the same channel and all other channels. We are most interested in linear multivariate modelling as this can be simply implemented and the number of prior assumptions is much smaller than most

nonlinear methods. It was decided to start with these methods and if needed add extra information to our findings using nonlinear and more complex techniques.

In recent years, MVAR-based approaches have been used on EEG, Local Field Potentials (LFP), and Electrocorticography (ECoG) signals for different purposes such as distinguishing between visually presented congruent and incongruent words (Astolfi et al., 2007), imagining the movement of a specific limb (Schlögl and Supp, 2006), visual face-versus-car discrimination (Philiastides and Sajda, 2006), and muscle contraction (Korzeniewska et al., 2011) tasks but only a limited number of studies have focused on auditory related tasks (Brancucci et al., 2005; Gourévitch et al., 2006; Giannakakis and Nikita, 2008; Korzeniewska et al., 2008, 2011; Sun et al., 2009) among which only a few worked with EEG (Brancucci et al., 2005; Sun et al., 2009; Giannakakis and Nikita, 2008) rather than LFP or ECoG. Brancucci et al. (2005) showed that there is an increase in the connection from the right to the left hemisphere in response to dichotic tones in a 3-channel MVAR model. Giannakakis and Nikita (2008) fitted an 11-channel MVAR on nonstationary evoked EEG in response to pure tones in a memorising task, introduced a new approach for estimating these MVAR parameters as they were fitted to nonstationary signals, and only demonstrated the connectivity between two of these channels to show that their approach worked adequately according to their standards. Sun et al. (2009) presented participants with audiovisual tasks and identified a connection responsible for audiovisual integration.

Some of these MVAR models are explained and implemented in the current chapter and applied on simulated data to test and evaluate the performance of the algorithms. The methods were then applied on recorded EEG data in response to auditory stimuli with the purpose of finding the connections responsible for access to speech in the brain.

7.2 Multi-Variate Auto-Regressive models

7.2.1 Defining the equation

In linear MVAR methods of N-channel EEG data, an MVAR process will be fitted to the multi-channel data as in Equation 7.1 (Astolfi et al., 2007), assuming that the data are stationary and the system is stable:

$$\sum_{j=0}^{p} A_j Y[k-j] = E[k], \tag{7.1}$$

in which, Y is assumed to be the observed EEG data and defined as:

$$Y = [y_1[k], y_2[k], ..., y_N[k]]^T, \tag{7.2}$$

where y_i is the signal in the i^{th} $(i = 1, 2, \ldots, N)$ channel of recorded EEG, A_j's are $N \times N$ matrices of model parameters with $A_0 = I$, p is the model order which is the number of time lags used for prediction of the present value, and $E[k] = [e_1[k], e_2[k], \ldots, e_N[k]]^T$ is zero-mean uncorrelated white noise in N channels with a nonsingular autocovariance matrix Σ_e. In other words, this model assumes that there are N uncorrelated white noise sources inside the brain which are combined linearly by A_j matrices and have generated the EEG data.

7.2.2 Model order

The order of the model can be estimated using different criteria (Lütkepohl, 1991). These criteria consider both the accuracy of fit and the complexity of the model at the same time, where the former is calculated by the autocovariance of residuals E after model estimation and the latter by the number of free parameters of the model. To use these criteria, a series of models with different model orders are fitted to the data (e.g. EEG) and the parameters of the models are estimated separately. Then, for each model order, the specified criterion, e.g. Akaike Information Criterion (AIC), is calculated. The model order that produces the lowest value for this criterion is then considered the best model order for that set of data, i.e. a model that does not have too many parameters but produces a low estimation error.

Each of the existing criteria in the literature may outperform the others depending on the sample size of data, i.e. the number of data points used for estimating the model. For example, Final Prediction Error (FPE) criterion works better than AIC in very small sample sizes but for moderate sample sizes, AIC might be a better choice than FPE (Lütkepohl, 1991). Unfortunately, there is no clear definition of small, moderate, or large sample sizes in the literature. Furthermore, in more complicated systems such as the EEG, these methods will only help to find an approximation of the model order and this reported order usually changes from one method to the other. As AIC and another method termed the Bayesian Information Criterion (BIC) (Porcaro et al., 2009) have been most widely used in EEG related studies and the results in the literature do not appear to be conclusive as to which method is better than the other, we chose both AIC and BIC for our model selection. These criteria are presented in Equations 7.3 and 7.4 (Lütkepohl, 1991):

$$AIC(p) = ln|\Sigma_e| + \frac{2pN^2}{KT}, \tag{7.3}$$

$$BIC(p) = ln|\Sigma_e| + \frac{ln(KT)}{KT}pN^2, \tag{7.4}$$

in which Σ_e is the autocovariance matrix of E in Equation 7.1 and $|.|$ denotes its determinant. p, N, K, and T indicate the model order, the number of channels, the number of epochs, and the number of time points in each epoch, respectively. In this equation, the first term calculates the accuracy of fit and the second term calculates the number of free parameters. With increasing model order p, the first term decreases, but the second term increases, such that there is a minimum which provides the optimal model order.

7.2.3 Estimating model parameters

The A_j's can be estimated using different estimation methods and approaches such as multichannel Yule-Walker and multi-variate Burg-type methods (Schlögl, 2006). Schlögl (2006) simulated some training and testing EEG data and showed that when there are a large number of data samples for estimating the parameters, all the widely used MVAR estimation methods produce similar prediction errors. However, if the number of data points is small, then the Burg-type methods such as the Vieira-Morf method (Morf et al., 1978) give the lowest estimation error among tested methods. For this reason, we opted for the Vieira-Morf method, the algorithm of which was implemented in *mvar.m* (Omidvarnia, A., 2011) file accessible from MATLAB File Exchange website and was used in this study after minor modifications to be used for multi-epoch datasets.

In the Vieira-Morf method, a forward and a backward error are defined using the data and the aim is to minimise these errors (Morf et al., 1978; Brockwell et al., 2005). For this purpose, a recursive approach is employed. In each step, the parameters of one order are calculated, a modification parameter which is called the reflection coefficient is computed using the correlation coefficients of the data, and the parameters of the previous orders are modified using this reflection coefficient. This process is repeated until the algorithm reaches the full order of the model (Morf et al., 1978; Brockwell et al., 2005). For multi-epoch data, a modified version of parameter estimation will be employed (Ding et al., 2000) where an averaged correlation matrix over all epochs will be used for parameter estimation in each step.

The number of unknown parameters of the model is pN^2 where p is the model order and N is the number of EEG channels. Theoretically, to estimate pN^2 parameters, pN^2 data points should be sufficient, however, in practice, this is not the case. As a rule of thumb, in practice, the number of available data points (NTK where N is the number of channels, T is the number of time points in one epoch, and K is the number of epochs) should be at least 10 times the total number of parameters (Korzeniewska et al., 2008; Boatman-Reich et al., 2010).

7.2.4 The transfer function

After the A_j matrices are estimated, for subsequent spectral analysis and to compute different connectivity measures, Equation 7.1 is transformed to the frequency domain using $A(f) = \sum_{j=0}^{p} A_j e^{-i2\pi j \frac{f}{F_s}}$ in which F_s is the sampling frequency (Astolfi et al., 2007). This then gives:

$$A(f)Y(f) = E(f), \tag{7.5}$$

in which A, Y, and E are the frequency representation of the same variables as in Equation 7.1.

The transfer function $H(f)$ can then be calculated as $A^{-1}(f)$. $H(f)$ at each frequency point is an $N \times N$ matrix in which H_{ij} represents the transfer function from the j^{th} channel to the i^{th} one. Equation 7.5 can then be written as:

$$Y(f) = H(f)E(f). \tag{7.6}$$

As explained before, E is the residual noise which is the contribution made by each channel that cannot be explained by any other channel or past samples of this channel.

After determining $H(f)$, different connectivity measures can be estimated some of which will be explained in section 7.3.

7.2.5 Validity of the model

After A_js are estimated, before calculating any connectivity measures using these parameters and the ensuing $H(f)$ matrix, the validity of the model estimation should be explored (Lütkepohl, 1991; Ding et al., 2000). This goal is usually achieved by checking both the whiteness of residuals of the model and the stability of the estimated parameters. The whiteness test ensures that there is no additional relationship between different channels over time which could not be explained by the estimated parameters, and stability ensures that the system will not diverge to infinity when driven by the input noise.

7.2.5.1 Test of whiteness

There are different methods for testing the whiteness of residuals (Lütkepohl, 1991) after model estimation. These methods usually define a test statistic which can be calculated

using the number of data points available for estimating the model and the correlation function values of the residuals over a predefined number of lags. The asymptotic distribution of this statistic is known. Then, using the value of the statistic computed from the results of estimation together with the predefined significance level, one can infer if the residuals obtained are white or not. The difference between the methods is in how the statistic is defined.

Each of the available statistics have their own advantages and disadvantages. For example, Auto-Correlation Function (ACF) method assumes that the auto-correlation function of white noise follows a normal distribution $N(0, \frac{1}{\sqrt{KT}})$, K and T being the number of epochs and data points in each epoch, respectively. To identify whether the residuals are white, a significance level is defined (say 5%) and a threshold is calculated for the values of the correlation function, e.g. for 5% it would be $\pm\frac{1.96}{\sqrt{KT}}$. If the number of coefficients of the correlation function over time which fall outside this threshold are more than the significance level (5% in this example), the null hypothesis of "residuals are white" is rejected. ACF is a very popular method because of its simplicity, however, it is a very conservative method (it rejects the null hypothesis less often than expected when the hypothesis is true) especially when the sample size is small (Lütkepohl, 1991).

A set of tests such as Box-Pierce (BP), Ljung-Box (LB), and Li-Mcleod (LM) (Lütkepohl, 1991; Miguel A. Arranz, 2005) commonly known as Portmanteau tests were thus introduced by different researchers all of which are supposed to asymptotically follow a χ^2 distribution with $N^2(h-p)$ degrees of freedom where N, h, and p are the number of channels, the number of lags for calculating the autocorrelation function, and the model order, respectively. These methods are not as simple as ACF to implement but they are less conservative than ACF. Even among these methods (Lütkepohl, 1991; Miguel A. Arranz, 2005), the level of conservativeness is different depending on the sample size and it has been shown that LB and LM tests have better properties than their predecessors in that their distribution in small samples are much closer to the asymptotic distribution. However, there needs to be a trade-off for selecting one of these two methods regarding their sensitivity in large samples and the variance of the distribution of the test statistic.

Still, as for the case of model order selection, there is no best method available for EEG data thus we decided to select LB. This test statistic is presented in Equation 7.7 and as explained above follows the χ^2 distribution with $N^2(h-p)$ degrees of freedom (Lütkepohl, 1991).

$$Q_h = KT'(KT'+2)\sum_{i=1}^{h}\frac{1}{KT'-i}tr(C_i'C_0^{-1}C_iC_0^{-1}), \tag{7.7}$$

in which Q_h is the LB statistic for h correlation lags. tr denotes the trace of the matrix, i.e. the sum of the elements on the main diagonal, K represents the number of epochs,

and $T' = T - p$, i.e. the number of data points that were used for calculating the covariance matrix C in each epoch. C_0 is the covariance matrix at lag zero and C_is are covariance matrices in lags $i = 1, \ldots, h$.

7.2.5.2 Test of stability

An MVAR model is deemed to be stable if the poles of its transfer function are all situated inside the unit circle. This fact can be tested by finding the roots of its characteristic polynomial $det(I - Cz^{-1}) = 0$ and showing that they all fall inside the unit circle (Lütkepohl, 1991) where C can be defined as Equation 7.8. The roots of this equation are also the eigenvalues of matrix C. Thus, if the absolute value of the largest eigenvalue of matrix C is smaller than 1, then it can be confirmed that the estimated model is stable (see Lütkepohl (1991) for the proof of this statement).

$$C = \begin{bmatrix} A_1 & A_2 & \ldots & A_{p-1} & A_p \\ I_N & 0 & \ldots & 0 & 0 \\ 0 & I_N & \ldots & 0 & 0 \\ \vdots & \vdots & \ddots & \vdots & \vdots \\ 0 & 0 & \ldots & I_N & 0 \end{bmatrix}_{pN \times pN}, \tag{7.8}$$

in which A_i's are matrices of model parameters for different time lags (see Equation 7.1). I_N's are $N \times N$ identity matrices with N being the number of channels. p is the model order and the size of C is $pN \times pN$.

Moreover, the condition of stability assures weakly stationarity (or Wide-Sense-Stationary (WSS)) as well (Lütkepohl, 1991). A process $Y[k]$ is WSS if its first and second moments, i.e. mean and covariance, are time independent, i.e. do not change over time. If the eigenvalues of C are all inside the unit circle, it can be shown that the time dependent factors in the mean and covariance equations are eliminated thus, the process is weakly stationary. Therefore, by testing the stability of estimated parameters, we can ensure that the process is stationary as well. Of course, this does not prove that the EEG from which this is estimated, is stationary.

After it is specified that the estimated parameters form a stable model and the residuals are white, $H(f)$ can be calculated and employed in computing various types of connectivity measures. These measures are explained in more detail in the following sections along with tests on synthetically generated data and their applications on recorded signals.

7.3 Connectivity measures

There are various connectivity measures that can be derived from MVAR-based model parameters. Each of these measures have their own advantages and disadvantages which will be explained along with the definition of some of these measures in the following subsections.

7.3.1 Pairwise Coherence

As explained in section 6.2.1, coherence between two signals identifies how much one signal has contributed to the other one but it will not provide any information about the direction of the information flow. The non-parametric coherence was explained in chapter 6. The model based coherence that can be derived from MVAR based parameters is presented in Equation 7.9 and can be used to compare the results with the non-parametric ones. This is another approach for determining that the MVAR parameters have been estimated properly. We can then move on to causality measures as explained in the following subsections.

$$Coh_{ij}(f) = \frac{S_{ij}(f)}{\sqrt{S_{ii}(f)S_{jj}(f)}}, \tag{7.9}$$

where Coh_{ij} is the coherence between channels i and j at different frequencies. $S(f)$ is the power spectrum matrix where S_{ij} specifies the cross spectrum between channels i and j and S_{ii} specifies the autospectrum of channel i. $S(f)$ can be calculated by Equation 7.10:

$$S(f) = H(f)\Sigma_e H^*(f), \tag{7.10}$$

in which $*$ denotes the conjugate transpose, Σ_e is the covariance matrix of residual noise $E(t)$ in Equation 7.1, and $H(f)$ is the transfer function of the system computed using Equation 7.6.

7.3.2 Directed Transfer Function

DTF is a multivariate measure of connectivity in the frequency domain (Korzeniewska et al., 2003). DTF of channel j to i was originally introduced as the squared magnitude of ij^{th} element in $H(f)$. For easier interpretation of strengths of connections, each element of $H_{ij}(f)$ was normalised by the sum of all the elements in row i that is all the inflows to channel i from all channels. The new measure was named normalised DTF

(nDTF) but for simplicity, we will use DTF notation instead of nDTF from now on in this study. Using the transfer function of Equation 7.6, DTF coefficients are defined as:

$$DTF_{ij}(f) = \frac{|H_{ij}(f)|^2}{\sum_{m=1}^{N} |H_{im}(f)|^2}, \tag{7.11}$$

in which DTF_{ij}'s are the causal influence of j^{th} channel over i^{th} channel at a frequency f and N is the number of channels. It should be noted that $\sum_{j=1}^{N} DTF_{ij}(f) = 1$ for each f i.e. all the information flow coming to one channel sum up to 1 at each frequency. DTF is a ratio between 0 and 1, one indicating that channel i is completely caused by channel j. This method eliminates the effects of other channels from the causal relation between i and j but a disadvantage of this approach is that it cannot differentiate between direct and indirect connections because of the inversion process that is performed on $A(f)$. This fact can be explained with a simple example. Assume that we have a first order three channel model with a coefficient a_1 from area 1 to 2 and a coefficient a_2 from area 2 to 3, $A(f) = \begin{bmatrix} 1 & 0 & 0 \\ a_1 & 1 & 0 \\ 0 & a_2 & 1 \end{bmatrix}$. Obviously, there is no direct connection from area 1 to 3 meaning that $DTF_{31}(f)$ thus $H_{31}(f)$ should be zero. $H(f)$ for this example is calculated by inverting the $A(f)$ matrix. So, $H(f) = A^{-1}(f) = \frac{1}{det(A)} \begin{bmatrix} 1 & 0 & 0 \\ -a_1 & 1 & 0 \\ a_1 a_2 & -a_2 & 1 \end{bmatrix}$. As can be seen, there seems to be a connection from the area 1 to 3 when it should be zero.

7.3.3 Direct Directed Transfer Function

To surmount the problem of direct-indirect causality discussed in the preceeding section, a direct Directed Transfer Function (dDTF) was introduced which combined the directionality characteristic of DTF with the ability of PDC (which will be explained in the next subsection) in distinguishing if a connection between two signals is mediated by a third signal (Korzeniewska et al., 2003). dDTF is obtained by multiplying full frequency Directed Transfer Function (ffDTF) given by Equation 7.12 and Partial Coherence (PCoh) given by Equation 7.13. In ffDTF the normalisation of DTF is done by a double summation over all inflows to channel i from all channels and all frequencies, making the denominator a value independent of the frequency.

$$ffDTF_{ij}(f) = \sqrt{\frac{|H_{ij}(f)|^2}{\sum_f \sum_{m=1}^{N} |H_{im}(f)|^2}}, \tag{7.12}$$

in which $ffDTF_{ij}$'s are the causal influence of the j^{th} channel over the i^{th} channel at a frequency f and N is the number of channels. It should be noted that $\sum_{f}\sum_{j=1}^{N} ffDTF_{ij}^2(f) = 1$ for each channel, i.e. all the information flow coming to one channel from all frequencies sum up to 1. ffDTF cannot distinguish between direct and indirect connections but it can give the direction of information correctly. On the other hand, PCoh which is given by Equation 7.13 is not a causal measure but it is non-zero only when there is a direct relation between two signals. Therefore, multiplying the two values at each frequency will produce a causal measurement that can eliminate indirect effects.

$$PCoh_{ij}(f) = \sqrt{\frac{M_{ij}^2(f)}{M_{ii}^2(f)M_{jj}^2(f)}}, \tag{7.13}$$

where $M_{ij}(f)$ is the minor of spectral matrix $S(f)$ in Equation 7.10. The ij^{th} minor of matrix $S(f)$ is the determinant of this matrix when its i^{th} row and j^{th} column are eliminated. dDTF is then computed as:

$$dDTF_{ij}(f) = PCoh_{ij}(f).ffDTF_{ij}(f), \tag{7.14}$$

Although dDTF can both determine the causality of a connection and cancel out indirect flows to a channel, it has the problem of "marrying parents of a joint child" (Winterhalder et al., 2005) which comes from the PCoh part of its equation. Winterhalder et al. (2005) shows that if x_1 is the sum of x_2 and x_3, even though there is no direct relation between x_2 and x_3, spurious significant connection would be reported between x_2 and x_3. This effect is called "marrying parents of a joint child".

7.3.4 Partial Directed Coherence

Partial directed coherence is another frequency representation of Granger causality which has clearer frequency domain connectivity than DTF (Baccala and Sameshima, 2001). Using the same autoregressive model as explained for DTF, the ratios of connectivity are calculated as in Equation 7.15:

$$PDC_{ij}(f) = \frac{|A_{ij}(f)|}{\sqrt{\sum_{k=1}^{N} A_{kj}(f)A_{kj}^*(f)}}, \tag{7.15}$$

where A_{ij} is the ij^{th} element of matrix $A(f)$ in Equation 7.5 and PDC_{ij} is the causal influence of j^{th} channel over i^{th} channel at a frequency f where the effect of channel j

over any channel k has been eliminated. It should be noted that $\sum_{i=1}^{N} PDC_{ij}^2(f) = 1$ for each f where N is the number of channels i.e. all the information flow going out of one channel sum up to 1 at each frequency. This is a ratio between 0 and 1, one indicating that channel i is completely caused by channel j. Squared Patial Directed Coherence (sPDC) was introduced by squaring PDC coefficient to increase the sensitivity of PDC (Astolfi et al., 2006) and was shown to produce lower estimation errors when applied on simulated data.

It is worth noting that DTF and PDC can be considered simultaneously. This way, one can find the direct connections using PDC and then using DTF, follow where the information started from and ended at.

In the next section, the data on which the connectivity methods were applied are explained along with the steps taken for measuring connectivity in these data, from selecting the appropriate initial parameters such as the model order to the significance tests employed after calculating the connectivity parameters.

7.4 Materials used in connectivity analyses

In this section, the simulated data that were used for testing the reliability of the above mentioned connectivity methods will be explained. Also, the recorded data on which the connectivity methods were applied and different pre-processing steps that were employed on these data (before connectivity analyses) are described. Then, the appropriate initial model parameters such as the model order and the number of channels and how these parameters were decided upon are mentioned. The model was fitted to the data according to section 7.4.3, the parameters were estimated and the significance of calculated connectivity measures using these parameters were tested as in section 7.4.4, the results of which are presented in section 7.5.

7.4.1 Data

7.4.1.1 Simulated data

Simulated data were generated to test the validity of the connectivity measurements and their implementations.

To simulate an MVAR EEG signal, a set of parameter matrices modelling three lags of MVAR for a 5-channel data ($N = 5$) were presumed as in Equations 7.16 and 7.17 which have a connectivity pattern as in Figure 7.1. The data in the five channels were simulated by assuming a set of white noises with equal power as model inputs assuming

a 1000 Hz sampling frequency and a one-epoch or a 100-epoch dataset. More details are presented in section 7.5.1.

$$A_1 = \begin{bmatrix} 0.95 & 0 & 0 & 0 & 0 \\ 0 & 0.2 & 0 & 0 & 0 \\ 0 & 0 & 0 & 0 & 0 \\ 0 & 0 & 0 & 0.5 & 0 \\ 0 & 0 & 0 & 0.1 & 0.55 \end{bmatrix}, A_2 = \begin{bmatrix} -0.76 & 0 & 0 & 0 & 0 \\ 0.5 & -0.76 & 0 & 0 & 0 \\ 0 & 0.4 & 0 & 0 & 0 \\ 0 & -0.8 & 0 & -0.98 & 0 \\ 0 & 0 & 0 & 0.5 & -0.1 \end{bmatrix},$$
$$A_3 = \begin{bmatrix} 0 & 0 & 0 & 0 & 0 \\ 0 & 0 & 0 & 0 & 0 \\ 0 & 0 & 0 & 0 & 0 \\ 0 & 0 & 0 & 0 & 0 \\ 0 & 0 & 0 & 0 & -0.7 \end{bmatrix}. \tag{7.16}$$

$$\begin{cases} y_1[k] = 0.95y_1[k-1] - 0.76y_1[k-2] + e_1[k] \\ y_2[k] = 0.5y_1[k-2] + 0.2y_2[k-1] - 0.76y_2[k-2] + e_2[k] \\ y_3[k] = 0.4y_2[k-2] + e_3[k] \\ y_4[k] = 0.5y_4[k-1] - 0.8y_2[k-2] - 0.98y_4[k-2] + e_4[k] \\ y_5[k] = 0.1y_4[k-1] + 0.5y_4[k-2] + 0.55y_5[k-1] \\ \qquad -0.1y_5[k-2] - 0.7y_5[k-3] + e_5[k] \end{cases} \tag{7.17}$$

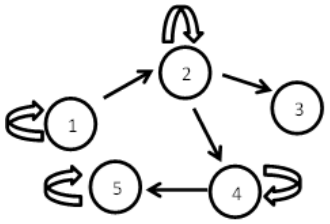

Figure 7.1: Connectivity pattern of signals presented in Equations 7.16

7.4.1.2 Recorded data

The recorded EEG data that were the main target of connectivity analyses in this chapter were the data in protocols S1 and S2 mentioned in section 3.2. This dataset was first pre-processed according to section 3.4.

The data were then either used with the 1000 Hz sampling frequency or low-pass filtered (with 100 Hz cut-off frequency) and downsampled to 250 Hz. The reason for trying both these sampling frequencies was that although most researchers downsample the data to 200-250 Hz, Porcaro et al. (2009) shows that decreasing the sampling frequency sometimes leads to missing some important connections. Porcaro et al. (2009) also shows

that using a narrow band filter would diminish the chance of picking a true connection. Furthermore, they demonstrate that increasing the cut-off frequency of the low pass filter to more than 150 Hz would destroy any evidence of connectivity completely. Thus, in our study, it was decided to use a low pass filter with a 120 Hz cut-off frequency (or in case of downsampling, a 100 Hz cut-off frequency), calculate the connectivity measures, and then average the values in different frequency bands.

The average value (over time) of each epoch was subtracted from that epoch and then the ensemble average of all epochs was subtracted from each epoch. The subtraction of the mean value is necessary for our modelling as the model assumes a zero mean process. By removing the ensemble average, the signal becomes mean stationary which is one of the requirements of MVAR modelling (Ding et al., 2000). Then, the signal in each epoch was normalised to the standard deviation (over time) of that epoch and then the values of each epoch were divided by the ensemble standard deviation of all epochs. The former was performed to equalise the effect of all epochs and the latter to make the results comparable over time. Also, dividing by the ensemble standard deviation leads to variance stationarity in the signal (Ding et al., 2000). After all this, one should be aware that the signal might still not be completely stationary.

The data were then divided to 200/500 ms non-overlapping time windows according to Figure 4.1 starting from 200/500 ms window before the onset. The length of the time window depended on the stimulus type being analysed and was the same as the lengths that were used for coherence analyses in chapter 6.1, e.g. 500 ms and 200 ms windows were used for words and tone bursts, respectively. These lengths will be mentioned again for each stimulus in the results section of this chapter.

7.4.2 Selecting the model order and number of channels

As explained in section 7.2.3, as a rule of thumb, the number of data points used for the estimation of MVAR parameters, i.e. NTK, should be at least 10 times the number of unknown parameters which is pN^2 (or $TK > 10pN$). Thus, there should be a trade-off between the number of channels that can be used for MVAR estimation and the model order. Furthermore, according to section 7.2.2, the order of the model for a specific number of channels can be decided using AIC and BIC methods.

As we were trying to compare our results with the previous chapters, the lengths of the windows were either 200/500 ms which resulted in 200/50 or 500/125 data points in each epoch for a sampling frequency of 1000 Hz or 250 Hz. Having in mind the comparability of results between different types of stimuli and also different sampling frequencies, and knowing the $TK > 10pN$ rule, different numbers of channels (13, 23, and 44) were selected symmetrically from the 66-channel data and AIC and BIC criteria

were calculated for $p = 1, .., 100$ for 500 ms windows and for $p = 1, .., 40$ for 200 ms windows. The results of AIC and BIC tests are presented in order to define methods.

For 250 Hz, AIC decreased gradually with the increase in the model order and no local minimum could be observed although around $p = 10$ the gradient of the decline in the curve started to decrease but for 1000 Hz sampling frequency, a minimum was observed around $p = 60$. On the other hand, BIC showed a minimum value and sometimes a flatness around and after model orders 10-15 for 250 Hz sampling frequency and 25-30 for 1000 Hz sampling frequency in all time windows and in all subjects. However, closer inspection showed that there was another minimum around model orders 50-60 in the case of 1000 Hz sampling frequency. Examples of these curves for one of the time windows in different subjects is presented in Figure 7.2 for 250 Hz and 1000 Hz sampling frequencies and EEG in response to words. These figures are AIC and BIC values in a 23-channel model, however, other channel numbers were also tested and produced similar results. As lower model orders would be much faster to estimate and have fewer parameters and probably more accurate parameter estimations, a model order of 15/25 was selected for 250/1000 Hz sampling frequencies. This can be considered a reasonable order as other studies have decided on similar model orders using AIC, e.g. Schlögl and Supp (2006) reports order 15 for 250 Hz sampling frequency and Kamiński et al. (2001) reports order 5 for 102 Hz sampling frequency. Note that although analyses started with these orders, whiteness test after parameter estimation showed that we required higher model orders to obtain uncorrelated residuals (see section 7.5.2.1).

After specifying the model order, to decide about the number of channels, the $TK > 10pN$ inequality was used. Depending on the stimulus type, sampling frequency, and window length, different number of channels could be used for each of the combination of these options to have a reliable estimate. However, to be consistent over all these options, the smallest number of channels was selected. For data in study S1/S2 (see section 3.2), 23/21 channels were chosen symmetrically from each map covering the whole head area. The selected channels are marked in Figure 7.3.

7.4.3 Measuring connectivity

After data were pre-processed according to section 7.4.1.2, the number of channels and the model order were selected, as in section 7.4.2. The MVAR model was fitted to each time window and its parameters were estimated. The model order was the same for all subjects and datasets as Figure 7.2 showed similar results over all subjects. Using these MVAR parameters, each of the connectivity methods explained in section 7.3 was calculated in each window and their values were averaged over different frequency bands of Figure 4.1 (with time-lengths similar to those used in chapter 6) for further significance analyses.

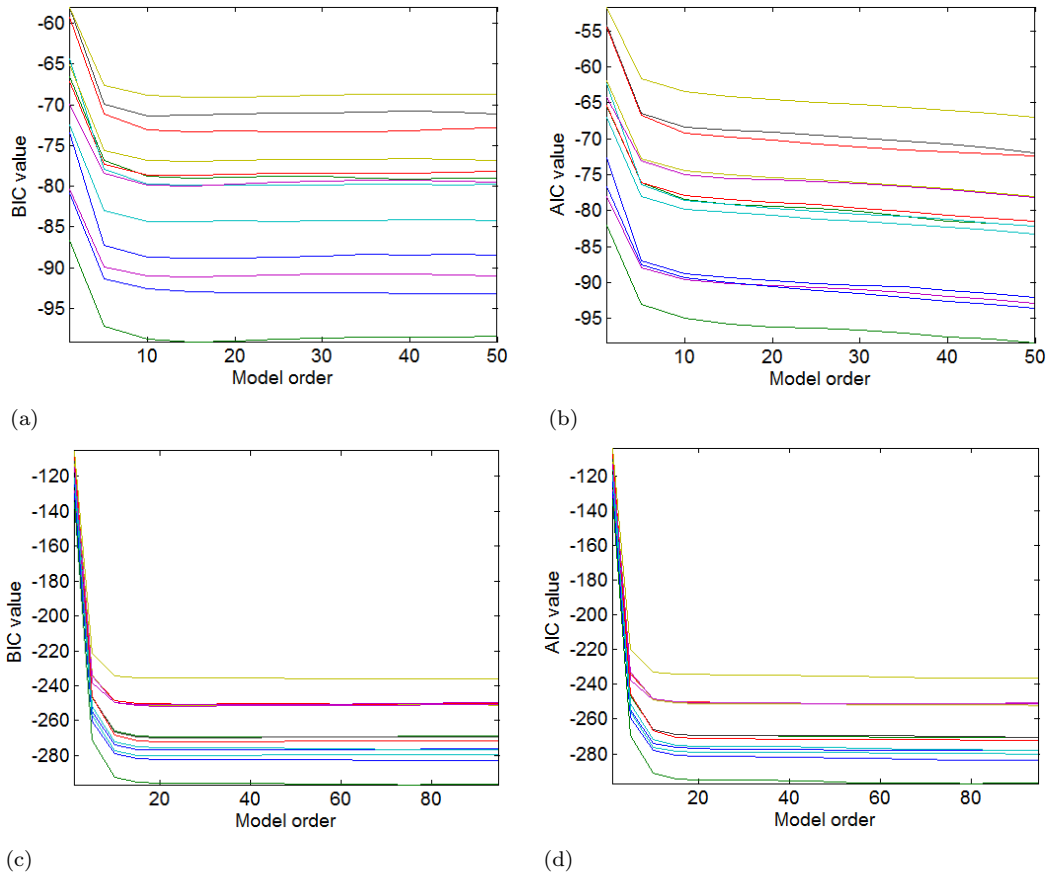

Figure 7.2: AIC and BIC values over different model orders in a 23-channel model for 250 Hz (a and b) and 1000 Hz (c and d) sampling frequencies in a 500 ms window in response to words, different curves are for different subjects.

7.4.4 Significance analyses

Similar to previous induced response and non-parametric coherence analyses, for each connectivity measure, the Friedman's test was applied to the value of the measure between each electrode pair over time in each frequency band. If a significance ($p<0.05$) change was detected over time, post-hoc analyses (Tukey's test) were applied to find the window after the onset that showed significant increase or decrease ($p<0.01$) from the baseline value. Although the p-value should be corrected for multiple comparisons, if it was corrected too much (using for example bonferroni correction), there would be the chance of missing weak connections (type II error) thus it was not corrected any further.

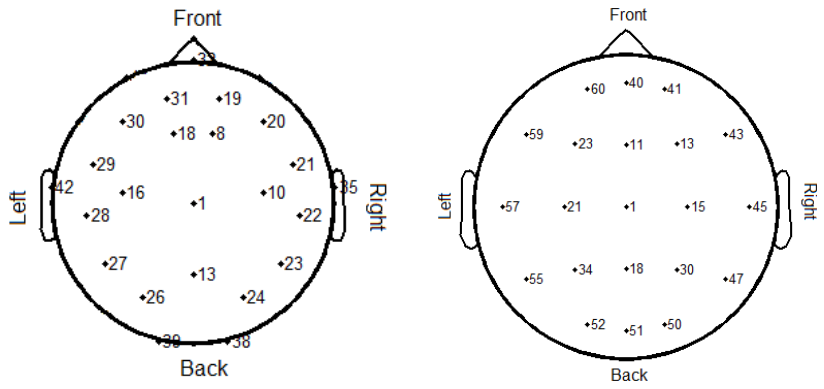

(a) (b)

Figure 7.3: Channels selected for connectivity analyses in study a) S1 and b) S2.

7.5 Results

7.5.1 Analyses on simulated data

First, matrices of Equation 7.16 were used to test the implementations (in MATLAB) of different connectivity measures and see if each one of them produce theoretically correct results. The matrices were fed directly to the algorithms assuming that they were estimated parameters of an MVAR model. The results are shown in Figure 7.4. In this figure, the direction of each connection is from each column to each row, e.g. position (2,3) in each of the measures means flow from channel 3 to channel 2. In each subfigure, the frequency is on the x-axis and the calculated value of that connectivity is along the y-axis. Note that all measures have values in the [0 1] range except for ffDTF and dDTF because of the difference in the normalisation of ffDTF from other methods. If a subfigure shows values other than zero in any frequency, even very small values, it means that there is a connection between the two channels in that direction (from column to row). As mentioned before, coherence is not a causal measure and in Figure 7.4, connections are seen between all channels in both directions just because they were directly or indirectly connected. However, PCoh only shows connections between directly connected channels but still it is a non-causal method, e.g. there is a connection from 1 to 2 as well as 2 to 1. PDC shows a correct causal flow between directly connected channels as does sPDC, e.g from 1 to 2 or from 2 to 4 but not from 1 to 4, and sPDC shows sharper changes compared to PDC. As expected, DTF and ffDTF show a directional information flow even in indirect paths, e.g from 1 to 4. However, this problem is resolved in dDTF as it is a multiplication of PCoh by ffDTF in the same subfigures. The correct relationships between different channels (for all measures) thus indicate that the algorithms have been implemented correctly. This step only proves the correct calculation of connectivity measures but still does not prove the correct MVAR parameter estimation, i.e. getting from the observed data to A_j matrices.

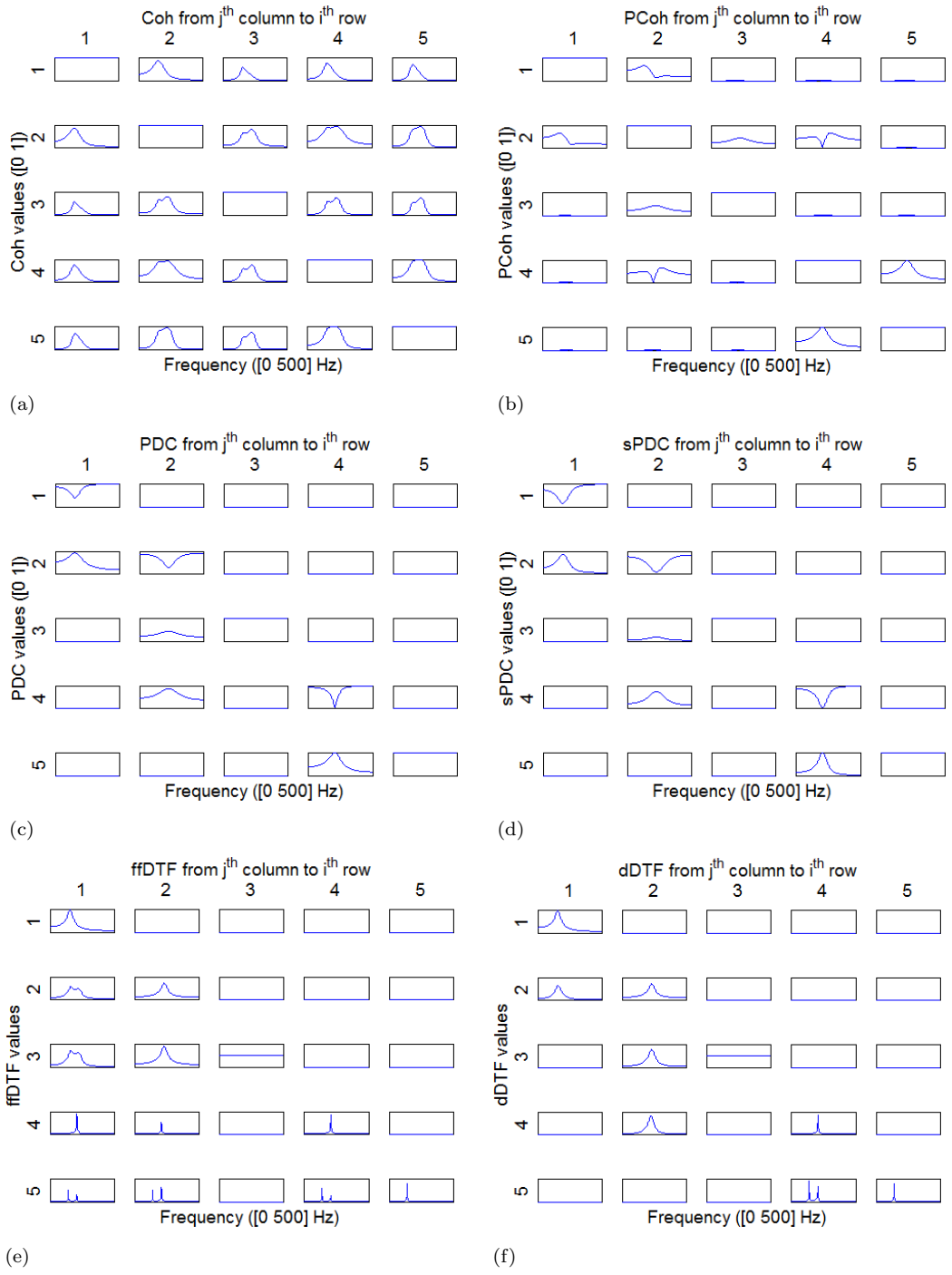

Figure 7.4: Different connectivity measures calculated directly from A matrices defined as in Equation 7.16, no simulated data. In each subfigure, the value of the measure is plotted versus frequency in [0 500] Hz range.

To test the MVAR estimation procedure (i.e. the multichannel system identification), the same parameter matrices (Equation 7.16) were employed. However, this time, data were simulated using Equation 7.17 as in section 7.4.1.1, first by simulating a one-epoch set of data and then by simulating 100 epochs. Each dataset was then fed to the Vieira-Morf estimation algorithm (see section 7.2.3) to calculate the MVAR coefficients

the results of which were parameter matrices similar to Equation 7.16. The estimated parameters were very close to the true parameters in both cases, however, the Mean Squared Error (MSE) over all estimated parameters was much smaller in the multi-epoch ($MSE = 5 \times 10^{-4}$) than one-epoch ($MSE = 5 \times 10^{-2}$) dataset. Moreover, the covariance matrix of residuals was a diagonally dominant matrix close to identity with off-diagonal elements of second/third decimal point in the one/multi-epoch dataset. This showed the independence of channels, and did more so in multi- than one-epoch dataset. Thus increasing the number of epochs, i.e. data points, helps in the accuracy of the estimation, as might be expected. The residual noise was also tested according to section 7.2.5.1 and was identified as being white meaning that there was no more information in the data that had not been picked by the estimated MVAR coefficients.

The connectivity measures were calculated using these estimated parameters and looked very similar to Figure 7.4. An example of the DTF and PDC measures obtained from estimated parameters is presented in Figure 7.5 for both the one-epoch and 100-epoch datasets. Comparing Figures 7.4 and 7.5 shows that DTF and PDC obtained from true parameters and estimated parameters are very similar except for a few discrepancies in the one-epoch dataset (e.g. $DTF(1,2)$, $PDC(1,5)$, or $PDC(3,5)$) which is resolved in the multi-epoch (100-epoch) version. As mentioned before, in multi-epoch datasets, the correlation matrix is calculated for each epoch and averaged over all epochs before estimating the parameters.

Other simulations were also performed using different sets of MVAR coefficients and the results of MVAR estimation and connectivity calculations were again similar to the true connectivity pattern as calculated from the original model on which the simulation is based.

7.5.2 Analyses on recorded data

The connectivity measures were then applied on recorded EEG data after further pre-processing of data as explained in section 7.4.1.2. As the results of word stimulation were clearer than any other stimulus in previous chapters, connectivity analyses were started using this stimulus.

7.5.2.1 Connectivity and words

In chapters 4 and 6, it was shown that there was an increase in the induced power and the non-parametric pairwise coherence in posterior electrodes in the [0 8] Hz frequency band for about 1 s after the onset. Although the connectivity estimation algorithms proved reliable on simulated data, it was important to make sure they would produce expected results in EEG data as well. It was decided that a reasonable approach for testing the

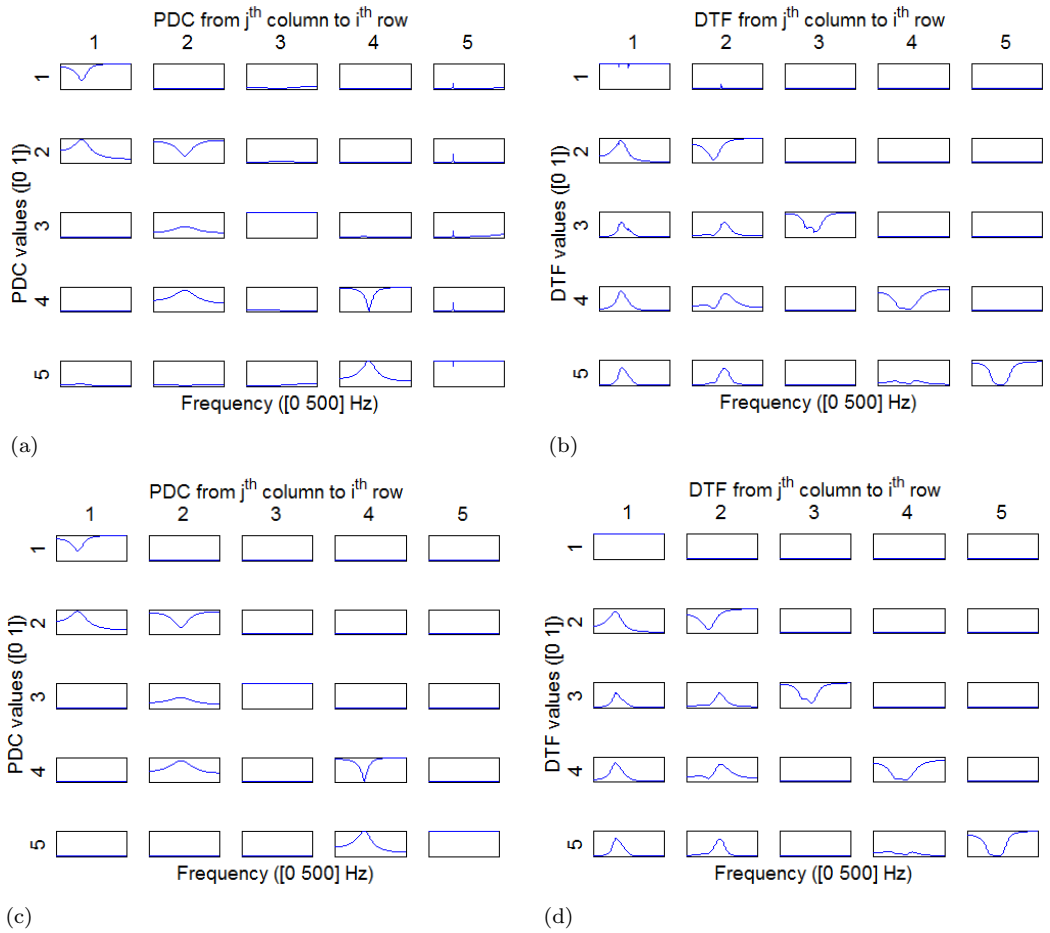

Figure 7.5: DTF and PDC measures derived from data simulated using A matrices defined as in Equation 7.16, for a one-epoch (a and b) and a multi-epoch (c and d) dataset. In each subfigure, the value of the measure is plotted versus frequency in [0 500] Hz range.

reliability of the outcome of MVAR parameter estimation on recorded EEG would be to calculate the model-based coherence values over time and apply significance analyses (see section 7.4.4) on these values and compare the reported significant connections with those of non-parametric estimations.

Pairwise coherence: For this purpose, the downsampled epoched data (see section 7.4.1.2) in response to words played to the right ear were segmented into 500 ms windows without overlapping starting from 500 ms before the onset. A bivariate auto regressive model of order 15 (see Figure 7.2) was fitted to all different channel pairs, its parameters were estimated, and the pairwise coherence (i.e. the parametric equivalent of the simple coherence) was calculated for all electrode pairs using these parameters. Similar to non-parametric coherence, the coherence values were then averaged in different frequency bands as indicated in Figure 4.1 in each time window, the baseline subtracted values are plotted in Figure 7.6 which are quite similar to those obtained from non-parametric coherence analyses in Figure 6.5. The Friedman's test and post-hoc analyses

were employed according to section 7.4.4 and connections showing significant coherence increase or decrease compared to the baseline window were identified in each frequency band. Figure 7.7 shows the connections with significant increase/decrease in the coherence compared to the baseline in different time-frequency ranges after the onset, in red/blue. This figure shows similar results to those obtained from non-parametric coherence in Figure 6.7 in that it clearly follows a similar pattern to that figure. This provides further evidence that the algorithms are correctly implemented. However, as the significance level is the same in the two approaches but the number of significant connections is smaller in the model-based coherence, it is reasonable to say that with the same level of significance, non-parametric coherence is more powerful than model-based one in detecting the changes in the signal (from the baseline to time windows after the onset). Now that the validity of parameter estimation and connectivity measurement algorithms have been established using simulated data and the pairwise model-based coherence on recorded data, we can move to analyses on more than two channels in recorded data.

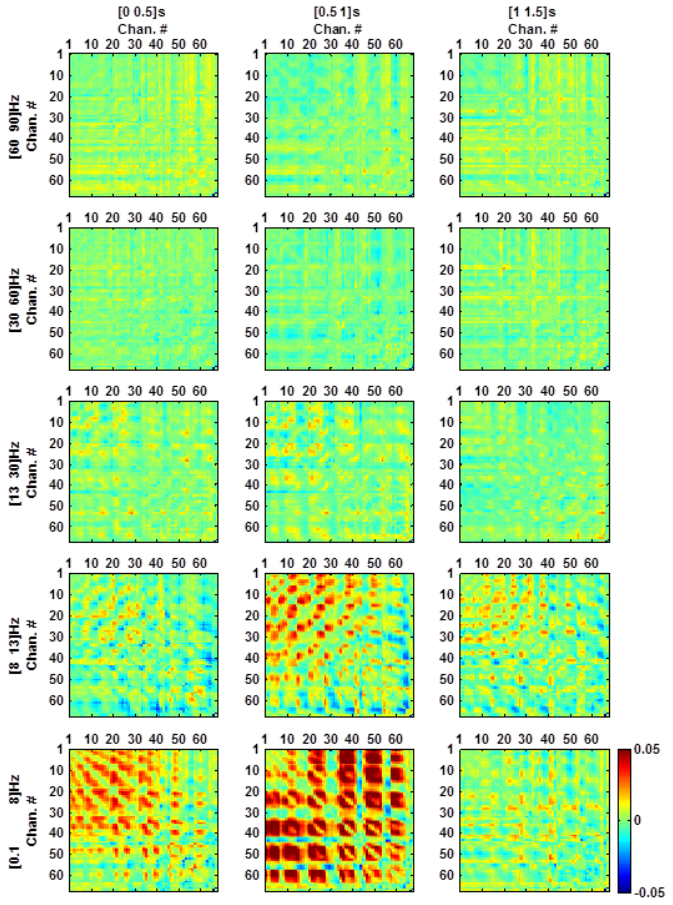

Figure 7.6: Words played to the right ear: model-based pairwise coherence after subtraction of baseline values, along time (columns) and over different frequency bands (rows). In each subfigure, rows and columns show channel numbers between which the coherence is computed. Blue/red indicates decreased/increased coherence compared to the baseline.

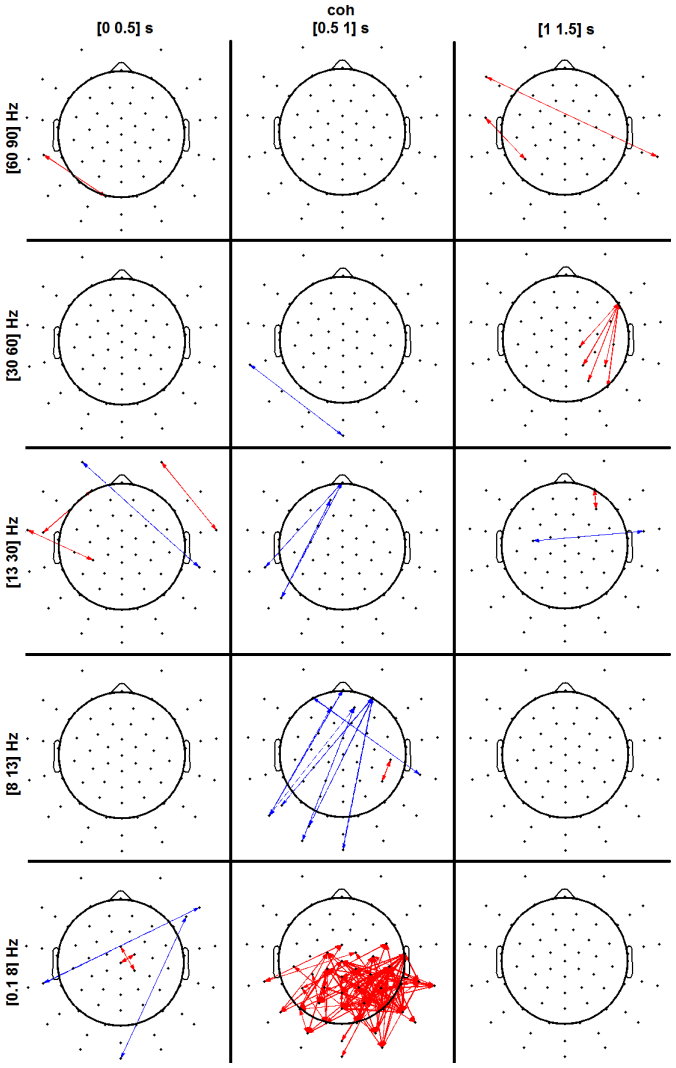

Figure 7.7: Words played to the right ear (MVAR estimated with p=15 and for F_s=250 Hz): Significant model-based pairwise coherence changes from the baseline (Friedman's test, p<0.05 - Tukey's test, p<0.01) in different time-frequency windows are marked by arrows. Red/blue arrows indicate increase/decrease in the coherence compared to the baseline. The stimulus onset occurs at zero seconds.

Multi-variate connectivity: The epoched EEG data in response to words when played to the right ear were employed. According to section 7.4.2, a set of 23 channels were selected symmetrically from the 66 channels. A new dataset was generated by decimating the signals in these channels to 250 Hz sampling frequency. MVAR analyses were applied on both sampling frequencies. The data were segmented into 500 ms windows according to section 7.4.1.2 and an MVAR model of order 15, 25, or 50 was fitted to the data and its parameters were estimated. In each time window, the whiteness of residuals and the stability of estimated model parameters were tested (see section 7.2.5). Although according to section 7.4.2, a model order of 15 should have been a good fit (i.e. small estimation error), whiteness tests showed that it would not result in white residuals in

all windows and all subjects. That is why other orders were also tested. Estimated parameters (i.e. A_j matrices in Equation 7.1) were then used to calculate different connectivity measures the first of which was the multi-channel (as opposed to pairwise) coherence to compare its results with those achieved from non-parametric coherence (see chapter 6) and model-based pairwise coherence (see Figure 7.7).

In each time window, each of the calculated measures were averaged in different frequency bands for each connection. For each measure and in each frequency band, Friedman's test was applied on the values of each connection over time and using post-hoc analyses, the connections that showed significant change from the baseline were marked (see section 7.4.4). Figures 7.8 and 7.9 show these results for multi-channel MVAR-based coherence in the theta frequency band over time when words were played to the right ear for different model orders and different sampling frequencies. Blue/red arrows indicate connections with significant decrease/increase of coherence compared to the baseline coherence in each time-frequency window. As almost no connections were marked significant in other time-frequency windows (as indicated in Figure 4.1) in any of the order or sampling frequency conditions, those results are not presented here. These figures again show similar results to the pairwise coherence (both model-based and FFT-based) results in that a significant increase in the coherence is observed in [0 8] Hz and [0 1]s time-frequency windows in posterior electrodes. From Figures 7.8 (model-based pairwise coherence) and 7.9 (model-based multi-channel coherence), it is also clear that the number of connections marked significant in this window decreases when increasing the model order and also when increasing the sampling frequency.

From the results of Figures 7.8 and 7.9, it was decided that a 250 Hz and a model order of 15 or 25 should be sufficient for further analyses. Although order 15 appears to detect more connections than 25, the former reported the residuals in some of the time windows of a few subjects as not white. So, order 25 was selected as the choice of MVAR order for future analyses as it reported whiteness of residuals for all time windows and subjects.

Similar statistical analyses on PDC and DTF only showed some random significant connections in DTF with a sampling frequency of 1000 Hz and model orders of 15 (see Figures 7.10) and 25 (see Figure 7.11) and even those connections changed in an apparently random way from one model order to another. Examples of the actual DTF values and the baseline subtracted values are presented in Figures 7.12 and 7.13 for a sampling frequency of 1000 Hz and a model order of 25. Due to displaying limitations, only the label of a few channels are used. The same channels as in Figure 7.3 are arranged in an ascending order. Results of PDC are not shown as the significant connections seemed even more random than those of DTF. As at this stage, the actual significance level was not as important as finding a change in the connectivity with regards to the baseline (similar to coherence), the α-value of the Friedman's test and post-hoc analyses were increased to see if clearer evidence of activity would be observed. Although, the

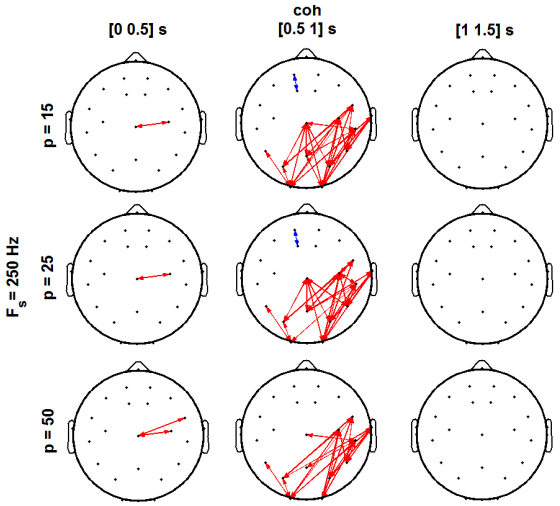

Figure 7.8: Words played to the right ear (F_s=250 Hz): Significant multichannel MVAR-based coherence changes from the baseline (Friedman's test, p<0.05 - Tukey's test, p<0.01) in the [0 8] Hz band are marked by arrows over time for different model orders. Red/blue arrows indicate increase/decrease in the coherence compared to the baseline. The stimulus onset occurs at zero seconds.

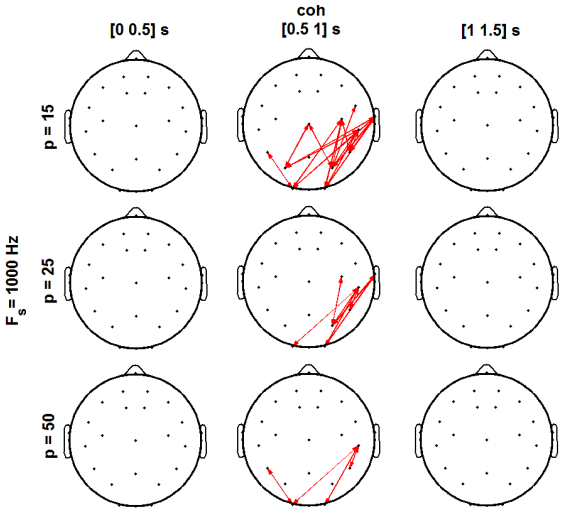

Figure 7.9: Words played to the right ear (F_s=1000 Hz): Significant multichannel MVAR-based coherence changes from the baseline (Friedman's test, p<0.05 - Tukey's test, p<0.01) in the [0 8] Hz band are marked by arrows over time for different model orders. Red/blue arrows indicate increase/decrease in the coherence compared to the baseline. The stimulus onset occurs at zero seconds.

number of significant connections increased (as expected), still no clear pattern could be detected in PDC and DTF contrary to the way it did in simple coherence estimates.

Similar steps with model order of 25 and sampling frequency of 250 Hz were repeated for EEG data in response to words when played to the left ear or binaurally and significance analyses were applied on the results, however, no clear pattern was obtained for any of

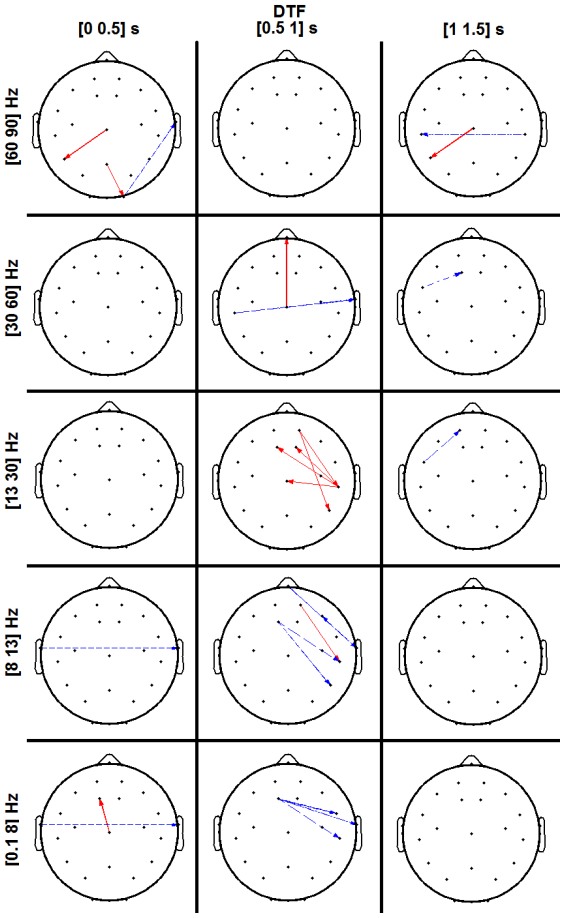

Figure 7.10: Words played to the right ear (MVAR estimated with p=15 and for F_s=1000 Hz): Significant DTF changes from the baseline (Friedman's test, p<0.05 - Tukey's test, p<0.01) in different time-frequency windows are marked by arrows. Red/blue arrows indicate increase/decrease in DTF compared to the baseline. The stimulus onset occurs at zero seconds.

the measures, not even in the coherence. Although it was initially expected that, in the case of words played to the left ear or binaurally, an increase in the coherence should be seen in lower frequency bands after the onset, the results obtained (i.e. no change in the coherence) were not unreasonable. According to the results obtained from FFT- and model-based coherence in Figures 6.7 to 6.9 of chapter 6 and Figures 7.7 to 7.9 of this chapter, it is clear that the number of connections reported as significant is lower for words played to the left ear or binaurally than when they were played to the right ear. Moreover, it was concluded that model-based coherence is less sensitive than FFT-based coherence in detecting the coherence change in the signal. Thus, not seeing any change in the coherence could very well be because of weaker ability of model-based coherence to detect changes (which were probably weaker in the data when words were played to the left ear or binaurally than when played to the right ear).

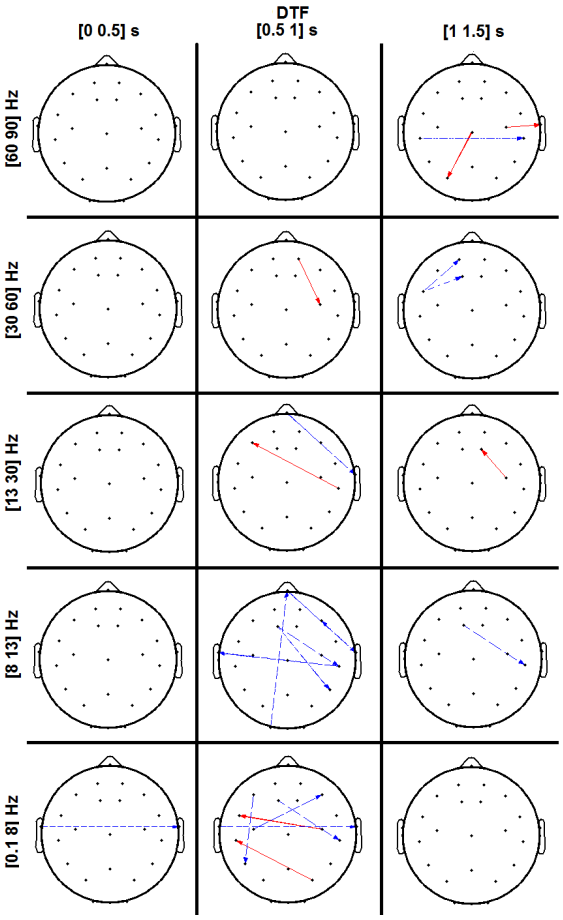

Figure 7.11: Words played to the right ear (MVAR estimated with p=25 and for F_s=1000 Hz): Significant DTF changes from the baseline (Friedman's test, p<0.05 - Tukey's test, p<0.01) in different time-frequency windows are marked by arrows. Red/blue arrows indicate increase/decrease in DTF compared to the baseline. The stimulus onset occurs at zero seconds.

7.5.2.2 Connectivity and sentences

Similar to word stimulus, EEG data in response to sentences were downsampled as in section 7.4.1.2 and segmented to different non-overlapping windows. For the results to be comparable with those obtained from induced response and FFT-based coherence, the lengths of these windows were selected as 1 s. Other pre-processing steps as explained in section 7.4.1.2 were applied on each window and 23 channels were selected. The 23-channel MVAR model of order 25 was fitted to the data in each window and the parameters were estimated. Using these parameters, different connectivity measures were estimated and averaged in different frequency bands, again according to Figure 4.1. Friedman's test and post-hoc analyses were applied on each connection over time (as in section 7.4.4) to find significant connectivity changes after the onset compared to the baseline. The results of the MVAR-based coherence is presented in Figures 7.14 for binaural sentence presentation. Red/blue arrows show significant increase/decrease compared to the baseline and each subfigure shows different changes over time in different

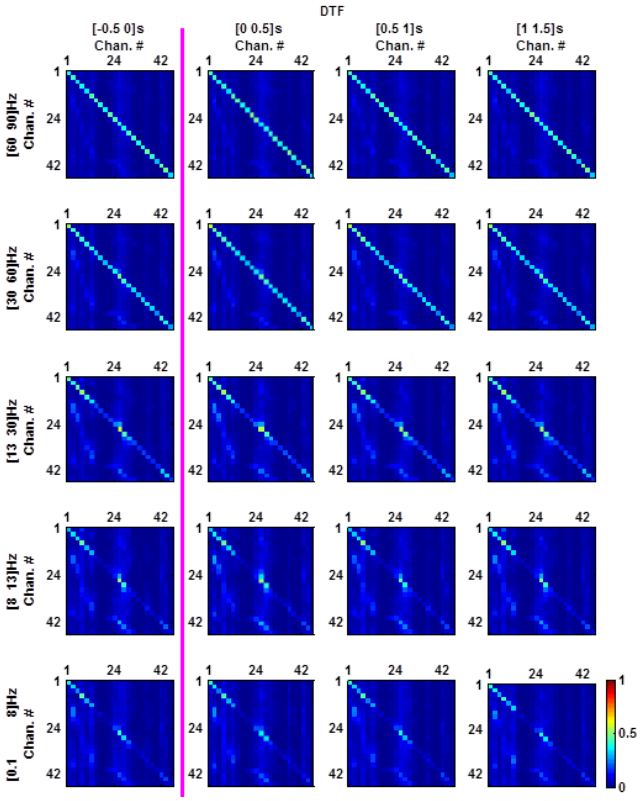

Figure 7.12: Words played to the right ear: DTF values (MVAR estimated with p=25 and for F_s=1000 Hz) along time (columns) and over different frequency bands (rows). In each subfigure, rows and columns show channel numbers between which DTF is computed. The direction is from each column to each row. The stimulus onset occurs at zero seconds and is indicated by the magenta line.

frequency bands. Similar to the results obtained from induced analyses and pairwise coherence, there is a notable increase in the coherence in the [0 8] Hz frequency band for about 2 s after the onset in binaural presentation though with fewer significant connections than those obtained from non-parametric pairwise coherence analyses. For left and right presentations, MVAR-based coherence showed no significant changes which again confirms that MVAR-based coherence is less sensitive than the model-based one in detecting changes over time.

Again, no clear change in any of the other connectivity measures could be detected in any of the presentations so the results are not presented here.

7.5.2.3 Connectivity and AM tones

The EEG in response to these stimuli showed no induced activity neither in power nor in FFT-based coherence thus, no change was expected from model-based coherence or any other connectivity measure in this case. Still, connectivity analyses were performed

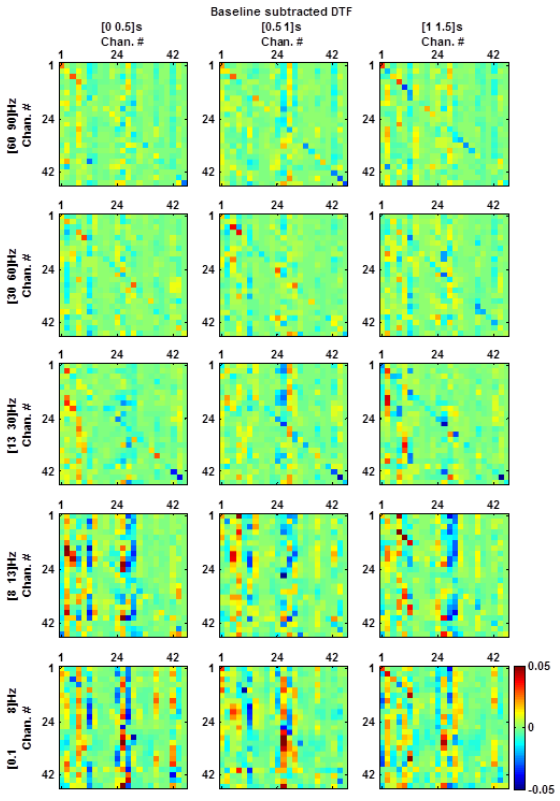

Figure 7.13: Words played to the right ear: DTF values (MVAR estimated with p=25 and for F_s=1000 Hz) after subtraction of baseline values along time (columns) and over different frequency bands (rows). In each subfigure, rows and columns show channel numbers between which DTF is computed. The direction is from each column to each row. Blue/red indicates decreased/increased coherence compared to the baseline. The stimulus onset occurs at zero seconds.

on these stimuli for different presentation ears and as expected, no pattern could be detected. As there was no connectivity, the results are not presented here.

7.5.2.4 Connectivity and tone bursts

The data from the PT protocol (see section 3.2.2) were pre-processed according to section 3.4 and downsampled to 250 Hz as in section 7.4.1.2. Each epoch was segmented into 200 ms non-overlapping windows and 21 channels of data were selected symmetrically. After further pre-processing, i.e. subtraction of the average and dividing by the standard deviation (as in section 7.4.1.2), a 21-channel MVAR model with an order of 25 was fitted to the data and its parameters were estimated. From these parameters, different connectivity measures were estimated in each time window before and after the onset and significance analyses were applied on them according to section 7.4.4, to test for the significance of changes over time compared to the baseline.

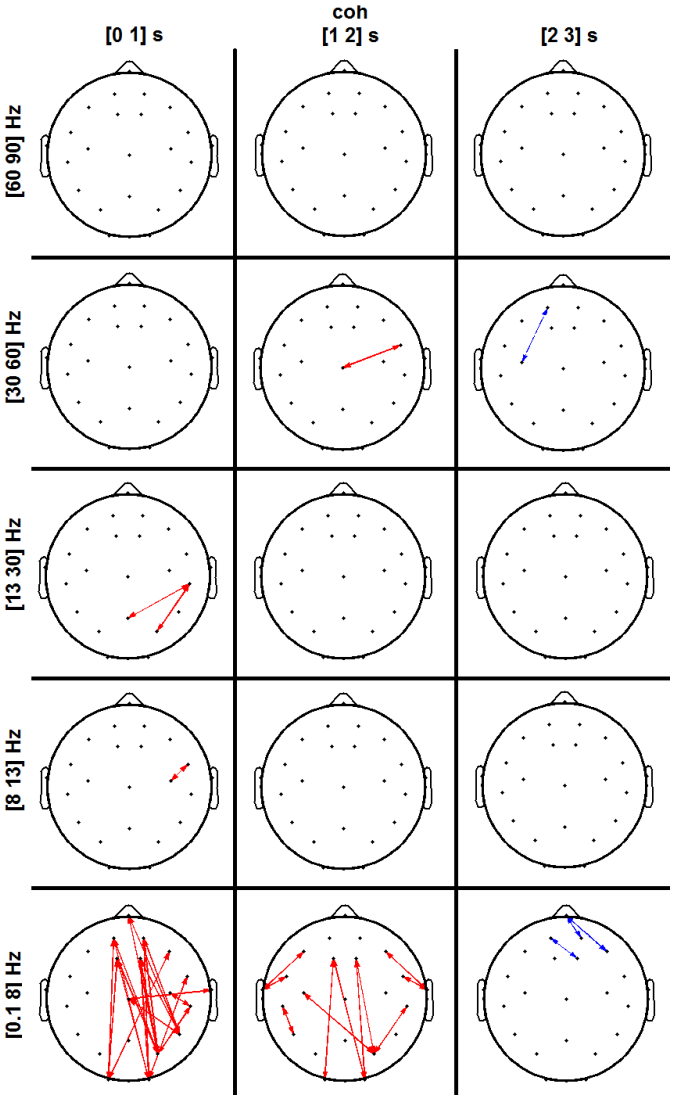

Figure 7.14: Sentences played binaurally (MVAR estimated with p=25 and for F_s=250 Hz): Significant MVAR-based coherence changes from the baseline (Friedman's test, p<0.05 - Tukey's test, p<0.01) in different time-frequency windows are marked by arrows. Red/blue arrows indicate increase/decrease in the coherence compared to the baseline. The stimulus onset occurs at zero seconds.

Using α-values mentioned in section 7.4.4 (0.05 for Friedman's and 0.01 for post-hoc analyses), no clear pattern could be observed in coherence whereas when the significance level was increased to 0.1 (for both Friedman's test and post-hoc), the arrows in Figure 7.15 were marked as significant, red/blue indicating an increase/decrease. Rows/-columns show coherence change over different frequencies/times. This figure starts to show similar results to that of FFT-based coherence in response to tone bursts (Figure 6.4), i.e. an increase in coherence in occipital electrodes in the beta band in [0.2 0.4] s time window followed by a decrease in coherence in frontal areas and simultaneously an increase in the occipital electrodes in [0.4 0.6] s time window. This result again confirms that model-based coherence is less sensitive than FFT-based coherence in detecting the

change over time as the observed change was achieved with a higher significance level. As before, no pattern could be detected in other connectivity methods when using the same statistical methods as before.

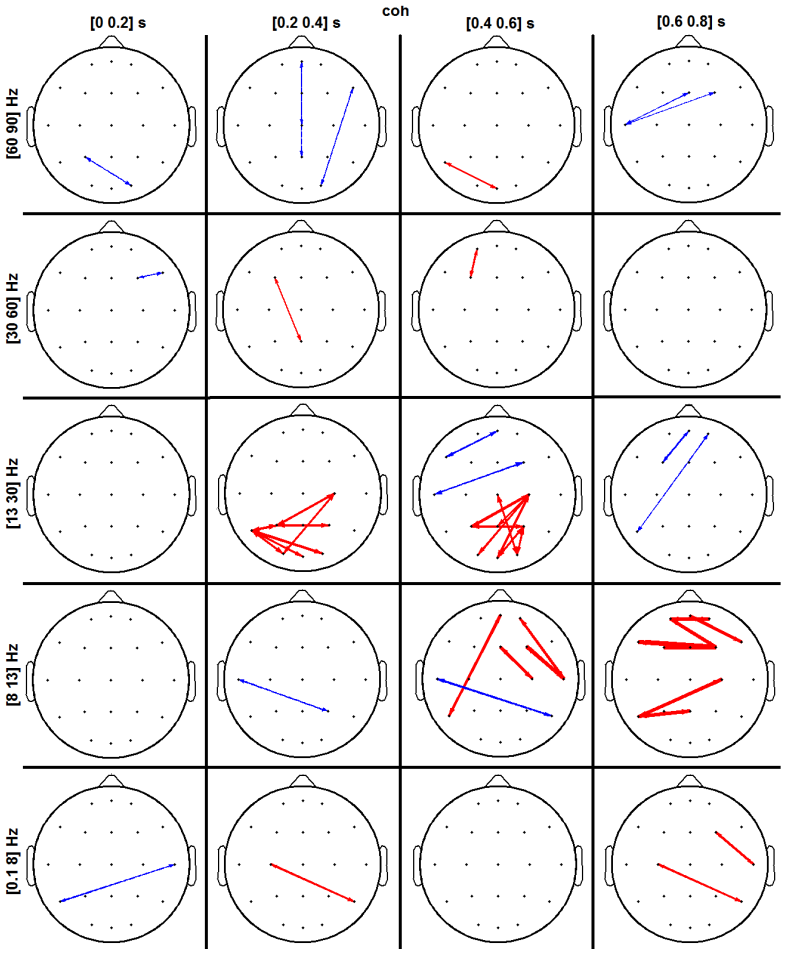

Figure 7.15: Tone bursts played to the right ear (MVAR estimated with p=25 and for F_s=250 Hz): Significant MVAR-based coherence changes from the baseline (Friedman's test, p<0.1 - Tukey's test, p<0.1) in different time-frequency windows are marked by arrows. Red/blue arrows indicate increase/decrease in the coherence compared to the baseline. The stimulus onset occurs at zero seconds.

7.6 Discussion

This chapter has introduced MVAR models and has explained how different connectivity measures (such as PDC and DTF) can be estimated from them. To test the algorithms, simulated data were generated and it was established that the algorithms for MVAR estimation and connectivity computation were providing the expected results. To make certain that the algorithms produced correct results on recorded data too, pairwise model-based coherence was estimated for all channel pairs in EEG dataset recorded in response to words played to the right ear, and its results were compared with

those obtained from FFT-based coherence in chapter 6. Pairwise model-based coherence showed an increase in the coherence in the same windows as pairwise FFT-based coherence though with fewer significant connections than FFT-based coherence. From this result, it was concluded that the MVAR estimation and connectivity calculation algorithms were implemented correctly, but that non-parametric approaches were more powerful than model-based ones in tracking changes in the signal.

In the next step, the multi-channel MVAR parameters (as opposed to pairwise that was explained in the previous paragraph) were used to calculate different connectivity measures such as coherence, DTF, and PDC for each stimulus type and presentation ear. Although in most cases, similar results were obtained for multi-channel-based coherence as for model-based and FFT-based pairwise coherence, i.e. the same time-frequency windows showed increase or decrease, no other measure reported any clear pattern in any of the stimulus types or presentation ears.

It is discussed in Porcaro et al. (2009) that decreasing the sampling frequency may affect the fine structure of the signal thus making measures less sensitive to the changes in the signal and so the statistical analyses may miss some connections. The main reason the data were downsampled in this chapter, other than decreasing the computation time, was for consistency with the approaches in chapter 6. Although the results are not presented in this chapter, MVAR measures were also calculated with the original 1000 Hz sampling frequency but though the results were again consistent for coherence, no change was observed in other connectivity measures. Moreover, the model order of 25 was selected carefully using AIC and BIC methods and according to the whiteness test as the primary model order. However, model orders of 15 and 50 were also tested and the results were again the same, i.e. no change in the connectivity pattern other than with coherence.

Of course the first reason for not seeing any significant change in effective connectivity might be the actual lack of connectivity change over time, although pairwise coherence did suggest otherwise. However, many other reasons may be behind the results obtained. It is quite possible that the change is not large enough (due to low SNR) and more subjects are needed for these analyses in order to detect any changes. In other words, if the number of stimuli presented or the number of subjects is increased, some connectivity may be detected. Also, it is possible that these measures are more sensitive to a change in the participant's state of mind, e.g. awake versus asleep, as shown in Kamiński et al. (2001) or two different stimuli versus each other, such as Go or NoGo (Ding et al., 2000) or visually congruent or incongruent words (Astolfi et al., 2007), rather than a change before and after the onset of a stimulus.

One factor that has not been addressed in this report and can affect connectivity is the effect of instantaneous connectivity on MVAR parameter estimation which should be the subject of future work. One of the initial assumptions of an MVAR model is that the

input noise has a diagonal covariance matrix at lag zero, i.e. there is no instantaneous connection between signals. Erla et al. (2009) showed that if there is instantaneous effect, i.e. noise in different channels are correlated at lag zero, connectivity measures derived from the conventional MVAR parameters may be misleading. Thus, they introduced an extended MVAR model which accounted for instantaneous activity as well. In MVAR estimations in this chapter, it was observed that the residuals of the model are not always uncorrelated at lag zero. Although this instantaneous connectivity may be considered as one factor affecting our results, it still does not explain the complete lack of significant connectivity observed. It has been demonstrated (Erla et al., 2009; Faes and Nollo, 2010; Faes et al., 2013) that instantaneous activity would introduce more connections in connectivity measures when in fact there is none, not the other way round, which is the case of the results in this chapter. Thus, if the instantaneous activity was to affect the results of this chapter, it would be expected to introduce spurious connections instead of leading to a lack of connectivity.

7.7 Summary

In this chapter, different MVAR based connectivity measurements where defined and their advantages and disadvantages were discussed. It was shown that these methods work well on simulated data and the MVAR estimation algorithms provide expected results on recorded EEG data using a comparison between model-based and FFT-based coherence analyses. Similar to FFT-based analyses, model-based analyses showed an increase in the coherence in the [0 8] Hz frequency band in the [0 1] s time window in response to words and a weak increase in the coherence in beta band in response to tone bursts. However, no change in other connectivity patterns such as DTF or PDC was observed in any of our stimulus conditions the possible reasons of which were presented in section 7.6. Further analyses and change of auditory presentation protocols are required before any definite conclusions can be derived from the results. Having established in chapters 4 and 6 that words and sentences lead to significant induced activity and changes in coherence, the aim of the current chapter was to add further insights into the change in the direction of information flow with these stimuli. The results achieved suggest that these methods are not effective in probing these stimulus responses further.

Chapter 8

Analyses of CI data

8.1 Introduction

As explained in chapter 2, section 2.3, a cochlear implant is a device that is implanted in the cochlea of patients with sensorineural hearing loss whose auditory nerves are not damaged. This device acts as a bypass to auditory hair cells and brings back some hearing to patients with severe to profound deafness.

Although patients can hear sounds after implantation of a CI, it has been shown that the areas of the brain that are activated after implantation are different to those of a normal hearing person and although the activation resembles that of a normal hearing subject after using the implant for a while, it does not reach an identical pattern (Kral and Tillein, 2006; Giraud et al., 2001; Limb et al., 2010; Strelnikov et al., 2010; Łukaszewicz et al., 2010). It was hypothesised in this project that abnormal activity patterns, in addition to the changes to the input sound exerted by the CI, might be one reason for the patient not perceiving more complex sounds such as words and sentences properly.

As the active areas of the brain have been shown to be different in CI users compared to normal hearing people (Łukaszewicz et al., 2010; Limb et al., 2010), most probably, the connectivity pattern also differs from that of normal hearing subjects. This question, i.e. assessing connectivity pattern in CI users, was the main motivation behind this project and does not appear to have been approached elsewhere other than by Castañeda-Villa et al. (2012) who only measured interhemispheric correlation, as a functional and not effective connectivity measure, in response to tone bursts and not more complex sounds. Both effective and functional connectivity were investigated in normal hearing people in previous chapters in response to different types of auditory stimuli, and connectivity was shown to change in delta and theta bands in response to words and sentences and in beta band in response to pure tones. The main purpose of this chapter was to approach the same question using EEG data recorded from CI users. The aim of this line of

investigation is to help in understanding access to speech in CI users and in finding potential approaches that can assist CI users benefit from their implant more efficiently. However, before this data can be used, CI artefacts should be removed from it in addition to other common EEG artefacts (refer to section 3.4).

Cochlear implants induce large-amplitude artefacts in EEG while the processor is on (i.e. processing sound) and it is shown to be a challenging artefact to remove from EEG data (Gilley et al., 2006; Li et al., 2010), refer to section 8.3 and Figure 8.1. Most of this chapter is dedicated to reducing this artefact in recorded EEG so that it can be used for connectivity analyses.

The next sections explain the steps taken for artefact rejection and response detection in CI data. As will be demonstrated, different artefact rejection approaches were used and the most reasonable (even if not the ideal) one for our data was identified. Note that for the artefact rejection procedure (section 8.3) to be clearer and for the flow of the chapter to be more understandable, in each section, the method used for artefact rejection is explained, its results are presented and a short discussion is laid out to specify why the next method was used. The results of connectivity analyses on the artefact rejected data are then presented in the last sections.

8.2 CI data collection

The process of patient recruitment and EEG recording is explained in detail in section 3.2.1. As explained, from each patient who consented to take part in the experiment, two sessions of EEG were recorded in response to different types of auditory stimuli. The first session was in the first week of their implant activation and the second session was after 3-6 months of activation. The details of participants are presented in Table 8.1. For full details on the stimulus presentation and recording procedure refer to section 3.2.1. The collected data were filtered and epoched around the onset of different stimuli according to section 3.4. Then, different artefact rejection approaches were applied on them (refer to section 8.3) before being used for response detection and connectivity analyses.

8.3 Artefact rejection

The process of artefact rejection is one of the most important preprocessing steps in the procedure of EEG analysis (refer to section 3.3). In CI users, in addition to the usual artefacts present in the EEG such as ECG, eye blink, movement, etc, the artefact from the cochlear implant should be removed from the data prior to other signal processing steps.

Table 8.1: Details of CI patients participated in this study.

Patient	Age (years)	Gender	CI Brand (Processor)	Coding Strategy	Implanted Ear	CI use (months) [a]
1 [b]	60	F	MEd-EL (OPUS 2)	FS4	Left	12
2	64	F	Advanced Bionics (Harmony)	HiRes-S	Right	4
3	42	M	Advanced Bionics (Harmony)	HiRes-S	Right	4
4	66	F	MEd-EL (RONDO)	FS4	Left	3

[a] How many months they used the CI before the second recording.
[b] This patent was only recorded once.

CI artefact on the EEG may come from the radio frequency transmission or the electrical pulses that stimulate the electrodes of the implant (Gilley et al., 2006). This artefact looks like a pedestal that starts slightly after the onset and ends slightly after the offset of the stimulus. This pedestal may be preceded or followed by a negative or positive overshoot. Figure 8.1 shows an example of such an artefact in response to tone bursts in patient 1, recording 2. The exact shape, magnitude, and length of this artefact depends on many factors such as the brand of the cochlear implant, the type of the stimulation (mono or bipolar), the stimulus type, the location of the reference electrode of the EEG system, the distance of the recording electrode from the implant, etc. Even the length of the slope of the onset and the offset can be affected by these factors (Gilley et al., 2006). However, generally, the artefact follows the envelope of the input sound and has a delay with regards to the stimulus onset which comes from the processing delay in the implant. Note that this delay may be different in consecutive epochs depending on where in a clock cycle the sound reaches the processor but in repeating sounds, the shape of the artefact remains the same. If the sound is too abrupt such as tone bursts, it may produce an overshoot or undershoot at onset and offset times. Thus, for tone bursts, the artefact usually looks like a pedestal as in Figure 8.1.

Different methods such as simple filtering, finding the best reference electrode position, manipulating the stimulus, Principal Component Analyses (PCA), and Independent Component Analyses (ICA) have been used to remove the CI artefact from EEG, each of which has its own advantages and disadvantages (Gilley et al., 2006; Li et al., 2010). For example, finding the best reference position is a time consuming approach but may generate the least artefactual signals compared to many other methods. Alternatively, manipulating the stimulus may help in easier identifying and removing the CI artefact but it would limit CI-related studies to a large extent. For the purpose of this study, different approaches were tried for artefact rejection and noise reduction of our data, the procedures of which are explained in the following sections.

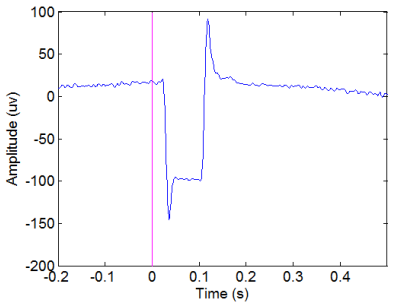

Figure 8.1: Ensemble average of EEG in an electrode close to the implant site for a Medel OPUS2 implant in response to tone bursts. The magenta line shows the onset of the stimulus.

It is worth noting that for speech stimuli, there is no gold-standard (like ALR for tone bursts) to compare the output of artefact rejection to, that is why the process of artefact rejection was not quite straight forward and different artefact rejection techniques had to be approached.

8.3.1 Independent Component Analysis

ICA assumes that the recorded EEG signals come from the same number of independent sources (or components) in the brain which are mixed linearly to produce the observed EEG signal (Castañeda-Villa et al., 2012). In the case of our study, the components can include eye-blinks, CI artefacts, ECG, the brain response to the stimulus, and background EEG activity. After identifying the artefact components and removing them from the mixture, one should be left with the clean signal. Among the existing artefact rejection techniques, ICA appeared to have more advantages compared to other methods for the purpose of this study. For example, it is not dependent on the type of the stimulus or the location of the reference electrode. ICA has been tested on different stimulus types such as pure tones and music-like tones and the process of visually selecting the artefactual components has been shown to be very helpful in removing the CI artefact (Agrawal et al., 2013; Sandmann et al., 2009; Gilley et al., 2006; Castañeda-Villa et al., 2012; Groppe et al., 2009). ICA was one step in artefact rejection of data used in previous chapters of this thesis and using the same technique in CI users would make the results more comparable. Thus, ICA and the process of visual artefactual component selection was initially deemed appropriate for the purpose of this study. Visual component selection using ICA is subjective and thus is not an ideal method for our data. As a result, other approaches were also tested for artefact rejection (refer to sections 8.3.1.1 to 8.3.1.4).

For the purpose of artefact rejection using ICA, similar to normal EEG, data from CI users were filtered in the [1 120] Hz frequency band, and then epoched for each stimulus type separately (refer to section 3.4 for epoch lengths). Electrode positions in

3D space were added to the data for future use in plotting the topographic maps of ICA components. Epochs deemed too noisy were removed from the data, based on visual analyses, and all epochs were zero-meaned. Channels that fell just over or around the transmitter (depending on the patient) were removed from the data as signs of amplifier saturation were evident in them and saturation effects would have negative effects on the performance of ICA. Extended Infomax ICA was then applied to the whole epoched data (including data before and after the onset) (Castañeda-Villa et al., 2012) using EEGLAB software (Delorme and Makeig, 2004). Using different approaches including manual and automatic methods, the artefactual components including the CI artefact, ECG, eye-blink, etc were identified and removed. The following sections explain these different methods.

8.3.1.1 ICA and visual component selection

The steps explained in Agrawal et al. (2013); Sandmann et al. (2009); Gilley et al. (2006); Castañeda-Villa et al. (2012); Viola et al. (2011) for visually selecting artefactual components were performed for identifying ICs related to the CI artefact. These steps are as follows: IC activations were inspected both in temporal and spatial domains, ICs with centroids originated around the implant location according to spatial (topographic) maps and which at the same time showed CI artefact characteristics in the temporal domain were removed. For example, for tone bursts, CI artefact characteristics resemble that of Figure 8.1, e.g. pedestal like ensemble average around the stimulus presentation time but with a small time delay, sometimes with sharp peaks around the onset or the offset time, etc.

Before artefact rejection was applied to EEG in response to words and sentences, it was tested on tone bursts as the evoked response to tone bursts after cleaning the data should be the well-known ALR. If our approach worked on tone bursts and an ALR could be observed after data cleaning, then it could be applied on other stimulus types with more confidence.

Tone bursts

The topographic maps of the channel Auditory Evoked Potentials (AEP), i.e. ensemble average over all epochs around the onset of the stimulus, before artefact rejection is presented in Figure 8.2 for one of the patients. The figure shows topographic maps at different times along the epoch in response to tone bursts after removing the saturated electrode (i.e. electrode 41 in this recording). Topographic maps are spatial representations of electrode activity over the whole scalp. In each map, the amplitude of EEG is colour coded where dark red/blue show high positive/negative amplitudes. For example, in this figure, at time 30 ms, a large negative activity is observed in electrodes close to the left ear and around the implant site. The same site shows large positive amplitudes

around 120 ms. These maps are spatial representations of the time domain signal of Figure 8.1. It is clear from the maps that the activation of the implant has dominated the activation from any other part of the brain and that there is about a 30-ms delay (the processing time) between the onset of the stimulus and the main activation of the implant. It may be noted that the implant even affects the EEG before the onset of the stimulus and also after the end of the stimulus, but not as strongly (note the activity contours around the implant site). Similar results were observed for other types of stimuli. Figure 8.3 shows the AEPs in different channels for the same data. The scale of the plot is presented at the bottom right corner of this figure.

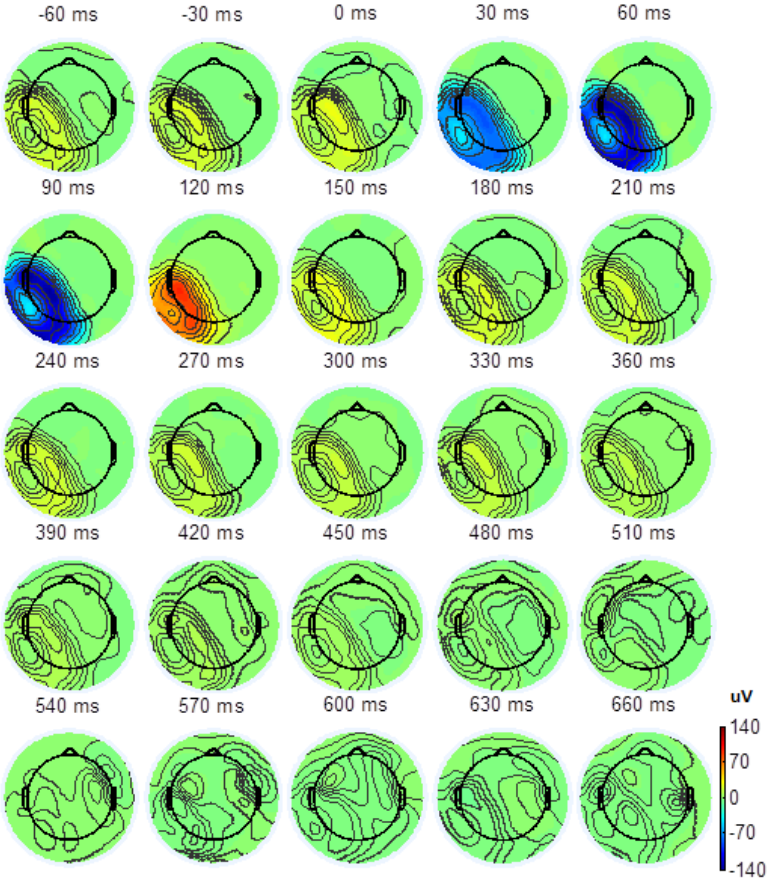

Figure 8.2: Topographic maps of channel AEPs at different times in response to tone bursts after removing electrode 41 in patient 1 recording 2, before artefact rejection. Each subfigure shows an axial view of the top of the head with the right side being the right of the head. The stimulus onset occurs at zero seconds.

As explained before, for visual IC rejection, the temporal and spatial distribution of IC activities should be used. An example of the spatial distribution (topographic map) and the ensemble averages (in time domain) of different ICs is presented in Figures 8.4 and 8.5, respectively, for the same data as in Figure 8.2. As one electrode (the one over the implant) had been removed before applying ICA, instead of 68, there are 67 components in Figure 8.4. Note that the scale of amplitude is different for different components in Figure 8.5 and that only a few components are presented in this figure. Figure 8.4 is

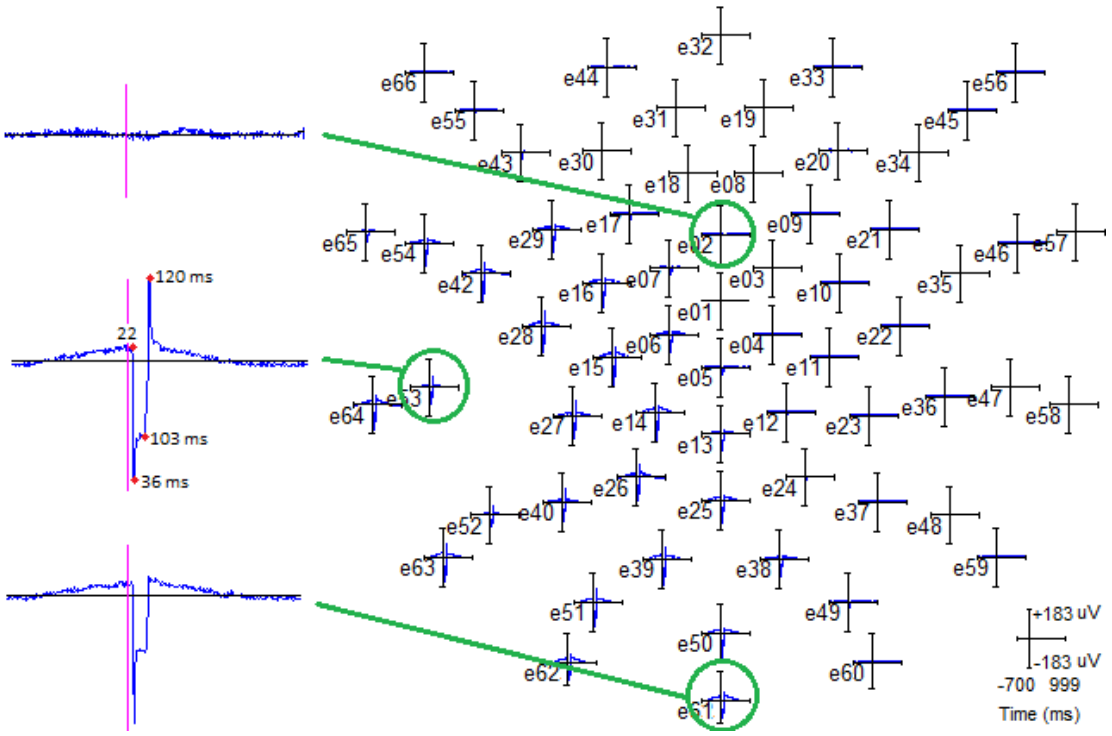

Figure 8.3: AEPs in response to tone bursts in all channels for the data in Figure 8.2 after removing electrode 41, before artefact rejection. The scale is presented at the bottom right corner. A larger view of some of the channels (circled in green) is presented on the left hand side of this figure. The magenta line marks the stimulus onset which occurs at zero seconds.

the spatial representation of the ICA demixing matrix. Dark red/blue areas for each IC means that this IC has a large positive/negative contribution from scalp electrodes close to that area. ICs such as 1, 2, and 3 that show large positive or negative activity around the implant site can be considered CI artefacts.

In this example, ICs with concentrated activity around the implant site (such as components 1, 3, 12, 26 in Figure 8.4) and at the same time show CI artefact characteristics in the temporal domain (like components 1, 3, 26 in Figure 8.5) were removed. For this dataset, components 1, 2, 3, 8, 12, 20, 26, 43, and 60 were removed because of their CI-related activities and components 4, 5, 10, 16, 17, and 18 were removed because of their clear contribution to ECG, eye blink, and main's noise (50Hz). As can be seen in this figure, some other ICs such as 41 show centroids around the implant site but because auditory activation can also arise from the same site and these ICs did not show any obvious CI artefact characteristics in the temporal domain, these components were not eliminated from the data.

After component rejection, the channel data were reconstructed and filtered with a low pass filter with cut off frequency of 30 Hz. The temporal and spatial maps of AEPs after artefact rejection are plotted in Figures 8.6 and 8.7, respectively. The AEPs look very similar to those of expected ALR except for a peak around 120 ms which should

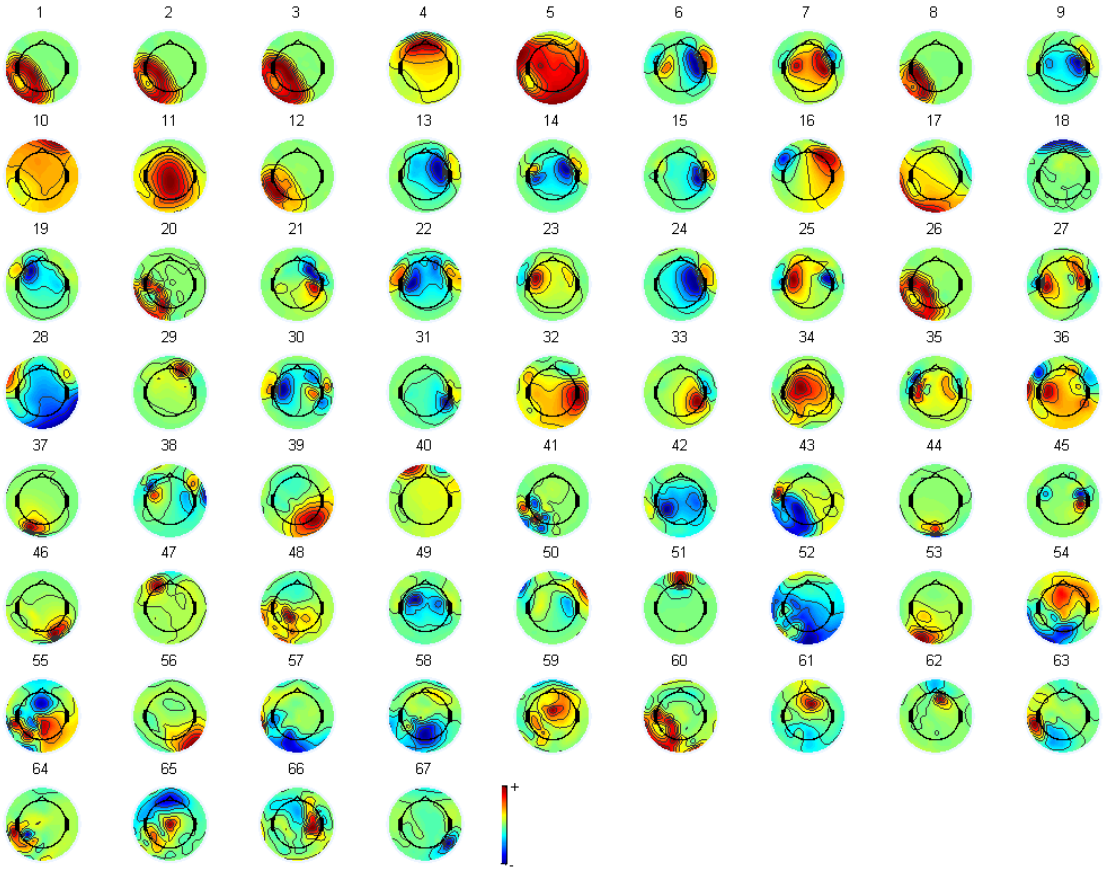

Figure 8.4: Topographic maps of 67 ICA components (i.e. spatial representation of the ICA demixing matrix) in response to tone bursts for the same data as in Figure 8.2, before artefact rejection. Each subfigure shows an axial view of the top of the head with the right side being the right of the head.

not be present in a typical ALR. This peak could have come from some artefact that had not been removed completely. However, the ensemble average of one of the ICs (component 11 in Figure 8.5) looked very much like the reconstructed AEP in channel 1 and contained the same peak around 120 ms, it was decided that it might actually be an extra peak that occurred in CI users. In fact, after artefact rejection of other datasets, this peak was observed consistently in most patients and recording sessions.

The same steps (visual component selection and elimination) were repeated for all patients and both recording sessions and the clean data were low-pass filtered to 30 Hz before ensemble averaging. The EEG response after artefact rejection looked similar to the expected ALR in most cases except for patient 3 recording 1 (Figure 8.8) that seems to be missing the P1 and N1 components of the ALR (see section 2.5.1). Also, in some cases, such as patient 2 recording 1 (Figure 8.9), an early (30-40 ms) negative or positive peak can be observed which might be the onset effect of the implant which has not be removed completely.

In all cases, as the onset and offset peaks of the CI artefact were close to the peaks

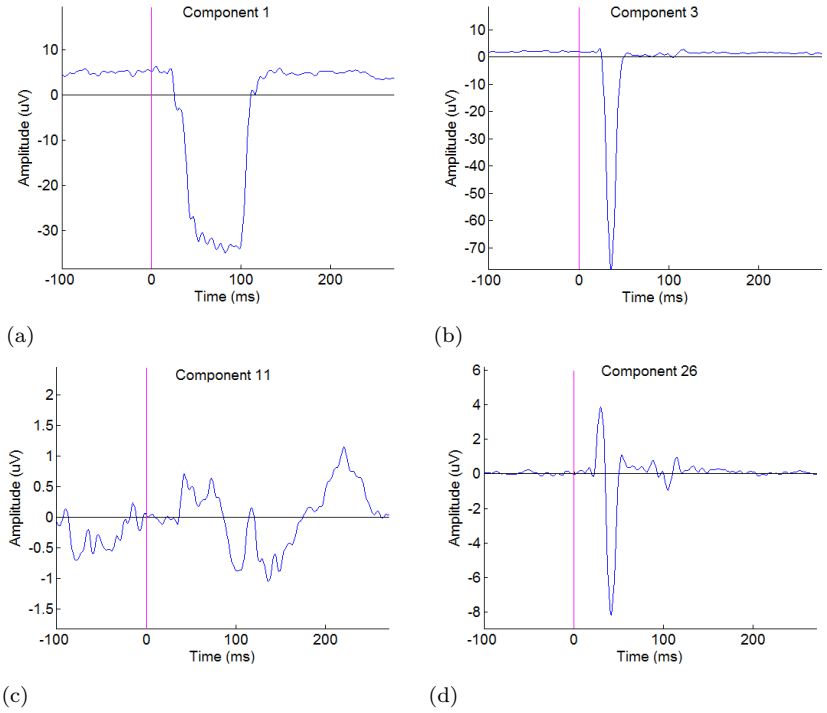

Figure 8.5: Ensemble average (a-d) of four different components of Figure 8.4. The stimulus onset occurs at zero seconds.

expected in ALR, there was some doubt as to the validity of the observed ALR. However, topographic maps of the observed EEG after artefact rejection (Figures C.2, C.4, C.6, C.8, C.10, and C.12) did not show concentration of activity close to the implant site, at least not around the main peaks of the ALR. Thus, it appears that ICA and visual component selection are effective approaches for rejection of CI artefact and the same approach was therefore employed to reject the CI artefact in EEG data in response to words.

Words

EEG data were pre-processed according to section 8.3.1, ICA was applied on the data, and artefactual components were selected visually. As previously, the data were then reconstructed from the rest of the components. Note that the CI artefact usually follows the envelope of the stimulus and when the components are averaged over epochs, this property would help in identifying the artefactual components (like the pedestal shape and large onset and offset effects in tone bursts). However, because in the case of words, there was no exactly repeating stimulus and the stimulus is not as fast changing as a tone burst, the artefact clues were not clearly evident from the ensemble average in temporal AEP maps. This made it more difficult to visually detect the artefact components using time domain responses to words. Also, more components showed mixed activity (from implant and non-implant sites) in topographic maps compared to the tone burst condition, which also made it impossible to only keep the response and reject the artefact. It soon became evident that this artefact rejection procedure was

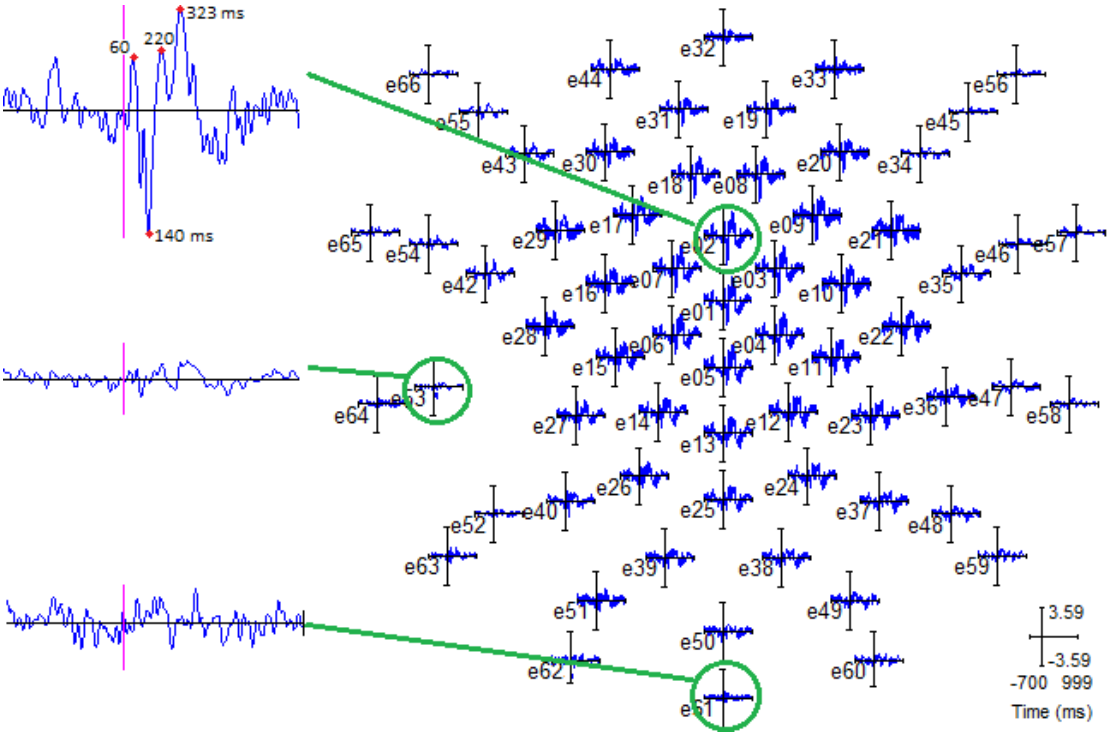

Figure 8.6: AEPs in all channels for the data in Figure 8.3 after artefact rejection by visually selecting ICA components (patient 1 recording 2 in response to tone bursts). Data were low pass filtered to 30 Hz after artefact rejection. The scale is presented at the bottom right corner. A larger view of some of the channels (circled in green) is presented on the left hand side of this figure. The magenta line marks the stimulus onset which occurs at zero seconds.

not as straight forward as before and artefact components were not as easy to identify as in tone bursts.

Figure 8.10 shows temporal AEP maps in a few electrodes in response to words in patient 2, recording 1 before artefact rejection, for electrode positions refer to Figure 3.1.a. Note that channel 23 falls almost over the implant transmitter in this patient. ICA was applied on these data after electrodes 23 and 36 were removed from the data as they were very close to the CI transmitter and electrode 45 was removed because it had not been connected properly. The topographic maps of ICA components in these data is presented in Figure 8.11. Dark red/blue areas for each IC means that this IC has a large positive/negative contribution from scalp electrodes close to that area. For example, ICs 4, 5, and 6 show high contribution from electrodes around the implant site and can be considered as artefact.

Using both temporal and spatial maps of ICs, components 4, 5, 6, 9, 12, 32, 39, 45, and 50 were marked as CI contaminated and were removed from the data along with some other components such as 1 and 13 that showed stereotypical artefacts such as eye-blink and 50 Hz noise. Channel data were reconstructed with the remaining ICs. As the evoked response to words had been seen in low frequency bands in normal hearing subjects,

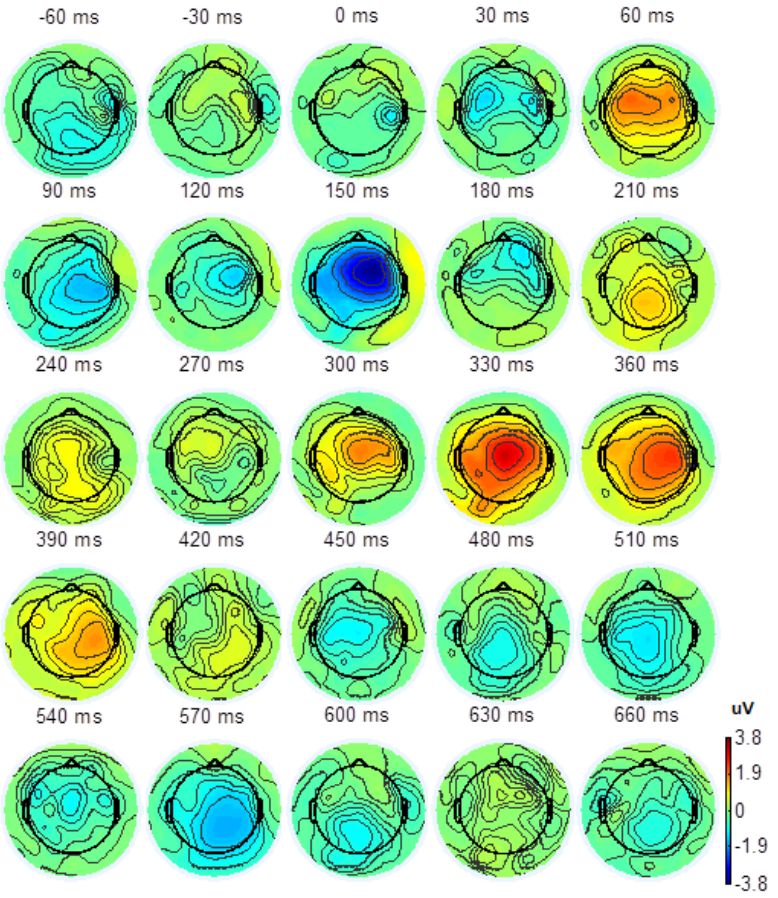

Figure 8.7: Topographic maps of channel AEPs at different times in response to tone bursts for the same data as in Figure 8.6 (patient 1 recording 2). Each subfigure shows an axial view of the top of the head with the right side being the right of the head. The stimulus onset occurs at zero seconds.

after reconstruction of data, thwy were first low-pass filtered with a cut-off frequency of 8 Hz and then the ensemble average over all epochs was calculated. The AEPs of a few channels after artefact rejection and low-pass filtering and the topographic maps of these AEPs over time are presented in Figures 8.12 and 8.13 for patient 2 recording 1.

Although the timings of the peaks are very similar to those obtained from normal hearing subjects (refer to Figures 3.2 and 3.3) especially in frontal electrodes, the flatness of the third peak (around 300 ms) raises the question of improper artefact rejection. Thus, the signal before low-pass filtering was also inspected. Figure 8.14 shows AEPs in the same channels after artefact rejection but before low-pass filtering. As the signal had last been filtered in the [1 120] Hz frequency band, and in this band no obvious change could be detected in AEPs in normal hearing subjects, the large changes with their big jumps in the signal (Figure 8.14, channels 1 and 35) appeared suspicious and might have come from an artefactual component. Thus, AEPs of ICA components were investigated and it appeared that the dominant component for the observed EEG was component number 3 which was not coming from the implant site (refer to Figure 8.11). Thus, the

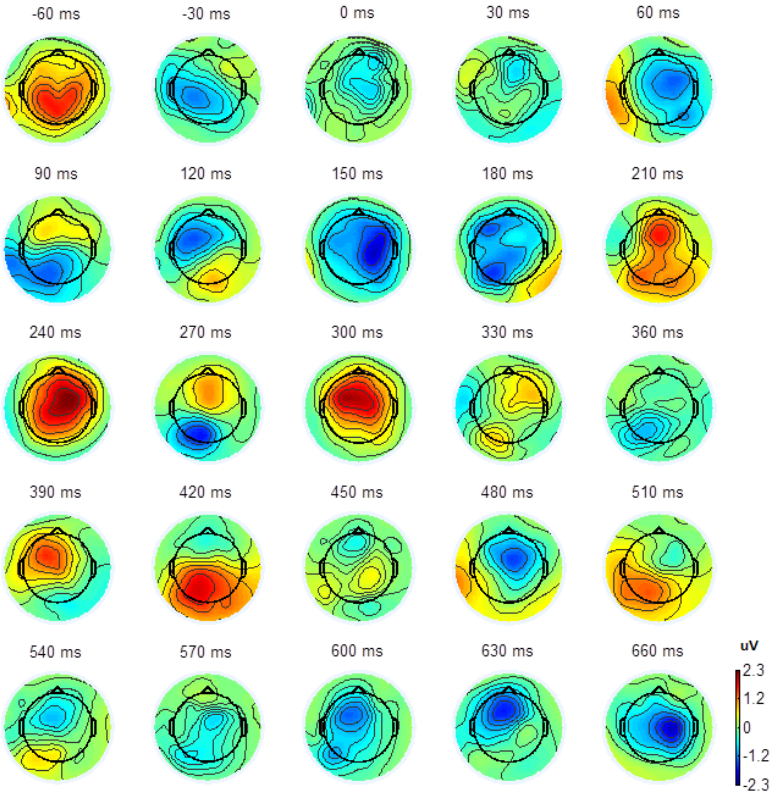

Figure 8.8: Topographic maps of channel AEPs over time in response to tone bursts, for Patient 3 recording 1 after artefact rejection. Each subfigure shows an axial view of the top of the head with the right side being the right and the left being the left of the head. The stimulus onset occurs at zero seconds.

question still persisted if this component, and a few others that looked similar to this one but were coming from different topographic areas, had to be removed from the data. Although it is a matter of opinion, in this study, these components were not eliminated. This issue clearly illustrates the concern in using visual methods for artefact rejection.

Similar problems, i.e. if a component should or should not be rejected, were observed in other patients and recording sessions in response to words. As a result, the step of selecting the ICs that may be deemed an artefact became a greater challenge than for tone-bursts.

Similar steps were taken for other patients and recording sessions and on average, 20 components ($\sigma = \pm 2.4$ components) were kept in each dataset. The AEPs of a few channels and the topographic maps of these AEPs over time after artefact rejection and low-pass filtering with 8 Hz are presented in Figures C.13 to C.24 in appendix C for all patients and different recording sessions in response to words. In most cases, clear peaks can be observed with timings close to those observed for normal hearing subjects (refer to Figures 3.2 and 3.3 for comparison); however, as mentioned before, the source may still be from the CI and not physiological.

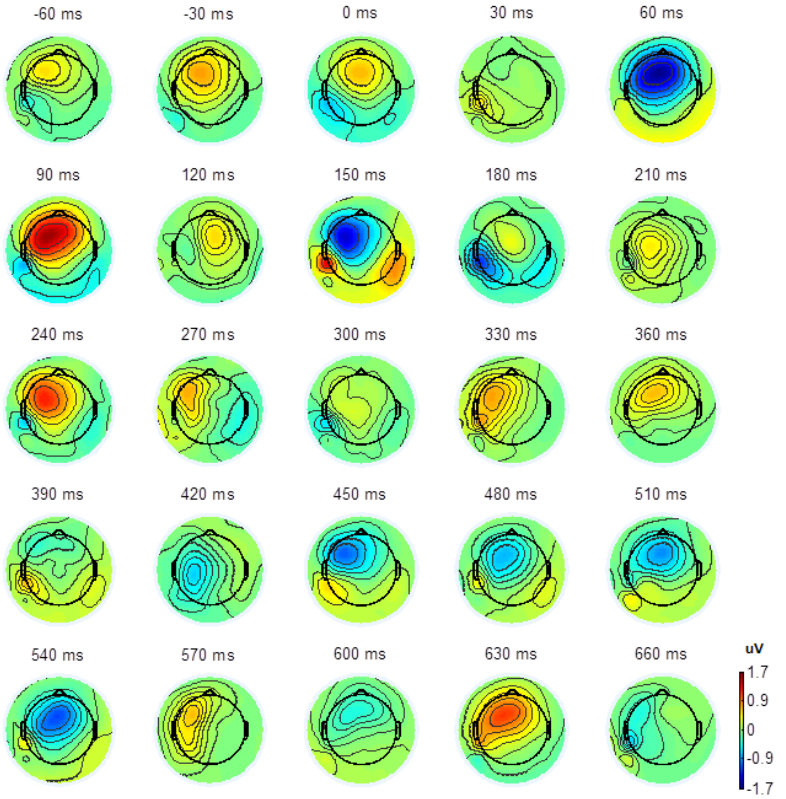

Figure 8.9: Topographic maps of channel AEPs over time in response to tone bursts, for Patient 2 recording 1 after artefact rejection. Each subfigure shows an axial view of the top of the head with the right side being the right and the left being the left of the head. The stimulus onset occurs at zero seconds.

Although around 40 components (out of about 65 components) have been removed from each dataset, we cannot be sure that the artefact has been completely removed. From visual inspection (especially of the unfiltered signal), concern remains that artefacts continue to be present in the signals. Removing ICA components visually could not be improved further for word stimuli and thus other approaches were pursued.

8.3.1.2 ICA with additional pre-processing

In the absence of a gold-standard, the primary criteria for judging the results were whether the additional processing notably changed results, removing more of what might be judged, visually, to be an artefact (see previous section), without removing what is likely to be the brain's response to stimuli. In this regard, with the use of ICA, the concern is removing too few components (and leaving artefact) or too many components (and removing some of the stimulus response). Thus, to improve the visual representation of artefacts in word stimuli (and make the artefact components stand out more clearly), different pre- and post-processing procedures were employed. Again, these methods were first tested on data from tone bursts.

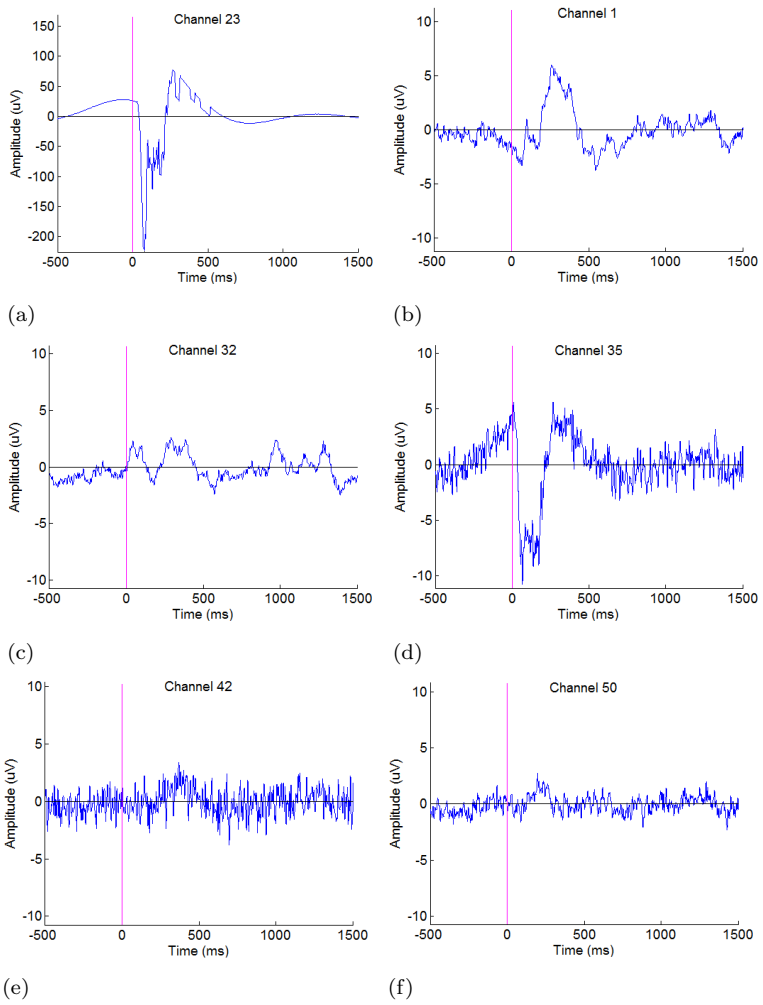

Figure 8.10: AEPs in response to words in a few channels before artefact rejection for patient 2, recording 1, for electrode positions refer to Figure 3.1.a. Note that the amplitude scale changes between subfigures. For channel locations refer to Figure 3.1.a. The stimulus onset occurs at zero seconds and the average length of words is 540±80 ms.

In the first approach, more electrodes around the implant transmitter site were removed. The rationale for this approach was to reduce the effect of large artefact amplitudes on ICA. In a second approach, the signals were low-pass filtered (for example to 30 Hz) before applying ICA following the suggestions in Sandmann et al. (2009) to decrease the high-frequency CI artefact. The former did not change the results and the latter produced more mixing of implant and non-implant activity in different components. These results are thus not presented here. The data were also filtered to lower frequency bands (such as 30 Hz) and then downsampled (to 100 Hz) before applying ICA. However, the fine structure of the signal was affected greatly and the number of data points decreased significantly so the ICA was not able to demix the channel signals effectively and most components showed dominant activity around the implant site. For example, Figures 8.15 and 8.16 show the results of applying ICA on low-pass filtered (30 Hz) data

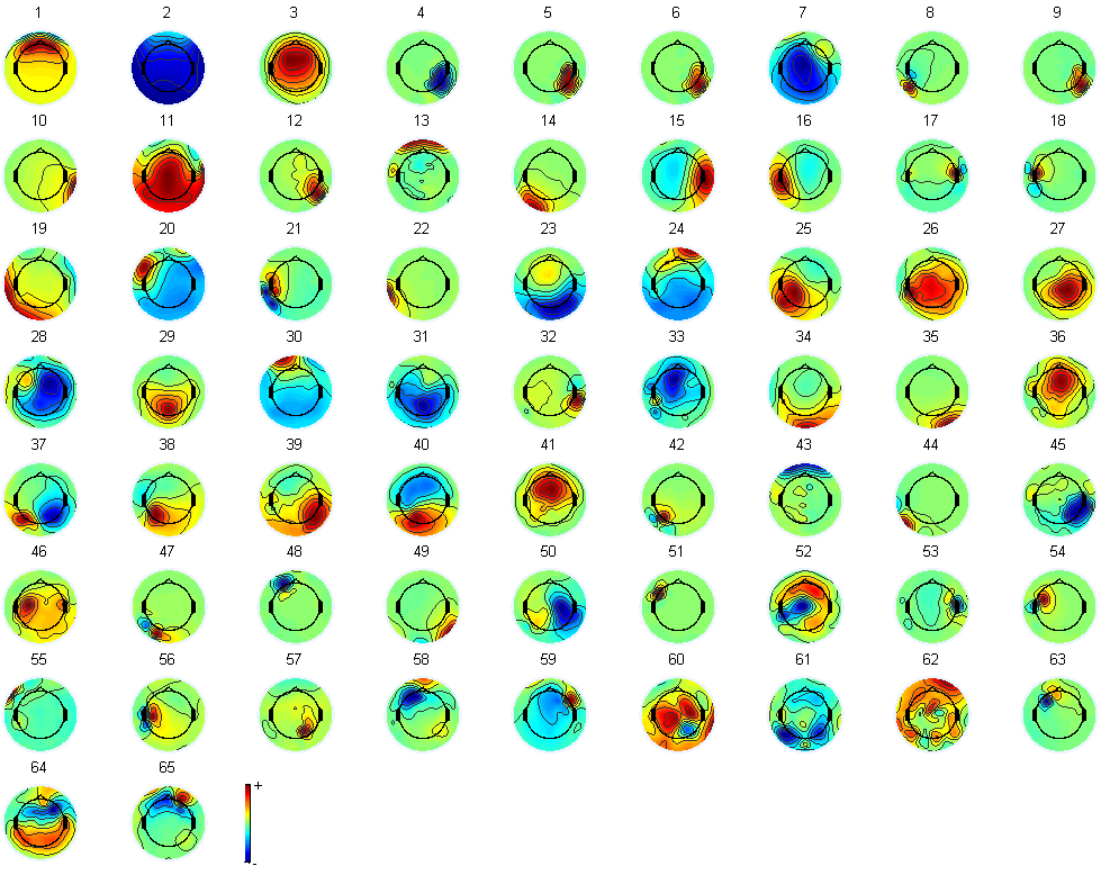

Figure 8.11: Topographic maps of 65 ICA components for patient 2 recording 1 in response to words before artefact rejection. Each subfigure shows an axial view of the top of the head with the right side being the right of the head.

in patient 1 recording 2 (i.e. the recording after the patient has been using the implant for about 12 months) before and after downsampling to 100 Hz, respectively. In these figures, dark red/blue areas for each IC means that this IC has a large positive/negative contribution from scalp electrodes close to that area. For example, IC numbers 1, 2, and 3, in both figures, show high contribution from electrodes around the implant site. In Figure 8.15, components 28, 35, and 52 and in Figure 8.16, components 18, 25, and 29 are examples of mixed CI- and non-CI-related activities because these components do not show concentrated activity around the implant site and their activity is scattered over different areas of the brain. Also, in both figures, more implant-related components (concentrated around the implant site) are present compared to the non-filtered data (compare with Figure 8.4). Thus, using the [1 120] Hz filter band appeared to be more appropriate than filtering to lower frequency bands such as [1 30] Hz and downsampling.

8.3.1.3 ICA and semi-automatic component selection

As visual selection of ICs appeared to be working more reliably on ICA of tone bursts than words, another approach investigated for improving ICA results for words. This

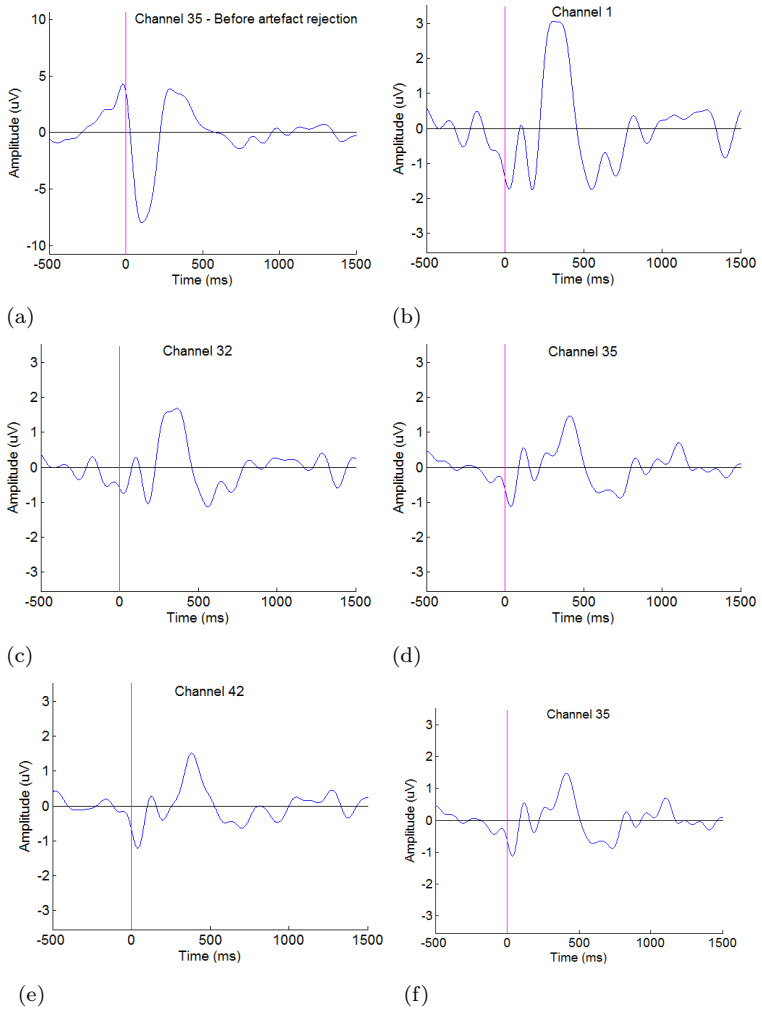

Figure 8.12: AEPs in response to words in a) a channel close to the implant site before artefact rejection and in b-f) five channels after artefact rejection for Patient 2 recording 1 after low-pass filtering to 8 Hz. For channel locations refer to Figure 3.1.a. The stimulus onset occurs at zero seconds.

approach was to use the demixing matrix calculated in response to tone bursts and use it for EEG in response to words. The reasoning behind this approach was that the sources of artefact were the same in both stimulus types. With this assumption in mind, in each dataset, ICA was applied on EEG in response to tone bursts and the artefactual ICs were identified for tones, then the demixing matrix was extracted for tones and multiplied by channel data in response to words. From the obtained ICs in words (obtained using demixing matrix from tones), the same ICs that had been marked in tone bursts as being artefactual, were removed and data were reconstructed. However, it was observed that this approach kept much of the CI artefact in the data. As an example, Figure 8.17 shows AEPs in a few channels resulting from this approach in patient 1 recording 2, in response to words. It is clear that the signal is not free from the artefact yet. The same approach was applied on other datasets. In some datasets, the result of this approach was similar to that obtained from visual selection and in some, the results

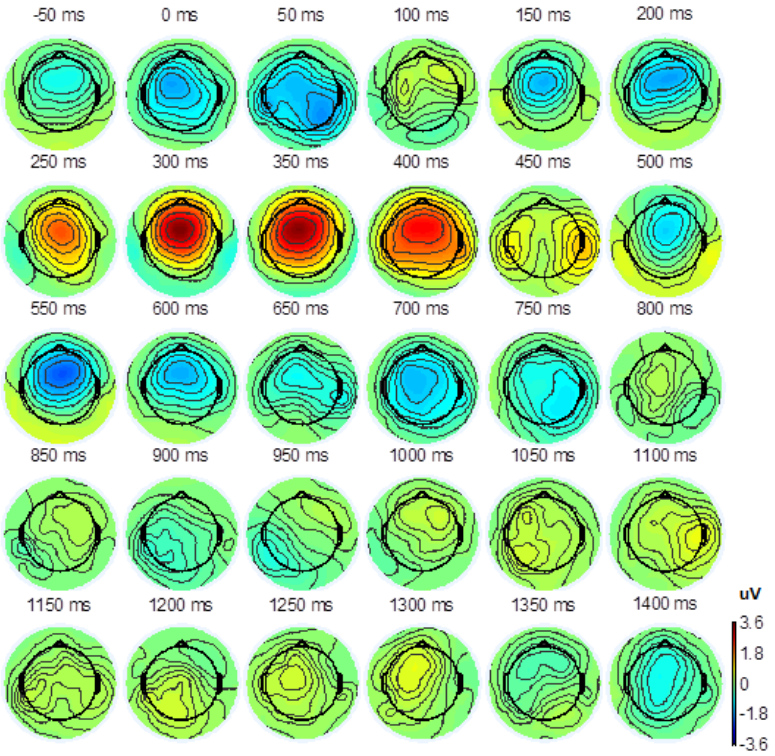

Figure 8.13: Topographic maps of channel AEPs over time in response to words, for Patient 2 recording 1 after artefact rejection (visual selection of ICA components), the same data as in Figure 8.12. Each subfigure shows an axial view of the top of the head with the right side being the right of the head. The stimulus onset occurs at zero seconds.

showed a large CI artefact. These results were quite dependent on the components that had been marked artefactual for tone burst stimulation leading to disproving the initial assumption that the sources of artefacts are the same in tone bursts and words. Thus, this approach was deemed inappropriate for the purpose of CI artefact rejection from EEG in response to words.

8.3.1.4 ICA and other approaches

Other approaches and measures were also tested for automatic component selection. As previously, the methods were first tested on EEG in response to tone bursts.

Power

It was observed visually that the broadband power in CI related components was higher than non-CI ones. Thus, to that effect, after applying ICA on EEG data in response to tone bursts, the broadband power was computed in each component before and after the stimulus onset for different epochs separately. In each component, a paired Wilcoxon signed-rank test was applied on power values before and after the onset and components showing significant increase ($p<0.05/68$, p-value corrected by the number

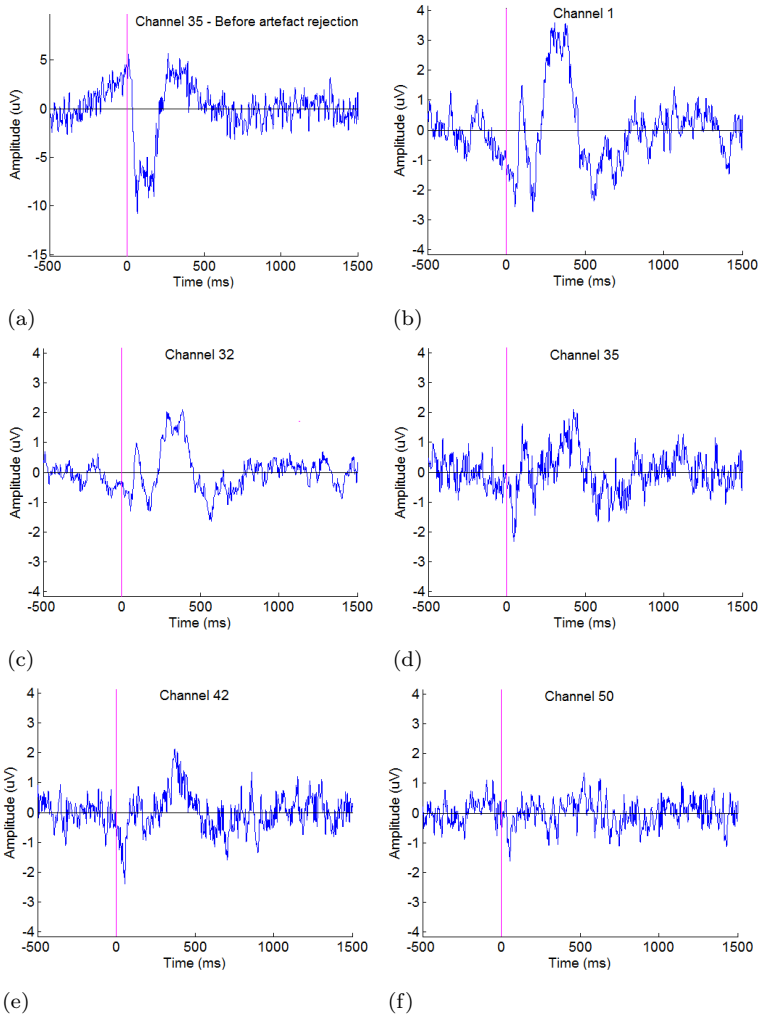

Figure 8.14: AEPs in response to words in a) a channel close to the implant site before artefact rejection and in b-f) five channels after artefact rejection for Patient 2 recording 1 before low-pass filtering. The stimulus onset occurs at zero seconds.

of components) in power after the onset were marked as CI-related components. This approach was applied on patient 1 recording 2 and showed promising results as it chose all components with centroid around the implant site along with a few components that had been marked to be CI-related by visual selection (refer to section 8.3.1.1). However, on some datasets (such as patient 2 and patient 3 both recordings), many of the obvious CI components (either through their AEP or their topographic map) were not marked as CI-related. For example, Figure 8.18 shows topographic maps of ICs in response to tone bursts in patient 2 recording 2. Using this approach, components 1, 5, 7, 36, 43, and 62 were correctly marked as CI-related but components such as 17 and 18 that were clearly CI-artefact (because they have centroid around the implant site), were falsely rejected. This approach was pursued with different frequency bands, time windows, and significance levels, however, every time either some of the artefact components were missed, or in the case of higher significance levels, some components that did not appear

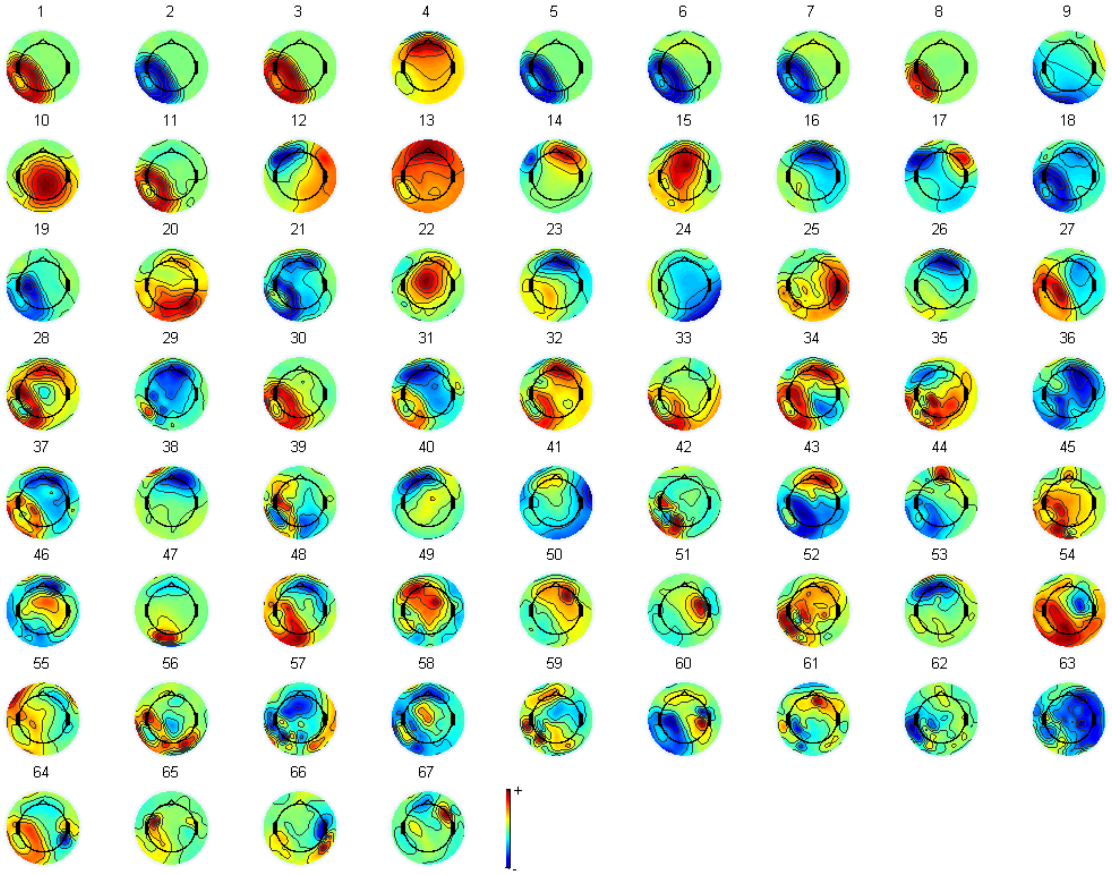

Figure 8.15: ICA components in response to tone bursts in patient 1 recording 2 after low-pass filtering of data to 30 Hz. Each subfigure shows an axial view of the top of the head with the right side being the right of the head.

to be CI-related were selected. Thus, this approach was dropped.

Kurtosis

Kurtosis is defined as the fourth normalised moment, describes the peakedness of the distribution, and is calculated as $K = E(x - \mu)^2/\sigma^4$ (Delorme et al., 2007); where, μ and σ are, respectively, the mean and the standard deviation of the distribution and E indicates the expected value. The value of kurtosis is around 3 for a Gaussian distribution. Having this property, Kurtosis is shown to be helpful in identifying artefact components after applying ICA on EEG (Delorme et al., 2007). For example, eye-blink-related components show very high kurtosis values and line noise from electrical sources show very low kurtosis values.

As some of the main characteristics of CI artefact are overshoots and undershoots specially around the stimulus onset and offset times, it was hypothesised that the kurtosis of CI-related components must be much higher than other components and that the kurtosis of these components should have a significant change after the stimulus onset compared to the baseline.

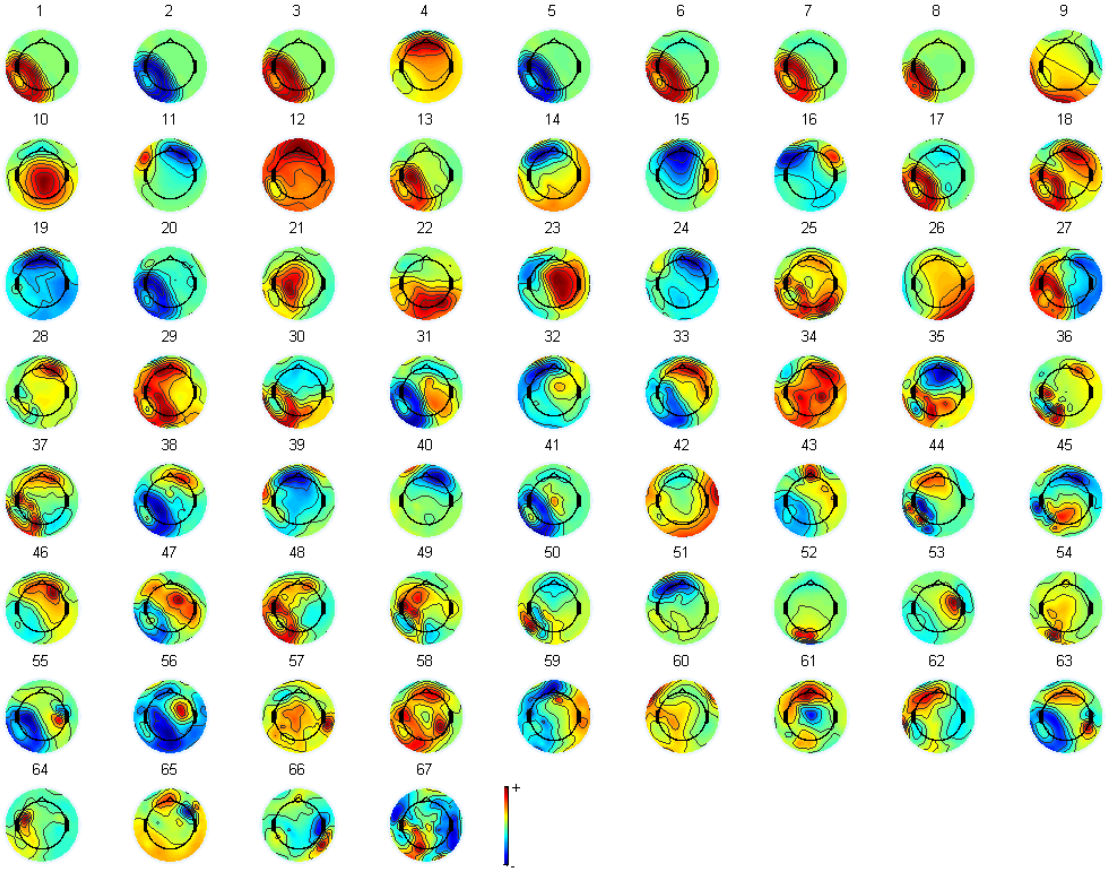

Figure 8.16: ICA components in response to tone bursts in patient 1 recording 2 after low-pass filtering of data to 30 Hz and resampling to 100 Hz. Each subfigure shows an axial view of the top of the head with the right side being the right of the head.

Thus, similar to power analyses, for each component, kurtosis was calculated before and after the onset for each epoch separately. Then, in each component, a paired Wilcoxon signed-rank test was applied on kurtosis values before and after the onset. Components with significant ($p<0.05/68$, p-value corrected by the number of components) increase after the onset compared to the baseline were marked as artefact. With this approach, there was the chance of falsely selecting a response-related component as being artefact but it was presumed that this problem could be controlled by setting an appropriate significance level. However, it was observed that even the obvious CI-related components could not always be detected by this approach even without correcting the α value. For example, in patient 2 recording 2 with ICA components as in Figure 8.18, components 17 and 36, which show clear artefact characteristics both in the spatial (centroid around the implant site) and temporal (not shown here) maps but not as strong as other CI-related components, were never selected even when the α level was set to 0.05.

Using kurtosis, another approach was employed. This time, after the kurtosis was computed for all epochs, it was averaged over all epochs for each component. Then, the mean value of the kurtosis over all components was subtracted from these values and

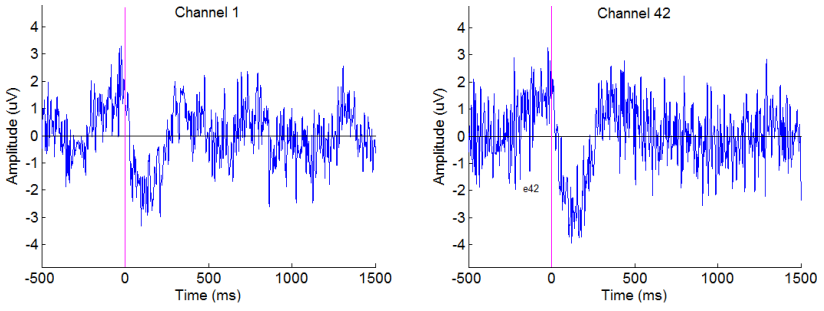

(a) (b)

Figure 8.17: AEPs in response to words after artefact rejection using the demixing matrix of tone bursts, in patient 1 recording 2. The stimulus onset occurs at zero seconds.

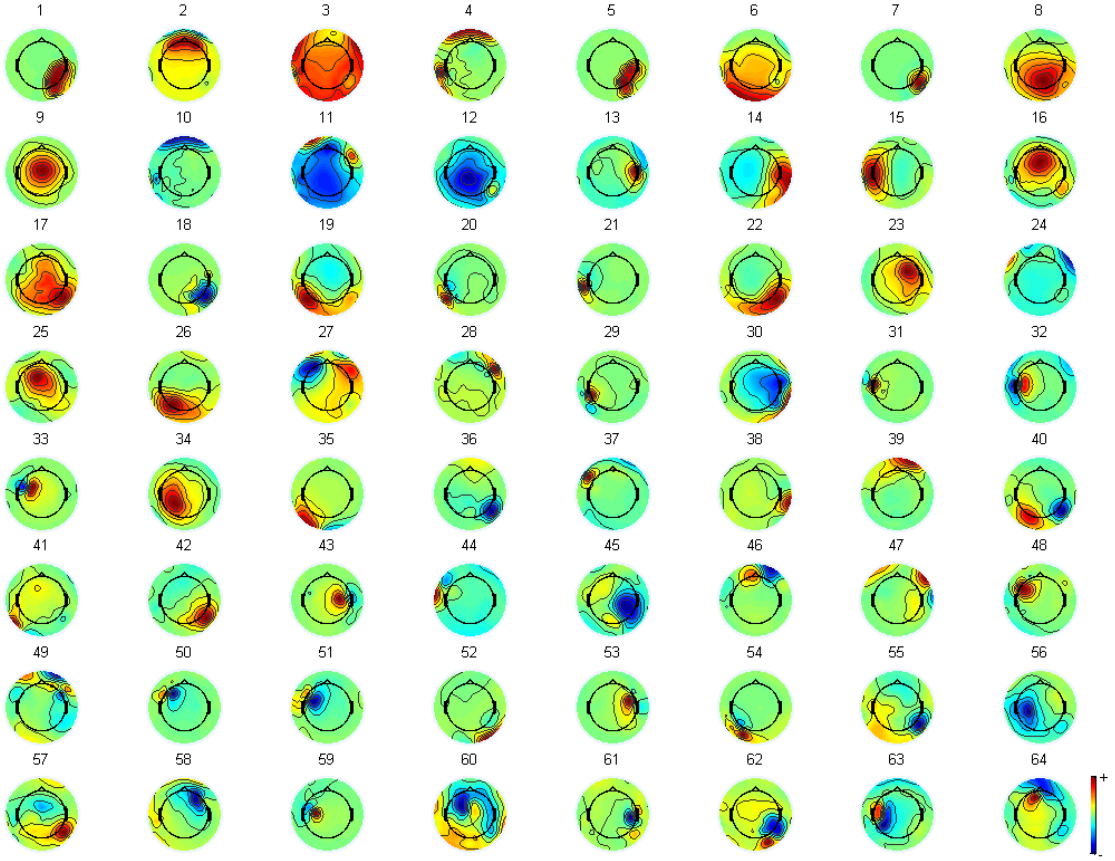

Figure 8.18: ICA components in response to tone bursts in patient 2 recording 2 before artefact rejection. Each subfigure shows an axial view of the top of the head with the right side being the right of the head.

they were normalised to their standard deviation to make a normal distribution. A threshold of ± 1.96, 2σ which is the 95% confidence interval of a normal distribution and σ is the standard deviation of the distribution, was set and components outside this range were marked as CI-artefacts. However, because in most datasets, a couple of

components had very high kurtosis values, they would affect the normality of the distribution and the z-values of all components would fall inside the threshold range. Thus, no components would be selected as artefact. To solve this problem, those very high kurtosis values were marked as artefact before z-transform and then were eliminated from the mean and standard deviation calculation. This time, more components were selected as artefactual, however, many of the artefactual components were missed again.

Therefore, the methods tried here based on kurtosis also appeared to be inappropriate for the purpose of CI artefact rejection using ICA.

Correlation

As explained in section 8.3.1.1, the CI artefact follows the envelope of the sound signal. It was presumed that the correlation of CI-related components with the envelope of the sound signal should be much higher than other components. This assumption was also tested on tone burst data. However, as different ICs pick various parts of the artefact, e.g. one component may only include the onset effect and the other one just the offset effect, the correlation would only be high in components that closely followed the whole tone burst envelope, i.e. were pedestal-like. This would again cause the same problem as other component selection methods, i.e. only the obvious CI-related components would be marked.

As an another approach using correlation, all epochs of each component were concatenated and the autocorrelation function of each component was estimated. As the CI artefact or the brain response are repeated in each epoch, the autocorrelation function of these components had to be periodic with a frequency equal to the reverse of the length of one epoch. Thus, if the FFT of the autocorrelation function was estimated in each component, those components with a significant increase in this frequency compared to the neighbour frequencies would be marked as CI- or response-related components. Because the CI artefact is assumed to be more time-locked to the stimulus and also larger than the brain response, we were hoping that CI-related components would produce higher correlation values and using a threshold on significance values would then separate these two groups. But this method did not work properly either.

As the correlation related approaches were not successful, no more details will be given.

Coherence

Assuming that the CI-artefact is more time-locked to the stimulus than the brain response, it was assumed that the Magnitude Squared Cohere (MSC) (refer to Equation 6.2) of each component with the stimulus would be much higher for CI related components than other components. If this assumption was true, we could find a threshold for keeping or removing a component. However, again, MSC was only very high in a few obvious CI-related components and this approach was also dropped. As this approach was unsuccessful, it will not be explained further.

The reason behind the poor performance of artefact rejection in this section could be that the artefact in those components was not strong enough to cause a significant change in the measured statistic but because of the temporal and spatial characteristics of that component, it could be visually detected. Also, it is possible that the time-locking of the response and weaker artefact components were similar and that their SNRs (response to noise or artefact to background noise) were in the same range. Because these measures could not find obvious artefactual components, we could not be confident about other selected or non-selected components either.

8.3.2 Plus minus averaging

As the shape of the tone stimulus is the same in all epochs, it was assumed that the CI artefact should appear similarly in all epochs in response to tone bursts and that it could be eliminated from each epoch by ensemble averaging and subtracting the ensemble average from each epoch. Subtracting the ensemble average would also remove the evoked response from the data, however, this was not a problem because the induced response would still remain in the data. Nevertheless, it was important that if the evoked response was being excluded, it was done thoroughly. Because of the phenomenon of the habituation of the brain, the evoked response would eventually subside after high number of presentations. Thus, the subtraction of the ensemble average may eliminate the evoked response from the early epochs but not from the last ones. To resolve this problem, Plus-Minus averaging (PMavg) method was examined. In PMavg, every other epoch is subtracted from the epoch before, leaving a dataset with only the induced response in each epoch and half the epochs in the original dataset. Note that this method could only be used for tone bursts and not words because words were changing from one epoch to the next one thus different CI artefacts arise in each epoch.

After epoching the data for the tone burst stimulus, the PMavg was applied on each channel. However, looking at the data after PMavg showed that there were still large onset and offset effects visible in the data, so strong that they were evident even without averaging. Figure 8.19 presents a few epochs of one dataset (patient 1, recording 2) before and after PMavg. The spectrogram of the evoked response in this dataset was calculated according to section 4.2.1. The sprectrogram of the evoked response in one channel (close to the implant site) of this dataset before and after PMavg is presented in Figure 8.20. These figures show that PMavg could eliminate most but not all of the low frequency contribution of the CI artefact. Also, it could not remove the high frequency contents of the CI artefact at all.

It was initially presumed that the artefact was perfectly time-locked to the stimulus, however, plotting all epochs in the same figure showed that there was a very small time shift (around 10 ms) in this artefact between epochs (see Figure 8.21) which is probably coming from CI sampling of the input sound. This time shift causes the PMavg to not

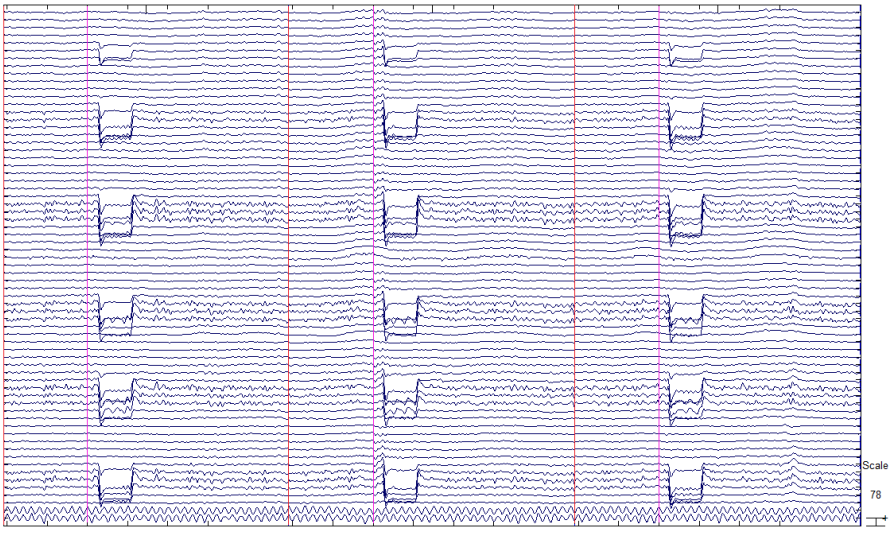

(a)

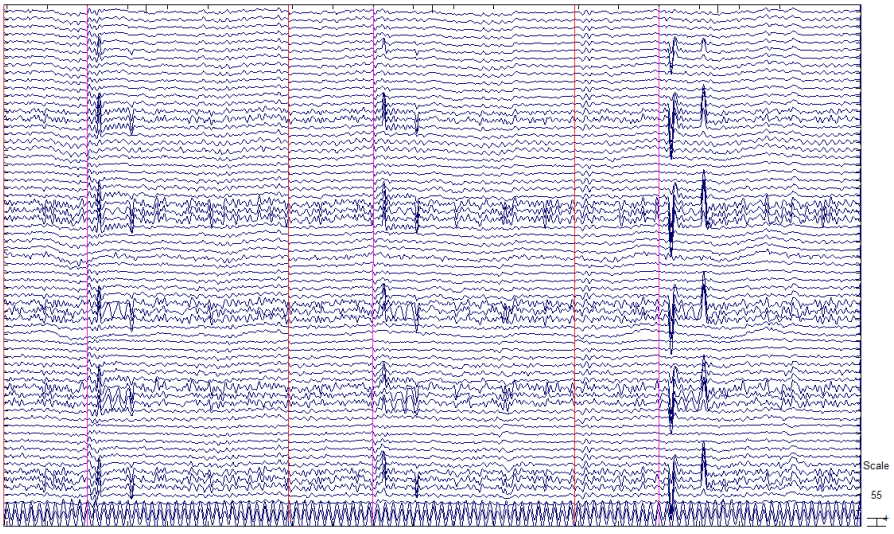

(b)

Figure 8.19: Three epochs of the EEG response to tone bursts in patient 1 recording 2 a) before and b) after PMavg in channels 1-40 and 42-68 (from top to bottom). Channel 41 is removed because it showed saturation effects. Red lines show the start of each epoch and magenta lines show the stimulus onset.

generate a perfectly artefact rejected data. Thus, this method also proved to be unfit for the purpose of artefact rejection in CI contaminated EEG.

8.3.3 Wiener filtering

Another method that seemed to be appropriate for CI artefact rejection was Wiener Filter (WF). In Wiener filtering, a desired signal is known and a second signal is filtered with the WF in a way that the output of the filter resembles the desired signal. Different filters are considered for the Wiener Filter in the literature one of which is the FIR filter

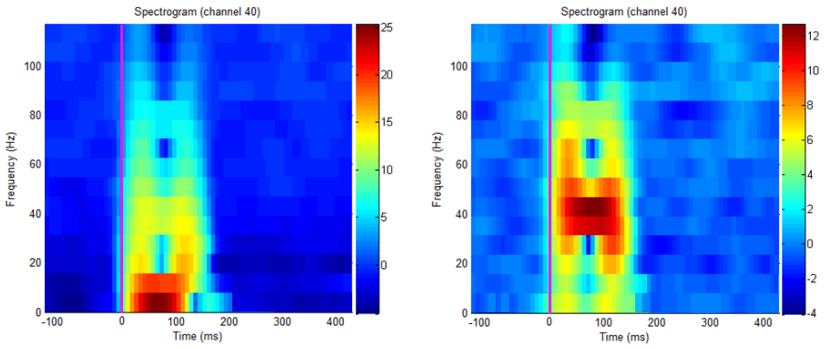

(a) (b)

Figure 8.20: The evoked response spectrogram of channel 40 in response to tone bursts in patient 1 recording 2 a) before and b) after PMavg. The magenta line indicates the start of the stimulus.

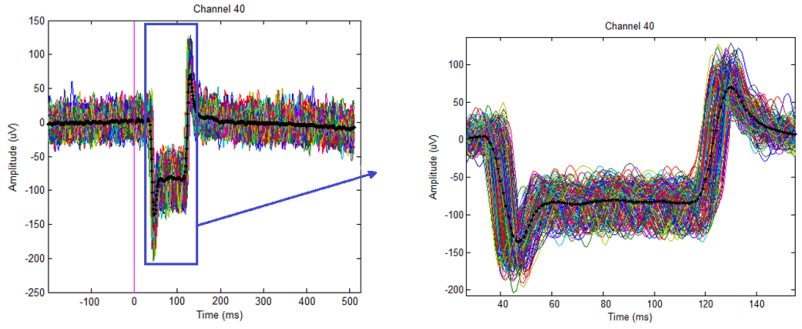

(a) (b)

Figure 8.21: a) All epochs of the EEG response to 2kHz tone bursts in a CI user filtered in 1-120Hz. b) A magnified version of Figure 8.21.a. The magenta line shows the onset of the stimulus. The black dotted line shows the ensemble average of all epochs.

(Vaseghi, 2008). To estimate the parameters of the filter, MSE between the estimated signal and the desired signal is minimised. One of the applications of WF is in noise reduction (Vaseghi, 2008).

In this research, based on a channel in which noise dominates, we try to find a filter that provides an estimate of artefact in another channel. By subtracting this estimate away, we may be able to reduce the artefact in that channel. In our application, the input of the filter will be a channel with a large artefact and the desired signal will be each one of the other channels separately. The output should resemble the desired signal and will be reduced from the desired signal to produce an artefact-free signal. The block diagram of this process is presented in Figure 8.22.

In this figure, Ch.1 is the highly artefact-affected channel, Ch.2 is the channel we intend to remove the artefact from, and $e(t)$ is the artefact rejected signal. N_1 and N_2 are artefacts in Ch.1 and Ch.2 and S is the potential response. Note that the evoked response of the brain would also be removed from the signal along with the artefact if it

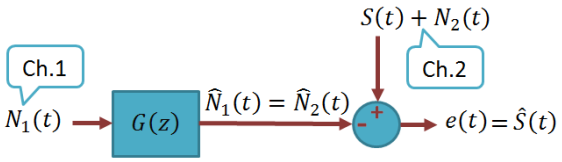

Figure 8.22: The block diagram of WF in EEG of a CI user

is present in both channels but the induced response would probably remain if it is not phase-locked between channels. If the evoked response is not present in both channels, we would be able to retrieve that response as well. For our further connectivity analyses, the induced response would suffice. The benefit of this method is that it could also be applied to words because each epoch would be artefact rejected separately and different epochs would not affect each other.

To formulate the problem, it is assumed that $\hat{X}$ is filtered by a Finite Impulse Response (FIR) Wiener Filter $G(z)$ and its MSE with $S(t)$ should be minimum; where, $S(t)$ is the desired signal. Thus:

$$\hat{X}(t) = \sum_{i=1}^{K} a_i X(t-i), \tag{8.1}$$

and

$$e(t) = S(t) - \hat{X}(t). \tag{8.2}$$

To estimate the parameters of the filter, MSE, i.e. $E\{e^2(t)\}$, is minimised and from there $\bar{a} = \bar{r}_{XS} R_X^{-1}$ is obtained where $\bar{a}$ is the vector of parameters of the filter, $\bar{r}_{XS}$ is the vector of cross-correlation between the input and the desired signal, and R_X is the autocorrelation matrix of the input (Vaseghi, 2008).

The method was first applied to tone bursts. As an example, in patient 1 recording 2, channel 40 was considered as the input N_1 of the Wiener filter because it was closest to the CI transmitter and was affected most by the CI artefact. Then, all other channels were considered as the desired signals $S + N_2$ one by one. As the artefact in different channels occurred simultaneously, an order 1 FIR filter was expected to suffice to eliminate the artefact, however, other orders were also tested. Some examples are presented in Figure 8.23 for two reference signals but always with channel 40 being the input of the filter. In this figure, a first order FIR filter was used. The notations on this figure match those of Figure 8.22. Each subfigure is an ensemble average over different epochs for each one of the noise and reference channels. The method clearly greatly reduced the artefact (compare $S+N_2$ and $\hat{S}$ in this figure), but was unable to eliminate it completely.

The same approach was repeated for higher orders of WF but again the artefact could not be removed completely, the results are not presented.

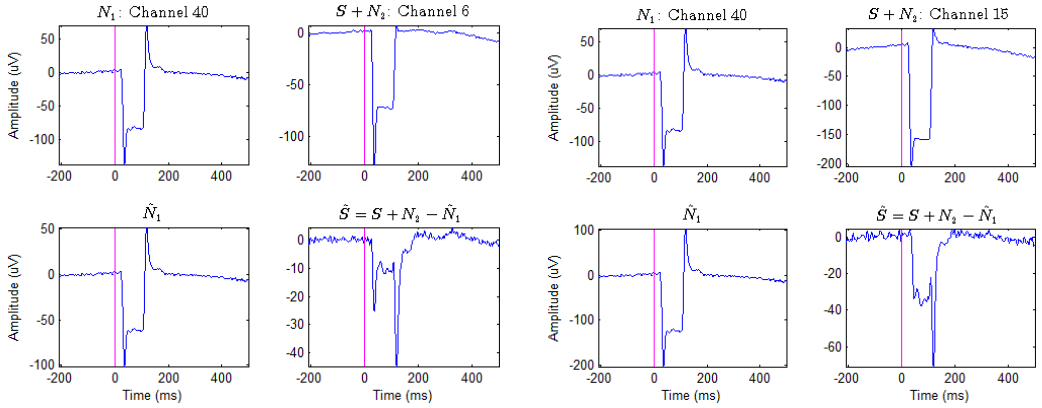

(a) (b)

Figure 8.23: Noise cancellation using WF with FIR filter order 1 in patient 1 recording 2 when listening to tone bursts. The input (Ch.1 of Figure 8.22) is the signal in channel 40 and the desired signal (Ch.2 of Figure 8.22) is the signal in a) channel 6 and b) channel 15, which are close to the implant site and in which an evoked response is expected. Each subfigure is the ensemble average over all epochs for that signal. $\hat{S}$ is the signal after artefact rejection. For the rest of notations refer to Figure 8.22.

The most probable explanation for the method not working is that although the artefact appears instantaneously over different channels, closer inspection showed that its shape changes from one channel to the other thus the artefact probably does not affect different channels linearly. For example, in some channels, it has as big an offset as the onset and sometimes the offset is much smaller than the onset and vice versa. A linear filter may not be helpful for removing the artefact in this case. Therefore, Wiener Filter also appeared to be an unsuitable method for cancelling the CI artefact in EEG.

8.3.4 Conclusion of the section

In this section, different methods were used for rejection of CI artefact in the data and for the sake of clarity, a brief summary of the conclusion is presented here. PMavg was considered only for repetitive stimuli such as tone bursts. Because of the small time-shift in the CI artefact between different epochs, the artefact could not be removed fully and a large onset and offset could be observed even without ensemble averaging. Wiener filter could also remove the artefact greatly, however, not completely. ICA was applied on the data and artefactual components were either identified visually or using different features of the signal such as the signal power. Using signal features, many of the components that were clearly artefacts (through visual inspection) would not be identified. Thus, these approaches could not be trusted. Removing artefacts by visual inspection was not ideal either as there were many components in each dataset that could not confidently

be marked as artefacts or selected as a response. However, the reconstructed data after artefact rejection would not show any clear artefacts (such as those in PMavg or WF) either and the evoked potentials after artefact rejection showed similar features as in normal hearing subjects. Thus, ICA and visual component selection was selected as the most suitable approach for the data used in our research (especially in response to words).

8.4 Response detection

Similar to steps taken in chapter 4, after artefact rejection of CI data, these data were tested for the presence of evoked and induced responses. It should be mentioned again that we are still not confident that the artefact rejected data are truly clean of artefacts, however, of the many options investigated, on balance ICA, together with visual inspection were deemed the most robust. These data will now be considered in exploratory analysis of induced responses and connectivity.

8.4.1 Response and tone bursts

Similar to section 4.2.1, in each patient, evoked and induced power spectra were calculated and normalised by the average power of the whole epoch and this was carried out in each frequency. As an example, Figures 8.24 and 8.25 show the evoked and induced powers, respectively, obtained in patient 2 recording 1. In Figure 8.24, an increase in most frequency bands can be observed just after the onset in all electrode groups. However, no clear induced response (consistent over different electrode groups) can be seen for this dataset, see Figure 8.25. The same steps were repeated for all other datasets.

As there are not enough datasets and they are recorded under dissimilar conditions (different implanted ear, different implant brands, etc), group significance analyses such as Friedman's test could not be performed on CI data. Thus, the bootstrap as explained in section 4.2.2 was employed to investigate the significance of observed responses. The tests were performed on evoked and induced power values after the onset compared to baseline values using the epochs within each recording. Note that similar to a brain response, CI-related artefact would be repeated in all epochs and if all CI-related components were not removed from the signal in the artefact rejected step, this artefact would be picked as a significant change from the baseline. Thus, bootstrap approach does not ensure that what is marked as significant is truly a brain response but just that the selected time-frequency point has significant power difference with the baseline (signal before the onset).

For the example in Figures 8.24 and 8.25, the result of bootstrap analyses (200 samples and α=0.05) on evoked and induced power spectra are presented in Figures 8.26 and

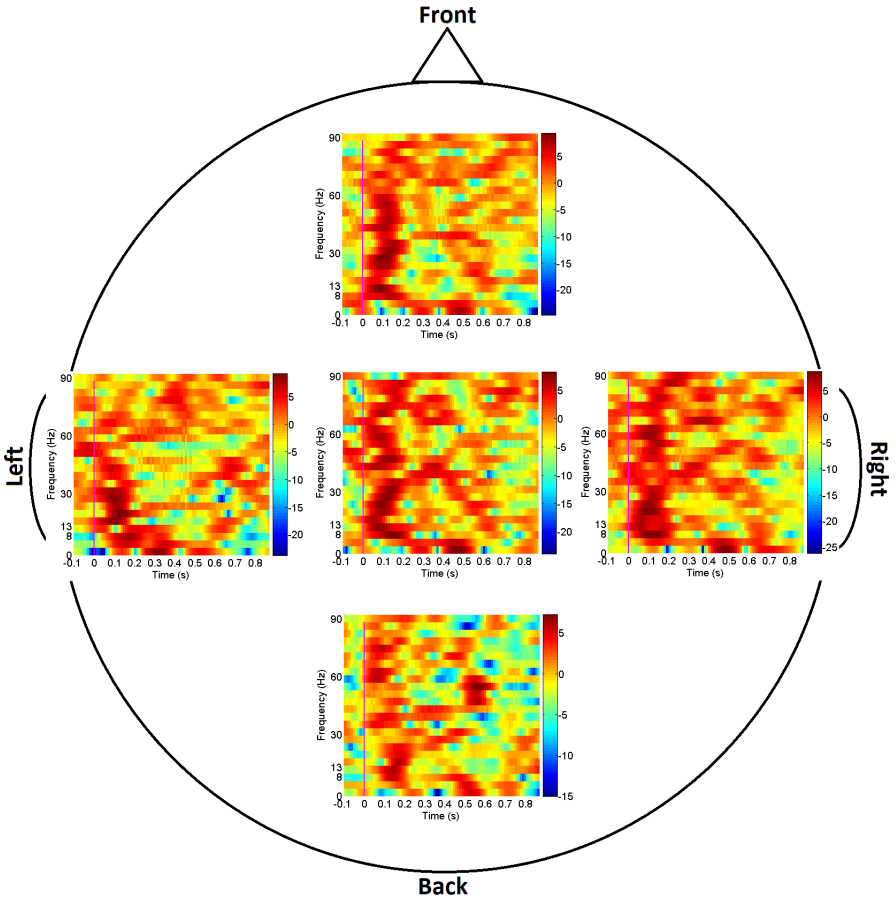

Figure 8.24: Average of evoked power over groups of electrodes shown by Figure 3.1.a in response to tone bursts in patient 2 recording 1 (right ear implanted), plotted in dB. The magenta line indicates the stimulus onset.

8.27. Green indicates no change and red means a significant change from the baseline. Note that these figures both show only the significant increase (and not decrease) from the baseline. Similar maps were also plotted for significant decrease though they are not presented here.

Statistical analysis (based on the 200-sample bootstrap approach with α=0.05) was applied to the evoked and induced responses from each patient and each recording session. For each recording session, the number of patients showing significant increase or decrease at a time-frequency point was counted and the results were plotted using colourmaps. Figures 8.28 and 8.29 show the number of patients showing significant increase in evoked and induced power in their second recording, respectively. Dark blue means no patient and red means all patients showing significant change at that time-frequency point. Only the results from the second recording session are presented here but the results of the first recording will also be discussed in this section. This approach may not be the best visualisation approach as the recording conditions of patients differ from one another (e.g. left or right ear presentation) and the results may be misleading, however, it could give us a sense of where the power is more concentrated in all patients.

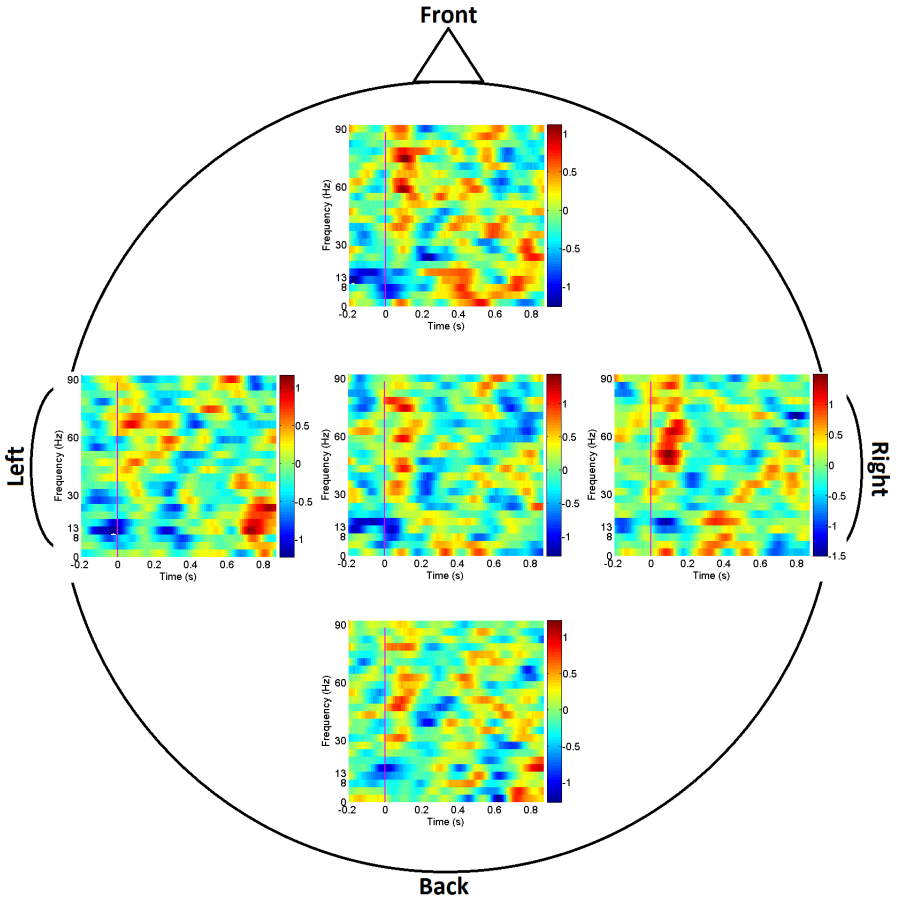

Figure 8.25: Average of induced power over groups of electrodes shown by Figure 3.1.a in response to tone bursts in patient 2 recording 1 (right ear implanted), plotted in dB. The magenta line indicates the stimulus onset.

These figures show that in response to tone bursts, there is a significant increase in the evoked power just after the onset in frequencies lower than 60 Hz in the second recording of all patients. A similar pattern was also observed in the first recordings. However, the induced power does not appear to follow a similar pattern in different patients in this recording session (in the first week after the implant was switch on). Bootstrap analyses on first recordings did not show any repetitive pattern either. As the maps on significant power decrease were not consistent over patients, those results are not presented here.

8.4.2 Response and words

After artefact rejection of data in response to words as in section 8.3.1.1, similar steps as in section 8.4 were followed to calculate the evoked and induced power spectra in each patient and recording session. Then, bootstrap analyses as in section 4.2.2 were applied to each dataset. For each recording session, i.e. recording 1 or recording 2, the number of patients showing significant increase or decrease in evoked or induced power after the onset compared to baseline was counted and plotted in colourmaps. The results of

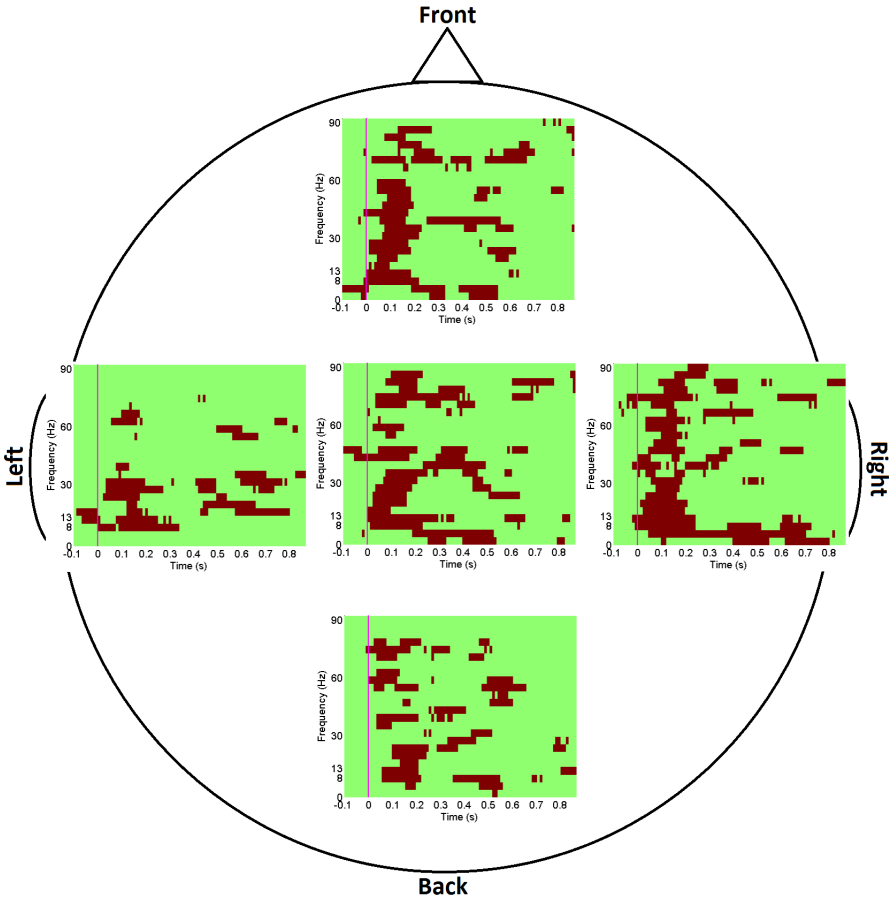

Figure 8.26: Significant increase in evoked power in response to tone bursts in patient 2 recording 1 (right ear implanted). Green indicates no change, red shows a significant time-frequency point. The magenta line indicates the stimulus onset.

this counting for the second recording session are shown in Figures 8.30 to 8.32. The results of the first recording session are not presented but discussed in this section. Most patients show an increase in evoked power in low frequency bands, i.e. 13 Hz and lower, and a decrease in induced power in beta band just after the onset in the second recording session. This evoked response pattern was evident in the first recording session as well. Some increase in induced power can also be observed in the [0 8] Hz frequency band around the ending of the words. The induced activity changes (either the increase or the decrease) were not evident in the first recording session.

8.5 Pairwise coherence

To compare the results obtained from power analyses with coherence analyses, data were first artefact rejected for each stimulus type according to section 8.3.1.1. Then, the data were pre-processed and FFT-based coherence was estimated between all channel

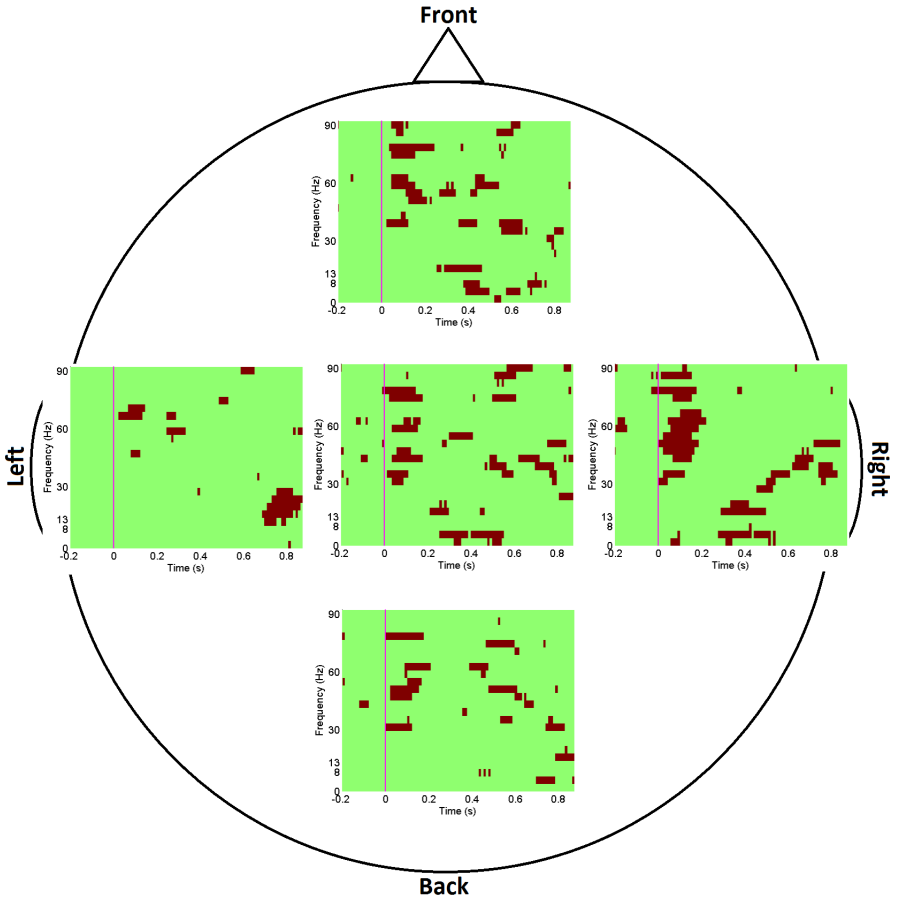

Figure 8.27: Significant increase in induced power in response to tone bursts in patient 2 recording 1 (right ear implanted). Green indicates no change, red shows a significant time-frequency point. The magenta line indicates the stimulus onset.

pairs over time in each recording session according to steps in section 6.3. After averaging coherence values in different time-frequency windows, the baseline coherence was subtracted from coherence values after the onset for each frequency band.

Group statistical analyses could not be employed similar to section 6.2.2 because of dissimilarities between recording conditions. Thus, for presentation purposes, in each dataset, the standard deviation of the coherence (in all time and frequency bands and between all pairs after subtraction baseline values) was estimated and four times this standard deviation (99.99% confidence interval) was set as the selection threshold. Any coherence change outside this ±threshold was kept as being a significant change. Similar to coherence figures in chapter 6 (such as Figure 6.4), connections showing significant increase/decrease were plotted in red/blue in each time-frequency window for each dataset. All datasets showed large changes in [0 8] Hz and [8 13] Hz frequency bands. However, the changes were not consistent over different datasets, i.e. some datasets showed significant increase and some showed significant decrease and the time windows in which changes occurred varied across datasets. Examples of these results are presented in

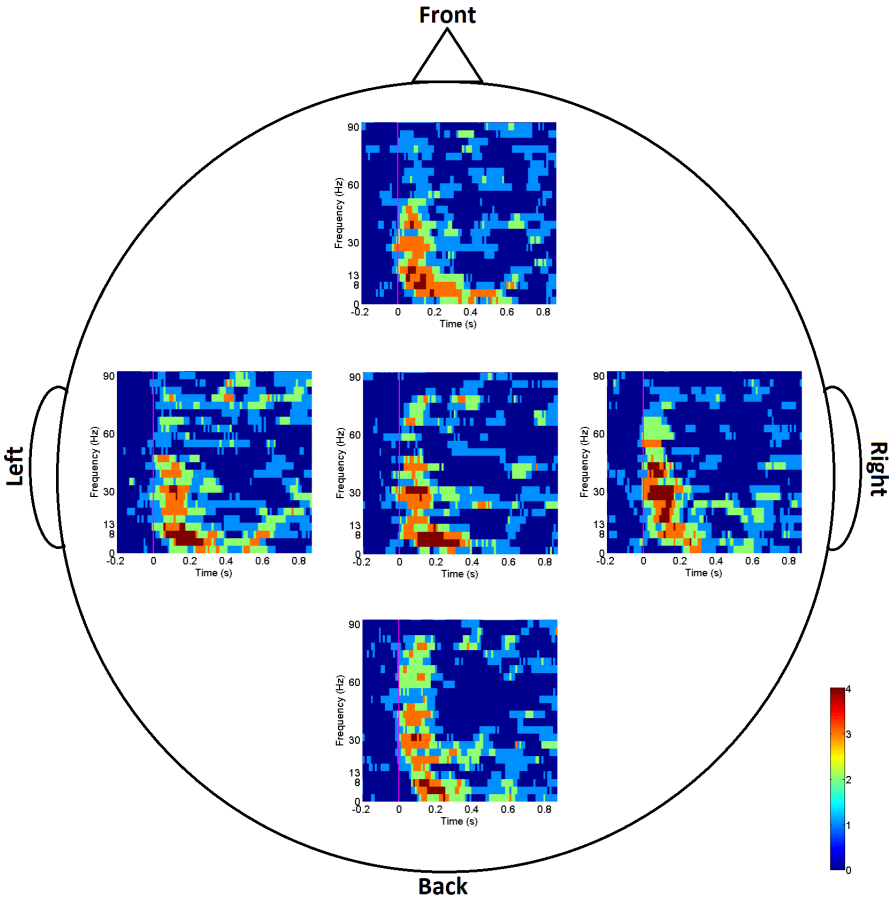

Figure 8.28: Number of patients showing significant increase in evoked power in the second session of recording while listening to tone bursts. Note that the implanted ear in two patients is the right and in the other two patients is the left ear. The magenta line indicates the stimulus onset.

Figures 8.33 and 8.34 for the second recording of patients 2 and 3, in response to tone bursts and words, respectively. As no significant pair was found in higher frequency bands (>13 Hz), these figures only focus on lower frequency bands (<13 Hz).

As can be seen, this diversity in significant changes in coherence occurred in response to both tone bursts and words and the significant windows of each recording were not consistent with the results observed for the induced responses, as was the case for normal hearing subjects.

8.6 Discussion

In this chapter, much effort was put into rejecting the CI artefact in EEG data recorded from CI users. Different methods and approaches were employed for this purpose but none of the methods were clearly able to remove the artefact in response to words. However, the most conventional approach, i.e. ICA and visual selection of artefactual

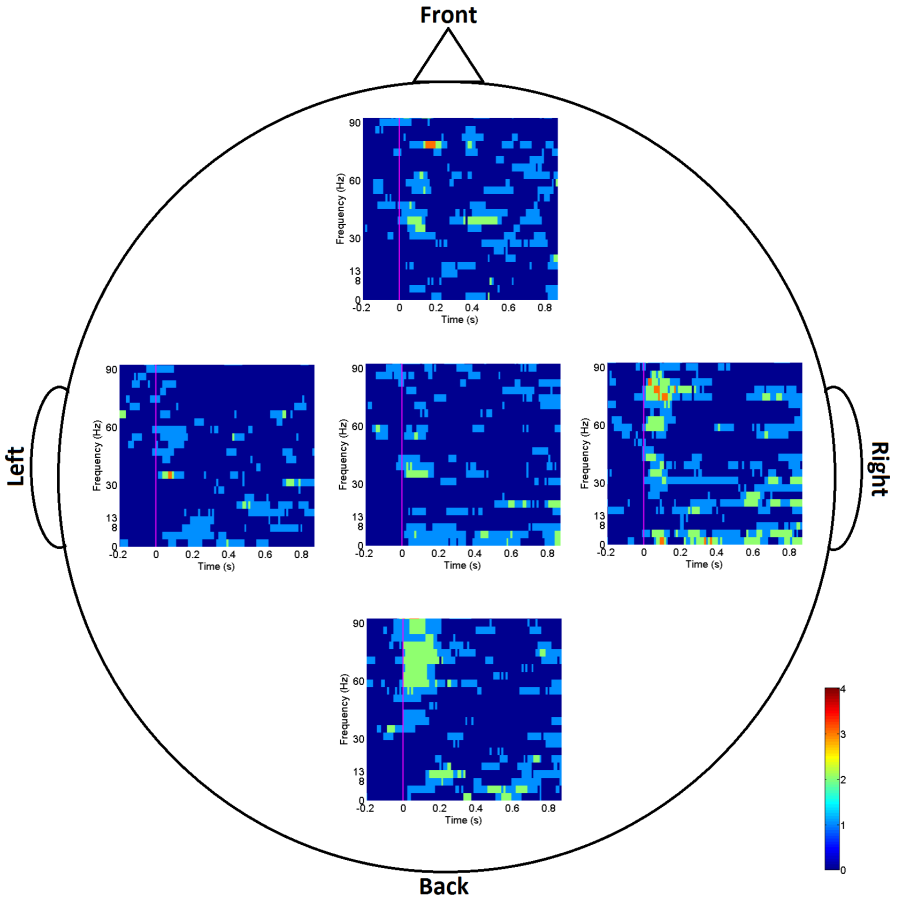

Figure 8.29: Number of patients showing significant increase in induced power in the second session of recording while listening to tone bursts. Note that the implanted ear in two patients is the right and in the other two patients is the left ear. The magenta line indicates the stimulus onset.

components (see section 8.3.1.1), was deemed the most promising and used for further analyses. While the literature suggests that ICA is able to remove the artefact, our experience is that this is rather more challenging. Artefact removal in the case of words has not been described before. This chapter thus serves to highlight challenges that might be expected in analysing the EEG response to speech in CI patients.

The results of visual component selection (see section 8.3.1.1) were considered the most reliable as the ensemble average of data after artefact rejection showed the so-called ALR response in most datasets. However, some peaks were observed in some datasets that could be due to artefacts from the implant because of their timings. For example, a peak around 120 ms in patient 1 recording 2 (Figure 8.6) or a negative peak around 50 ms in patient 2 recording 2 (Figure C.3) in response to tone bursts. As topographic maps of the cleaned data did not show any activity around the implant site around these peaks, these peaks were not classified as artefacts and components containing these peaks were not removed from the data. However, the question still remained if they should have been regarded as artefacts. Thus, other approaches were employed to improve the efficiency

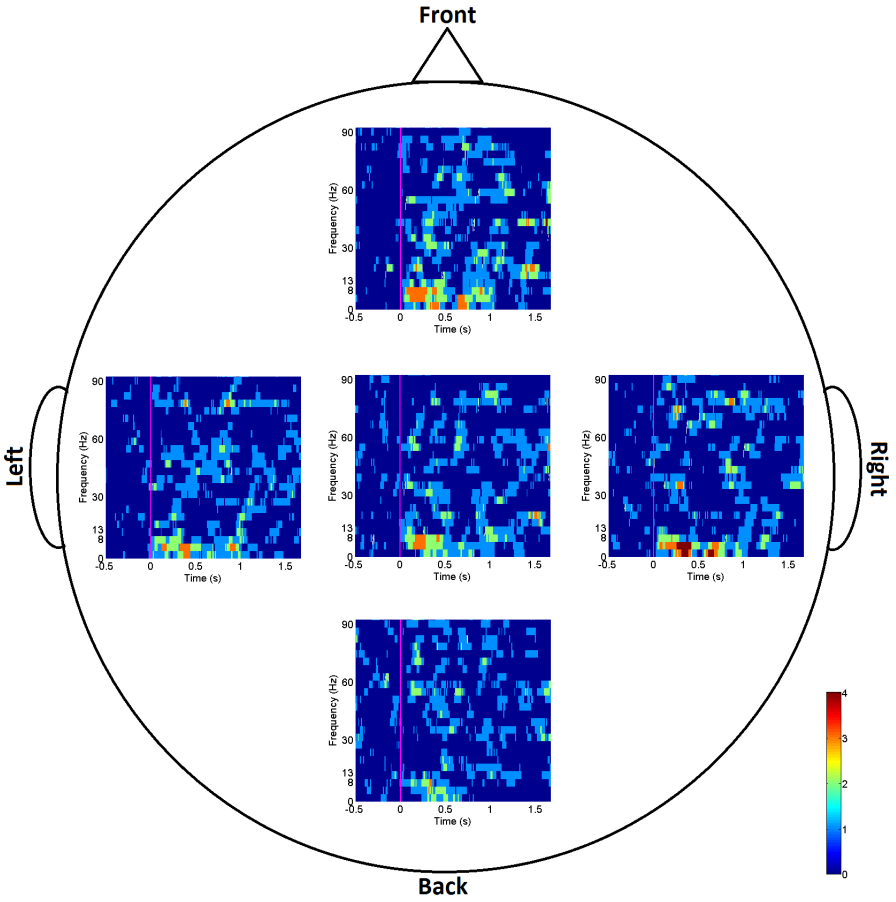

Figure 8.30: Number of patients showing significant increase in evoked power in the second session of recording while listening to words. Note that the implanted ear in two patients is the right and in the other two patients is the left ear. The magenta line indicates the stimulus onset.

of ICA according to suggestions in the literature (Agrawal et al., 2013; Sandmann et al., 2009; Gilley et al., 2006; Castañeda-Villa et al., 2012), e.g. filtering the data to other than [1 120] Hz or downsampling the data before applying ICA. However, components showed more mixing of CI- and non-CI-related activity than before, probably because the onset and offset peaks of the CI were very close to desired ALR peaks and filtering or downsampling mixed the two peaks which caused ICA to not be able to distinguish between them. Also, the length of epochs were changed to shorter time ranges around the response and artefact activities but the components obtained were quite similar to those with longer epochs. In addition, the electrodes around the implant site were all removed before applying ICA but again, no obvious improvement was achieved. Viola et al. (2012) suggested the use of longer tones (such as 400 ms) so that at least the offset is well outside the response range and then they used semi-automatic approaches to find the CI-related artefacts. This point should be considered in future work on tone-based stimuli, however, it still can not help in more complex stimuli such as words, which are key in assessing patients responses to speech. .

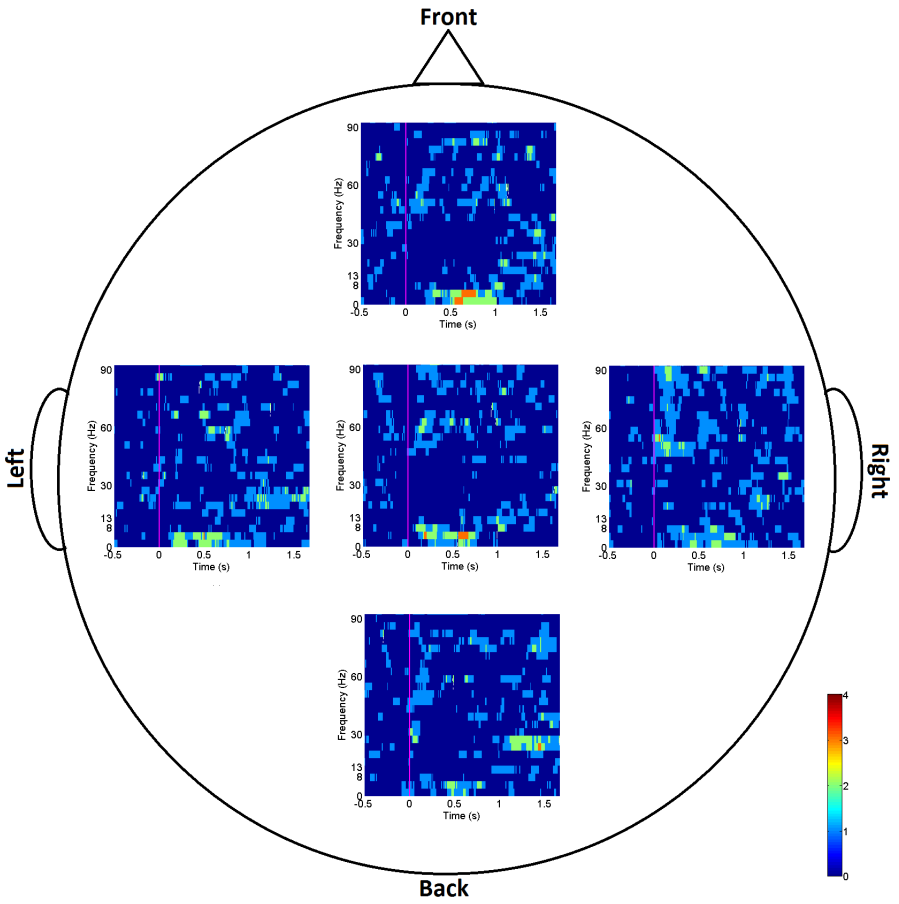

Figure 8.31: Number of patients showing significant increase in induced power in the second session of recording while listening to words. Note that the implanted ear in two patients is the right and in the other two patients is the left ear. The magenta line indicates the stimulus onset.

As visual component selection appeared fairly effective for tone bursts, it was also applied on EEG in response to words. However, it was not as easy as before to identify the CI-related components as the components had more mixed activity (containing both CI- and non-CI-related activity) than before and the artefact cues such as onset and offset peaks were missing from these data because of the shape of the stimuli. Tone bursts have much sharper increase and decrease at the beginning and ending of the sound compared to words which cause bigger onset and offset artefacts and are thus more identifiable in ICA components. Nonetheless, visual component selection was performed in these data. In most cases, an ALR-like response (P1-N1-P2) could be observed after artefact rejection similar to those of normal hearing subjects in response to words. However, because some components could not confidently be marked as non-CI-artefacts, we were not fully confident about the observed results. So, other approaches were employed to manually or semi-automatically remove CI-artefacts (see sections 8.3.1.2 to 8.3.3) from the EEG in response to words. However, none of these approaches produced clearly improved results and it was decided (see section 8.3.4) that the visual selection was the best approach among the ones tested in this chapter for CI-artefact rejection in response

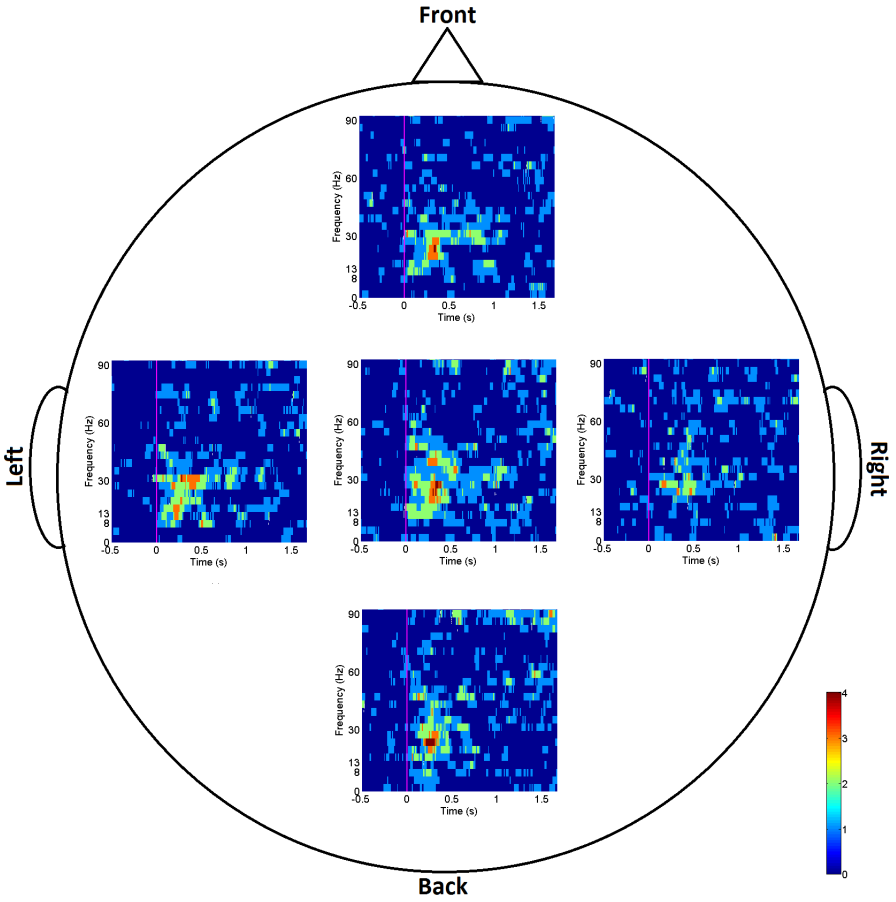

Figure 8.32: Number of patients showing significant decrease in induced power in the second session of recording while listening to words. Note that the implanted ear in two patients is the right and in the other two patients is the left ear. The magenta line indicates the stimulus onset.

to words. The possible reasons for each method not working properly on CI data are explained at the end of each section in this chapter.

One other method that could prove helpful for this purpose but was not approached in this research was the use of another ICA estimation algorithm called Temporal Decorrelation Source Separation (TDSEP) (Castañeda-Villa and James, 2007) instead of Infomax ICA. Castañeda-Villa and James (2011) showed that because TDSEP used the temporal structure of the signal, it produced clearer AEPs than Infomax and FastICA especially in lower SNRs. They had also used Mutual Information and clustering to automatically find the response-related components which showed promising results for the type of stimulus they were using (Castañeda-Villa and James, 2007). However, the level of artefact in their recordings was quite low compared to those in the current research and it might not work as effectively with our data. For our research, TDSEP requires careful and close investigation for the stimuli in this study which can be pursued in future work.

Although visual selection of ICA components was not the ideal approach in this study, it produced the most promising results (visually and looking at evoked responses) among

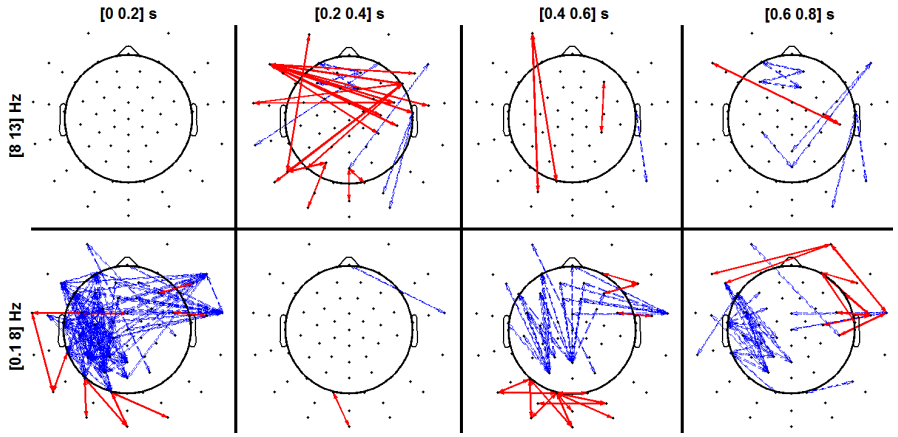

(a)

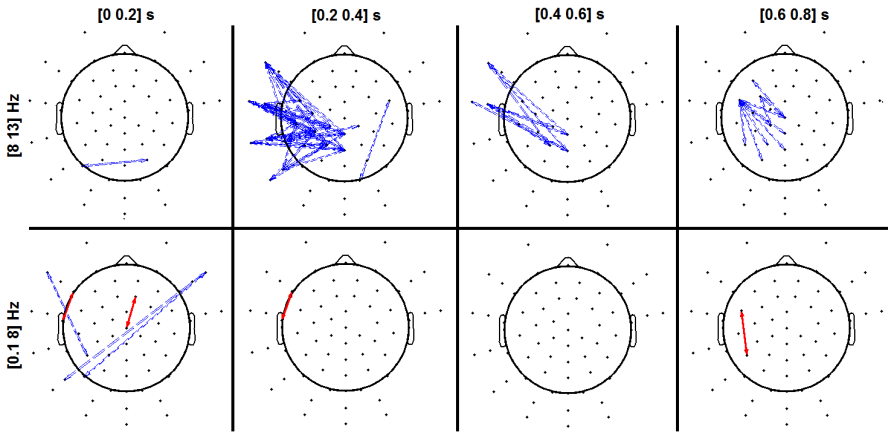

(b)

Figure 8.33: Significant coherence changes from the baseline in different time-frequency windows in response to tone bursts are marked by arrows in a) patient 2 recording 2 and b) patient 3 recording 2. Red/blue arrows indicate increase/decrease in the coherence compared to the baseline. Thicker arrows indicate larger difference from the baseline. The stimulus onset occurs at zero seconds.

the investigated methods and was used to remove the CI artefact in both words and tone bursts.

The evoked and induced power spectra of cleaned data were calculated. Using bootstrap analyses, all patients showed significant evoked activity in response to tone bursts in similar time-frequency areas as normal hearing subjects in both recording sessions. But no consistent induced activity could be detected except for a 200-ms increase in [60 90] Hz band. In both recording sessions, this increase was present in 2-3 patients. In response to words, evoked power showed increased activity in lower frequency bands in both recordings but an increase in induced activity (in low frequency bands) was only evident in the second recordings. Also in the second recordings, most patients showed a decrease in induced power in the beta band in the first 500 ms window after the onset

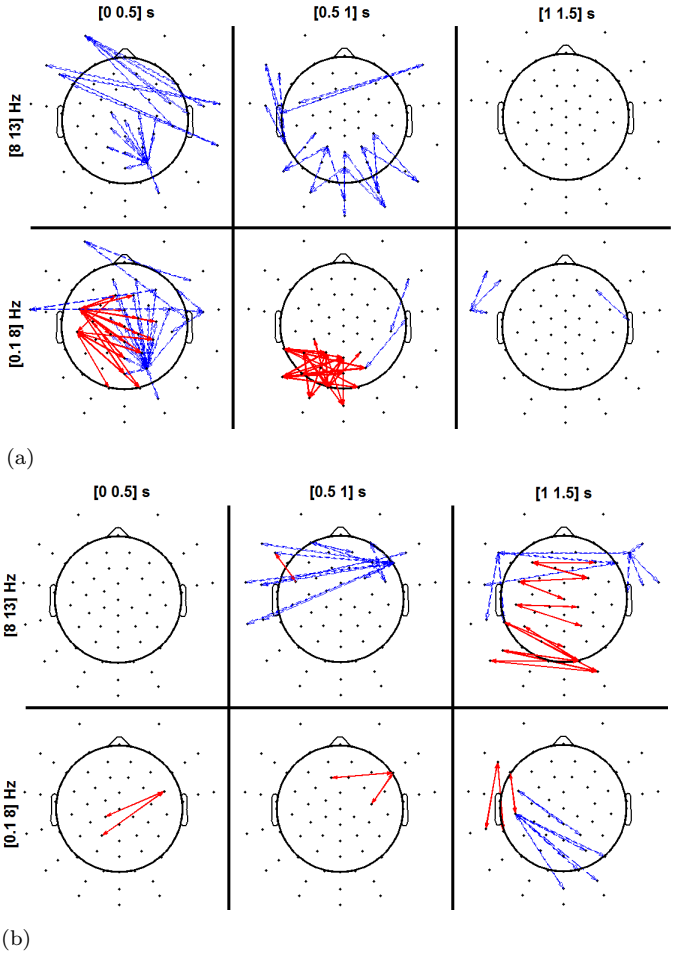

Figure 8.34: Significant coherence changes from the baseline in different time-frequency windows in response to words are marked by arrows in a) patient 2 recording 2 and b) patient 3 recording 2. Red/blue arrows indicate increase/decrease in the coherence compared to the baseline. Thicker arrows indicate larger difference from the baseline. The stimulus onset occurs at zero seconds.

but this decrease was not evident in the first recordings. As we were not fully confident about artefact rejection, the analyses were not extended to sentences and AM tones.

Although some consistency was present in evoked and induced response analyses, pairwise coherence analyses did not show any consistency over different patients or recording sessions, neither in response to tone bursts nor words. This inconsistency may be coming from a not ideal artefact rejection, however, it can also be coming from genuine differences between patients. This is worth investigating in the future, for example, by closer (time-wise) repeating recording sessions in the same patients.

In our analyses, it was observed that the level of artefact was different in each patient and even between the two recording sessions. It was thus concluded that the brand of the implant, the processing strategy, and the level of sound on the processor might have different effects on the shape and magnitude of the artefact, and thus the result of the artefact rejection. Detailed analyses of the CI artefact probably requires close

collaboration with the manufacturers as the way in which stimuli are generated depends on the device and details of the electrical signals generated by the CI are not readily evident from the published information.

8.7 Summary

In this chapter, different methods of artefact rejection were used to remove the CI-related artefact from the EEG recorded from tones and words. It appeared that although not ideal, applying ICA on the data and selecting artefact components visually was the most effective approach for the type of data in this study. Evoked and induced power spectra were calculated and it was shown that an evoked activity could be observed in response to both stimuli. The induced activity was not as consistent, especially between two recording sessions but in the second recording, some consistency could be observed (an increase in power in frequencies lower than 8 Hz for about one second after the onset and a decrease in beta and lower gamma frequency bands for about half a second after the onset). The pairwise coherence was then calculated and significant changes after the onset were marked, but the results were very different between patients and recording sessions although they were consistent with results from induced power.

Chapter 9

Discussion, Conclusions, and Future Work

9.1 Discussion

As mentioned before, connectivity analysis is the process of detecting relationships between different brain areas (David et al., 2006a). In one type of classification, functional connectivity refers to the existence of a relationship between activity from different brain regions and effective connectivity refers to the direction of the information flow in these regions (David et al., 2006a). Different methods of measuring brain connectivity exist in the literature (Sakkalis, 2011; Florin et al., 2011; David et al., 2006a; Castañeda-Villa et al., 2012). The main purpose of the current work was to asses the suitability and reliability of a few of these methods in response to auditory stimulation, specifically speech. The final (and future) aim of the project was to compare the connectivity patterns of normal hearing subjects and CI users to detect if there were specific connections causing the low (or lack of) speech perception in the latter group. The imaging technique used for this research was EEG as it has high temporal resolution, is appropriate for follow-up studies, is cost effective, and is more compatible with cochlear implants than other imaging techniques. Much research has focused on the brain response to auditory stimulation in CI users (Ponton et al., 2001; Sharma et al., 2005a; Kral et al., 2006; Nava et al., 2009a; Sharma et al., 2009; Sasaki et al., 2009; Limb et al., 2010) but first, they mostly only focus on simple stimuli such as tone bursts in EEG studies and second, almost none has approached the topic of connectivity in these patients.

In the current research, multichannel EEG was recorded in normal hearing subjects and cochlear implant users in response to both simple and complex sounds, i.e. tones, words, and sentences (see chapter 3). Tones were presented because the shape of the brain response to this stimulus is known from the literature (Hall, 2007) and this could be initially used for testing the employed methods. Speech stimuli were presented as

more complex sounds to elicit higher order processing in the brain. Preliminary response detection showed significant evoked responses (phase-locked and time-locked response to stimuli) to all types of stimuli in normal hearing subjects (see chapter 3). Unlike ALR that covers frequencies up to 30 Hz (Hall, 2007), the response to words and sentences was only evident in frequencies lower than 13 Hz. As the sound was not too loud (62 dB SPL), it is possible that the response was not strong enough to introduce higher frequencies in the evoked response. In addition, as the words and sentences were not identical in different epochs, it is possible that the SNR was not as strong as that of identical repeating stimuli. In addition to the evoked responses, induced response (time-locked but not phase-locked to stimuli) (Gruber et al., 2001; Gurtubay et al., 2004; Graichen et al., 2009) may also be present in EEG. The presence of this response had to also be checked before estimating some of the connectivity measures (namely MVAR-based methods) because these methods only work on stationary signals. The first step to make the data stationary was to remove the evoked response from the data thus the necessity to reveal other types of response, such as induced response or phase-synchronisation, in the data.

Preliminary induced response detection approaches based on envelope detection and single subject analyses did not show any induced activity in the data (see appendix A) and were strongly affected by noise and artefacts in the signal. Therefore, the data were cleaned of artefacts using ICA analyses and visual inspection of noisy epochs and this time, time-frequency analyses were employed. Different normalisation steps and statistical analyses were tested on simulated data to find the most appropriate methods for the purpose of this project (see appendix B). Short-time FFT analyses were used and evoked and induced power spectrograms were calculated for each set of simulated data. At each frequency over time, powers were normalised to the baseline power of that frequency or the power of that frequency over the whole time range being analysed. Even without the presence of any simulated response, employing the former approach reported a significant response after the onset, which probably came from the distribution of the averaged power not being normal. Thus, the latter (normalisation by the average power over the whole epoch) was selected as the appropriate approach. After the normalisation approach was decided on, following common approaches used in the literature, different statistical analyses methods were also employed on simulated data but most of them showed very high false positive rates. T-test showed high false positive rates because of the dependency between pairwise statistical tests (all values after the onset were compared with the same baseline) and one-way ANOVA had a high false positive rate because the values over time were coming from the same subject and were not independent. In bootstrap analyses, the pool of random data that was generated and the averaging that followed would make the distribution of values incomparable with the original distribution at each time-frequency point and thus higher rate of false positives (than expected) was observed. Repeated measures ANOVA and Friedman's test were

the only ones that produced correct number of false positives in simulated data. However, repeated measures ANOVA may be affected by outliers in recorded EEG. Thus, Friedman's test was selected as the most appropriate method for significance analysis in response detection, comparing power values before and after the onset.

Selected methods (short-time Fourier transform, normalisation to the power of the whole epoch, and Friedman's test) were then applied on EEG recorded from normal hearing subjects in response to all types of stimuli and presentation ears. In response to tone bursts and AM tones, no change in the induced power could be detected after the onset compared to the baseline. In AM tones, it was expected to observe an increase in the power around the frequency of modulation, i.e. 15 Hz or 80 Hz (Hall, 2007). The reason for not seeing this effect was probably the low number of stimuli with regards to the sound level, or the fact that the stimulus was presented as a burst rather than a continuous tone. In response to words, an increase in delta and theta powers and a decrease in beta power could be observed around the end of the words in central and posterior electrodes in both monaural and binaural presentations. Sentences evoked similar responses, i.e. increase in delta and theta powers and decrease in beta power. Other studies have also reported changes in these frequency bands when auditory speech was involved (Kim and Chung, 2008; Hirata et al., 2007; Bastiaansen et al., 2002; Bastiaansen and Hagoort, 2006), however, the presentation protocols were very different from those used in this research. It is worth mentioning that in both cases (words and sentences), more patients showed increase in the [0 8] Hz frequency band in right ear and binaural presentations than the left ear presentation. Various reasons can cause this difference such as lower SNRs in a few subjects in left ear presentation, different word or sentence lists for each presentation condition, or in fact different brain responses depending on the presentation ear. Investigating the reason requires more sophisticated experiments with different protocols and would usefully be the target of future research. In the future, other approaches such as alignment of data to the end of the words can also be employed.

Knowing that the data included both evoked and induced responses, different connectivity methods were tested using the data. DCM as an effective connectivity method was initially employed (David et al., 2006a) as it is a biophysically informed model, it works on source-level (inside the brain) signals, and it considers the non-linearities of the system. Although its validity had been previously tested with regard to some aspects (Daunizeau et al., 2011; David et al., 2006a; Garrido et al., 2007; Kiebel et al., 2007), there were still some doubts about its reliability especially because some concerns had been raised previously about the effectiveness of the model (Lohmann et al., 2012, 2013). So, before using DCM, its reliability was tested. The model was going to be tested for its reproducibility in one subject in the same session (by randomly selecting different sets of epochs and applying DCM on each set) and then in the same subject over two different sessions, and see if the results were consistent. However, in the first phase, we found out that by changing the operating system or the version of SPM8 or MATLAB, DCM

estimation would strongly be affected and the significant connections or the best model reported would differ dramatically when the software combination changed. One reason for this problem might be the difference in error accuracy in each one of these software systems. Because of too complicated calculations and large loops in the algorithm, even slightly different accuracies could become large in higher iterations and as the algorithm advances. So, we advised that researchers approach this method cautiously (Hosseini et al., 2014c,b, 2013b) and moved on to other connectivity methods.

In the next step, non-parametric pairwise coherence (Miranda de Sá et al., 2001) was used to make sure that there was functional connectivity between electrodes before going any further with effective connectivity analyses. This step was also used as a confirmation of the results obtained from previous power-based analyses for induced response detection and as a basis for testing the reliability of model estimations in the following steps (MVAR-based models). Coherence analyses confirmed that in the same time-frequency windows that power analyses reported induced activity, there were also significant changes of coherence compared to the values before the onset in word and sentence stimuli. The areas that showed significant coherence changes were also in line with those showing significant induced power changes. In addition, similar to power analyses, right ear and binaural presentations reported more significant connections than left ear presentation in these stimuli (words and sentences). Coherence changes in the theta frequency band had been observed in the literature in response to words (Weiss and Muller, 2013; Weiss and Mueller, 2003; Weiss and Rappelsberger, 2000), however, in these studies, the evoked response was not removed from the data and the presentation protocol and the purpose of the study was quite different from the current research. In AM tones, like power analyses, there was no significant change of coherence. However, in tone bursts, unlike power analyses, coherence showed significant changes in the beta band for about 400 ms starting around 200 ms after the stimulus onset. As no change could be observed in power analyses for this stimulus, this may be explained by three possibilities: coherence being more sensitive than power in detecting induced activity (Simpson et al., 2000), phase-synchronisation of response to the stimulus without the change in the power (Makeig et al., 2002), or (the more probable) phase-synchronisation between channels (Fuentemilla et al., 2006, 2008). These analyses proved that there was functional connectivity between electrodes in response to different types of sound.

After the existence of functional connectivity in response to different stimuli was established, directional (effective) connectivity was investigated. After dropping DCM, simpler linear methods based on multi variate autoregressive models were approached (Sakkalis, 2011). MVARs have far fewer prior assumptions and parameters compared to nonlinear methods thus they are likely to be more robust than those methods. The validity of estimated models were tested by checking the whiteness of residuals and stability of estimated parameters (Lütkepohl, 1991). Then, from estimated MVAR parameters, different effective connectivity measures such as DTF (Korzeniewska et al., 2003) and

PDC (Baccala and Sameshima, 2001) were computed. A few more validity tests were performed before applying autoregressive models to multiple channels: first, simulated data were generated, their DTF and PDC values were calculated and compared with the values expected from theory for these simulations and showed correct results. Second, a bivariate model was estimated for all pairs of channels, model-based pairwise coherence was calculated from estimated parameters, and significant connections were marked. These results were compared with those obtained from pairwise coherence and showed consistent results. Third, a multi-variate model was fitted to a few channels, parameters were estimated, coherence was calculated for all channel pairs using these multi-variate (and not bivariate) parameters, and significant connections were specified. Again, the results were consistent with those of non-parametric coherence and bivariate model-based coherence. All these steps indicated the reliability of the implemented algorithms and estimation procedures. After these preliminary validity tests, the estimated parameters from multi-channel models were used for calculating effective connectivity measures such as DTF and PDC. However, no clear change of connectivity could be observed from the baseline in any of the employed measures. Not choosing an appropriate model order or sampling frequency may cause some significant connections to disappear (Porcaro et al., 2009). Thus, different model orders and sampling frequencies were used but still no significant change in the connectivity could be achieved. The first potential reason for not seeing any changes in effective connectivity was the actual lack of effective connectivity; however that was not very likely as coherence showed significant changes. Most studies report significant changes in connectivity between two different states in subjects or two different stimulus types, e.g. awake versus asleep (Kamiński et al., 2001), Go versus NoGo stimulus(Ding et al., 2000), or visually congruent or incongruent words (Astolfi et al., 2007). So, it is possible that these methods are more sensitive in comparing two different conditions rather than a specific response against baseline (resting) condition. Many studies that report changes from the baseline condition work with LFP or ECoG signals which usually have higher SNRs than surface EEG, or these studies have more data points than our study both of which lead to more accurate parameter estimates (Baccala and Sameshima, 2001; Kamiński et al., 2001; Korzeniewska et al., 2003; Kamiński et al., 2005; Gourévitch et al., 2006; Boatman-Reich et al., 2010; Korzeniewska et al., 2011). Thus, low SNR (i.e. weak induced responses) and not enough data points might be the more plausible reasons for the methods to not be able to pick any significant effective connectivity changes. To resolve these problems, other protocols may be helpful, such as repeating identical words or sentences or presenting continuous speech. Also, in our work, the covariance matrix of residuals is not an identity matrix hinting at electrical conduction between electrodes. Using extended MVAR analysis that take into account the instantaneous relations might have some positive effects on the results (Erla et al., 2009; Faes and Nollo, 2010; Faes et al., 2013) and can be the target of future work.

Although effective connectivity analyses did not show promising results, induced response analyses and non-parametric coherence had encouraging outcomes. Thus, they were selected to be applied on case studies in CI users. Before these methods could be employed on these data, strong artefacts due to the electrical signal generated by the CI had to be removed from EEG signals. Different artefact rejection approaches were used to remove CI artefacts from the data among which ICA and visually selecting the artefactual components were ultimately deemed the most suitable among the techniques tested. However, even with this approach, we could not be sure if the artefact had been removed completely as the onset and offset effect of the CI was in the same time range as the brain response. ICA had been previously shown to be suitable for removing CI artefact in response to tone bursts (Viola et al., 2012; Castañeda-Villa et al., 2012; Sandmann et al., 2009) but in this study, even in response to tone bursts, artefact rejection with ICA was not an easy task as most of the components showed effects of CI artefact in them. Different cut-off frequencies for filtering and different sampling frequencies were tested (Agrawal et al., 2013; Sandmann et al., 2009; Gilley et al., 2006; Castañeda-Villa et al., 2012) but still detection of artefactual components was not very convincing. In future work, other presentation protocols such as presentation of longer tones (Viola et al., 2012) could help the artefactual IC identification as the onset and offset effect of the implant would fall well outside the response range. However, in the case of speech presentation, it is obviously not a suitable approach. Other artefact rejection techniques such as ICA with TDSEP algorithm (Castañeda-Villa and James, 2007) can also be approached in the future. Although ICA was not the ideal approach, it was used for rejecting artefacts in response to tone bursts and words, and the power and coherence analyses described above were applied on the cleaned data. As there were only a handful of datasets available and even those had not been recorded under identical conditions, statistical analyses could not be performed. However, analyses on single subjects (case studies) showed some consistency in evoked and induced responses over subjects. For example, in response to words, most subjects showed an increase in the evoked power in frequencies lower than 13 Hz in both recording sessions but induced activity was only observed in the second recording session by an increase in the [0 8] Hz frequency band and a decrease in the beta band. Of course it was only case-studies, these results were similar to those achieved in normal hearing subjects. Better artefact rejection techniques and more carefully recorded datasets (in respect of electrode placement, test of loudness, etc) are required before a definitive conclusion can be derived from power and connectivity analyses on data recorded from cochlear implanted patients.

9.2 Conclusions

The brain consists of different task-related areas. The unique relationship between these areas is what makes a person capable of perceiving a stimulus or performing an action.

This relationship can be defined as the brain connectivity. Various tasks rely on different connectivity patterns of the brain and the study of this so called brain connectivity for a specific task may enable us to detect the cause of discrepancies in perception of that task in a particular individual. One of the applications of connectivity measurement can be on hearing impaired people who have been implanted with a cochlear implant either unilaterally or bilaterally. One of the reasons for the lack of speech perception in cochlear implant users especially in adults may be the alteration of their connectivity pattern after deafness that has not been reorganised back to the normal condition even after implantation.

There is a wide range of studies around the issue of brain activity in cochlear implant users. These studies have answered many questions in this area such as the best age for cochlear implantation or the effect of a second implant in children and adults. Some of them even reported that the activated areas during speech perception in CI users are different from normal hearing individuals but even though some of these differences are reported, it is still an open question how these new areas are connected to each other and what the information flow pathway is in CI users. We assume that connectivity analyses can inform us if the activity of a specific connection in the brain has changed after implantation. This knowledge will not only increase our understanding of the underlying activities of the brain during speech perception, but also help researchers seek methods that can aid CI users benefit more from their implants. These methods may vary from new therapy techniques to non-invasive stimulation of the brain targeting an ill connection. Moreover, it may be seen as a predictive method of patient performance after their first or second implantation.

Following objectives mentioned in the introduction, this research started with response detection in EEG in normal hearing subjects in response to different types of stimuli such as tones bursts and words. Analyses were carried out using both power spectrum of the signal and coherence analyses over different electrodes. Significant changes in both phase-locked and non-phase-locked activity of the brain was observed in response to all types of stimuli in different frequency bands of the EEG signal. After the existence of the response was confirmed, connectivity analysis were performed on the data. These analyses were initially carried out using DCM, however, it was soon determined to be a poor technique for the application of this project as the available MATLAB toolbox (SPM8) that has implemented this method showed varying results in different combinations of SPM8 and MATLAB versions and the operating systems being used, possibly because of different error precisions of the software. The direction of the research was then switched to more simple linear connectivity methods which were based on autoregressive modelling of a multi-channel system such as EEG. It was shown that these methods worked properly on synthetically generated data, however, in recorded EEG data, no significant directional connectivity could be detected although the functional

connectivity measures (i.e. coherence) calculated from the parameters of the model were consistent with the results obtained from non-parametric analyses.

The other objective of the thesis was to measure connectivity in response to auditory stimulation in CI users. Much effort was made to remove the CI artefact from these data using different approaches mentioned in the literature. However, artefact rejection, especially in response to speech, proved quite challenging in EEG recorded from CI users and needs more carefully designed presentation protocols and more targeted investigations in the future. Artefact rejection was eventually carried out using ICA, in this project. Although proper significance analyses could not be applied on the results because of the non-identical recording conditions and the low number of subjects, preliminary analyses showed similar changes in the brain activity of these patients to normal hearing subjects, using power and non-parametric coherence analyses. As the employed connectivity analyses did not prove suitable on normal data, these methods were not applied on data recorded from cochlear implanted patients.

Some parts of this research were published in Hosseini et al. (2014b,c, 2015, 2014a, 2013b,a, 2011a,b).

9.3 Future Work

In section 9.1, a more detailed version of potential future work of our research is discussed at the end of each paragraph. A list of these points are mentioned as follows:

- Approaching the question of response detection by aligning epochs to the end of the words or sentences
- Distinguishing if evoked response to speech can be detected easier by coherence analyses
- Introducing new auditory stimulation protocols which might be more feasible for investigations of connectivity using speech both in normal hearing subjects and hearing impaired patients, such as presentation of continuous speech, presenting louder and longer sounds, using repeating stimuli, recording multiple sessions from the same subjects for testing the repeatability, etc
- Looking into non-linear approaches in conjunction with linear ones to investigate connectivity in response to auditory stimulation
- Approaching MVAR-based methods using equations that embed instantaneous relations between electrodes
- Extending connectivity to source (cortex) level signals rather than sensor (electrode) level only

- Investigating other approaches of EEG artefact rejection in CI users, specifically in response to speech and testing new stimulus presentation protocols for improving artefact rejection, probably in close contact with the manufacturers of CI devices
- Continuing investigation on brain connectivity in CI and hearing aid users
- Using all the mentioned investigation to introduce objective methods of speech perception assessment in hearing impaired patients and to improve fitting the CI or the hearing aid in these groups and to identify approaches for helping them benefit most from their implants

Appendix A

Preliminary Response Detection Approach

A.1 Introduction

Two main methods of determining the existence of induced response in the data are 1) time-frequency spectrum and 2) envelope detection in different frequency bands (e.g. as in Table 2.1) (Pfurtscheller and da Silva, 1999; Allen and MacKinnon, 2010) and then comparing the pre- and post-stimulus power in that frequency band (for more information on induced response see chapter 4). These two methods were employed initially to prove the existence of the induced response in the recorded data and the results are presented in the following sections.

It will be shown that these approaches failed to detect the response therefore more in depth analyses were employed as in appendix B on simulated data to find the most appropriate method for induced response detection for the purpose of this study.

A.2 Time-Frequency Spectrum

For this purpose, EEG signals were epoched (sectioned) around the stimulus onset time. The pre-stimulus time which can also be called the baseline was 700 ms/700 ms/1000 ms and the post-stimulus time was 2 s/2 s/4 s for AM tones/words/sentences. The time-frequency spectrum of each epoch was calculated using a 256 point FFT over 256 ms windows of the epochs with steps of 56 ms over time (200 ms overlapping windows) and then estimating its power. In each epoch and at each time point, the power was averaged in different frequency band. Then, two different baseline correction approaches were employed. The baseline correction was achieved by 1) dividing the power of each frequency band at each time point by the average power of the baseline in the same

frequency band and 2) subtracting the average power of the baseline in a frequency band from the power of the same frequency band at each time point in the epoch. Therefore, each epoch provided one sample of power value for every time point and frequency band.

To test the significance of the power change from the baseline at each time point after the stimulus onset, an obvious approach at the time was to use a t-test. In each frequency band and at each time point, t-test was applied to the power at that time point (over all epochs) in comparison to the average baseline power in the same frequency band (over all epochs).

In the case of dividing by the baseline power, the t-test selects almost every time-frequency point after the stimulus onset as a significant change over baseline i.e. even the smallest positive change after the onset is regarded as a significant change. Figure A.1 shows an example of the results in this case for one subject in response to words in channel 1 but this patterns repeats itself in all stimulus types and all subjects. In Figure A.1.a, the left column shows the normalised power in all trials in different frequency bands and the right column shows the average power (over all trials) in the same frequency band. In Figure A.1.b, in each frequency band, the p-values show the significance of the power at each time point being different from the baseline power in that frequency band. This problem might have come from the fact that the distribution of power is not normal and is skewed towards zero. Thus, the power values after the onset are being divided by smaller values more than larger values. This division may affect the distribution of power after the onset and take the mean value away from zero. This approach thus deemed inappropriate for the purpose of our study.

In the case of subtracting the baseline power, the t-test would show almost no significant point after the stimulus onset. Even when one subject showed significant change in a time-frequency range, other subjects might not show significance in that range. The pattern of significant time-frequency ranges is so different between subjects that it cannot be reliable in group analyses. Examples of this dispersion of results can be viewed in Figure A.2 in four different subjects. Assuming there is some response in the data that could not be detected with this approach, one reason may be that the FFT window that is being used is too long and the response too short thus the power of the response is averaged and smoothed in this window. It is also possible that the response is not strong enough to be easily detected which this approach.

As no significant response could be detected with this analyses, another approach was pursued which is presented in the following section.

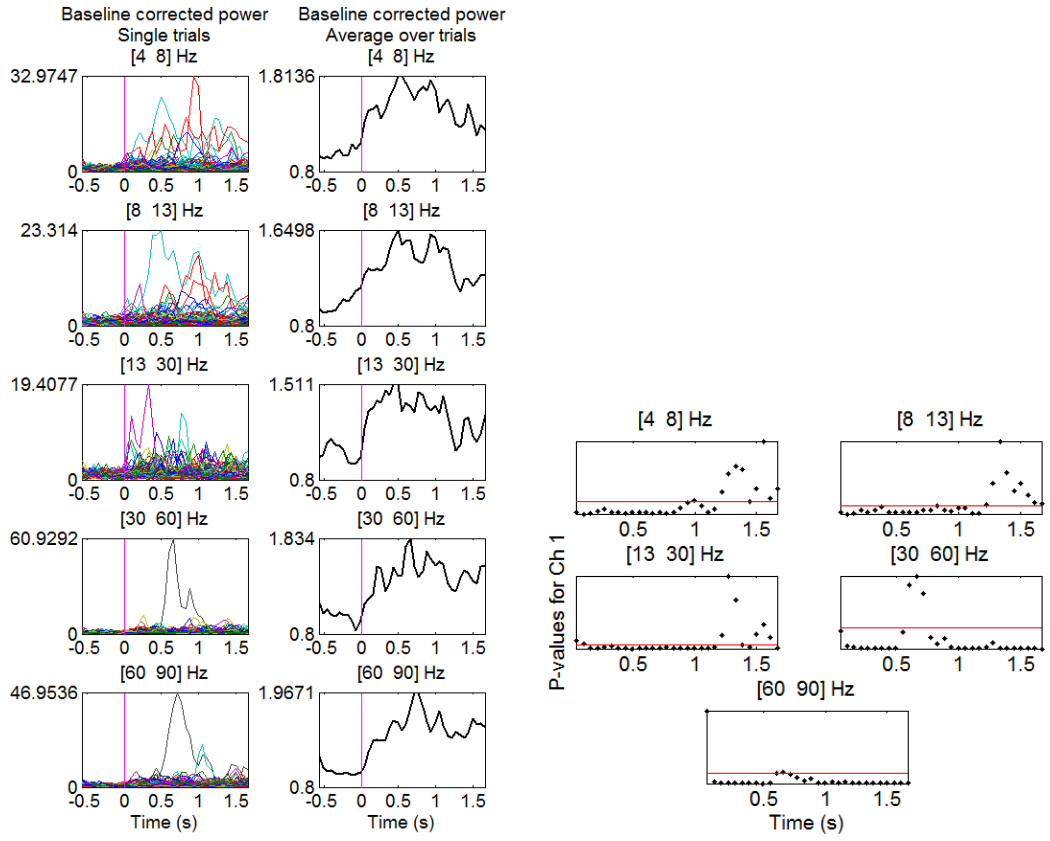

(a) (b)

Figure A.1: a) Left column: the power of signal in different frequency bands for each trial. Right column: the average power over all trials for each frequency band. The magenta line shows the onset of the stimulus. b) p-values of t-test at each time point after the stimulus onset. For presentation purposes, the actual amount of p-values are not indicated but the red line shows 5% significance level. Lower than this level means a significant p-value. All figures are related to EEG channel 1 for word stimuli presented binaurally. Baseline correction is achieved by division of power at each time point by the average baseline power in the same frequency band.

A.3 Envelope Detection

Similar analyses were performed in the same frequency bands by filtering the original signal and then extracting its envelope instead of applying time-frequency spectrum hoping that the smoothing would be less in this case and the peaks more evident. The results were still very similar to that of the spectra and it can be because of the not-so-ideal gain of the narrow band pass filter which acts similar to smoothing in time-frequency spectrum. Because of the similarities of envelope detection and spectra analysis, the results of envelope detection are not presented here. Therefore, this approach was not pursued any further.

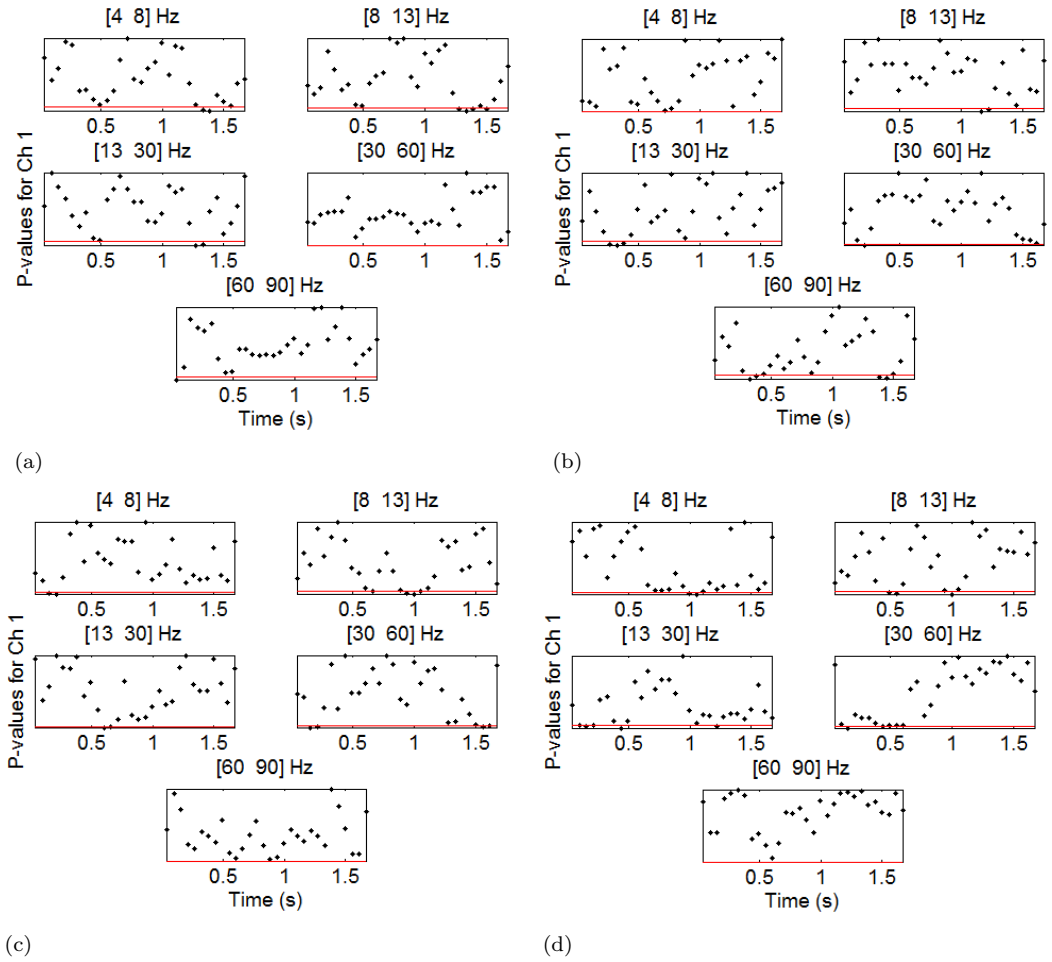

Figure A.2: p-value graphs of different frequency bands in EEG channel 1 of four different subjects (a-d) for word stimuli presented binaurally. In this case, baseline correction is achieved by subtraction of baseline power of each frequency band from the power of each time point in the same frequency band. There is no repetitive pattern in all subjects from which a reliable conclusion can be inferred. For presentation purposes, the actual amount of p-values are not indicated but the red line shows the 5% significance level.

A.4 TF Analyses and ALR

As the data being tested was an unconventional set of data (recorded using S1), it was not known if not getting a significant change after the stimulus onset was due to the use of an inappropriate algorithm or the lack of a response in the data. So, two sets of data in response to tone bursts were used. One set was from protocol S2 and another set that was recorded independently by the researcher of the current project from an adult subject with a similar protocol to protocol S2 but with almost three times the number of stimuli (480 stimuli). The SNR of the independent recording was almost two times the SNR of the dataset from protocol S2.

First, the data were epoched in [-0.5 1] s time range and then, filtered in [1 30] Hz frequency band. An ensemble average was then calculated over all epochs in channel 1 and the three main peaks of an ALR (P1-N1-P2) were visually inspected and detected in both cases. Then, the TF analyses method (section A.2-baseline subtraction) was employed to find the same peaks in [1 30] Hz frequency band. The t-test was successful in finding the response in the dataset with the higher SNR (Figure A.3) but not in the one with the low SNR (Figure A.4). Figures A.3 and A.4 show the ensemble average of trials in channel 1 in response to tone bursts in the two datasets. Also, it shows the power in single trials and the average power over all trials along with the significance of the power being different from the baseline at each time point after the onset.

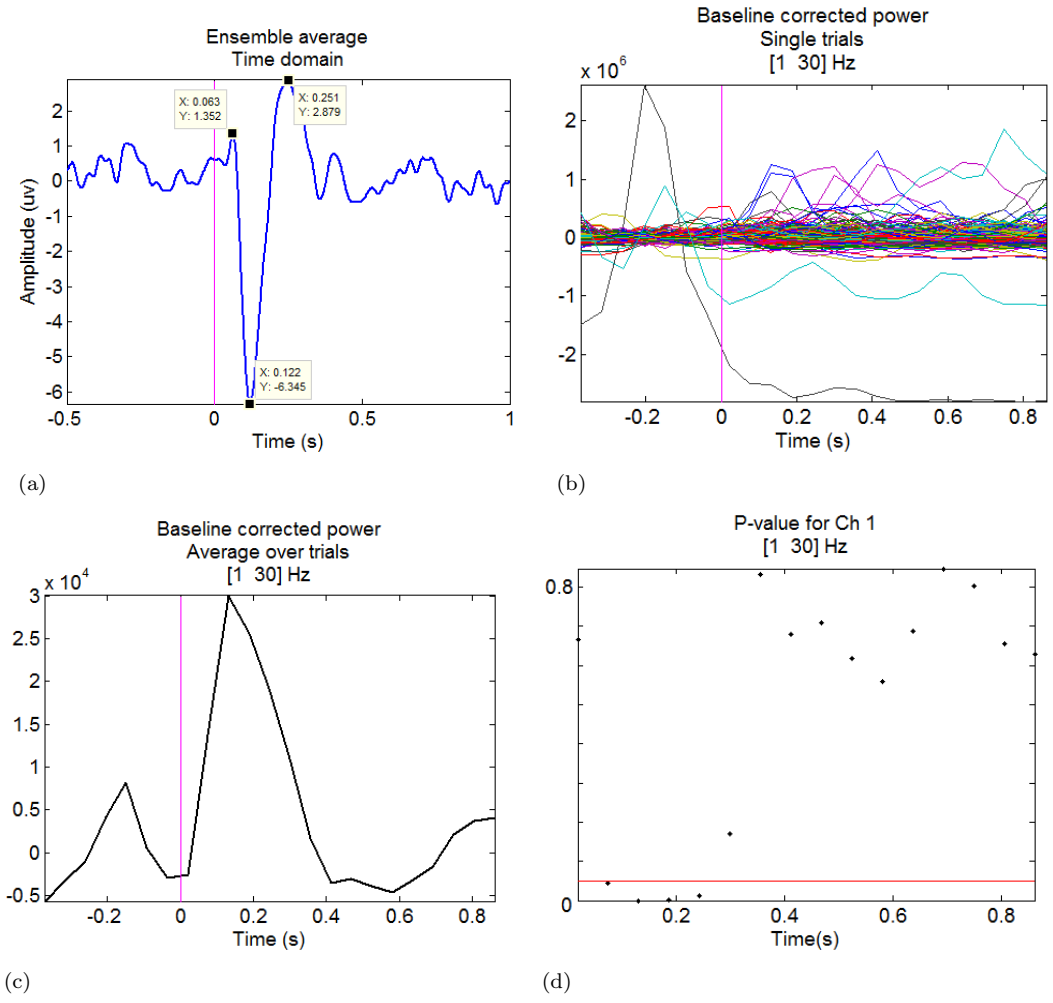

Figure A.3: Data from channel 1 of the independent recording. a) Ensemble average. The magenta line indicates the onset of the stimulus. b) Power (with baseline subtraction) in [1 30] Hz frequency band in single trials. The magenta line indicates the onset. c) the average power in [1 30] Hz frequency band over all trials. The magenta line indicates the onset. d) p-values of t-test at each time point after the stimulus onset. For presentation purposes, the actual amount of p-values are not indicated but the red line shows 5% significance level.

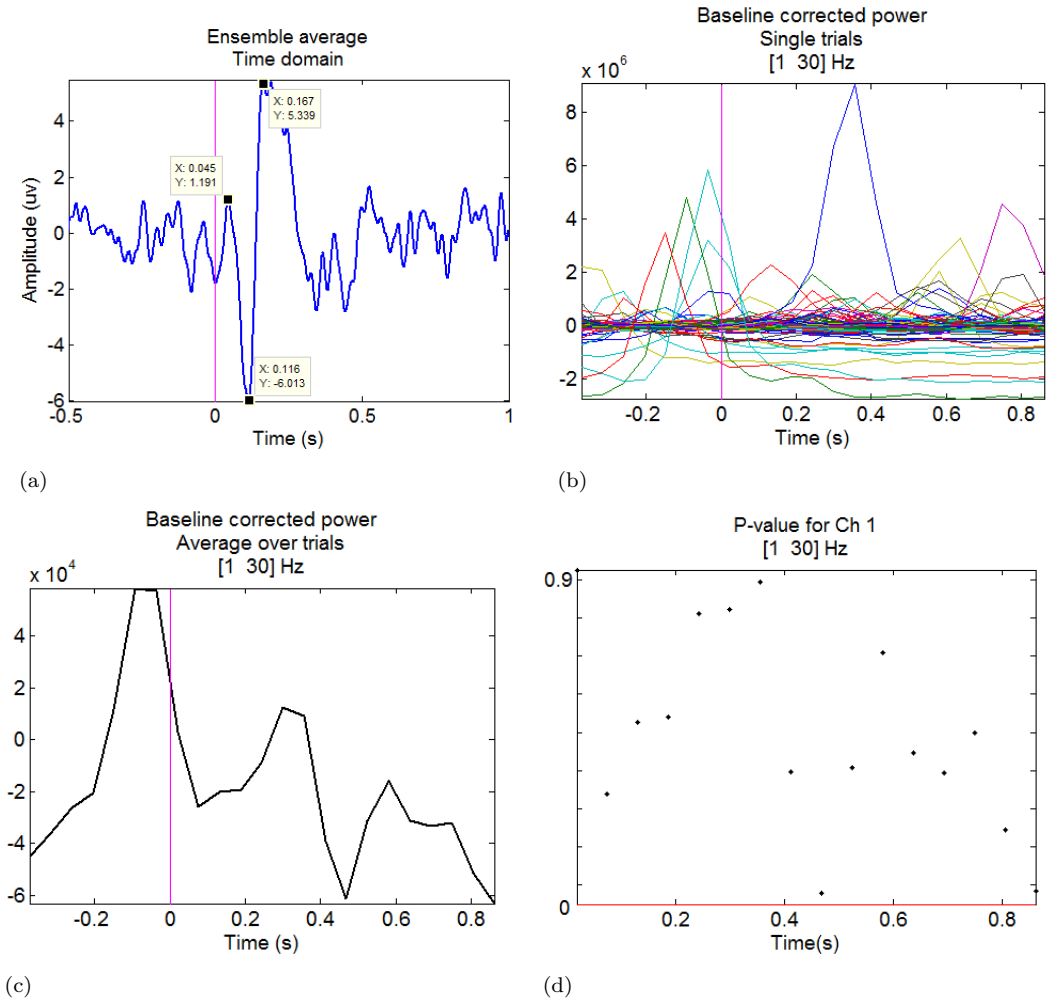

Figure A.4: Data from channel 1 of the dataset from protocol S2. a) Ensemble average. The magenta line indicates the onset of the stimulus. b) Power (with baseline subtraction) in [1 30] Hz frequency band in single trials. The magenta line indicates the onset. c) the average power in [1 30] Hz frequency band over all trials. The magenta line indicates the onset. d) p-values of t-test at each time point after the stimulus onset. For presentation purposes, the actual amount of p-values are not indicated but the red line shows 5% significance level.

These results demonstrate that the success of the mentioned algorithms depends very much on the quality of the signal. In the case of the examples in Figure A.4, in the dataset from protocol S2, the eye-blinks that happened in the baseline were the main reason for the lack of response detection. So, it was still possible that there was some response in the data from protocol S1 but the mentioned response detection algorithms would only work properly if artefacts were removed from EEG signals first.

A.5 Summary

In this appendix, two main methods of detecting induced response in EEG data were employed on the recorded data but were shown to be highly sensitive to the SNR of the signal. As the success of our targeted brain connectivity measures is dependent on the existence of the induced response in EEG data, it was very important to make sure if there is any induced response in the recorded EEG. That is why, further down the line, more analyses were employed for induced response detection in our data. These approaches are explained in appendix B.

Appendix B

Response Detection in Simulated Data

B.1 Introduction

As mentioned before, detecting the presence of induced response in our data was a very important step before going further to connectivity analyses (see to 4). To make sure that the approaches employed for this purpose are reliable, they were first applied on simulated data. This appendix focuses on these simulations and their results.

The methods that will be used are explained first and then the simulated data that were generated for testing each of the methods are discussed. The results of applying different approaches on simulated data are presented next. It should be pointed out that in each section presented on simulations, a brief discussion follows the results so that the process of rejecting or selecting a method is more understandable throughout the whole appendix. A more comprehensive discussion will be laid out at the end of the appendix.

B.2 Methods

The following methods will be applied on simulated data first and if appropriate, then will be employed for induced response detection in recorded data. For more details of recorded data see chapter 3 and for more information on the simulated data see section B.3 of this appendix.

B.2.1 Time-Frequency (TF) analyses

Trautner et al. (2006) shows that by averaging the Fourier transform of EEG over all trials and then calculating the power of the Fourier transform, the phase-locked activity of the brain will be restored and any activity that is non-phase-locked to the stimulus will be averaged out. On the other hand, by first calculating the power of the Fourier transform of each trial and then averaging the power spectra over all trials, one will be left with a linear combination of both the phase-locked and non-phase-locked activity of the brain. The phase-locked activity can thus be subtracted from this spectrum so that the non-phase-locked activity can be retained. If the non-phase-locked activity is time-locked to the stimulus, it will stand out in the averaged spectrum and can be regarded as an event-related response which is also called the induced response.

To obtain the power changes after the stimulus onset in the recorded EEG, the short time Fourier transform of each epoch was performed over the whole epoch for each simulated subject data with 256 ms windows and 250 ms overlap. Same as Trautner et al. (2006), to obtain the power spectrum of the evoked response for each dataset, firstly, Fourier transforms of all epochs were averaged and then, the power of this averaged Fourier transform was computed. Moreover, to compute the power spectrum of the induced response for each dataset, the power of the Fourier transform in each epoch was computed, the power was averaged over all epochs, and the power spectrum of the evoked response was subtracted from this average.

Because the range of the power in EEG spectrum decreases by increasing the frequency and for assessing the evoked and induced response an average will be computed in specific time-frequency areas of the spectrum, some sort of normalisation is needed to bring the power of all frequencies to a similar range. Two normalisation approaches were employed:

1. Baseline normalisation: Each one of the evoked and induced spectra were normalised to the average power of its baseline (time range before the stimulus onset) at each frequency. This normalisation will show the percentage of change of the power after the stimulus onset compared to the baseline (Hannemann et al., 2007).

2. Epoch power normalisation: Each one of the evoked and induced spectra were normalised to the average power of its whole time course at each frequency. This normalisation brings all frequency bands to a similar range and enhances the visibility of peaks (Zanto et al., 2005).

After normalisation, power was averaged in specific time-frequency areas in the spectrum of the evoked and the induced response in each simulated subject. This was performed to reduce the number of significance tests required. These areas were selected as in Figure B.1 for simulated data.

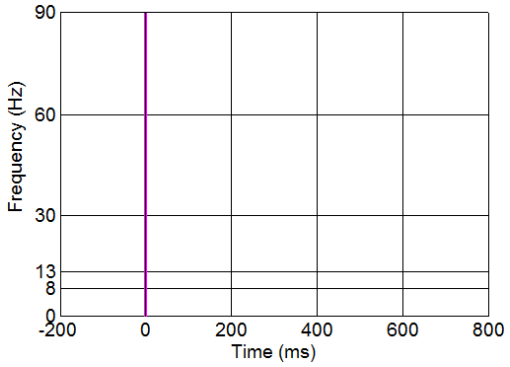

Figure B.1: Areas in the power spectrum in which an average power was calculated. The magenta line shows the onset time of the stimulus.

B.2.2 Significance tests

To test the significance of power changes after the stimulus onset, in both the induced and the evoked response, different methods of significance analyses were used. These methods are explained below, note that for t-test and ANOVA, the normality of the distribution of data was first checked by Kolmogrov-Smirnov test:

1. T-test: For pairwise paired t-tests, the power in every window after the stimulus onset was compared with the power of its peer (the same frequency band) in the baseline with a significant level of 5%. In each group, the number of observations was equal to the number of simulated subjects. The p-value for the t-test was not corrected for multiple comparisons because in recorded EEG, especially in induced response detection, if it is corrected too much, we may miss the change if it is not large enough.

2. Bootstrap: In bootstrap analyses, first the actual event-related induced and evoked spectra were calculated as explained in section B.2.1 and averaged according to Figure B.1 for each simulated subject separately. Then, in each time-frequency area of Figure B.1, the values were averaged over all subjects. To find out if the value in each area was significantly different from the baseline (thus showing an event related change), a non-event-related distribution of power values was required for that time-frequency area.

   To produce a non-event-related distribution of the spectrum, after the time-varying FFT of all trials was calculated and before any power computations were performed, FFT values were selected randomly with replacement from the baseline of all trials and were situated as FFT values of the whole duration of all epochs. It is worth mentioning that the randomly selected FFT value will be placed in the same frequency band as it was selected from. To explain it further, assume that after FFT calculations, a 50 x 60 x 100 (Frequency x Time x Trials) matrix of FFT values is obtained. After randomisation, again, a 50 x 60 x 100 matrix is generated

but this time all the values in this matrix come only from the baseline FFT values. After the randomised spectrum was generated, the evoked and induced powers were calculated for this new set of trials, the same as before and the power was averaged in areas marked by Figure B.1. This procedure was repeated 200 times for each subject so that in the end, for each time-frequency area of the evoked or induced spectrum, 200 values were calculated for each subject, i.e a matrix of 5 x 5 x 200 (Time x Frequency x Bootstrap) obtained. Then, in each time-frequency area of Figure B.1, bootstrap values were averaged over subjects so that in the end, for each area, 200 values were remained to make the distribution of the non-event-related power in that window. The lower/upper 5% value of the 200 bootstrap samples were identified for each time-frequency area. If the event-related average power in that area was lower/higher than this 5% value, that area was assumed to have a significant group decrease/increase compared to the baseline thus having a significant event-related change of power.

Ideally, instead of generating random power spectra by randomly selecting FFT values, datasets should be generated randomly in the time domain and the whole TF analyses and power averaging should be performed on these random datasets. Because the process of estimating the FFT-based power spectrum from the time-domain signal is very time consuming and doing that 200 times for each dataset would take a lot of time, the above mentioned approach, also used in EEGLAB toolbox (Delorme and Makeig, 2004), was employed instead.

3. One way ANOVA: For ANOVA analysis, after the average power in each window of Figure B.1 was calculated, a one-way ANOVA was applied to groups of powers over time (i.e. five groups [-200 0] ms, [0 200] ms, [200 400] ms, [400 600] ms, and [600 800] ms according to Figure B.1) in each frequency band separately, i.e. one-way ANOVA was applied five times (five frequency bands). The number of observations in each group was the same as the number of simulated subjects. If the p-value was smaller than 5% in a frequency band, post-hoc analysis (tukey's test) were performed at 5% significance level to find the areas after the stimulus onset that had significant power change compared to the baseline in that frequency band.

4. Repeated measures ANOVA: This test is similar to ANOVA only that it is applied on groups of observations that are not independent from each other. Therefore, the same steps as in one-way ANOVA were taken except that one-way ANOVA was replaced with repeated measures ANOVA.

5. Friedman's test: Friedman test is the non-parametric version of repeated measures ANOVA. Therefore, the same steps as in repeated measures ANOVA were taken except that repeated measures ANOVA was replaced with Friedman's test.

B.3 Simulated Data

As mentioned before, simulated data were produced to assess the reliability of the methods of computing the evoked and induced response and testing their significance. This section explains how these data were generated and what was the purpose of its generation.

B.3.1 White noise with no simulated response

This set of data was used to find the more appropriate normalisation and significant analysis methods for this project. Thirty sets of data with the same number of channels, data points, and trials as our ALR data (see section 3.2.2) were simulated using white noise, to account for three recordings from 10 subjects in Protocol S2 (see section 3.2.2.2).

As the significance level in significant analyses was set to 5% and no event-related activity had been added to the signal, it was expected that only 5% of the time-frequency areas (see Figure B.1) after the stimulus onset (1 out of 20) show significant change from the baseline power in every statistical test employed. The method that meets this condition can be regarded as the appropriate one for this project.

B.3.2 White noise with simulated evoked response

This dataset was simulated to find out if the methods that were deemed reliable using the simulated data in section B.3.1 would also have reliable results when it came to an existing evoked response in the data, i.e. if they could detect the time-frequency areas with evoked activity in them.

Thirty sets of data with the same number of channels, data points, and trials as our ALR data (see section 3.2.2) were simulated using white noise, to account for three recordings from 10 subjects in Protocol S2 (see section 3.2.2.2). Gaussian bells as in Figure B.2.a or 10 Hz sine waves as in Figure B.2.b were generated and added to the white noise in all trials. Adding the same Gaussian bell or the same sine wave to all trials of white noise can act as an evoked response. The peak of the evoked response in the Gaussian bell was located around 250ms and the bell started around 100 ms and ended around 400 ms after the onset. The 10 Hz sine wave was only added to the first 200 ms of data after the onset.

For the purpose of testing the sensitivity of significance tests to the SNR, sine wave evoked responses were simulated with different SNR levels simulated using different levels of peak amplitude in the sine wave. SNR is defined as the percentage of amplitude change from the baseline to the peak amplitude in the sine wave.

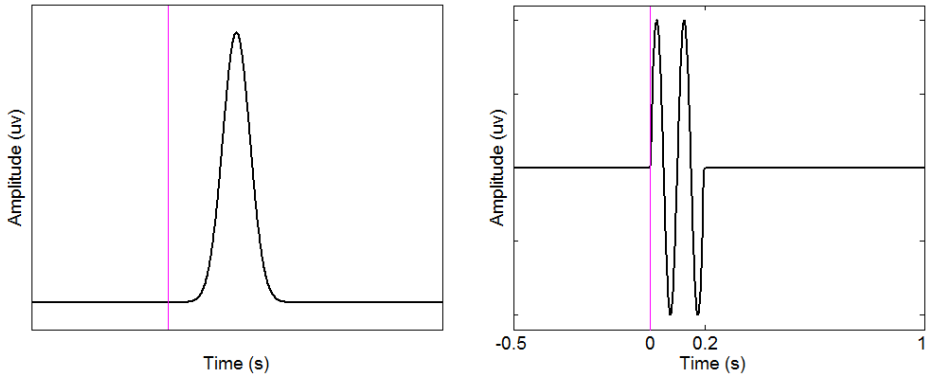

(a) (b)

Figure B.2: a) Gaussian window that was added to or multiplied by the white noise to simulate the evoked or the induced response. The timing of the peak and the width of the Gaussian bell depended on the type of the response simulated. b) A 200ms sine wave was generated with different phases and added to background noise to simulate induced response in the data.

B.3.3 White noise with simulated induced response

This dataset was simulated to find out if the methods that were deemed reliable using the simulated data in section B.3.1 would also have reliable results when it came to an existing induced response in the data, i.e. if they could detect the time-frequency areas with induced activity in them.

Thirty sets of data with the same number of channels, data points, and trials as our ALR data (see section 3.2.2) were simulated using white noise, to account for three recordings from 10 subjects in Protocol S2 (see section 3.2.2.2). Similar to simulated evoked responses, Gaussian bells as in Figure B.2.a and 10 Hz sine waves as in Figure B.2.b were generated. This time, Gaussian bells were multiplied by white noise in each trial. Multiplying the same Gaussian window to all trials of white noise can act as an induced response. The peak of the Gaussian bell was located around 500ms and the bell started around 400 ms and ended around 600 ms after the onset. However, for simulating the 10 Hz induced response, the 200 ms sine wave was generated with random phases and then added (not multiplied) to the white noise in different trials in the first 200 ms window after the onset.

For the purpose of testing the sensitivity of significance tests to the SNR, sine wave induced responses were simulated with different SNR levels simulated using different levels of peak amplitude in the sine wave. SNR is defined as the percentage of amplitude change from the baseline to the peak amplitude in the sine wave.

B.3.4 White noise with simulated phase synchronisation

This dataset was simulated to find out if the methods that were deemed reliable using the simulated data in section B.3.1 would also have reliable results when it came to an existing response in the data in the form of phase synchronisation and how phase synchronisation presents itself in induced and evoked spectra.

Zero phase: Thirty sets of EEG data with the same number of channels, data points, and trials as our ALR data (see section 3.2.2) were simulated using white noise, to account for three recordings from 10 subjects in Protocol S2 (see section 3.2.2.2). The FFT of the signal in [0 500] ms range was calculated for each trials and the FFT value at 10 Hz was replaced by its absolute value in each trial. This would make the 10 Hz frequency to have zero phase at 0 ms. An inverted FFT was applied to this new FFT vector. This way, the power of 10 Hz in the signal is kept the same before and after the onset but the phase has become synchronised in all trials for the first 500 ms time window after the onset.

Random phase: The same procedure as "zero-phase" was repeated but this time, the amplitude of FFT at 10 Hz was kept the same but its phase was randomly selected from $[-\frac{\pi}{6}\ \frac{\pi}{6}]$ rad range for different trials. This approach would simulate a phase synchronisation but with a bit of a jitter.

B.4 Results

In this section, methods mentioned in section B.2 will be applied on simulated data so that the most reliable ones are found and then used on recorded EEG data in chapter 4.

B.4.1 Testing the normalisation approaches

Thirty sets of evoked potentials were simulated as in section B.3.2. In each dataset, power was calculated in different areas of Figure B.1 for the first 22 channels following the steps in section B.2.1 and baseline normalisation. As in recorded EEG data, the spectra will be averaged over a few electrodes, more than one electrode were used in these simulations as well. At the time, we thought that we may use more than 20 electrodes around the vertex in recorded EEG that is why 22 electrodes were selected in simulations. Pairwise t-test was then applied to power values before and after the stimulus onset. By choosing a 5% significance level for each t-test, we expected an increase in the type-I error but what was not expected was for the t-test to report all changes after the onset to be significant and this was exactly what happened. The average spectrogram over all trials, 22 channels, and all 30 datasets is presented in

Figure B.3.a. By looking more closely at power values before and after the onset, a very small increase could be visually detected both in the distribution of power values and in the average power over 30 datasets. In Figure B.3.a, this small change is noticeable by the dark blue and light blue colours before and after the stimulus onset. It was thus concluded that by normalising the values after the onset to the average power of the baseline, a bias is applied to the power after the onset even when there was no actual increase in the power. So, the high number of false positives in the t-test seemed to be coming from the normalisation approach that was used and that normalisation to the baseline was not a reliable normalisation approach.

As the baseline normalisation was unreliable, power analyses were repeated by normalising power spectra to the whole epoch power (see B.2.1). The average spectrogram over all trials, 22 channels, and all 30 datasets after this type of normalisation is presented in Figure B.3.b. This time, only a few number of areas including the ones with evoked response present in them showed significant change with pairwise t-test. These areas are marked by black windows in Figure B.3.b.

Similar analyses were repeated with only white noise and no simulated response (see section B.3.1) and similar results were obtained, i.e. with baseline normalisation all areas after the baseline were marked significant and with whole epoch power normalisation only a few random areas were selected as significant.

From the simulations in this section, it was decided that normalisation to the power of the whole epoch was more acceptable than the baseline power normalisation. Still, it was not quite certain that t-test is an appropriate method for significance analyses. In the next sections, the reliability of t-test and other significance analyses methods is studied.

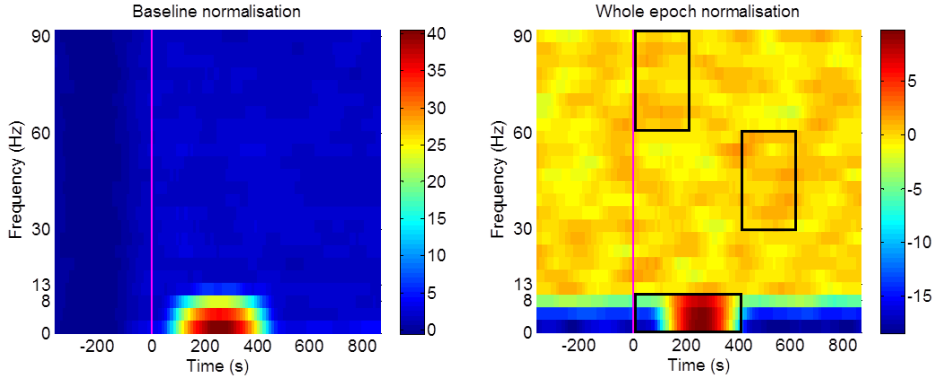

Figure B.3: The average spectrum over all trials, 22 electrodes centred around the vertex, and all datasets after a) baseline normalisation and b) whole epoch power normalisation (see section B.2.1). The magenta line shows the onset of the stimulus. The unit of the colour bars is dB.

B.4.2 Testing significance methods

It is possible that some significance analyses methods, even the ones currently being used in publications, may produce more or less false positives than expected depending on the data, the preprocessing steps taken, and the final features estimated from the data (in this case the power values). This fact will make the method either insensitive or over-sensitive to a change in the desired feature. In this section we aim to find an appropriate and reliable method for analysing the significance of power changes observed after the stimulus onset.

Our methods include both parametric (t-test and ANOVA) and non-parametric (bootstrap and Friedman's test) approaches. One of the limitations of using our parametric approaches is that each group of observations should have a normal distribution. Although power values do not have normal distributions on their own, in the case of our TF analyses, as the power spectra are averaged over trials and also over a group of time-frequency points (each of which have a χ^2 distribution with 2 degrees of freedom (Groth, 1975)) in each area of Figure B.1, it was assumed that the values that enter these analysis had normal distributions (as they had χ^2 distribution with a very large degree of freedom $\gg 50$). This assumption was also confirmed with a Kolmogorov-Smirnov test ($p<0.05$). Therefore, the condition of normal distribution was established.

B.4.2.1 T-test

In applying the t-test to our data, because of multiple comparisons of areas after the onset with a same group before the onset (baseline) and the comparison dependency that followed, it was assumed that the number of false positives should be higher than expected. To check for this problem, simulated datasets with no response present were generated (see section B.3.1), TF and power analyses were applied with normalisation to the whole epoch power (see section B.2.1), and the number of areas marked significant after the onset using the t-test were counted (see section B.2.2). As there was no response present in the data, if the comparisons were all independent, the distribution of the number of significant areas detected should have followed a binomial distribution with a 5% success rate in 20 runs (20 areas after the onset) of the significant test as in Figure B.4. If the same procedure (from generating 30 datasets to counting the number of significant areas) was repeated 100 times, the probabilities shown in Figure B.4 would be multiplied by 100 demonstrating that about 36 tries should show no significance at all, about 37 tries should show significance in only one area, about 18 tries should show significance in 2 areas and so on.

This whole scenario was carried out and Figure B.5 shows the results of these analyses. In this figure, the number of areas after the onset showing significant decrease or increase in the evoked or induced power compared to the baseline in each repeat (out of 100) is

presented (top row) along with its probability density function over 100 repeats (bottom row), i.e. the number of repeats that showed significant change in 0, 1, 2, etc areas. As can be seen in the bottom row, the distribution in simulated data (in blue) does not follow the expected binomial distribution (in red) and this is because separate t-tests are not independent from each other. The χ^2 goodness of fit was applied on the two distributions (blue and red curves in Figure B.5) and it confirmed that they were significantly different from each other ($p<0.05$) in all cases. For this reason, t-test was deemed inappropriate for this application.

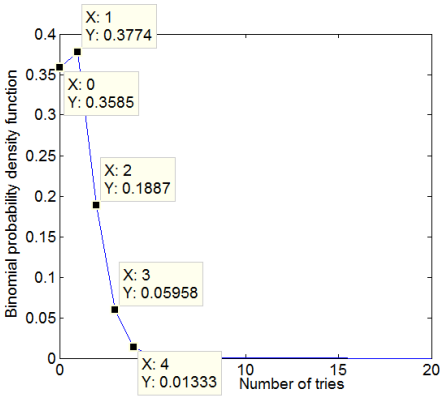

Figure B.4: The binomial distribution for 5% success rate in 20 independent tries.

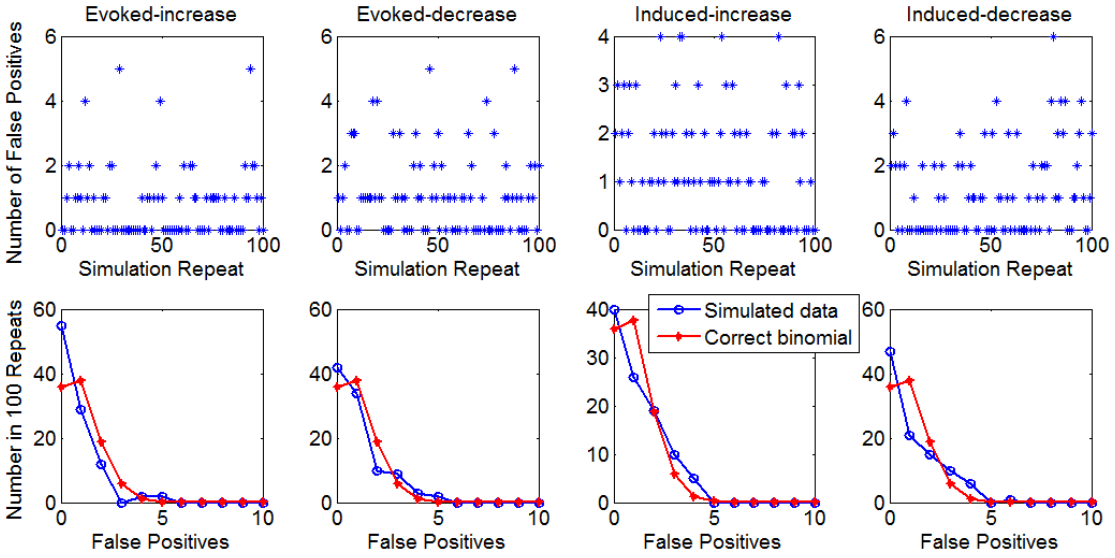

Figure B.5: False positives reported by t-test. Top row: number of windows showed significant decrease or increase in evoked or induced power after the onset compared to the baseline in each repeat of the simulations. Bottom row: the distribution of false positives in 100 repeats of simulations (in blue), i.e. the number of repeats that showed significant change in 0, 1, 2, etc areas, and the binomial distribution with a 5% success rate in 20 independent tests and 100 repeats of the same procedure (in red).

B.4.2.2 Bootstrap

The same procedure as in the t-test validation was employed for the bootstrap (see section B.4.2.1). As before, 30 sets of data were simulated using white noise without any response present as in section B.3.1. TF and power analyses were applied with normalisation to the whole epoch power (see section B.2.1) and the number of areas marked significant after the onset using bootstrap were counted (see section B.2.2).

As in the t-test, in one set of data, a false positive distribution as in Figure B.4 was expected for significant detection of areas in Figure B.1. Repeating the analyses 30 times (as it was a time consuming approach, it was repeated 30 times instead of 100 times like the t-test), it was expected that all probabilities be multiplied by 30, i.e. about 10 repeats should show no significance at all, about 11 repeats should show significance in only one area, about 5 repeats should show significance in 2 areas and so on. Reasoning behind this claim has been presented in section B.4.2.1. Figure B.6 depicts the number of areas showing significant change compared to the baseline in each repeat and the distribution of these values over 30 repeats, i.e. the number of repeats that showed significant change in 0, 1, 2, etc areas. This figure demonstrates that the distribution of simulated data (blue line) does not follow the expected binomial distribution (red line) and the number of false positives tends to be much higher than expected. This was also tested with the χ^2 goodness of fit and it showed that the two distributions presented in the bottom row of Figure B.6 are significantly different from each other ($p<0.05$)

It is clear from Figure B.6 that the number of false positives for 5% significance level is around 25-30% when using bootstrap so it is not an appropriate method for our application. The reason behind this problem can be the way the bootstrap has been handled here. After the induced and evoked responses were estimated for the first simulated data (the target data), power values in each area of Figure B.1 were still dependent on each other because in the process of power spectrum computation, an overlapping moving window had been used; whereas, in the bootstrap sample pool, this dependency had been removed because of the random selection of FFT values from the baseline. Therefore, the average values calculated in areas of Figure B.1 in the two conditions (main data and bootstrap pool) should not be compared together as we should not expect them to be in the same range. If the ideal method (generating random data in time domain) had been used, it might not have had this problem but it was a very time consuming method so it was dropped and the efficiency of ANOVA was tested instead.

B.4.2.3 One-way ANOVA

Other than normality of the distribution of observations in each group, ANOVA assumes that different groups should have similar variances (Stephan et al., 2012) which is the

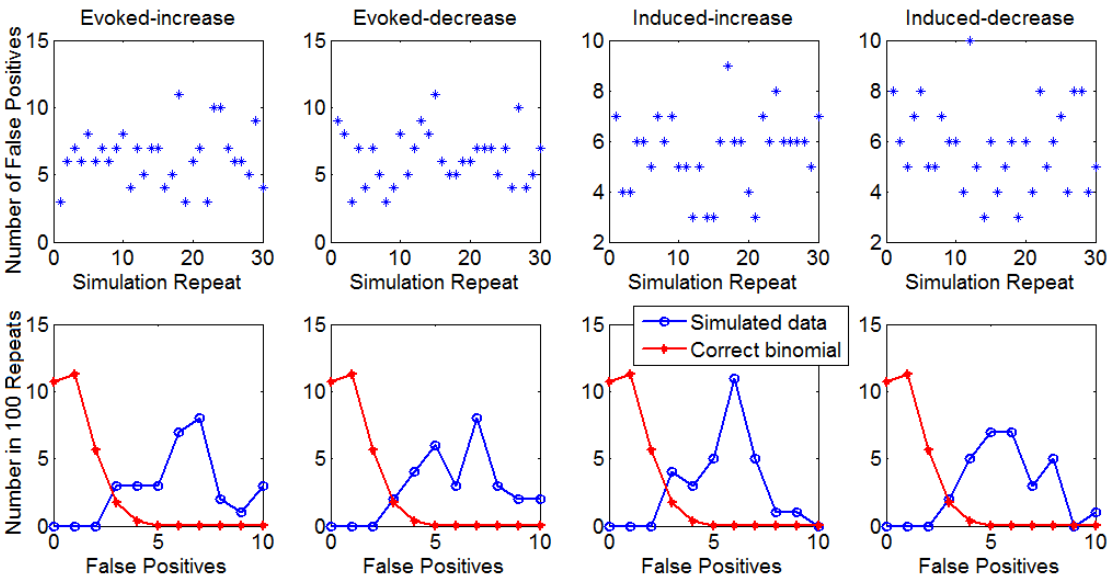

Figure B.6: False positives reported by bootstrap. Top row: number of windows showed significant decrease or increase in evoked or induced power after the onset compared to the baseline in each repeat of the simulations. Bottom row: the distribution of false positives in 30 repeats of simulations (in blue), i.e. the number of repeats that showed significant change in 0, 1, 2, etc areas, and the binomial distribution with a 5% success rate in 20 independent tests and 30 repeats of the same procedure (in red).

case in our computations as power values are normalised and they have fallen in a similar range after normalisation. Another limitation for ANOVA is that all observations should be mutually independent (Stephan et al., 2012) and as simulations are performed using independent white noise, independency of observations in each group is met. But, as different groups of power values are calculated for the same dataset over time, the independency of observations over different groups is not met. It is shown in this section how this dependency affects the results.

To test ANOVA, as in section B.3.1, 30 sets of data were simulated using white noise without any response present. Induced and evoked power calculations were performed by following the steps in section B.2.1 and normalisation to the whole epoch power. ANOVA was then applied to these estimated powers as explained in section B.2.2. As mentioned in section B.2.2, ANOVA was repeated five times, each time on one of the frequency bands of Figure B.1. As ANOVA is repeated five times with 5% success rate, it was expected that the probability of reporting false positives should follow the binomial distribution as in Figure B.8 (for reasoning behind this see section B.4.2.1). When this whole procedure (from simulating the 30 datasets to counting the number of significant reports) was repeated 100 times, the distribution of false positives should have followed the distribution of Figure B.7 when multiplied by 100, i.e. about 77 repeats should

show no significance at all, about 20 repeats should show significance only once, about 2 repeats should show significance twice and so on.

Figure B.8 shows the distribution of false positives reported by one-way ANOVA in evoked and induced power of simulated data (in blue) along with the correct binomial distribution (in red). Although, visually, the two distributions seem to match, their similarity was tested with a χ^2 goodness of fit ($p<0.05$) and it showed that they are significantly different. Simulations show higher false positives than expected and this difference is probably coming from the dependence between different groups.

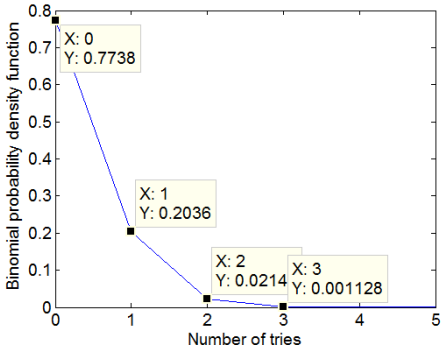

Figure B.7: The binomial distribution for 5% success rate in 5 independent tries.

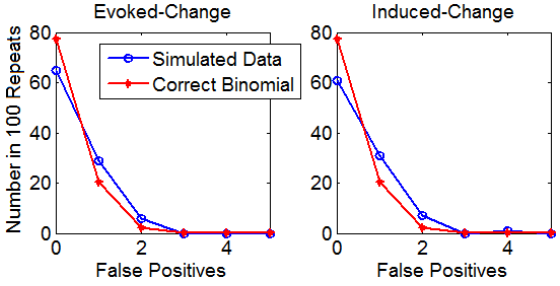

Figure B.8: False positives reported by one-way ANOVA. The distribution of false positives in 100 repeats of simulations (in blue), i.e. the number of repeats that showed significant change 0, 1, 2, etc times, and the binomial distribution with a 5% success rate in 5 independent tests and 100 repeats of the same procedure (in red).

To make sure that the dependence between groups is the reason behind higher false positives, further simulations were performed. This time, random 30x5 matrices sampled from a χ^2 distribution with 100 degrees of freedom were generated, representing average powers in five time windows and 30 subjects. These matrices were generated five times to account for different frequency bands and then the whole procedure was repeated 100 times to account for 100 repeats of the test as in previous analyses. One-way ANOVA was applied on these matrices and the normalised versions of these matrices (averaging values over time and dividing all time values by this average value). The results of these simulations are not presented here but they showed that the matrices without normalisation still produce correct number of false positives but the problem

of more false positives is observed after the normalisation step. Normalisation to the average power introduces a dependency over different groups and as was observed with simulations of Figure B.8 produces more false positives than expected. Therefore, other significance tests were sought for the purpose of our study.

The last simulations (producing random matrices) were also tested with repeated measures ANOVA and its non-parametric version (Friedman's significance test) and they were not affected by the normalisation step, i.e. they produced the expected false positive distribution both before and after normalisation step. For this reason, it was decided that these methods might be appropriate candidates for our significance analysis so their reliability was further tested with simulated white noise signals. These simulations are presented in the next sections.

B.4.2.4 Repeated measures ANOVA

The assumptions of repeated measures ANOVA are the same as one-way independent ANOVA (see section B.4.2.3) except for the independency condition between groups of observations (Howell, 2010). With repeated measures ANOVA, different groups can have dependent values as in longitudinal studies with more than one measurement from the same group of subjects and then looking for differences between different measurements (similar to the case of this project). This method was analysed in two steps. The distribution of false positives was tested first, after repeated measures ANOVA and then, after applying post-hoc analyses.

For testing the reliability of repeated measures ANOVA, the exact same steps as in section B.4.2.3 were taken, i.e. simulating 30 sets of data, calculating power, and counting the number of times repeated measures ANOVA reported significance and then repeating these analyses 100 times. The only difference was replacing one-way ANOVA with repeated measures ANOVA. It was expected that the distribution of false positives using repeated measures ANOVA in each set of data should follow Figure B.7 and repeating the procedure 100 times should produce the same distribution with probability values multiplied by 100 (for reasoning behind this, see B.4.2.3). This means that about 77 repeats should show no significance at all, about 20 repeats should show significance only once, about 2 repeats should show significance twice and so on.

Figure B.9 shows the number of repeats showing significance 0, 1, 2, etc times in simulations (in blue) along with the correct binomial distribution which is the distribution in Figure B.7 multiplied by 100 (in red). This figure shows that the two distributions follow each other closely and the test of χ^2 goodness of fit confirms that the two distributions are not significantly different ($p>0.05$). So, repeated measures ANOVA produced expected number of false positives and proved reliable upto this point.

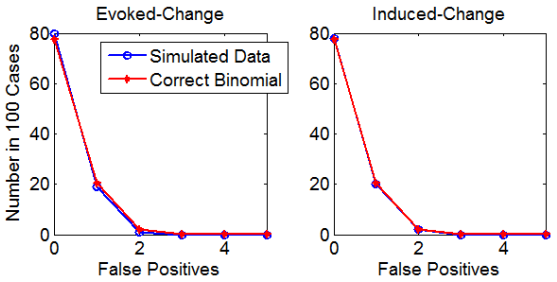

Figure B.9: False positives reported by repeated measures ANOVA. The distribution of false positives in 100 repeats of simulations (in blue), i.e. the number of repeats that showed significant change 0, 1, 2, etc times, and the binomial distribution with a 5% success rate in 5 independent tests and 100 repeats of the same procedure (in red).

The next step was to check the reliability of post-hoc analyses (Tukey's test) after repeated measures ANOVA. For this purpose, again 30 datasets were generated as in section B.3.1, TF analyses were applied on them, and powers were averaged in areas marked by Figure B.1. Every time repeated measures ANOVA reported a p-value less than 0.05, post-hoc analyses were performed using Tukey's method to find the areas after the onset that were significantly ($p<0.05$) different from the baseline and the number of areas after the onset that showed significant difference with the baseline were counted in all frequency bands. This procedure was repeated 100 times to find the distribution of this number. This distribution should then be compared with the expected (correct) distribution (similar to analyses in section B.4.2.1 for the t-test) to find out if the number of reported false positives was what was expected. Figure B.10, in the top row, shows the number of false positives in evoked or induced power of simulated data in each repeat. In the bottom row, the distribution of these false positives over 100 repeats is plotted (in blue) along with the expected distribution.

In this case, finding the correct distribution theoretically was not as straight forward as the t-test and bootstrap methods because for a random dataset, an α value of 0.05 only means that in 5% of cases when repeating the repeated measures ANOVA, a significant difference between the 5 groups will be seen. It does not guarantee that all these 5% cases would show a significant difference between a group in the baseline and a group after the onset. So, to produce the correct distribution, we can not simply use a 5% success rate. The desired success rate is probably much smaller than 5% and not easy to estimate.

So, instead of finding a theoretical binomial distribution, an experimental distribution was estimated. For this purpose, random 30x5 matrices sampled from a χ^2 distribution with 100 degrees of freedom were generated representing average powers in 5 time areas and 30 subjects, first column being the baseline power and the rest being the power in time areas after the onset. Each value in the matrix was divided by the average value of its row to account for the normalisation procedure that was employed in simulated

signals. Repeated measures ANOVA and post-hoc analyses were then applied on these normalised matrices assuming that they were power values calculated in areas of Figure B.1 and the number of areas in all frequency bands after the onset showing significant difference with the baseline was counted for all 100 repeats. The distribution of false positives obtained through these analyses was called correct distribution. In the bottom row of Figure B.10, this distribution is plotted in red. Test of χ^2 goodness of fit confirmed that the two distributions, from simulated data (in blue) and the correct distribution (in red), were not significantly different from each other ($p>0.05$) thus it was concluded that repeated measures ANOVA produced expected number of false positives and may be reliable in recorded EEG as well.

Still, as ANOVA focuses on the mean value of each group, outliers (if present) in recorded EEG may affect the results of significance analyses. For this reason, the non-parametric version of repeated measures ANOVA which is called Friedman's test and is not susceptible to outliers was also tested to replace repeated measures ANOVA if suitable.

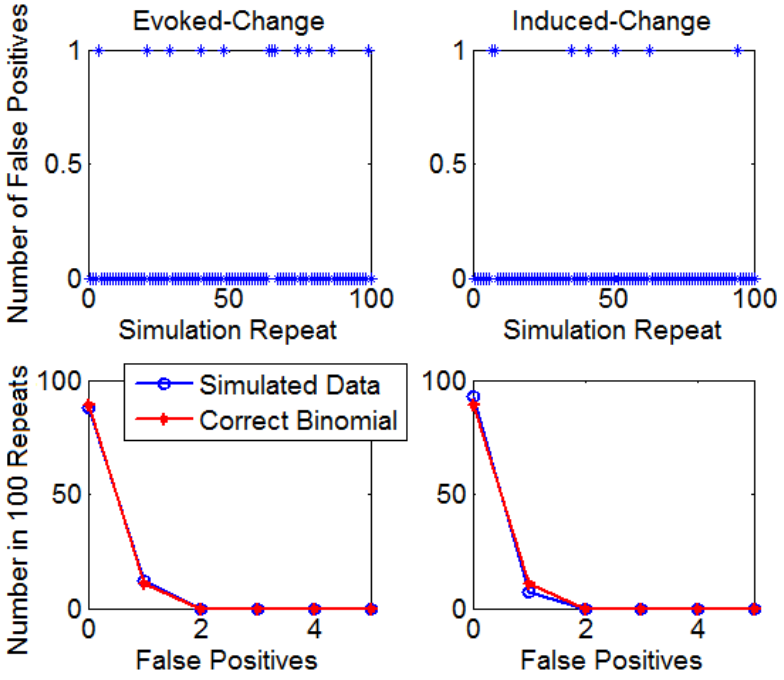

Figure B.10: False positives reported by Tukey's test after repeated measures ANOVA. Top row: number of windows showed significant change in evoked or induced power after the onset compared to the baseline in each repeat of the simulations. Bottom row: the distribution of false positives in 100 repeats of simulations (in blue), i.e. the number of repeats that showed significant change in 0, 1, 2, etc areas, and the correct distribution obtained experimentally (in red).

B.4.2.5 Friedman's test

Friedman's test was first applied on white noise with no response present. As it proved to be reliable on this set of data, it was also tested on simulated data with evoked and induced response present in them. The results of these analyses are presented in this section.

1. Friedman and white noise: As mentioned before, Friedman's test is not affected by outliers thus it may be a more appropriate method than repeated measures ANOVA in recorded EEG. Two assumptions that Friedman's test makes are that observations in different groups have similar continuous distributions and that observations in each group are mutually independent (Stephan et al., 2012). Both these conditions are met by generating simulated data using white noise thus it was reasonable to apply this test on these data.

   The exact same steps as in section B.4.2.4 were taken to examine the reliability of Friedman's test and the post-hoc analyses afterwards. The only difference was that repeated measures ANOVA was replaced with Friedman's test. Therefore, we are not going into all the details here again. The distribution of false positives obtained from simulated data was estimated and is shown in Figure B.7 (in blue) along with the correct binomial distribution. This figure shows that the two distributions follow each other closely and the test of χ^2 goodness of fit confirms this judgement ($p>0.05$). Up to this point, Friedman's test can be considered a suitable method.

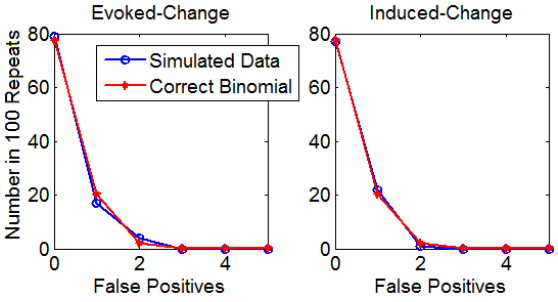

Figure B.11: False positives reported by Friedman's test. The distribution of false positives in 100 repeats of simulations (in blue), i.e. the number of repeats that showed significant change 0, 1, 2, etc times, and the binomial distribution with a 5% success rate in 5 independent tests and 100 repeats of the same procedure (in red).

   The next step was to test post-hoc analyses after Friedman's test. Again, this step was exactly the same as testing post-hoc after repeated measures ANOVA (see section B.4.2.4). First, the distribution of false positives from simulated data was estimated and then, the correct distribution was obtained experimentally by generating random matrices as explained in section B.4.2.4. These two distributions are plotted in Figure B.12, from simulations (in blue) and the expected one (in

red). χ^2 goodness of fit confirmed that the two distributions were not significantly different from each other ($p>0.05$) thus the Friedman's test produced expected number of false positives and is reliable for applying on recorded EEG data when there was no response present.

Although repeated measures ANOVA and Friedman's test both work properly in simulated data, Friedman was decided to be a more appropriate choice for the current project as recorded EEG may contain outliers and ANOVA will be affected by these outliers whereas Friedman will not. Still, one more test was required to reliably choose Friedman's test as the most appropriate method for our purposes, its sensitivity to existing response. To find out if it was sensitive enough to detect any response in the data, it was also applied on simulated data with evoked and induced response present in them. The results of these simulations are presented next.

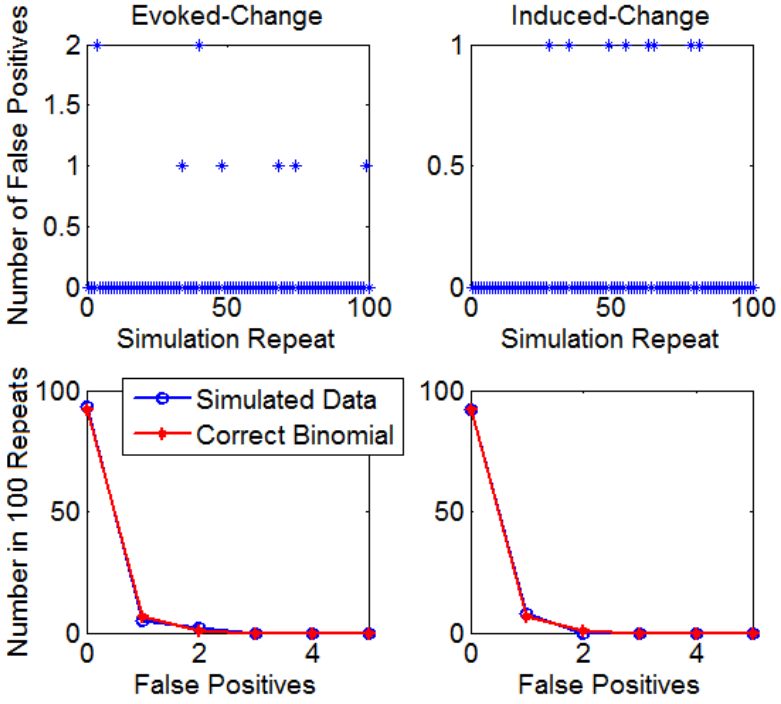

Figure B.12: False positives reported by Tukey's test after Friedman's test. Top row: number of windows showed significant change in evoked or induced power after the onset compared to the baseline in each repeat of the simulations. Bottom row: the distribution of false positives in 100 repeats of simulations (in blue), i.e. the number of repeats that showed significant change in 0, 1, 2, etc areas, and the correct distribution obtained experimentally (in red).

2. Friedman and simulated evoked response: To test the sensitivity of Friedman's test to existing evoked response in the data, 30 datasets were simulated as in section B.3.2 using the Gaussian bell. TF analyses and average power calculations in areas of Figure B.1 were performed according to steps in section B.2.1 with normalisation to whole epoch power. Figure B.13 shows the average induced and evoked spectra

over all trials of channel 1 and all 30 datasets. Using Friedman's test and post-hoc analyses, significant changes in power after the onset compared to the baseline was only observed in the evoked spectrum (not the induced spectrum) and the areas marked by the black windows. It should be noted that in this figure, a bit of blue area has also been selected as significant. The reason behind this is that the power is averaged over the whole 200 ms areas in different frequency bands (as in Figure B.1) so the significance result is over the whole window and not only the parts plotted in red. So, Friedman's test could correctly detect the evoked response in this case but what if the level of the response was lower or higher than this case?

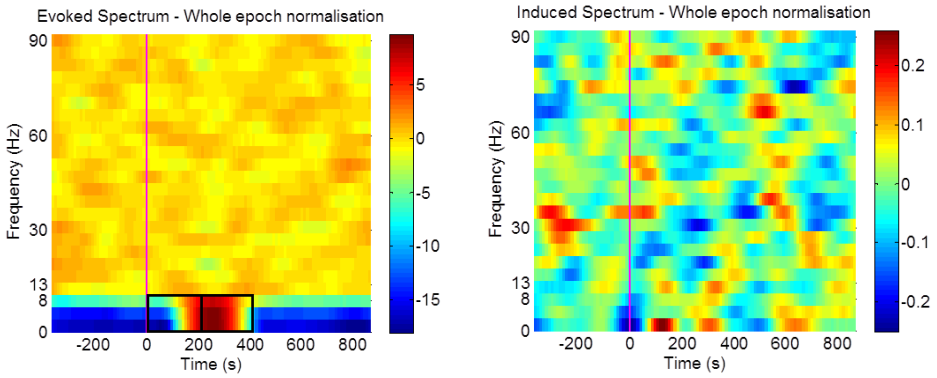

(a) (b)

Figure B.13: Average a) evoked and b) induced power in channel 1 over all trials and 30 datasets with simulated evoked response using the Gaussian bell. Areas marked with black windows show significant power increase compared to the baseline. The magenta line shows the onset of the stimulus. The unit of the colour bars is dB.

To test the sensitivity of Friedman's test to the level of evoked response SNR, datasets were simulated as in section B.3.2, this time with the simulated evoked response being the 10 Hz sine wave. For each level of SNR, 30 datasets were generated and the procedure of response detection was performed on each SNR level. This procedure was repeated 50 times for each SNR level (see section B.3.2 for the definition of SNR). By adding this 10 Hz to the white noise, only [8 13] Hz frequency band in [0 200] ms and [200 400] ms areas will be affected. The detection rate of these two time frequency areas over 50 simulations of each SNR level is presented in Figure B.14. This figure shows that, using Friedman's test, the evoked response is highly detectable down to SNR=0.02 and only gradually decreases for SNRs lower than 0.02. No induced response is detected in any of SNR levels, as expected.

3. Friedman and simulated induced response: To test the sensitivity of Friedman's test to existing induced response in the data, 30 datasets were simulated as in section B.3.3 using the Gaussian bell. TF analyses and average power calculations in areas of Figure B.1 were performed according to steps in section B.2.1 with

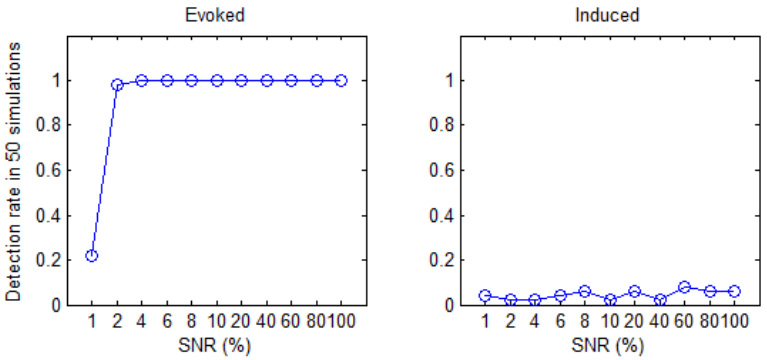

Figure B.14: Detection rate versus SNR level for 50 simulations of the evoked response. As expected, no induced response is detected when only evoked response is present.

normalisation to whole epoch power. Figure B.15 shows the average induced and evoked spectra over all trials of channel 1 and all 30 datasets. Using Friedman's test and post-hoc analyses, significant change in power after the onset compared to the baseline was only observed in the induced spectrum (not the evoked spectrum) and the areas marked by the black windows. As the Gaussian bell was multiplied by the white noise, it had affected all frequency bands thus what we see in this figure is completely reasonable. So, Friedman's test could correctly detect the induced response in this case but what if the level of the response was lower or higher than this case?

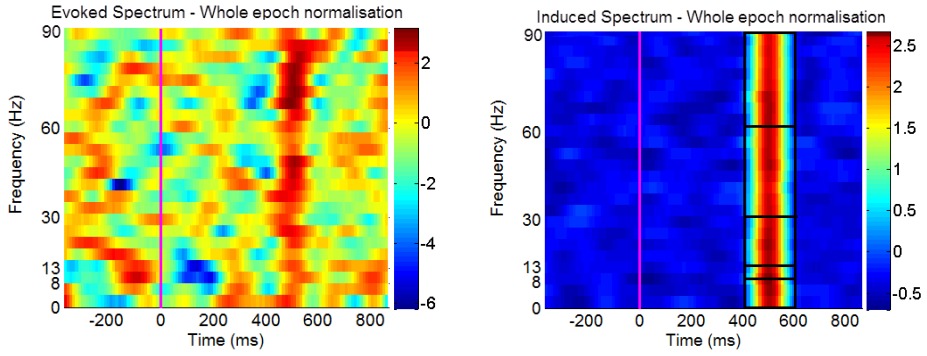

(a) (b)

Figure B.15: Average a) evoked and b) induced power in channel 1 over all trials and 30 datasets with simulated induced response using the Gaussian bell. Areas marked with black windows show significant power increase compared to the baseline. The magenta line shows the onset of the stimulus. The unit of the colour bars is dB.

To test the sensitivity of Friedman's test to the level of induced response SNR, datasets were simulated as in section B.3.3, this time with the simulated induced response being the 10 Hz sine wave. For each level of SNR, 30 datasets were generated and the procedure of response detection was performed on each SNR level. This procedure was repeated 50 times for each SNR level (see section B.3.3

for the definition of SNR). By adding this 10 Hz to the white noise, only [8 13] Hz frequency band in [0 200] ms and [200 400] ms areas will be affected. The detection rate of these two time frequency areas over 50 simulations of each SNR level is presented in Figure B.14. This figure shows that the induced response is highly detectable down to SNR=0.06 and only decreases for SNR's lower than 0.06. Comparing this figure with Figure B.14 indicates that the induced response is harder to detect than the evoked response but still Friedman's test can detect it to a very low SNR level. Furthermore, it can be seen in Figure B.16 that although there is no evoked response simulated in these sets of data, in SNR's higher than 0.2, Friedman's test is detecting significant evoked response. However, looking at the evoked and induced spectra in this case, shows that in higher SNRs, the induced response presents itself as an evoked response in the data as well. Thus, this problem does not come from the Friedman's test but rather the type of data and changing the significance test would not help in resolving this problem. This result suggests that in recorded EEG, we should approach the results with caution if we observe both induced and evoked response in the same time-frequency areas.

Now, we are satisfied that Friedman's test along with the selected post-hoc test (Tukey's) will be able to detect the existence of the induced or the evoked response in recorded EEG data to a reasonable degree, depending on the level of SNR. As a final stage and for understanding different types of responses in EEG data, phase synchronisation was also simulated and its results are presented next.

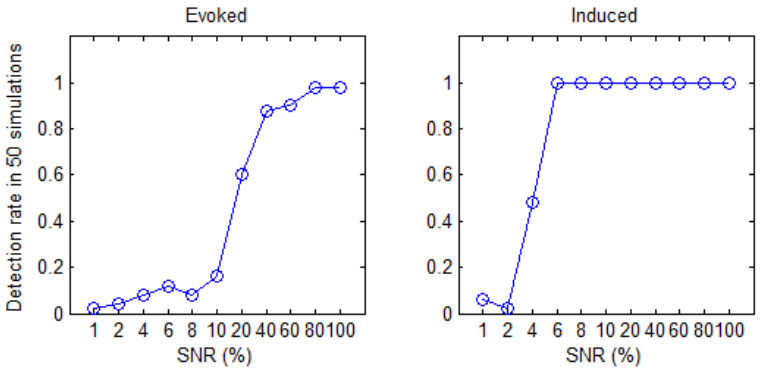

Figure B.16: Detection rate versus SNR level for 50 simulations of the induced response. Note that although there is no evoked response present in the data, for large SNR's (¿0.2), the induced response also presents itself as an evoked response in the data.

4. Friedman and phase synchronisation: To find out how phase synchronisation presents itself in evoked and induced spectra, two groups of 30 datasets were simulated as in section B.3.4, one with a zero-phase 10 Hz and the other with a random-phase 10 Hz. TF analyses, power averaging with normalisation to the whole epoch power, and Friedman's significance analyses were applied on each group separately (see section B.2).

As phase synchronisation can also be regarded as a phase-locked response, it was expected that this response was observed as an evoked response in our analysis. Figures B.17 and B.18 present the induced and evoked spectra for the zero-phase and the random-phase dataset, respectively. Black windows show significant increase and white windows show significant decrease compared to the baseline. As expected, a significant increase in the evoked power can be seen around 10 Hz in [0 400] ms areas in both cases (zero and random phase datasets). This suggests that the methods of response detection work properly even in case of phase synchronisation (although it can not differentiate between evoked response and phase synchronisation). However, an unexpected significant decrease can be seen in the same window in the induced response. This result is also reasonable. As there really is no evoked response in the data and the increase in the evoked power only comes from phase locking because of synchronisation, subtracting the evoked power from the averaged induced power introduces a hole in the induced power in the same time-frequency area as the significant evoked power was observed in.

This result can be very helpful in the future when dealing with recorded EEG data to discriminate between evoked power and phase synchronisation.

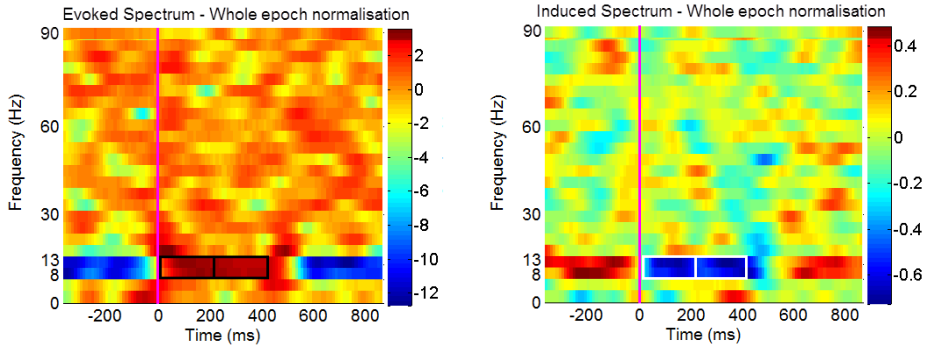

(a) (b)

Figure B.17: Average a) evoked and b) induced power in channel 1 over all trials and 30 datasets with simulation of zero-phase phase synchronisation. Areas marked with the black/white window shows significant power increase/decrease compared to the baseline. The magenta line shows the onset of the stimulus. The unit of the colour bars is dB.

B.5 Discussion

In section B.4.1, it was shown that normalisation of time-frequency spectra to the baseline power would introduce a bias to the power after the onset. This bias would force significant analysis methods to report a power change after the onset compared to the baseline power even when there was no response present. As the power has a χ^2 distribution which is skewed towards zero, normalising all values by the average power of the

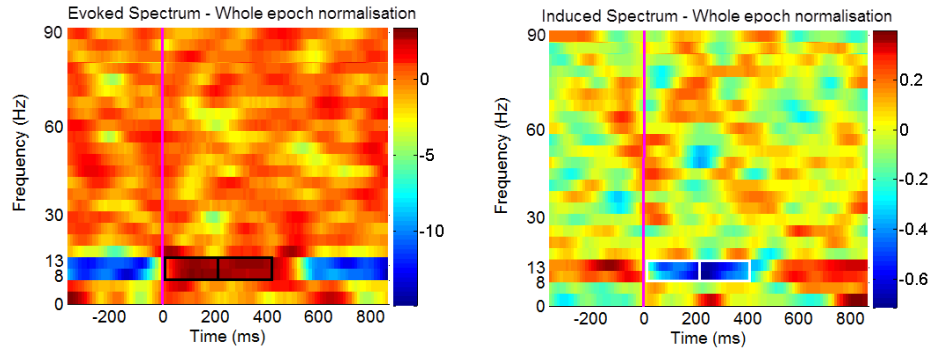

(a) (b)

Figure B.18: Average a) evoked and b) induced power in channel 1 over all trials and 30 datasets with simulation of random-phase phase synchronisation. Areas marked with the black/white window shows significant power increase/decrease compared to the baseline. The magenta line shows the onset of the stimulus. The unit of the colour bars is dB.

baseline may introduce this bias to the power values after the onset which have not been used for calculating the average power (used for normalisation). As significant analysis would be applied on average powers in specific time-frequency areas (Figure B.1) and because the power decreases by increasing the frequency, some sort of normalisation was needed to bring all powers to a similar range so that in averaging the effect of higher frequencies were not lost. Thus, normalisation to the baseline was replaced by normalisation to the average power of the whole epoch so that all power values (in each frequency bin) contribute to the normalisation value equally. It was shown that this normalisation was appropriate as it produced expected number of false positives in significant analyses and was selected as the main normalisation method for recorded data. It is worth noting that many studies have used baseline normalisation as their normalisation method (Hannemann et al., 2007; Sanderson, 2010; Friedrich et al., 2013; Gurtubay et al., 2004) but probably because they compare power values after the onset in different conditions (and not values before and after the onset), they did not face the same problem as we did with baseline normalisation.

In section B.4.2, different types of significant analysis were used on simulated data and all of them except Friedman's test were deemed inappropriate for the the purpose of this study. T-test was used because it was a simple and common significance test but was rejected because the pair-wise tests in each frequency band were not independent, i.e. all windows after the onset in one frequency band were compared with the same window in the baseline, therefore it would produce more false positives than expected. Group bootstrap analyses was employed but to save time, instead of making a pool of all data in time domain and calculating the spectra for each and every one of them, spectra were calculated once over the whole epoch and a pool of power values of the baseline was generated. As the values defined as the baseline were independent of each other and the values of the original signals were dependent, the average powers obtained from

these two groups were not comparable and much larger number of false positives were obtained. Thus, group bootstrap was also dropped. One-way ANOVA was initially used because it neither had the problem of repeating dependent tests nor the incomparable values but because the groups of power values were not independent, this method also produced more false positives than expected. In the end, repeated measures ANOVA and Friedman's test were tested and they both showed promising results when tested on simulated data with no response present, however, Friedman's test would have been a better choice for applying on recorded EEG data in case of outliers. Friedman's test was then applied on simulated data with different types of response present and it could detect the response properly. Therefore, Friedman's test was selected to be applied on recorded EEG data.

B.6 Summary

In this appendix, different response detection methods were employed on simulated data to find out which one was the most reliable one for applying to recorded EEG data.

From all the simulations in this section, it was concluded that the most reliable way of normalisation of the spectra for our application is normalising to the power of the whole epoch and the most reliable significance test is Friedman's test. In Friedman's test, the distribution of false positives for 0.05 significance level over 100 sets of simulated data followed the expected binomial distribution when the simulated data contained no simulated response. Moreover, Friedman could correctly detect the induced and evoked responses in simulated data with evoked and induced response present; though, the detectable SNR was much higher in induced response than the evoked response confirming that it was much more difficult to find an induced response in the data than an evoked response. Also, simulations showed that if there was an increase in the evoked response and in the same time-frequency area a decrease in the induced response was observed, this response may be a phase synchronisation and not an additive evoked response.

Appendix C

CI data after artefact rejection

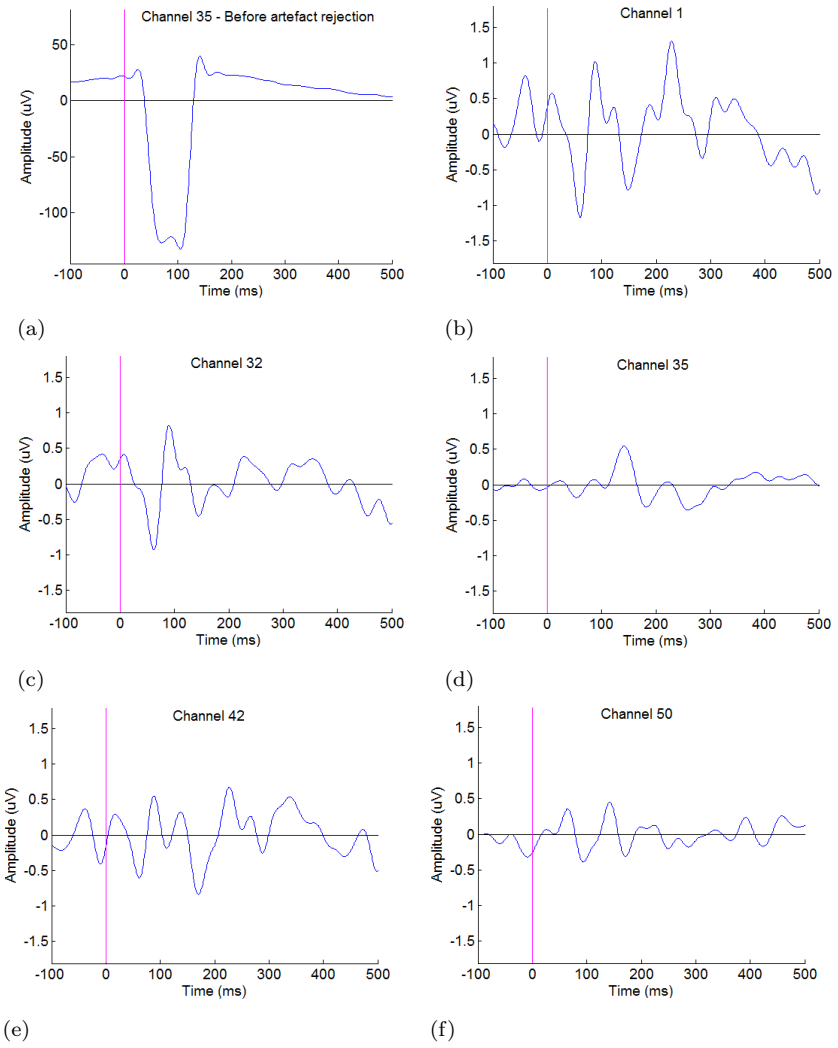

Figure C.1: AEPs in response to tone bursts in a) a channel close to the implant site before artefact rejection and in b-f) five channels after artefact rejection, for Patient 2 recording 1. The stimulus onset occurs at zero seconds.

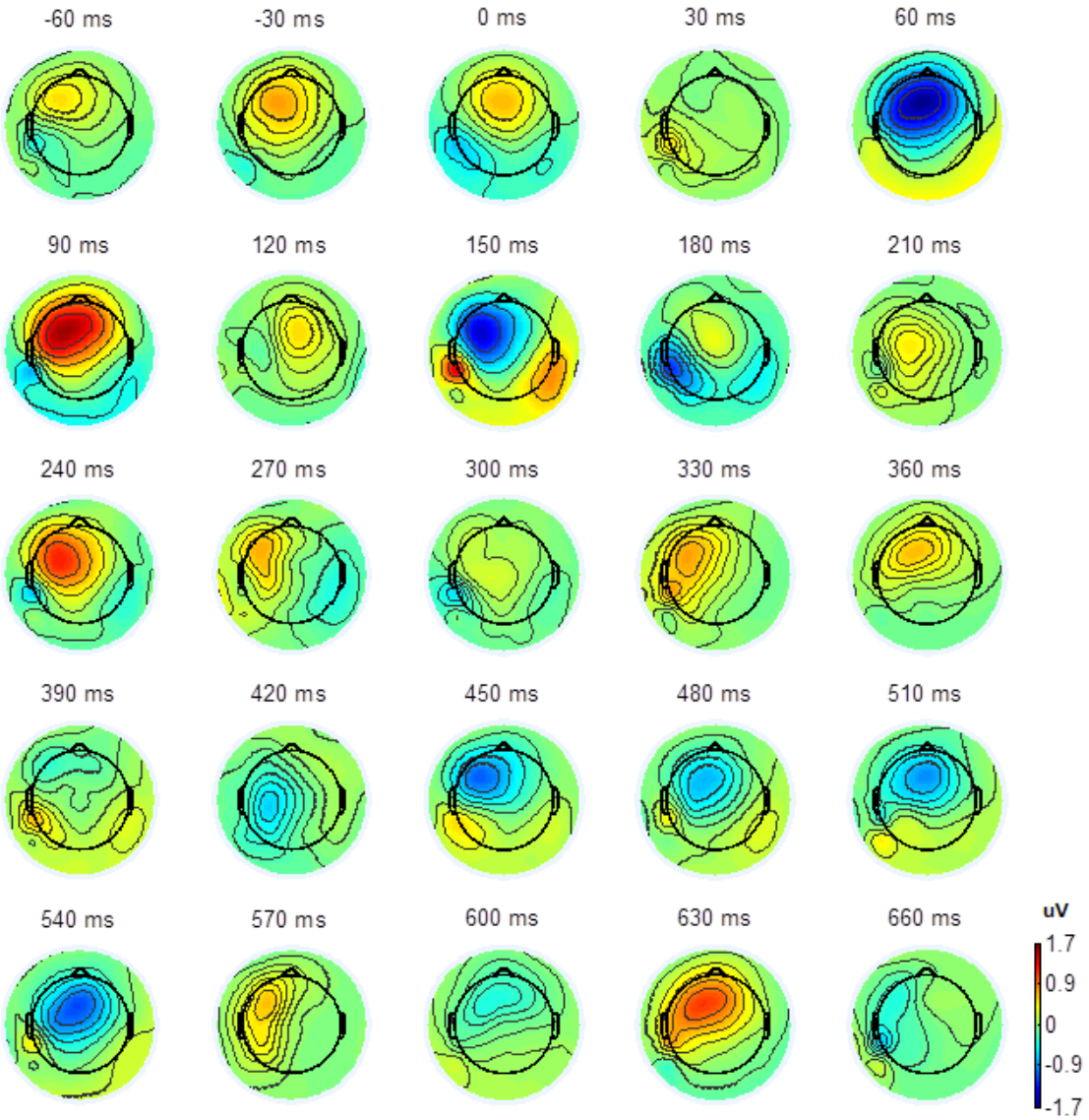

Figure C.2: Topographic maps of channel AEPs over time in response to tone bursts, for Patient 2 recording 1 after artefact rejection, the same data as in Figure C.1. Each subfigure shows an axial view of the top of the head with the right being the right and the left being the left of the head. The stimulus onset occurs at zero seconds.

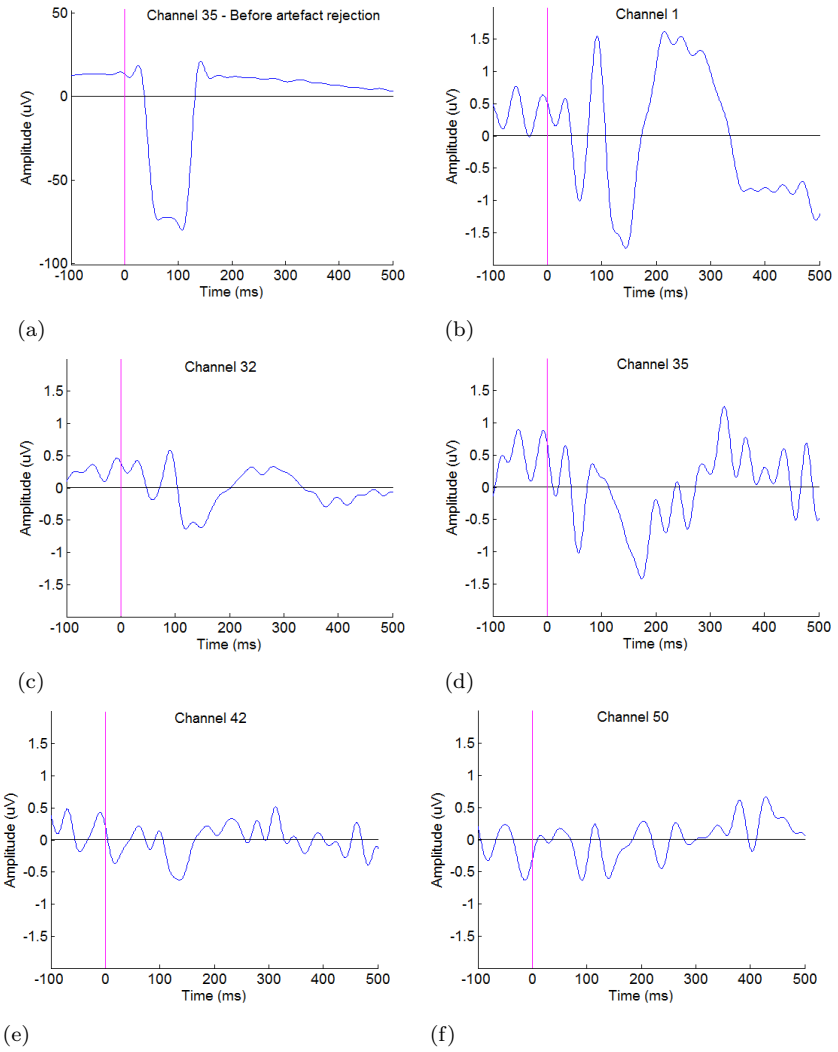

Figure C.3: AEPs in response to tone bursts in a) a channel close to the implant site before artefact rejection and in b-f) five channels after artefact rejection, for Patient 2 recording 2. The stimulus onset occurs at zero seconds.

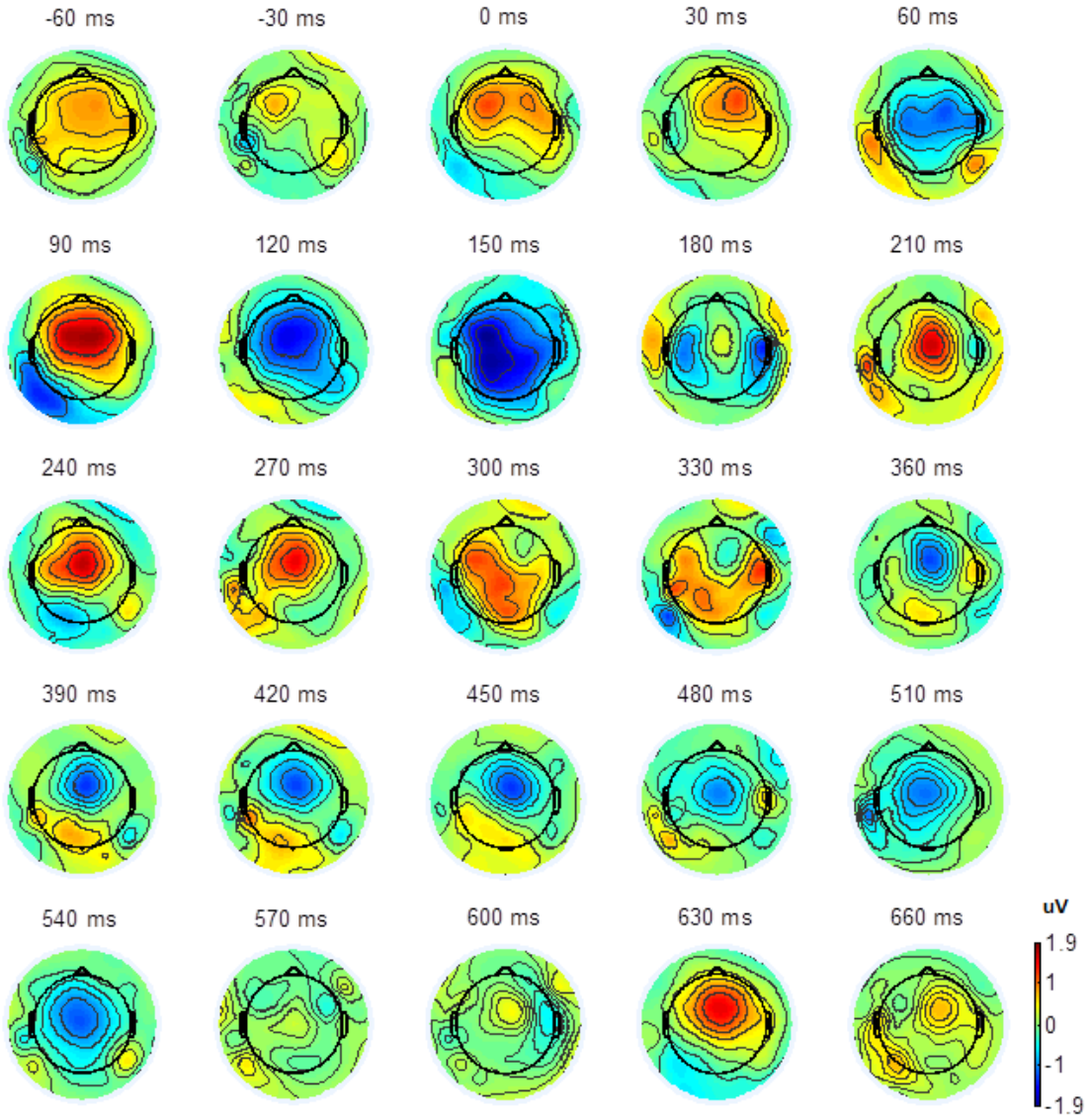

Figure C.4: Topographic maps of channel AEPs over time in response to tone bursts, for Patient 2 recording 2 after artefact rejection, the same data as in Figure C.3. Each subfigure shows an axial view of the top of the head with the right being the right and the left being the left of the head. The stimulus onset occurs at zero seconds.

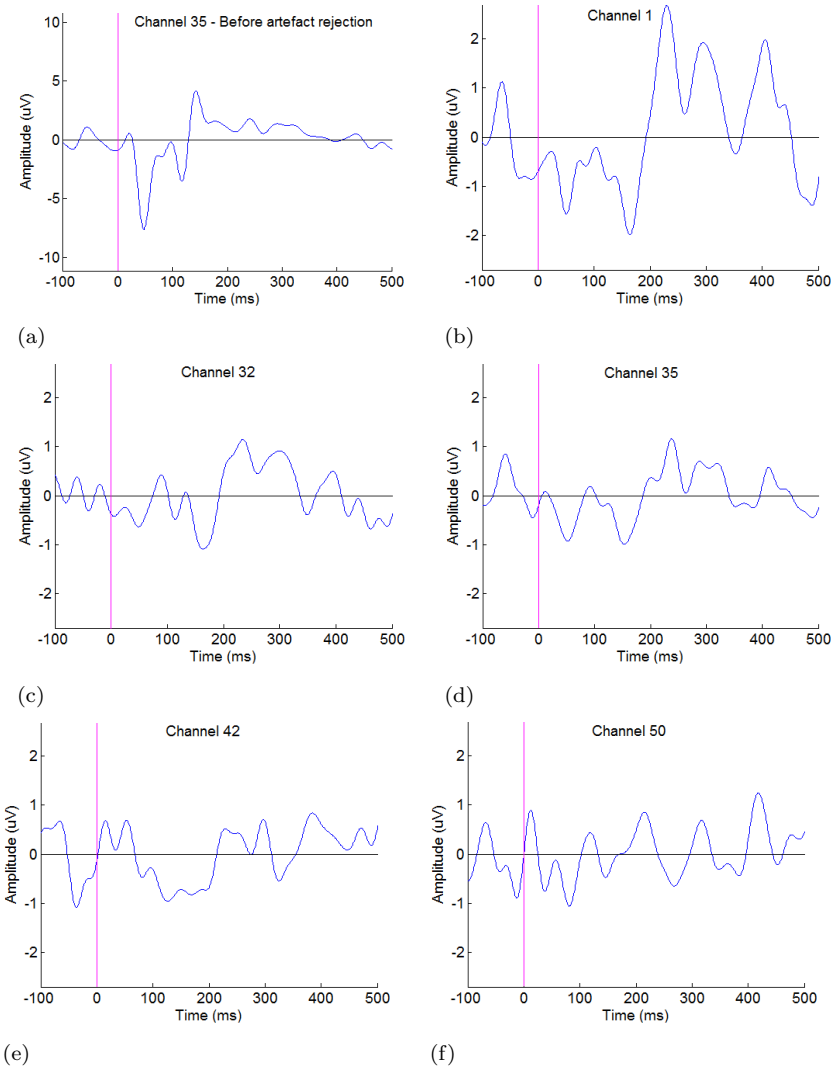

Figure C.5: AEPs in response to tone bursts in a) a channel close to the implant site before artefact rejection and in b-f) five channels after artefact rejection, for Patient 3 recording 1. The stimulus onset occurs at zero seconds.

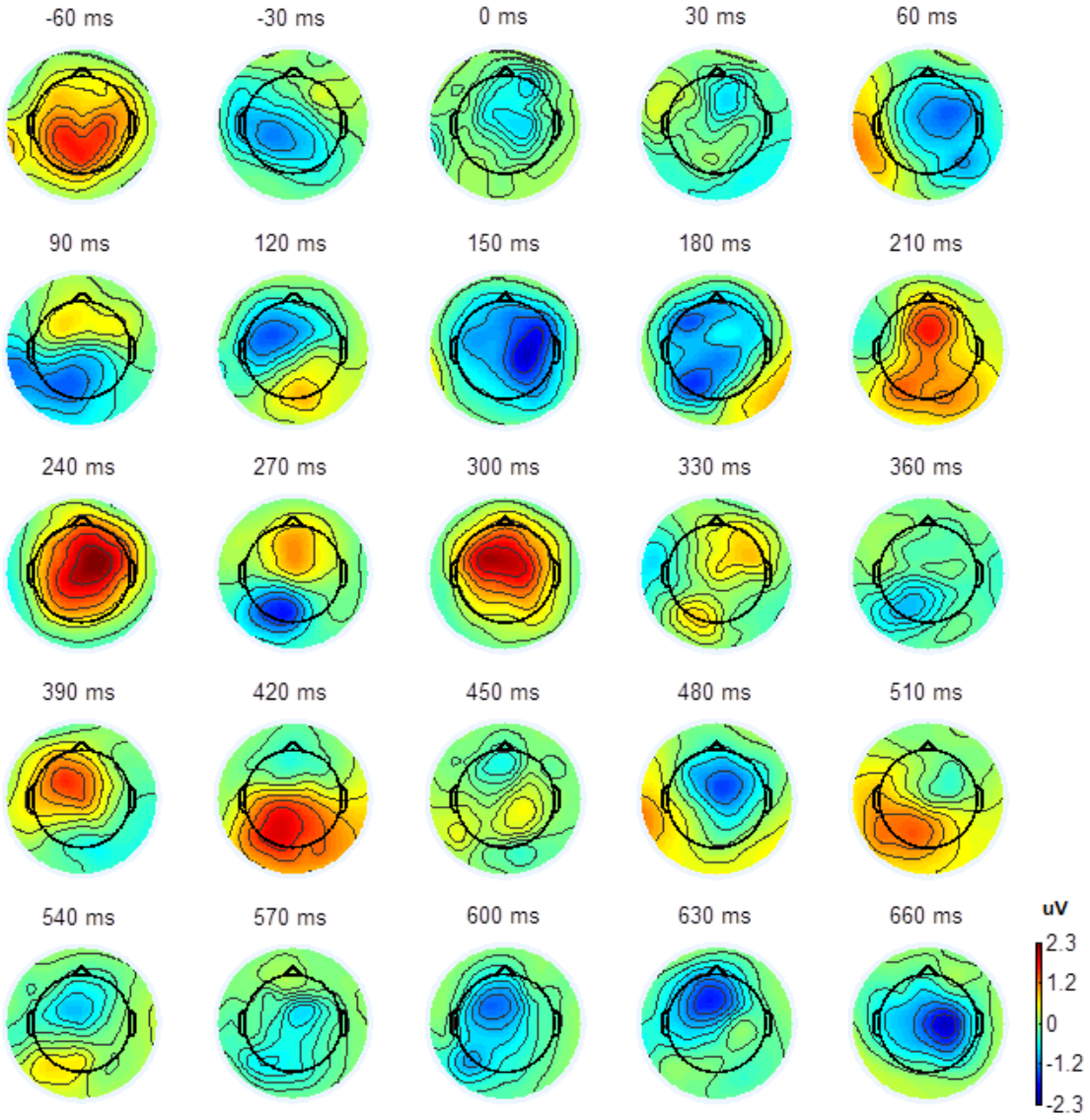

Figure C.6: Topographic maps of channel AEPs over time in response to tone bursts, for Patient 3 recording 1 after artefact rejection, the same data as in Figure C.5. Each subfigure shows an axial view of the top of the head with the right being the right and the left being the left of the head. The stimulus onset occurs at zero seconds.

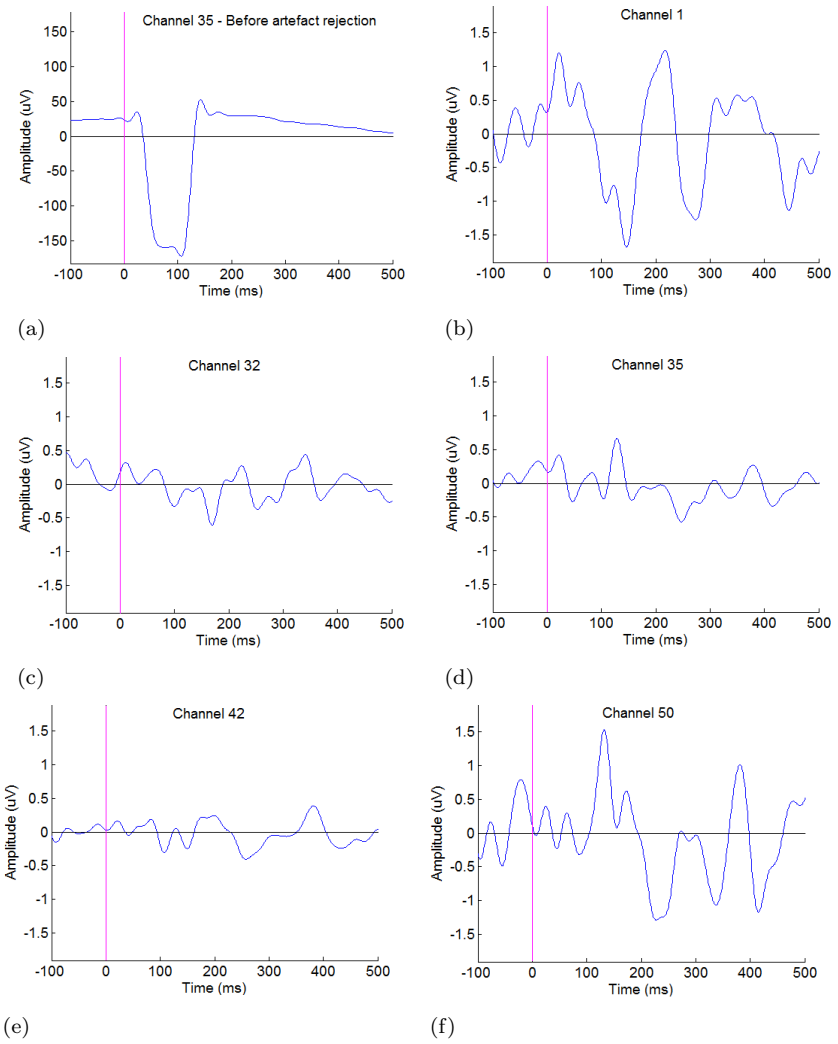

Figure C.7: AEPs in response to tone bursts in a) a channel close to the implant site before artefact rejection and in b-f) five channels after artefact rejection, for Patient 3 recording 2.The stimulus onset occurs at zero seconds.

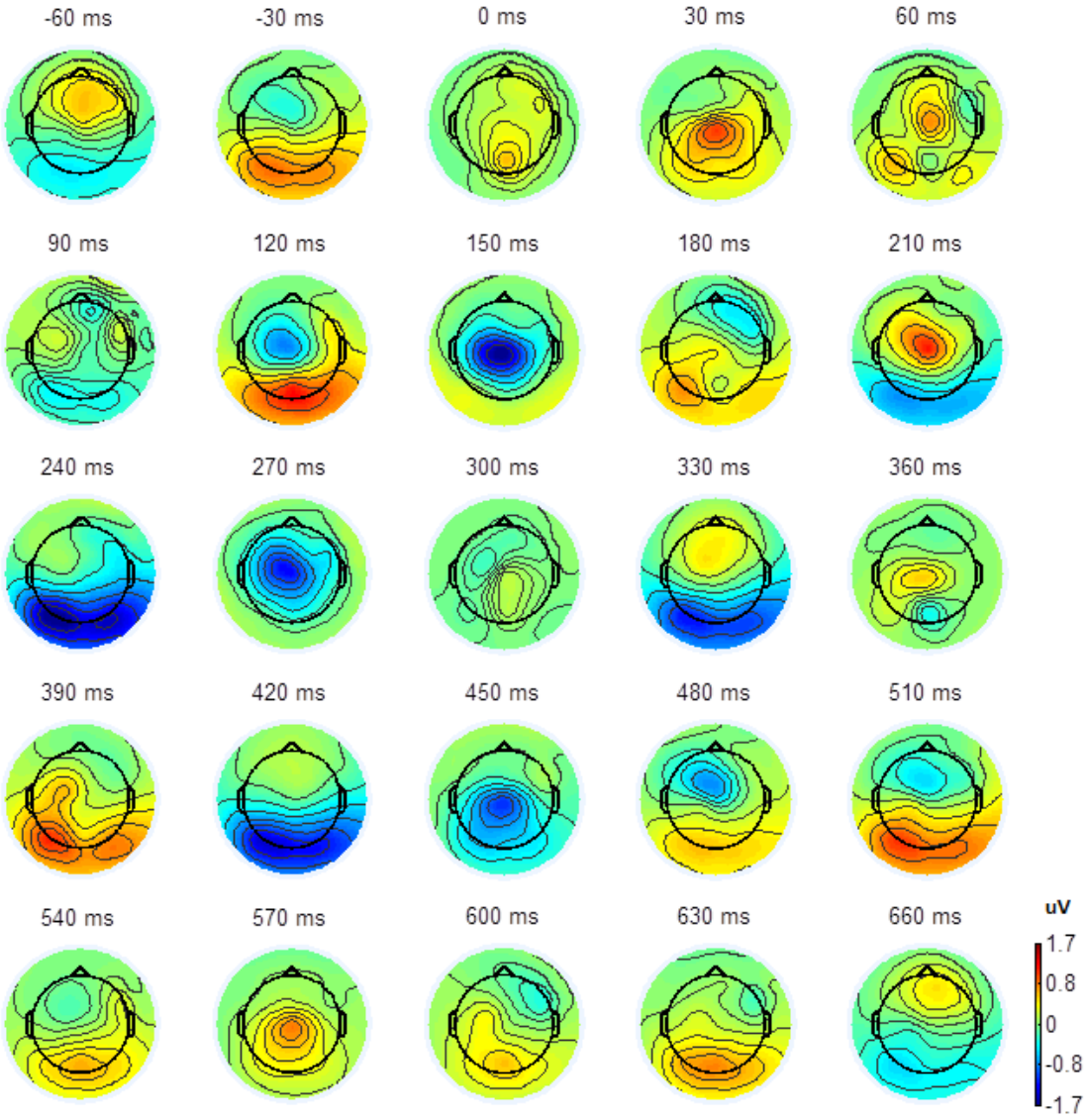

Figure C.8: Topographic maps of channel AEPs over time in response to tone bursts, for Patient 3 recording 2 after artefact rejection, the same data as in Figure C.7. Each subfigure shows an axial view of the top of the head with the right being the right and the left being the left of the head. The stimulus onset occurs at zero seconds.

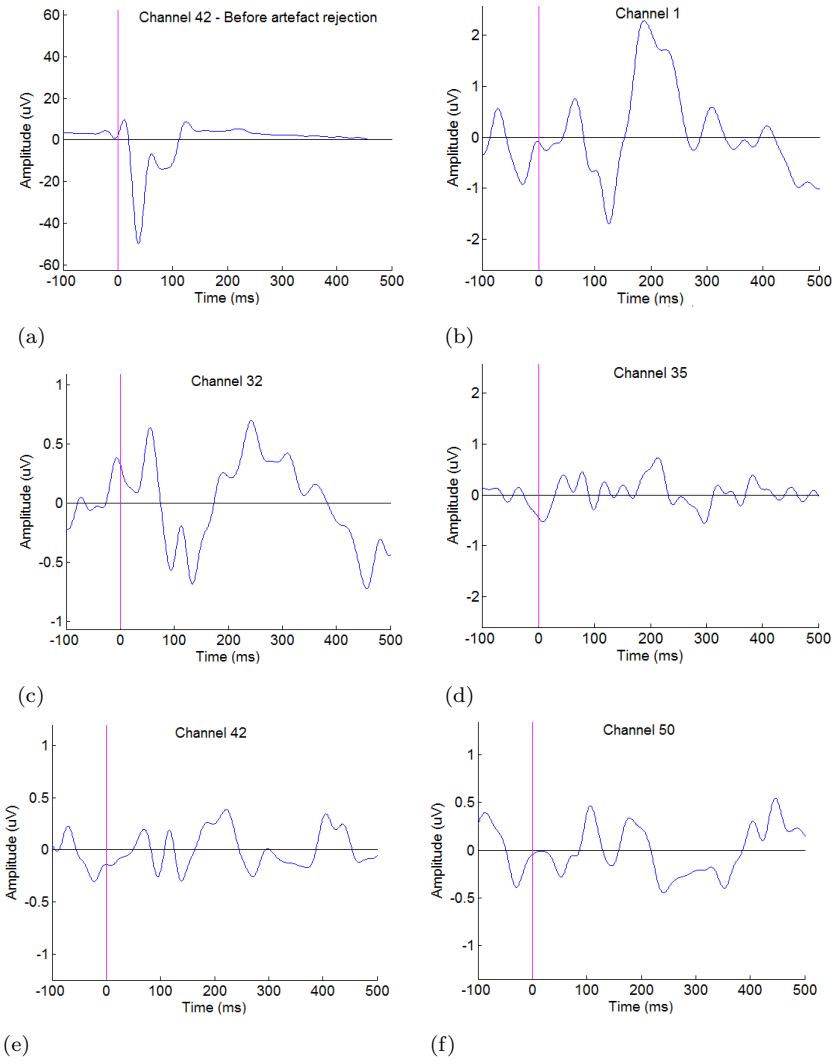

Figure C.9: AEPs in response to tone bursts in a) a channel close to the implant site before artefact rejection and in b-f) five channels after artefact rejection, for Patient 4 recording 1. The stimulus onset occurs at zero seconds.

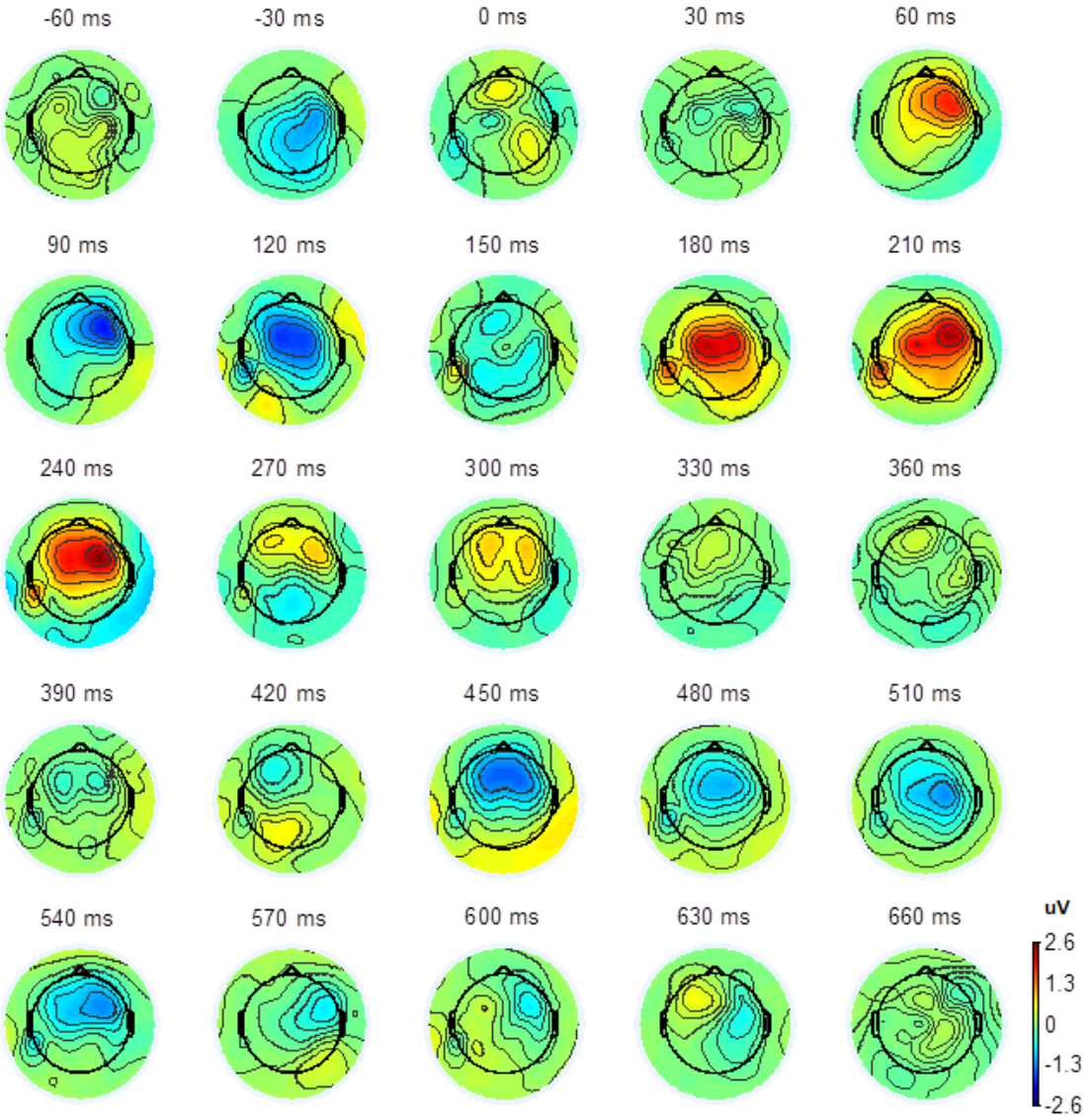

Figure C.10: Topographic maps of channel AEPs over time in response to tone bursts, for Patient 4 recording 1 after artefact rejection, the same data as in Figure C.9. Each subfigure shows an axial view of the top of the head with the right being the right and the left being the left of the head. The stimulus onset occurs at zero seconds.

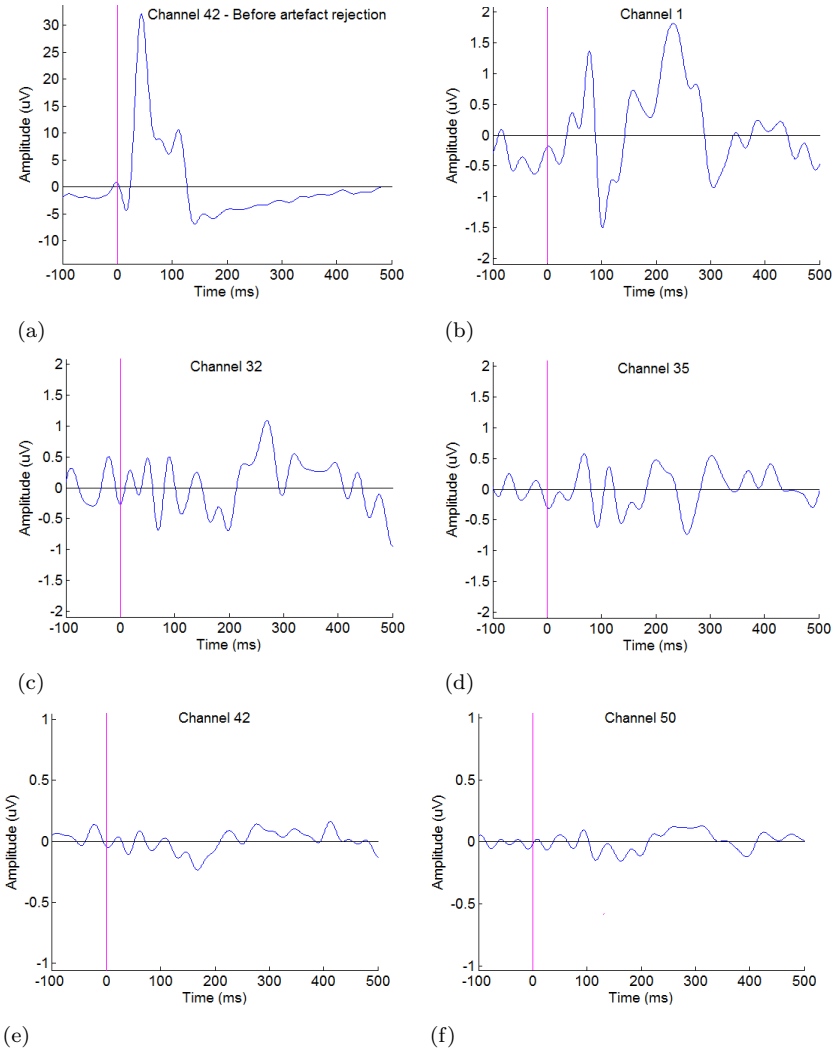

Figure C.11: AEPs in response to tone bursts in a) a channel close to the implant site before artefact rejection and in b-f) five channels after artefact rejection, for Patient 4 recording 2. The stimulus onset occurs at zero seconds.

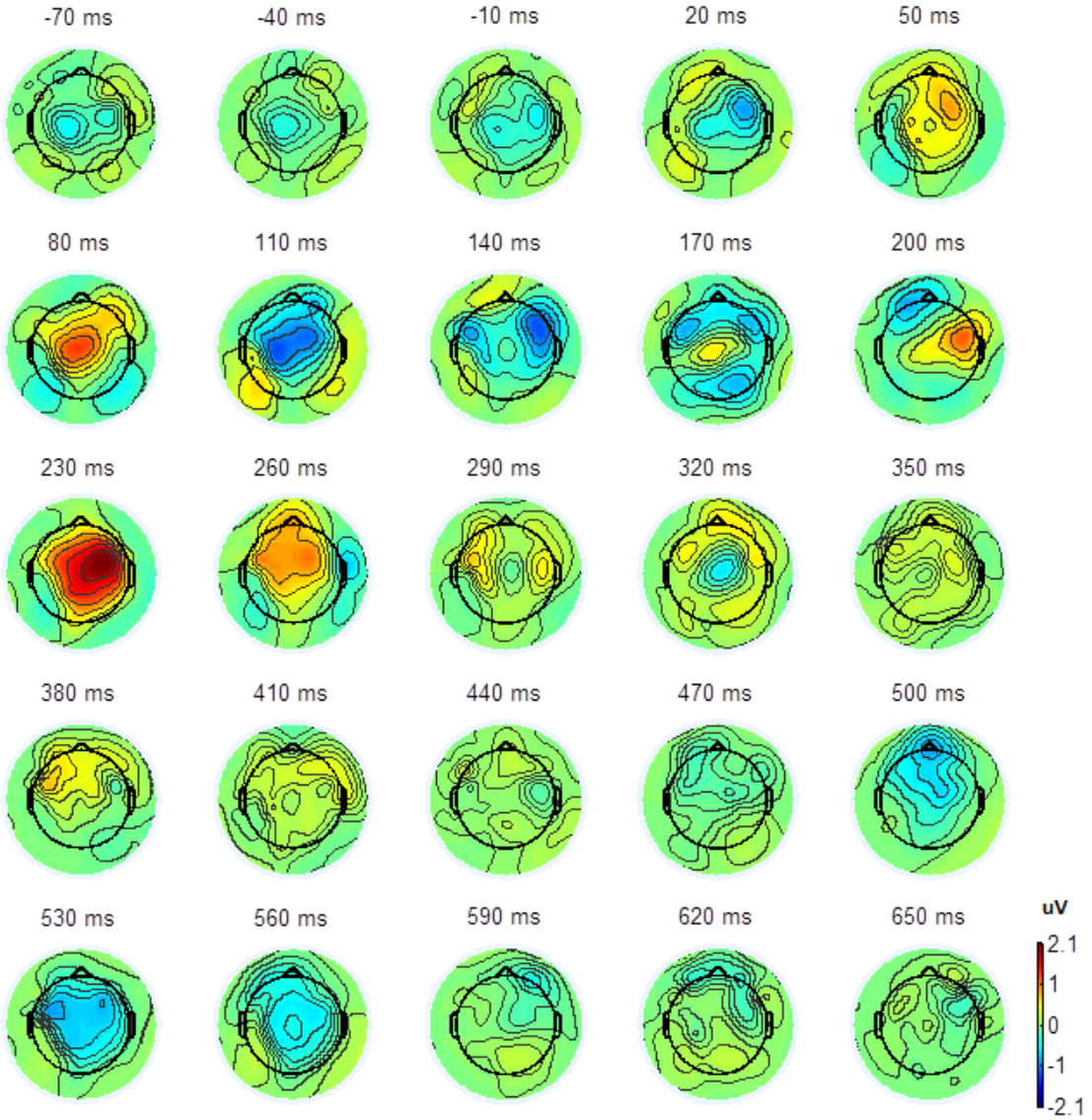

Figure C.12: Topographic maps of channel AEPs over time in response to tone bursts, for Patient 4 recording 2 after artefact rejection, the same data as in Figure C.11. Each subfigure shows an axial view of the top of the head with the right being the right and the left being the left of the head. The stimulus onset occurs at zero seconds.

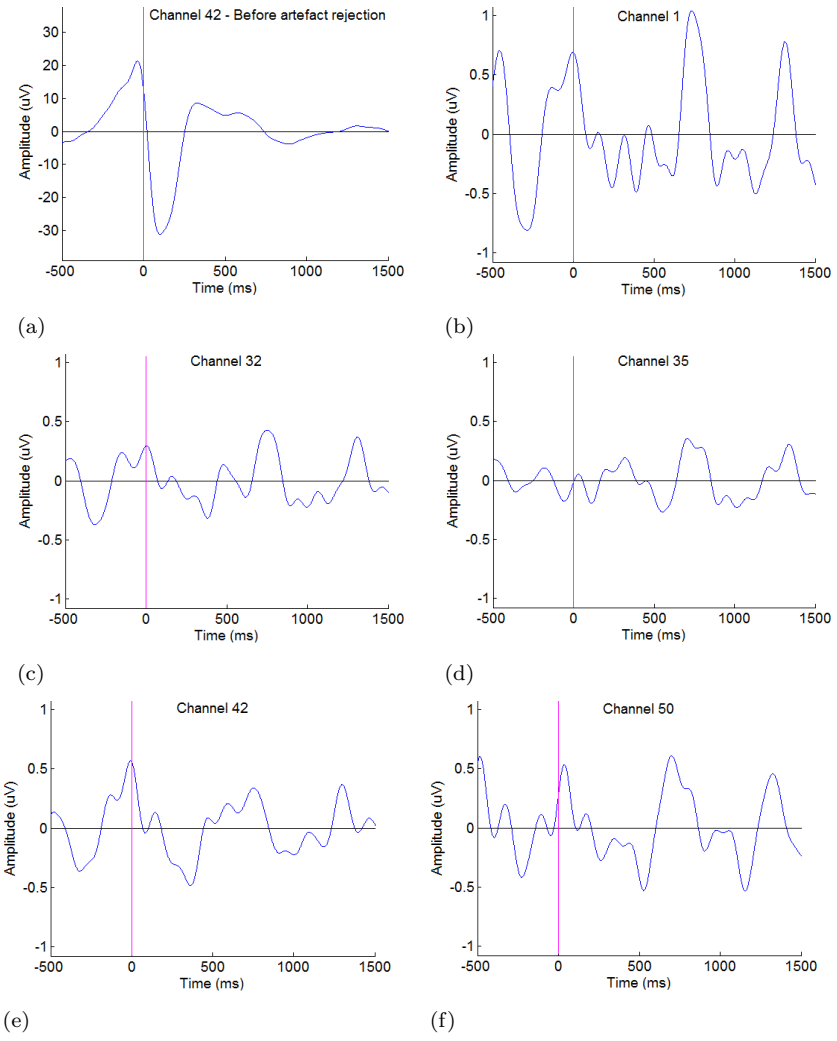

Figure C.13: AEPs in response to words in a) a channel close to the implant site before artefact rejection and in b-f) five channels after artefact rejection for Patient 1 recording 2 after low-pass filtering to 8 Hz. The stimulus onset occurs at zero seconds.

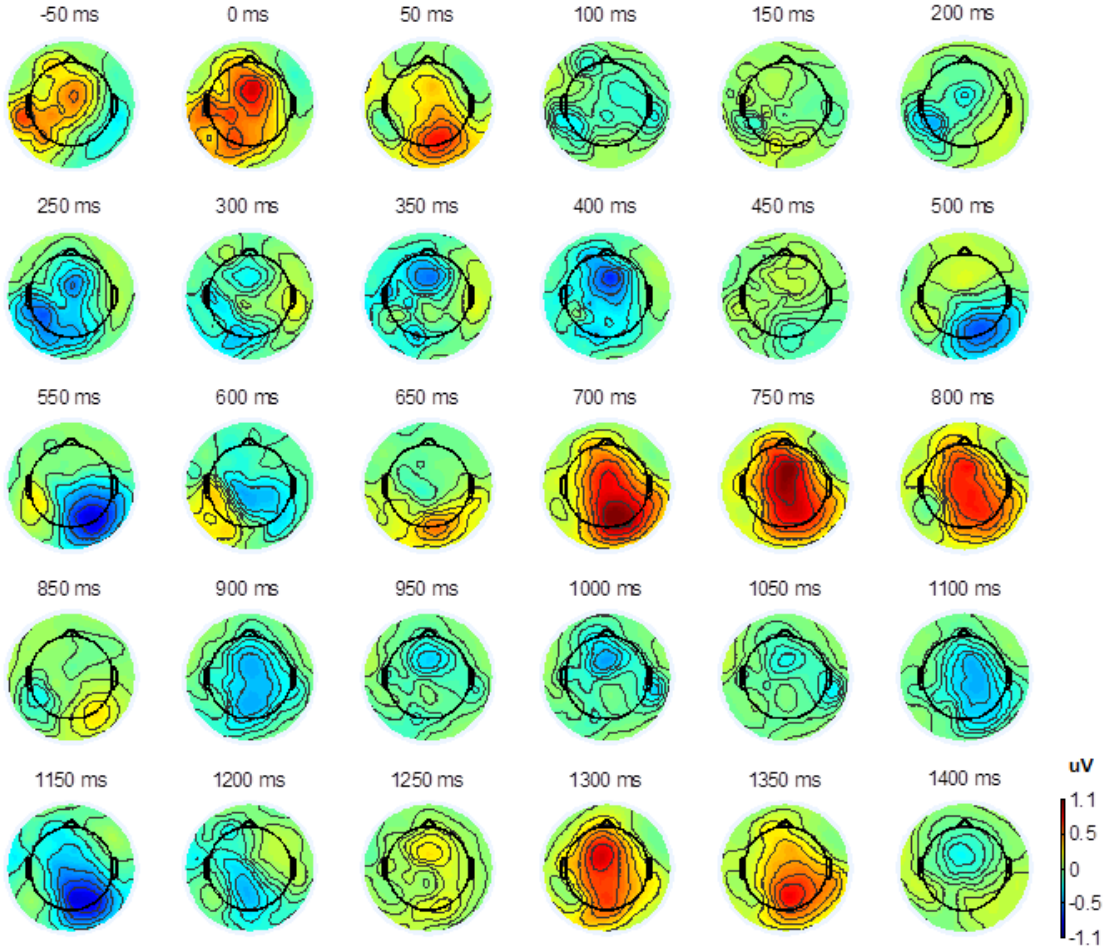

Figure C.14: Topographic maps of channel AEPs over time in response to words, for Patient 1 recording 2 after artefact rejection, the same data as in Figure C.13. Each subfigure shows an axial view of the top of the head with the right being the right and the left being the left of the head. The stimulus onset occurs at zero seconds.

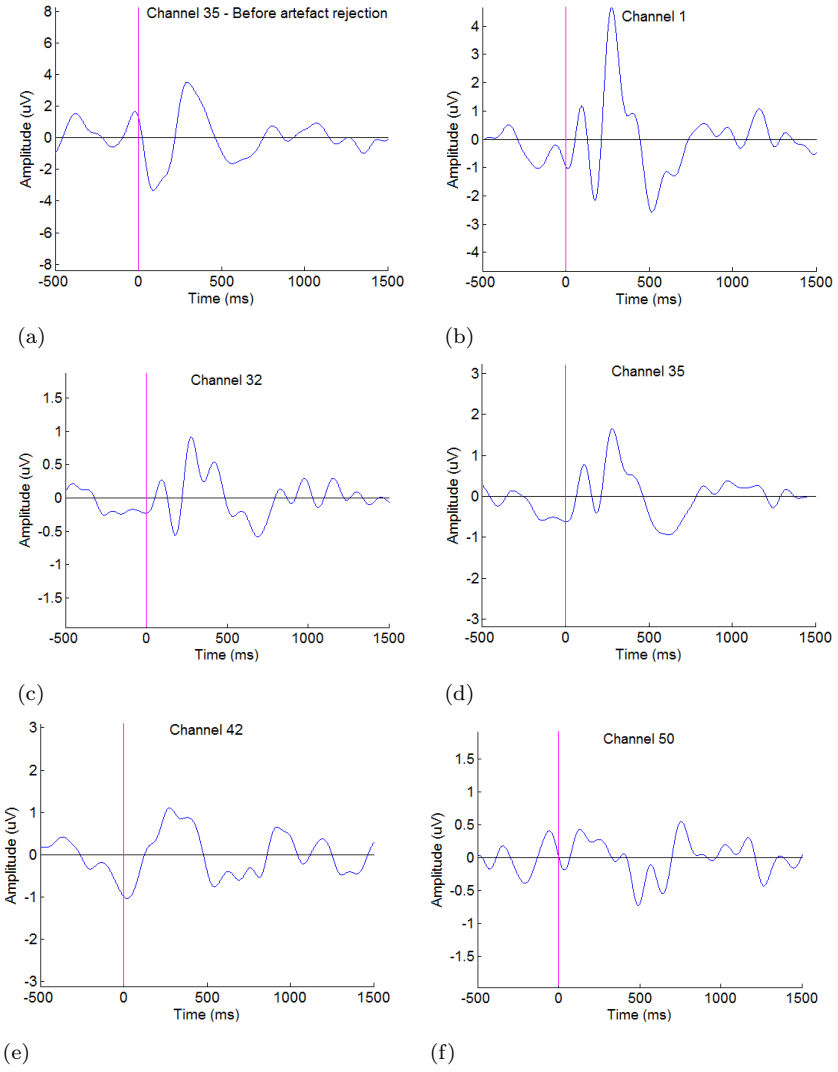

Figure C.15: AEPs in response to words in a) a channel close to the implant site before artefact rejection and in b-f) five channels after artefact rejection for Patient 2 recording 2 after low-pass filtering to 8 Hz. The stimulus onset occurs at zero seconds.

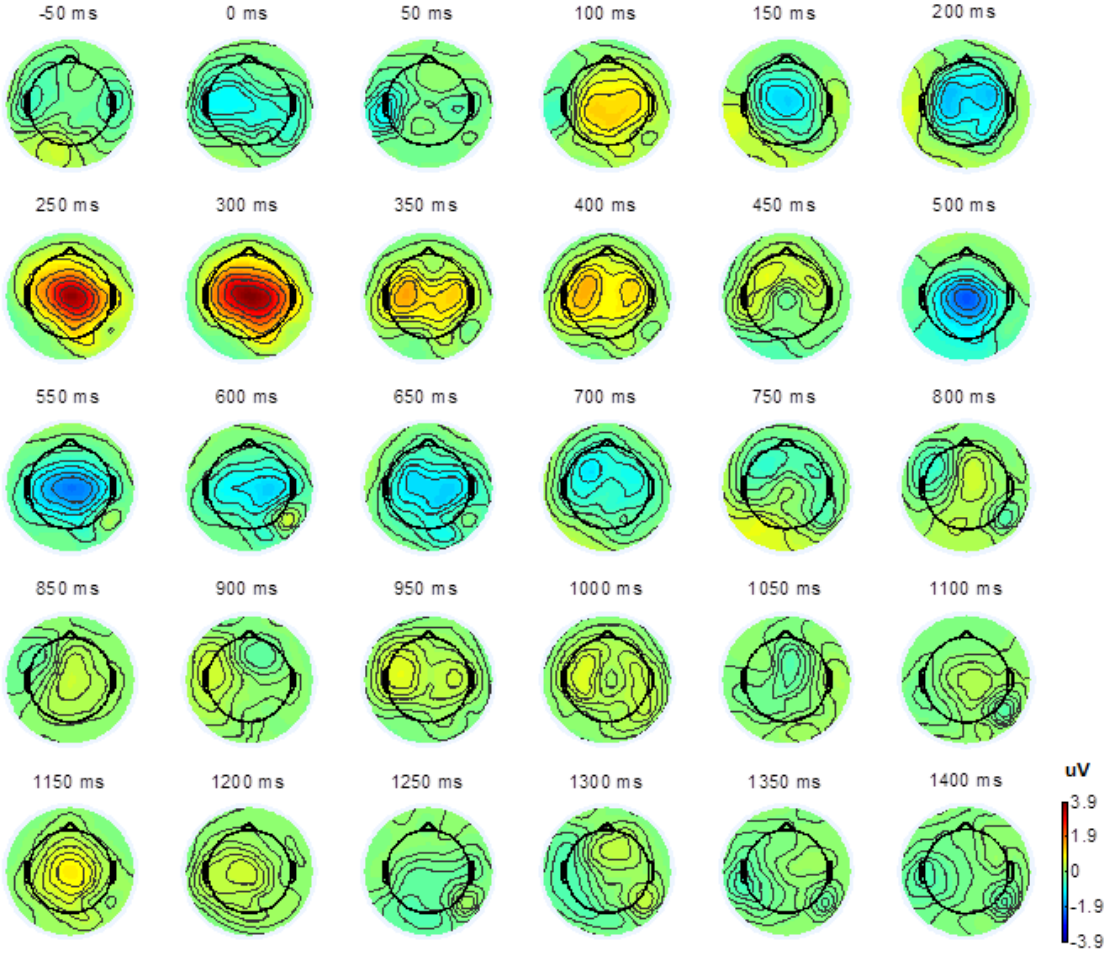

Figure C.16: Topographic maps of channel AEPs over time in response to words, for Patient 2 recording 2 after artefact rejection, the same data as in Figure C.15. Each subfigure shows an axial view of the top of the head with the right being the right and the left being the left of the head. The stimulus onset occurs at zero seconds.

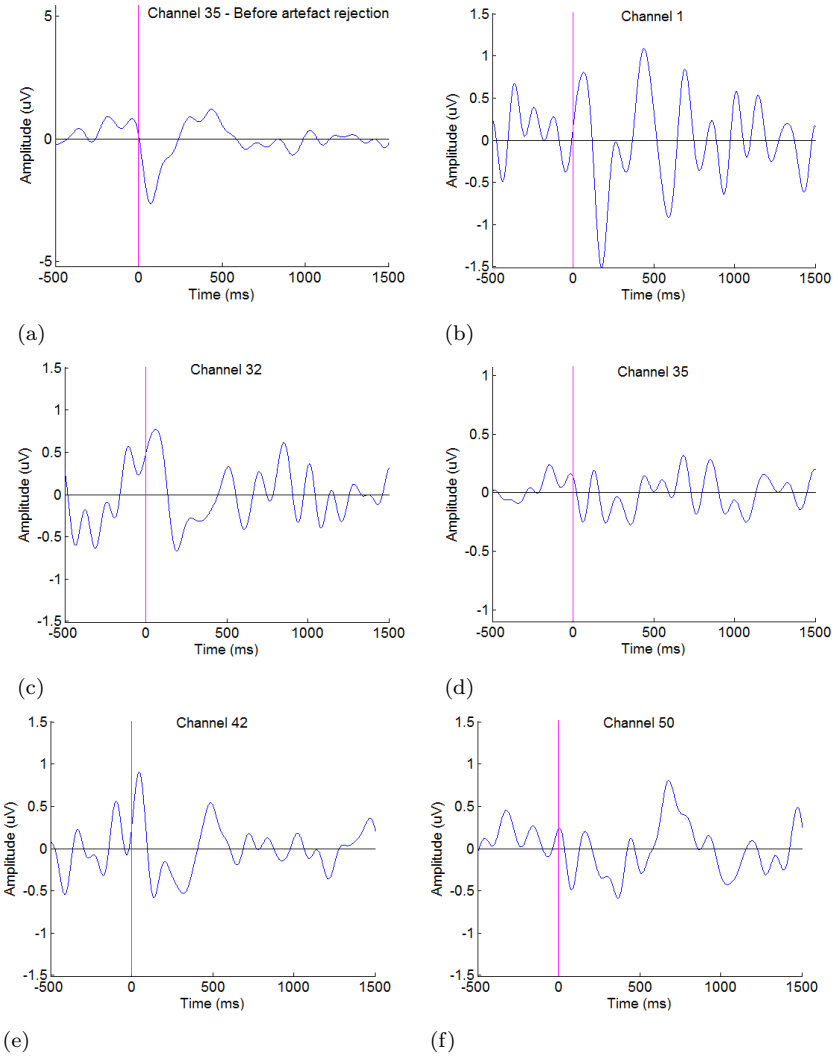

Figure C.17: AEPs in response to words in a) a channel close to the implant site before artefact rejection and in b-f) five channels after artefact rejection for Patient 3 recording 1 after low-pass filtering to 8 Hz. The stimulus onset occurs at zero seconds.

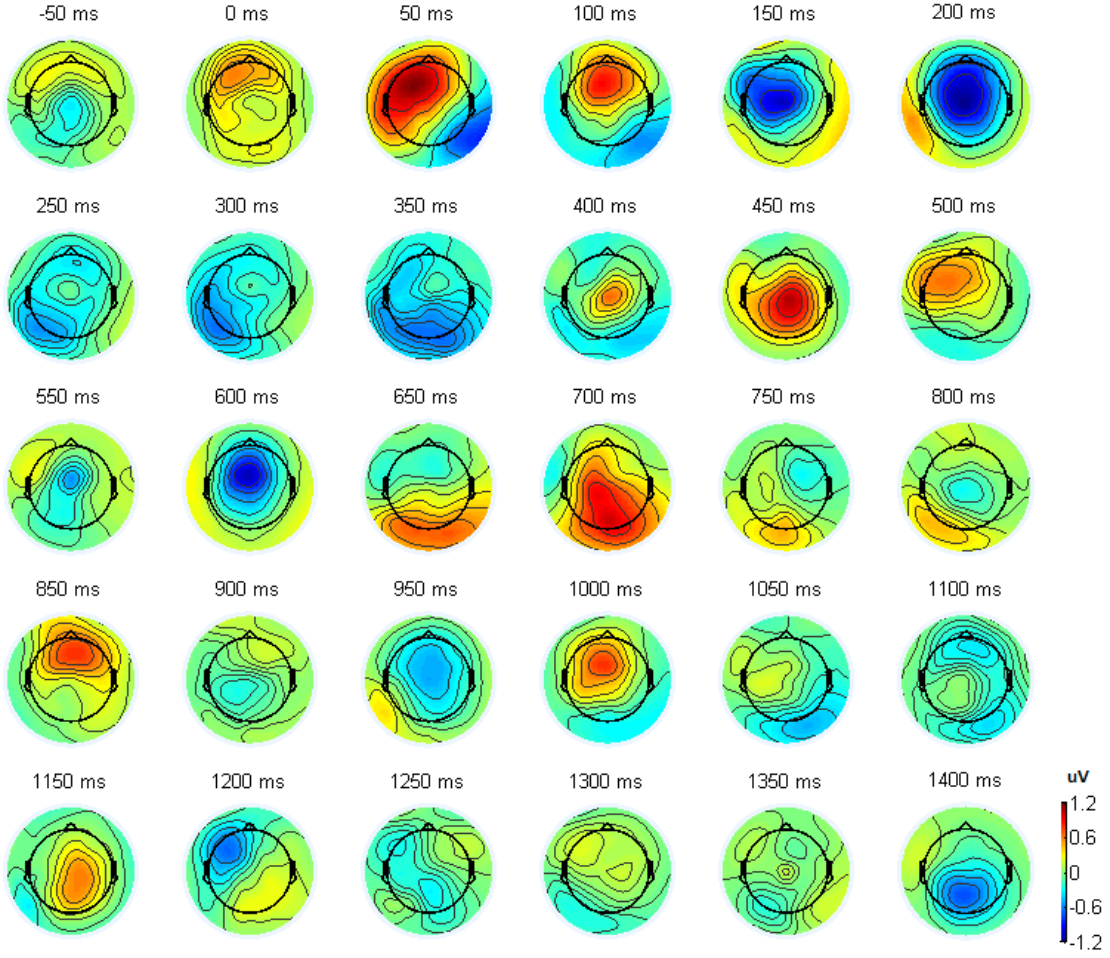

Figure C.18: Topographic maps of channel AEPs over time in response to words, for Patient 3 recording 1 after artefact rejection, the same data as in Figure C.17. Each subfigure shows an axial view of the top of the head with the right being the right and the left being the left of the head. The stimulus onset occurs at zero seconds.

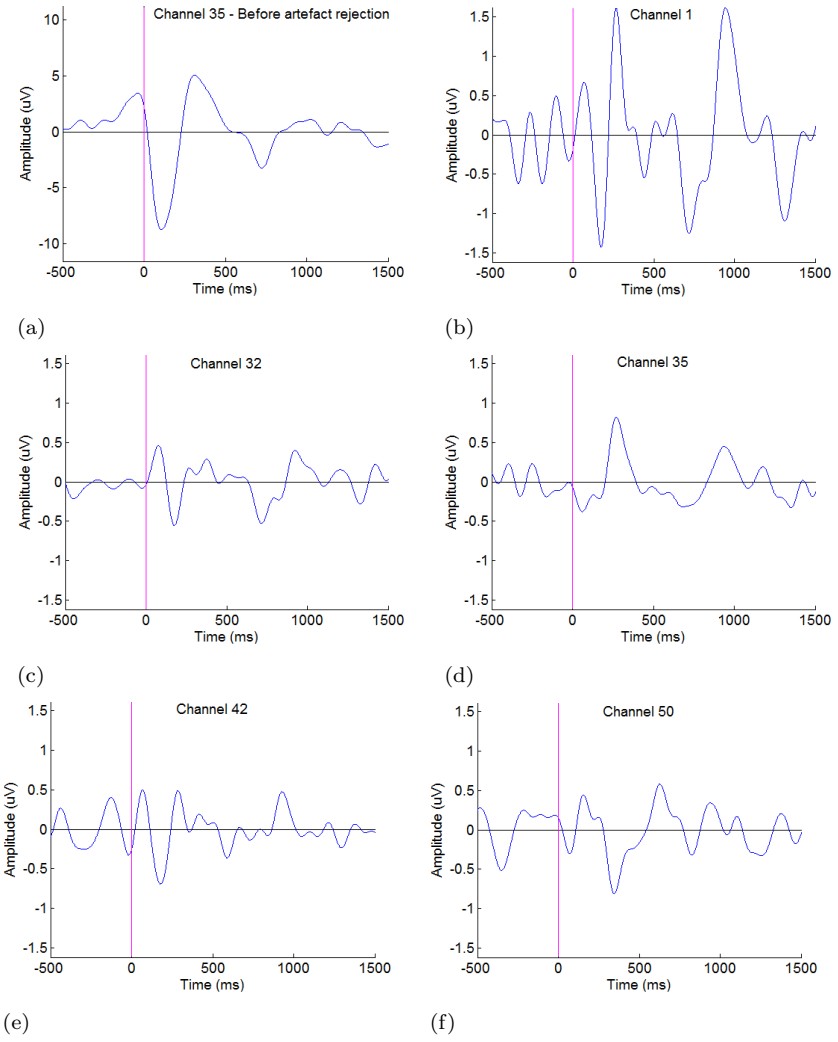

Figure C.19: AEPs in response to words in a) a channel close to the implant site before artefact rejection and in b-f) five channels after artefact rejection for Patient 3 recording 2 after low-pass filtering to 8 Hz. The stimulus onset occurs at zero seconds.

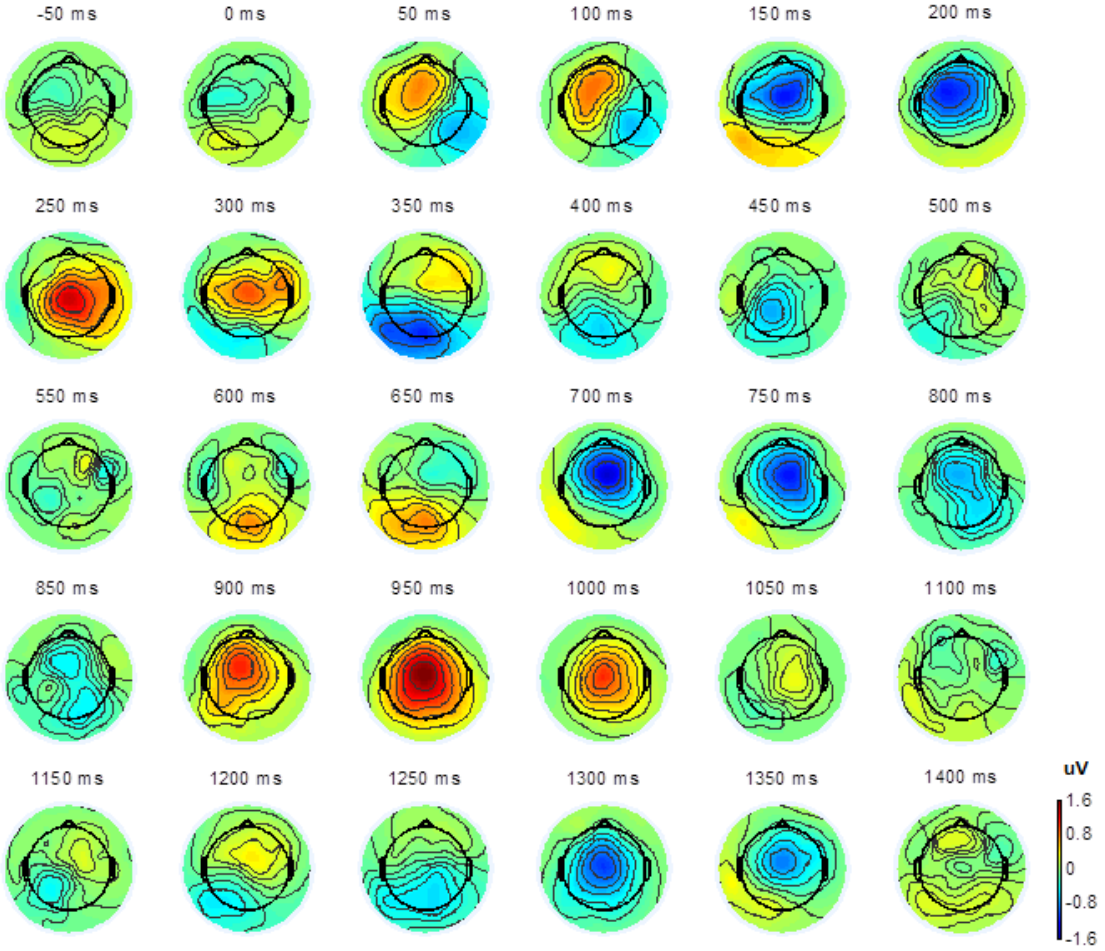

Figure C.20: Topographic maps of channel AEPs over time in response to words, for Patient 3 recording 2 after artefact rejection, the same data as in Figure C.19. Each subfigure shows an axial view of the top of the head with the right being the right and the left being the left of the head. The stimulus onset occurs at zero seconds.

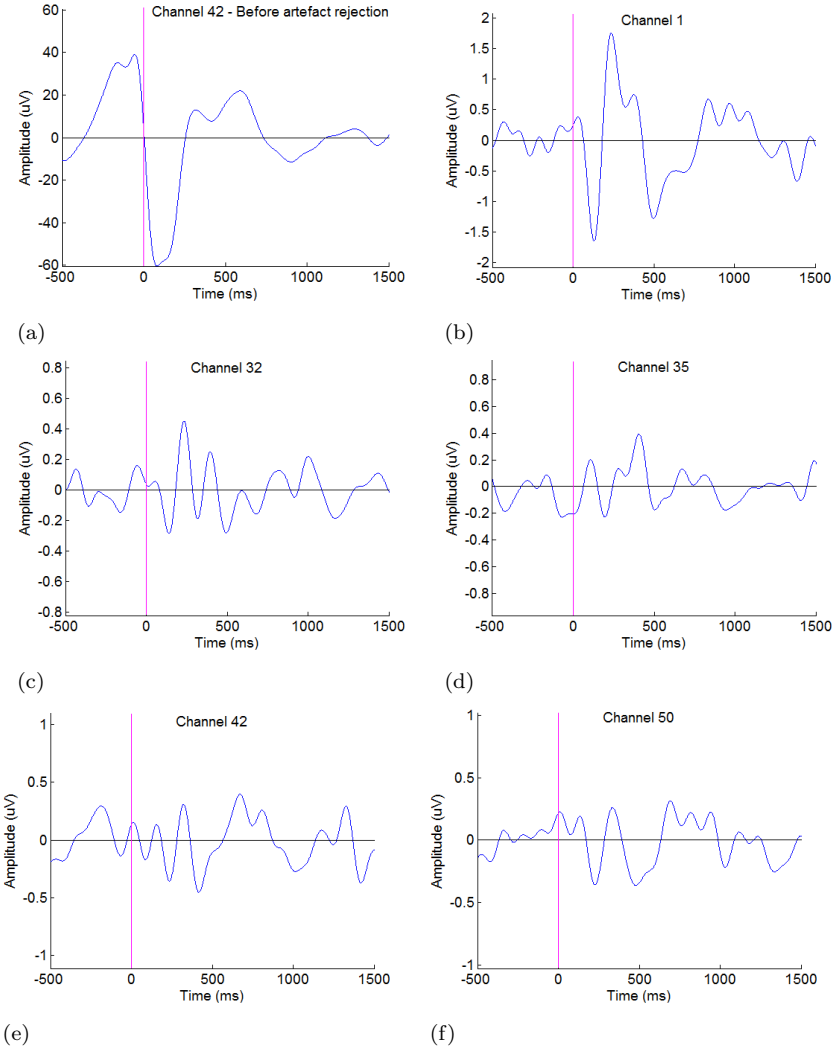

Figure C.21: AEPs in response to words in a) a channel close to the implant site before artefact rejection and in b-f) five channels after artefact rejection for Patient 4 recording 1 after low-pass filtering to 8 Hz. The stimulus onset occurs at zero seconds.

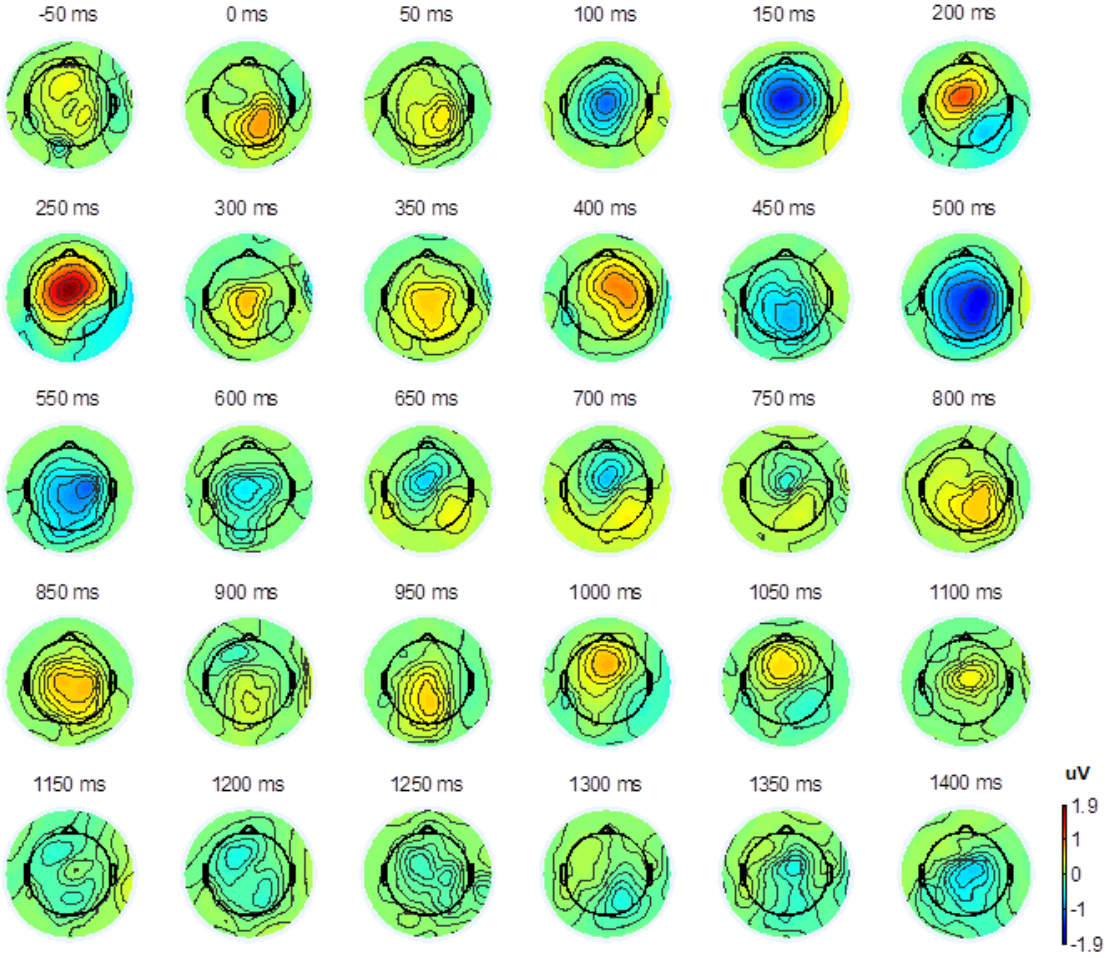

Figure C.22: Topographic maps of channel AEPs over time in response to words, for Patient 4 recording 2 after artefact rejection, the same data as in Figure C.21. Each subfigure shows an axial view of the top of the head with the right being the right and the left being the left of the head. The stimulus onset occurs at zero seconds.

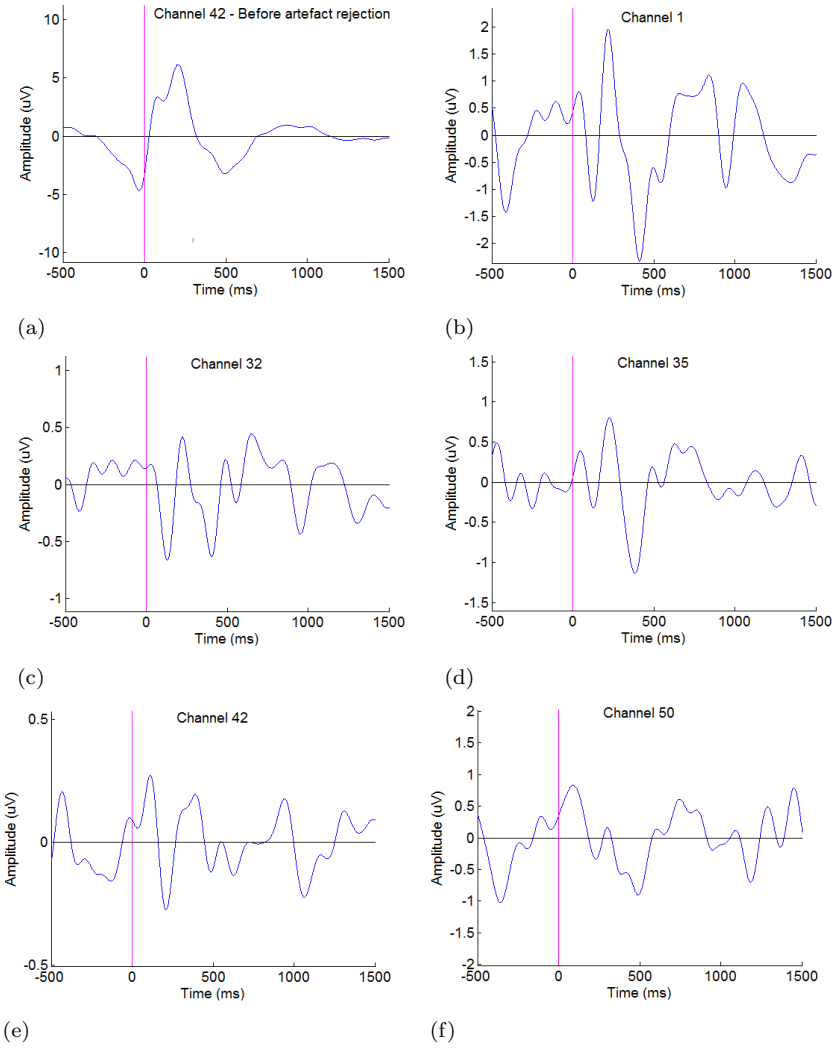

Figure C.23: AEPs in response to words in a) a channel close to the implant site before artefact rejection and in b-f) five channels after artefact rejection for Patient 4 recording 2 after low-pass filtering to 8 Hz. The stimulus onset occurs at zero seconds.

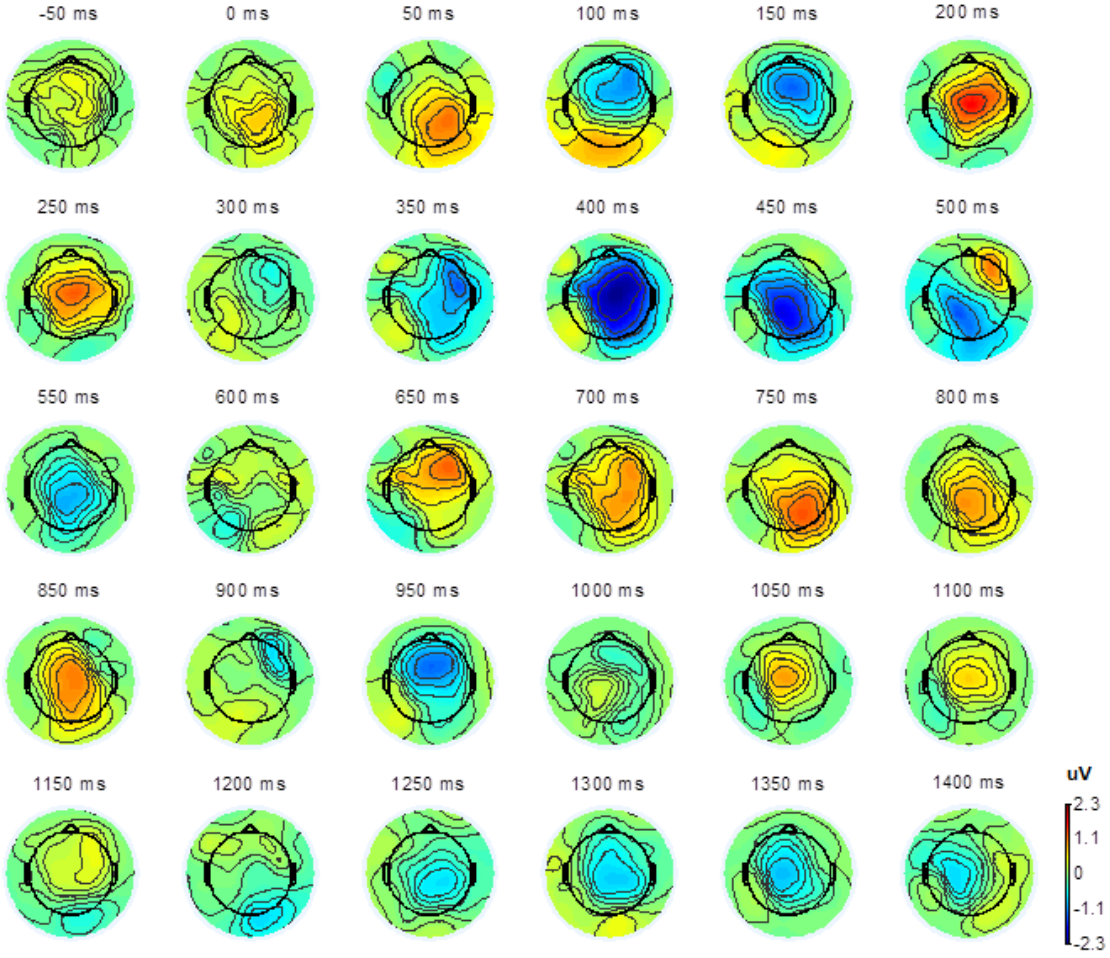

Figure C.24: Topographic maps of channel AEPs over time in response to words, for Patient 4 recording 2 after artefact rejection, the same data as in Figure C.23. Each subfigure shows an axial view of the top of the head with the right being the right and the left being the left of the head. The stimulus onset occurs at zero seconds.

References

Agrawal, D., Thorne, J. D., Viola, F. C., Timm, L., Debener, S., Buchner, A., Dengler, R., and Wittfoth, M. (2013). Electrophysiological responses to emotional prosody perception in cochlear implant users. *NeuroImage: Clinical*, 2:229–238.

Allen, D. P. and MacKinnon, C. D. (2010). Time-frequency analysis of movement-related spectral power in EEG during repetitive movements: a comparison of methods. *Journal of Neuroscience Methods*, 186(1):107 – 115.

Asp, F., Eskilsson, G., and Berninger, E. (2011). Horizontal sound localization in children with bilateral cochlear implants: effects of auditory experience and age at implantation. *Otology & Neurotology*, 32(4):558–564.

Astolfi, L., Cincotti, F., Mattia, D., Marciani, M. G., Baccala, L. A., de Vico Fallani, F., Salinari, S., Ursino, M., Zavaglia, M., and Babiloni, F. (2006). Assessing cortical functional connectivity by partial directed coherence: simulations and application to real data. *IEEE Transactions on Biomedical Engineering*, 53(9):1802–1812.

Astolfi, L., Cincotti, F., Mattia, D., Marciani, M. G., Baccala, L. A., de Vico Fallani, F., Salinari, S., Ursino, M., Zavaglia, M., Ding, L., Edgar, J. C., Miller, G. A., He, B., and Babiloni, F. (2007). Comparison of different cortical connectivity estimators for high-resolution EEG recordings. *Human Brain Mapping*, 28(2):143–157.

Au, D. K., Hui, Y., and Wei, W. I. (2003). Superiority of bilateral cochlear implantation over unilateral cochlear implantation in tone discrimination in chinese patients. *American Journal of Otolaryngology*, 24(1):19–23.

Babajani-Feremi, A., Gumenyuk, V., Roth, T., Drake, C. L., and Soltanian-Zadeh, H. (2012). Connectivity analysis of novelty process in habitual short sleepers. *NeuroImage*, 63(3):1001 – 1010.

Baccala, L. A. and Sameshima, K. (2001). Partial directed coherence: a new concept in neural structure determination. *Biological Cybernetics*, 84(6):463–474.

Bastiaansen, M. and Hagoort, P. (2006). Oscillatory neuronal dynamics during language comprehension. In Neuper, C. and Klimesch, W., editors, *Event-Related Dynamics of Brain Oscillations*, volume 159 of *Progress in Brain Research*, pages 179 – 196. Elsevier.

Bastiaansen, M. C., van Berkum, J. J., and Hagoort, P. (2002). Event-related theta power increases in the human EEG during online sentence processing. *Neuroscience Letters*, 323(1):13 – 16.

Baumgartner, W., Jappel, A., Frei, K., Stach, M., Eckl-Dorna, J., and Hamzavi, J. (2004). Bilateral cochlear implantation - 9-year results. *International Congress Series*, 1273(0):459 – 461.

Baumgartner, W. D., Pok, S. M., Egelierler, B., Franz, P., Gstoettner, W., and Hamzavi, J. (2002). The role of age in pediatric cochlear implantation. *International Journal of Pediatric Otorhinolaryngology*, 62(3):223–228.

Bench, J., Kowal, A., and Bamford, J. (1979). The BKB (Bamford-Kowal-Bench) sentence lists for partially-hearing children. *British Journal of Audiology*, 13(3):108–112.

Binder, J., Frost, J., Hammeke, T., Bellgowan, P., Springer, J., Kaufman, J., and Possing, E. (2000). Human temporal lobe activation by speech and nonspeech sounds. *Cerebral Cortex*, 10(5):512–528.

Blesch, A. and Tuszynski, M. H. (2009). Spinal cord injury: plasticity, regeneration and the challenge of translational drug development. *Trends in Neurosciences*, 32(1):41–47.

Bluestone, C. D., Alper, C., Arjmand, E., Stool, S., and Casselbrant, M. (2002). *Pediatric Otolaryngology*. Saunders.

Boatman-Reich, D., Franaszczuk, P. J., Korzeniewska, A., Caffo, B., Ritzl, E. K., Colwell, S., and Crone, N. (2010). Quantifying auditory event-related responses in multichannel human intracranial recordings. *Frontiers in Computational Neuroscience*, 4(4).

Boly, M., Garrido, M. I., Gosseries, O., Bruno, M. A., Boveroux, P., Schnakers, C., Massimini, M., Litvak, V., Laureys, S., and Friston, K. (2011). Preserved feedforward but impaired top-down processes in the vegetative state. *Science*, 332(6031):858–862.

Boothroyd, A. (1968). Developments in speech audiometry. *British Journal of Audiology*, 2(1):3–10.

Boothroyd, A. (2004). Measuring auditory speech perception capacity in very young children. *International Congress Series*, 1273(0):292 – 295. Cochlear Implants. Proceedings of the VIII International Cochlear Implant Conference.

Brademann, G., Müller-Deile, J., Maaß, J., Frese, K., Vogel, A., Kortmann, T., and Maune, S. (2003). Is the bilateral cochlear implantation necessary for avoidance of auditory deprivation in deaf children? *International Congress Series*, 1254(0):301 – 306.

Brancucci, A., Babiloni, C., Vecchio, F., Galderisi, S., Mucci, A., Tecchio, F., Romani, G., and Rossini, P. (2005). Decrease of functional coupling between left and right auditory cortices during dichotic listening: an electroencephalography study. *Neuroscience*, 136(1):323 – 332.

Breakspear, M. (2013). Dynamic and stochastic models of neuroimaging data: a comment on Lohmann et al. *NeuroImage*, 75:270–274.

British Academy of Audiology (BAA), British Cochlear Implant Group (BCIG), and ENT-UK (2007). Cochlear implants for deafness in children and adults. https://www.nice.org.uk/guidance/ta166/documents/. NICE Health Technology Appraisal, Accessed Online 30-05-2015.

British Cochlear Implant Group (BCIG) (2012). BCIG annual update on UK cochlear implant provision. http://www.bcig.org.uk/wp-content/uploads/2014/12/Pie-Charts-for-Number-of-Cochlear-Implants-2011-2012.pdf. Annual Update, Accessed Online 30-05-2015.

Brockwell, P. J., Dahlhaus, R., and Trindade, A. A. (2005). Modified Burg algorithms for multivariate subset autoregression. *Statistica Sinica*, 15:197–213.

Brown, H. R. and Friston, K. J. (2012). Dynamic causal modelling of precision and synaptic gain in visual perception - an EEG study. *NeuroImage*, 63(1):223–231.

Carter, G. C., Knapp, C., and Nuttall, A. H. (1973). Estimation of the magnitude-squared coherence function via overlapped fast Fourier transform processing. *IEEE Transactions on Audio and Electroacoustics*, 21(4):337–344.

Carter, L., Golding, M., Dillon, H., and Seymour, J. (2010). The detection of infant cortical auditory evoked potentials (CAEPs) using statistical and visual detection techniques. *Journal of American Academy of Audiology*, 21(5):347–356.

Castañeda-Villa, N., Cornejo, J. M., James, C. J., and Maurits, N. M. (2012). Quantification of LLAEP interhemispheric symmetry by the intraclass correlation coefficient as a measure of cortical reorganization after cochlear implantation. *International Journal of Pediatric Otorhinolaryngology*, 76(12):1729–1736.

Castañeda-Villa, N. and James, C. (2007). Objective source selection in blind source separation of AEPs in children with cochlear implants. In *Engineering in Medicine and Biology Society, 2007. EMBS 2007. 29th Annual International Conference of the IEEE*, pages 6223–6226.

Castañeda-Villa, N. and James, C. (2011). Independent component analysis for auditory evoked potentials and cochlear implant artifact estimation. *Biomedical Engineering, IEEE Transactions on*, 58(2):348–354.

Chadha, N. K., Papsin, B. C., Jiwani, S., and Gordon, K. A. (2011). Speech detection in noise and spatial unmasking in children with simultaneous versus sequential bilateral cochlear implants. *Otology & Neurotology*, 32(7):1057–1064.

Chan, H. L., Chu, J. H., Fung, H. C., Tsai, Y. T., Meng, L. F., Huang, C. C., Hsu, W. C., Chao, P. K., Wang, J. J., Lee, J. D., Wai, Y. Y., and Tsai, M. T. (2013). Brain connectivity of patients with Alzheimer's disease by coherence and cross mutual information of electroencephalograms during photic stimulation. *Medical Engineering & Physics*, 35(2):241–252.

Ching, T. Y. and Dillon, H. (2013). A brief overview of factors affecting speech intelligibility of people with hearing loss: implications for amplification. *American Journal of Audiology*, 22(2):306–309.

Chittka, L. and Brockmann, A. (2005). Perception space - the final frontier. *PLoS Biol*, 3(4):e137.

Choi, J. W., Lee, J. K., Ko, D., Lee, G.-T., Jung, K.-Y., and Kim, K. H. (2013). Fronto-temporal interactions in the theta-band during auditory deviant processing. *Neuroscience Letters*, 548(0):120 – 125.

Cooray, G., Garrido, M. I., Hyllienmark, L., and Brismar, T. (2014). A mechanistic model of mismatch negativity in the ageing brain. *Clinical Neurophysiology*. in press.

Das, S. and Buchman, C. A. (2005). Bilateral cochlear implantation: current concepts. *Current Opinion in Otolaryngology & Head and Neck Surgery*, 13(5):290–293.

Daunizeau, J., David, O., and Stephan, K. E. (2011). Dynamic causal modelling: a critical review of the biophysical and statistical foundations. *NeuroImage*, 58(2):312–322.

D'Ausilio, A., Bufalari, I., Salmas, P., and Fadiga, L. (2012). The role of the motor system in discriminating normal and degraded speech sounds. *Cortex*, 48(7):882–887.

David, O. and Friston, K. J. (2003). A neural mass model for MEG/EEG: coupling and neuronal dynamics. *NeuroImage*, 20(3):1743–1755.

David, O., Harrison, L., and Friston, K. J. (2005). Modelling event-related responses in the brain. *NeuroImage*, 25(3):756–770.

David, O., Kiebel, S. J., Harrison, L. M., Mattout, J., Kilner, J. M., and Friston, K. J. (2006a). Dynamic causal modeling of evoked responses in EEG and MEG. *NeuroImage*, 30(4):1255–1272.

David, O., Kilner, J. M., and Friston, K. J. (2006b). Mechanisms of evoked and induced responses in MEG/EEG. *NeuroImage*, 31(4):1580–1591.

Delorme, A. and Makeig, S. (2004). EEGLAB: an open source toolbox for analysis of single-trial EEG dynamics including independent component analysis. *Journal of Neuroscience Methods*, 134(1):9 – 21.

Delorme, A., Sejnowski, T., and Makeig, S. (2007). Enhanced detection of artifacts in EEG data using higher-order statistics and independent component analysis. *NeuroImage*, 34(4):1443 – 1449.

Desseilles, M., Schwartz, S., Dang-Vu, T. T., Sterpenich, V., Ansseau, M., Maquet, P., and Phillips, C. (2011). Depression alters "top-down" visual attention: a dynamic causal modeling comparison between depressed and healthy subjects. *NeuroImage*, 54(2):1662–1668.

Dima, D., Roiser, J. P., Dietrich, D. E., Bonnemann, C., Lanfermann, H., Emrich, H. M., and Dillo, W. (2009). Understanding why patients with schizophrenia do not perceive the hollow-mask illusion using dynamic causal modelling. *NeuroImage*, 46(4):1180 – 1186.

Ding, M., Bressler, S. L., Yang, W., and Liang, H. (2000). Short-window spectral analysis of cortical event-related potentials by adaptive multivariate autoregressive modeling: data preprocessing, model validation, and variability assessment. *Biological Cybernetics*, 83(1):35–45.

Doesburg, S. M., Green, J. J., McDonald, J. J., and Ward, L. M. (2012). Theta modulation of inter-regional gamma synchronization during auditory attention control. *Brain Research*, 1431(0):77 – 85.

Dunn, C. C., Tyler, R. S., Witt, S. A., Gantz, B., and Rubinstein, J. (2004). Frequency and electrode contributions to localization in bilateral cochlear implants. *International Congress Series*, 1273(0):443 – 446.

Erla, S., Faes, L. Tranquillini, E., Orrico, D., and Nollo, G. (2009). Multivariate autoregressive model with instantaneous effects to improve brain connectivity estimation. *International Journal of Bioelectromagnetism*, 11(2):74–79.

Faes, L., Erla, S., Porta, A., and Nollo, G. (2013). A framework for assessing frequency domain causality in physiological time series with instantaneous effects. *Philosophical Transactionas. Series A, Mathematical, Physical, and Engineering Sciences*, 371(1997):20110618.

Faes, L. and Nollo, G. (2010). Extended causal modeling to assess Partial Directed Coherence in multiple time series with significant instantaneous interactions. *Biological Cybernetics*, 103(5):387–400.

Faes, L., Pinna, G., Porta, A., Maestri, R., and Nollo, G. (2004). Surrogate data analysis for assessing the significance of the coherence function. *Biomedical Engineering, IEEE Transactions on*, 51(7):1156–1166.

Fallon, J. B., Irvine, D. R., and Shepherd, R. K. (2008). Cochlear implants and brain plasticity. *Hearing Research*, 238(1-2):110–117.

Faulkner, K. F. and Pisoni, D. B. (2013). Some observations about cochlear implants: challenges and future directions. *Neuroscience Discovery*, pages 1 – 9.

Fitzakerley, J. (2007). Tonotopic maps. http://www.d.umn.edu/~jfitzake/Lectures/UndergradPharmacy/SensoryPhysiology/Audition/TonotopicMaps.html. [Online; accessed 8-September-2014].

Fitzpatrick, E. M., Jacques, J., and Neuss, D. (2011). Parental perspectives on decision-making and outcomes in pediatric bilateral cochlear implantation. *International Journal of Audiology*, 50(10):679–687.

Florin, E., Gross, J., Pfeifer, J., Fink, G. R., and Timmermann, L. (2011). Reliability of multivariate causality measures for neural data. *Journal of Neuroscience Methods*, 198(2):344 – 358.

Friederici, A. D. (2002). Towards a neural basis of auditory sentence processing. *Trends in Cognitive Sciences*, 6(2):78–84.

Friedrich, E. V., Scherer, R., and Neuper, C. (2013). Stability of event-related (de-) synchronization during braincomputer interface-relevant mental tasks. *Clinical Neurophysiology*, 124(1):61 – 69.

Friston, K., Daunizeau, J., and Stephan, K. E. (2013). Model selection and gobbledygook: response to Lohmann et al. *NeuroImage*, 75:275–278.

Friston, K., Harrison, L., Daunizeau, J., Kiebel, S., Phillips, C., Trujillo-Barreto, N., Henson, R., Flandin, G., and Mattout, J. (2008). Multiple sparse priors for the M/EEG inverse problem. *NeuroImage*, 39(3):1104 – 1120.

Friston, K. J., Harrison, L., and Penny, W. (2003). Dynamic causal modelling. *NeuroImage*, 19(4):1273–1302.

Fuentemilla, L., Marco-Pallarés, J., and Grau, C. (2006). Modulation of spectral power and of phase resetting of EEG contributes differentially to the generation of auditory event-related potentials. *NeuroImage*, 30(3):909 – 916.

Fuentemilla, L., Marco-Pallarés, J., Münte, T., and Grau, C. (2008). Theta EEG oscillatory activity and auditory change detection. *Brain Research*, 1220(0):93 – 101.

Gantz, B. J., Tyler, R. S., Rubinstein, J. T., Wolaver, A., Lowder, M., Abbas, P., Brown, C., Hughes, M., and Preece, J. P. (2002). Binaural cochlear implants placed during the same operation. *Otology & Neurotology*, 23(2):169–180.

Garrido, M. I., Kilner, J. M., Kiebel, S. J., Stephan, K. E., Baldeweg, T., and Friston, K. J. (2009). Repetition suppression and plasticity in the human brain. *NeuroImage*, 48(1):269–279.

Garrido, M. I., Kilner, J. M., Kiebel, S. J., Stephan, K. E., and Friston, K. J. (2007). Dynamic causal modelling of evoked potentials: a reproducibility study. *NeuroImage*, 36(3):571–580.

Gelfand, S. (2004). *Hearing: An Introduction to Psychological and Physiological Acoustics, Fourth Edition*. Taylor & Francis.

Geweke, J. F. (1984). Measures of conditional linear dependence and feedback between time series. *Journal of the American Statistical Association*, 79(388):907–915.

Giannakakis, G. and Nikita, K. S. (2008). Estimation of time-varying causal connectivity on EEG signals with the use of adaptive autoregressive parameters. In *Engineering in Medicine and Biology Society, 2008. EMBS 2008. 30th Annual International Conference of the IEEE*, pages 3512–3515.

Gilley, P. M., Sharma, A., Dorman, M., Finley, C. C., Panch, A. S., and Martin, K. (2006). Minimization of cochlear implant stimulus artifact in cortical auditory evoked potentials. *Clinical Neurophysiology*, 117(8):1772–1782.

Gilley, P. M., Sharma, A., and Dorman, M. F. (2008). Cortical reorganization in children with cochlear implants. *Brain Research*, 1239(0):56 – 65.

Giraud, A., E., T., and R., F. (2001). Imaging plasticity in cochlear implant patients. *Audiology Neurotology*, 6:381–393.

Godar, S. P. and Litovsky, R. Y. (2010). Experience with bilateral cochlear implants improves sound localization acuity in children. *Otology & Neurotology*, 31(8):1287–1292.

Gola, M., Magnuski, M., Szumska, I., and Wróbel, A. (2013). EEG beta band activity is related to attention and attentional deficits in the visual performance of elderly subjects. *International Journal of Psychophysiology*, 89(3):334 – 341.

Golding, M., Dillon, H., Seymour, J., and Carter, L. (2009). The detection of adult cortical auditory evoked potentials (CAEPs) using an automated statistic and visual detection. *International Journal of Audiology*, 48(12):833–842.

Gordon, K. A., Papsin, B. C., and Harrison, R. V. (2005). Effects of cochlear implant use on the electrically evoked middle latency response in children. *Hearing Research*, 204(12):78 – 89.

Gourévitch, B., Bouquin-Jeannès, R., and Faucon, G. (2006). Linear and nonlinear causality between signals: methods, examples and neurophysiological applications. *Biological Cybernetics*, 95(4):349–369.

Graichen, U., Witte, H., and Haueisen, J. (2009). Analysis of induced components in electroencephalograms using a multiple correlation method. *BioMedical Engineering OnLine*, 8(1):1–8.

Granger, C. W. J. (1969). Investigating causal relations by econometric models and cross-spectral methods. *Econometrica*, 37(3):424–38.

Grech, R., Cassar, T., Muscat, J., Camilleri, K. P., Fabri, S. G., Zervakis, M., Xanthopoulos, P., Sakkalis, V., and Vanrumste, B. (2008). Review on solving the inverse problem in EEG source analysis. *Journal of NeuroEngineering and Rehabilitation*, 5:25.

Groppe, D. M., Makeig, S., and Kutas, M. (2009). Identifying reliable independent components via split-half comparisons. *NeuroImage*, 45(4):1199–1211.

Groth, E. J. (1975). Probability distributions related to power spectra. *The Astrophysical Journal Supplement Series*, 29(286):285–302.

Gruber, T., Giabbiconi, C. M., Trujillo-Barreto, N. J., and Müller, M. M. (2006). Repetition suppression of induced gamma band responses is eliminated by task switching. *The European Journal of Neuroscience*, 24(9):2654–2660.

Gruber, T., Keil, A., and Müller, M. M. (2001). Modulation of induced gamma band responses and phase synchrony in a paired associate learning task in the human EEG. *Neuroscience Letters*, 316(1):29 – 32.

Gurtubay, I., Alegre, M., Labarga, A., Malanda, A., and Artieda, J. (2004). Gamma band responses to target and non-target auditory stimuli in humans. *Neuroscience Letters*, 367(1):6 – 9.

Hackney, C. M. (1987). Anatomical features of the auditory pathway from cochlea to cortex. *British Medical Bulletin*, 43(4):780–801.

Haenschel, C., Baldeweg, T., Croft, R. J., Whittington, M., and Gruzelier, J. (2000). Gamma and beta frequency oscillations in response to novel auditory stimuli: A comparison of human electroencephalogram (EEG) data with in vitro models. *Proceedings of the National Academy of Sciences*, 97(13):7645–7650.

Hall, J. (2007). *New Handbook for Auditory Evoked Responses*. Pearson Allyn and Bacon.

Hannemann, R., Obleser, J., and Eulitz, C. (2007). Top-down knowledge supports the retrieval of lexical information from degraded speech. *Brain Research*, 1153(0):134 – 143.

He, S., Teagle, H. F., Roush, P., Grose, J. H., and Buchman, C. A. (2013). Objective hearing threshold estimation in children with auditory neuropathy spectrum disorder. *Laryngoscope*, 123(11):2859–2861.

Hear & Say (2013). About the hear and say centre. http://www.butterflyappeal.com/About.html. [Online; accessed 8-September-2014].

Hiemstra, C. and Jones, J. D. (1994). Testing for linear and nonlinear granger causality in the stock price- volume relation. *The Journal of Finance*, 49(5):1639–1664.

Hirata, M., Koreeda, S., Sakihara, K., Kato, A., Yoshimine, T., and Yorifuji, S. (2007). Effects of the emotional connotations in words on the frontal areas - a spatially filtered MEG study. *NeuroImage*, 35(1):420 – 429.

Holt, R. F., Svirsky, M. A., Neuburger, H., and Miyamoto, R. T. (2004). Age at implantation and communicative outcome in pediatric cochlear implant users: Is younger always better? *International Congress Series*, 1273(0):368 – 371.

Hong, X. and Tong, S. (2012). Cortical functional connectivity under different auditory attentional efforts. In *Engineering in Medicine and Biology Society (EMBC), 2012 Annual International Conference of the IEEE*, pages 6196–6199.

Hosseini, P. T., Bell, S., Brinton, J., and Simpson, D. (2013a). Brain's induced response to auditory stimulation. In *Abstracts of the 11th Annual Southampton Neuroscience Meeting*, Southampton, UK.

Hosseini, P. T., Bell, S., Brinton, J., and Simpson, D. (2014a). Brain activity in response to auditory stimuli. In *Proceedings of the 8th IEEE EMBS PGBiomed conference*.

Hosseini, P. T., Bell, S., Wang, S., and Simpson, D. (2015). Induced activity in EEG in response to auditory stimulation. *Biomedical Signal Processing and Control*, 22(0):31 – 43.

Hosseini, P. T., Sear, E., Sanderson, A., Verschuur, C., Lutman, M., Brinton, J., and Wang, S. (2011a). Cortical processing of speech simulation of cochlear implants. In *Abstracts of the 9th Annual Southampton Neuroscience Meeting*, Southampton, UK.

Hosseini, P. T., Simpson, D., Bell, S., Brinton, J., and Wang, S. (2013b). Comments on DCM as an effective connectivity measurement tool in EEG analysis. In *Proceedings of the 7th UK and RI Postgraduate Conference in Biomedical Engineering and Medical Physics*, page 23. University of Surrey.

Hosseini, P. T., Verschuur, C., Lutman, M., and Wang, S. (2011b). Cortical processing of distorted speech. In *Abstracts of British Society of Audiology Annual Conference*, Nottingham, UK.

Hosseini, P. T., Wang, S., Bell, S., Brinton, J., and Simpson, D. (2014b). Is the software package embedding dynamic causal modeling robust? In *XIII Mediterranean Conference on Medical and Biological Engineering and Computing 2013*, volume 41 of *IFMBE Proceedings*, pages 1686–1689. Springer International Publishing.

Hosseini, P. T., Wang, S., Brinton, J., Bell, S., and Simpson, D. M. (2014c). Reliability of dynamic causal modeling using the Statistical Parametric Mapping toolbox. *International Journal of System Dynamics Applications*, 3(2):1–17.

Howard, M. F. and Poeppel, D. (2010). Discrimination of speech stimuli based on neuronal response phase patterns depends on acoustics but not comprehension. *Journal of Neurophysiology*, 104(5):2500–2511.

Howard, M. F. and Poeppel, D. (2012). The neuromagnetic response to spoken sentences: co-modulation of theta band amplitude and phase. *NeuroImage*, 60(4):2118 – 2127.

Howell, D. C. (2010). *Statistical methods for psychology*. Wadsworth, Belmont, California.

Huang, S., Chang, W.-T., Belliveau, J. W., Hämäläinen, M., and Ahveninen, J. (2014). Lateralized parietotemporal oscillatory phase synchronization during auditory selective attention. *NeuroImage*, 86(0):461 – 469.

Hyvärinen, A. and Oja, E. (2000). Independent component analysis: algorithms and applications. *Neural Networks*, 13(4-5):411–430.

Ikeda, K., Hayashi, A., Matsuda, O., and Sekiguchi, T. (2010). An ignoring task improves validity of cortical evoked response audiometry. *Neuroreport*, 21(10):709–715.

Jalili, M. and Knyazeva, M. G. (2011). EEG-based functional networks in schizophrenia. *Computers in Biology and Medicine*, 41(12):1178–1186.

James.mcd.nz (2010). Brain surface gyri [gfdl http://www.gnu.org/copyleft/fdl.html or cc-by-sa-3.0-2.5-2.0-1.0 http://creativecommons.org/licenses/by-sa/3.0], via wikimedia commons from wikimedia commons. http://commons.wikimedia.org/wiki/File:Brain_Surface_Gyri.SVG. [Online; accessed 8-September-2014].

Jansen, B. and Rit, V. (1995). Electroencephalogram and visual evoked potential generation in a mathematical model of coupled cortical columns. *Biological Cybernetics*, 73(4):357–366.

Johnson, Erik (2009). Draw a line with an arrowhead. http://www.mathworks.co.uk/matlabcentral/fileexchange/278-arrow-m. [Online; accessed 4-March-2014].

Kamiński, M., Ding, M., Truccolo, W. A., and Bressler, S. L. (2001). Evaluating causal relations in neural systems: granger causality, directed transfer function and statistical assessment of significance. *Biological Cybernetics*, 85(2):145–157.

Kamiński, M., Zygierewicz, J., Kuś, R., and Crone, N. (2005). Analysis of multichannel biomedical data. *Acta Neurobiologiae Experimentalis (Wars)*, 65(4):443–452.

Karrasch, M., Krause, C. M., Laine, M., Lang, A., and Lehto, M. (1998). Event-related desynchronization and synchronization during an auditory lexical matching task. *Electroencephalography and Clinical Neurophysiology*, 107(2):112 – 121.

Kempton, M., Dima, D., Roiser, J., Stephan, K., Friston, K., and Frangou, S. (2010). PW01-148 - effective connectivity within the network of fearful facial affect recognition in patients with bipolar disorder compared to healthy controls. *European Psychiatry*, 25, Supplement 1(0):1564 –. 18th European Congress of Psychiatry. February 27, March 2, 2010 - Munich, Germany.

Kiebel, S. J., David, O., and Friston, K. J. (2006). Dynamic causal modelling of evoked responses in EEG/MEG with lead field parameterization. *NeuroImage*, 30(4):1273 – 1284.

Kiebel, S. J., Garrido, M. I., and Friston, K. J. (2007). Dynamic causal modelling of evoked responses: the role of intrinsic connections. *NeuroImage*, 36(2):332–345.

Kim, J. S. and Chung, C. K. (2008). Language lateralization using MEG beta frequency desynchronization during auditory oddball stimulation with one-syllable words. *NeuroImage*, 42(4):1499 – 1507.

Kirmizi-Alsan, E., Bayraktaroglu, Z., Gurvit, H., Keskin, Y. H., Emre, M., and Demiralp, T. (2006). Comparative analysis of event-related potentials during Go/NoGo and CPT: decomposition of electrophysiological markers of response inhibition and sustained attention. *Brain Research*, 1104(1):114 – 128.

Knight, R., Hillyard, S., Woods, D., and Neville, H. (1980). The effects of frontal and temporal-parietal lesions on the auditory evoked potential in man. *Electrophysiology and Clinical Neurophysiology*, 36:112–124.

Korzeniewska, A., Crainiceanu, C. M., Kuś, R., Franaszczuk, P. J., and Crone, N. E. (2008). Dynamics of event-related causality in brain electrical activity. *Human Brain Mapping*, 29(10):1170–1192.

Korzeniewska, A., Franaszczuk, P. J., Crainiceanu, C. M., Kuś, R., and Crone, N. E. (2011). Dynamics of large-scale cortical interactions at high gamma frequencies during word production: event related causality (ERC) analysis of human electrocorticography (ECoG). *NeuroImage*, 56(4):2218–2237.

Korzeniewska, A., Mańczak, M., Kamiński, M., Blinowska, K. J., and Kasicki, S. (2003). Determination of information flow direction among brain structures by a modified directed transfer function (dDTF) method. *Journal of Neuroscience Methods*, 125(12):195 – 207.

Kral, A. and Sharma, A. (2012). Developmental neuroplasticity after cochlear implantation. *Trends in Neurosciences*, 35(2):111 – 122.

Kral, A. and Tillein, J. (2006). Brain plasticity under cochlear implant stimulation. *Advances in Otorhinolaryngology*, 64:89–108.

Kral, A., Tillein, J., Heid, S., Klinke, R., and Hartmann, R. (2006). Cochlear implants: cortical plasticity in congenital deprivation. *Progress in Brain Research*, 157:283–313.

Krause, C. M., Åström, T., Karrasch, M., Laine, M., and Sillanmäki, L. (1999). Cortical activation related to auditory semantic matching of concrete versus abstract words. *Clinical Neurophysiology*, 110(8):1371 – 1377.

Krause, C. M., Korpilahti, P., Pörn, B., Jäntti, J., and Lang, H. A. (1998). Automatic auditory word perception as measured by 40 Hz EEG responses. *Electroencephalography and Clinical Neurophysiology*, 107(2):84 – 87.

Kühn-Inacker, H., Shehata-Dieler, W., Müller, J., and Helms, J. (2004). Bilateral cochlear implants: a way to optimize auditory perception abilities in deaf children? *International Journal of Pediatric Otorhinolaryngology*, 68(10):1257–1266.

Lachaux, J.-P., Rodriguez, E., Martinerie, J., and Varela, F. J. (1999). Measuring phase synchrony in brain signals. *Human Brain Mapping*, 8(4):194–208.

Li, X., Nie, K., Karp, F., Tremblay, K., and Rubinstein, J. (2010). Characteristics of stimulus artifacts in EEG recordings induced by electrical stimulation of cochlear implants. In *Biomedical Engineering and Informatics (BMEI), 2010 3rd International Conference on*, volume 2, pages 799–803.

Lightfoot, G. and Kennedy, V. (2006). Cortical electric response audiometry hearing threshold estimation: accuracy, speed, and the effects of stimulus presentation features. *Ear Hear*, 27(5):443–456.

Limb, C., Molloy, A., Jiradejvong, P., and Braun, A. (2010). Auditory cortical activity during cochlear implant-mediated perception of spoken language, melody, and rhythm. *Journal of the Association for Research in Otolaryngology*, 11(1):133–143.

Litovsky, R. Y., Parkinson, A., Arcaroli, J., Peters, R., Lake, J., Johnstone, P., and Yu, G. (2004). Bilateral cochlear implants in adults and children. *Archives of Otolaryngology Head & Neck Surgery*, 130(5):648–655.

Lohmann, G., Erfurth, K., Müller, K., and Turner, R. (2012). Critical comments on dynamic causal modelling. *NeuroImage*, 59(3):2322–2329.

Lohmann, G., Müller, K., and Turner, R. (2013). Response to commentaries on our paper: Critical comments on dynamic causal modelling. *NeuroImage*, 75(0):279 – 281.

Łukaszewicz, Z., Soluch, P., Niemczyk, K., and Lachowska, M. (2010). Korelacja zmian w funkcjonowaniu słuchowo-werbalnym pacjentów po wszczepieniu implantu

ślimakowego z ich oceną w badaniu pozytonowej emisyjnej tomografii komputerowej (PET). *Otolaryngologia Polska*, 64(7):10 – 16.

Lütkepohl, H. (1991). *Introduction to multiple time series analysis*. Springer-Verlag.

Lv, J., Simpson, D. M., and Bell, S. L. (2007). Objective detection of evoked potentials using a bootstrap technique. *Medical Engineering & Physics*, 29(2):191–198.

Lynskey, J. V., Belanger, A., and Jung, R. (2008). Activity-dependent plasticity in spinal cord injury. *Journal of Rehabilitation Research and Development*, 45(2):229–240.

Maiorova, L., Martynova, O., Fedina, O., and Petrushevskii, A. (2014). An fMRI study of impairments to speech perception in patients with vascular sensory aphasia. *Neuroscience and Behavioral Physiology*, 44(7):740–747.

Makeig, S., Jung, T.-P., Bell, A. J., Ghahremani, D., and Sejnowski, T. J. (1997). Blind separation of auditory event-related brain responses into independent components. *Proceedings of the National Academy of Sciences*, 94(20):10979–10984.

Makeig, S., Westerfield, M., Jung, T., Enghoff, S., Townsend, J., Courchesne, E., and Sejnowski, T. J. (2002). Dynamic brain sources of visual evoked responses. *Science*, 295(5555):690–694.

Manrique, M., Cervera-Paz, F. J., Huarte, A., Perez, N., Molina, M., and Garcia-Tapia, R. (1999). Cerebral auditory plasticity and cochlear implants. *International Journal of Pediatric Otorhinolaryngology*, 49 Suppl 1:S193–197.

Marreiros, A. C., Kiebel, S. J., and Friston, K. J. (2010). A dynamic causal model study of neuronal population dynamics. *NeuroImage*, 51(1):91–101.

Marsella, P., Scorpecci, A., Vecchiato, G., Maglione, A. G., Colosimo, A., and Babiloni, F. (2014). Neuroelectrical imaging investigation of cortical activity during listening to music in prelingually deaf children with cochlear implants. *International Journal of Pediatric Otorhinolaryngology*, 78(5):737 – 743.

Martini, F. and Bartholomew, E. F. (1997). *Essentials of anatomy & physiology*. Upper Saddle River, N.J. : Prentice Hall.

Marzetti, L., Della Penna, S., Nolte, G., Franciotti, R., Stefanics, G., and Romani, G. L. (2007). A cartesian time–frequency approach to reveal brain interaction dynamics. *Brain Topography*, 19(3):147 – 154.

Mattout, J., Phillips, C., Daunizeau, J., and Friston, K. J. (2007). Bayesian inversion of EEG models. In Friston, K., Ashburner, J., Kiebel, S., Nichols, T., and Penny, W., editors, *Statistical Parametric Mapping: The analysis of functional brain images*. Academic Press.

May, A. (2011). Experience-dependent structural plasticity in the adult human brain. *Trends in Cognitive Sciences*, 15(10):475–482.

Meyer, M., Zysset, S., von Cramon, D. Y., and Alter, K. (2005). Distinct fMRI responses to laughter, speech, and sounds along the human peri-sylvian cortex. *Brain Research Cognitive Brain Research*, 24(2):291–306.

Miguel A. Arranz (2005). Portmanteau test statistics in time series. http://packages.tol-project.org/docs/ndmtest.pdf. [Online; accessed 24-Sep-2014].

Miranda de Sá, A., Infantosi, A., and Simpson, D. (2001). A statistical technique for measuring synchronism between cortical regions in the EEG during rhythmic stimulation. *Biomedical Engineering, IEEE Transactions on*, 48(10):1211–1215.

Miranda de Sá, A., Infantosi, A., and Simpson, D. (2002). Coherence between one random and one periodic signal for measuring the strength of responses in the electroencephalogram during sensory stimulation. *Medical and Biological Engineering and Computing*, 40(1):99–104.

Morf, M., Vieira, A., Lee, D. T. L., and Kailath, T. (1978). Recursive multichannel maximum entropy spectral estimation. *IEEE Transactions on Geoscience Electronics*, 16(2):85–94.

Nash-Kille, A. and Sharma, A. (2014). Inter-trial coherence as a marker of cortical phase synchrony in children with sensorineural hearing loss and auditory neuropathy spectrum disorder fitted with hearing aids and cochlear implants. *Clinical Neurophysiology*, 125(7):1459 – 1470.

National Institute for Health and Clinical Excellence (NICE) (2009). *Cochlear implants for children and adults with severe to profound deafness (TA166)*. National Institute for Health and Clinical Excellence (NICE), London, UK.

Nava, E., Bottari, D., Bonfioli, F., Beltrame, M. A., and Pavani, F. (2009a). Spatial hearing with a single cochlear implant in late-implanted adults. *Hearing Research*, 255(1-2):91–98.

Nava, E., Bottari, D., Portioli, G., Bonfioli, F., Beltrame, M. A., Formigoni, P., and Pavani, F. (2009b). Hearing again with two ears: recovery of spatial hearing after bilateral cochlear implantation. *Neuropsychologia*, 47(3):928–932.

Obleser, J. and Kotz, S. A. (2011). Multiple brain signatures of integration in the comprehension of degraded speech. *NeuroImage*, 55(2):713 – 723.

Omidvarnia, A. (2011). Time-varying EEG connectivity: A time-frequency approach. http://www.mathworks.co.uk/matlabcentral/fileexchange/33721-time-varying-eeg-connectivity--a-time-frequency-approach. [Online; accessed 10-Sep-2014].

Osnes, B., Hugdahl, K., Hjelmervik, H., and Specht, K. (2011). Increased activation in superior temporal gyri as a function of increment in phonetic features. *Brain and Language*, 116(2):97–101.

Palva, S. and Palva, J. M. (2007). New vistas for α-frequency band oscillations. *Trends in Neurosciences*, 30(4):150 – 158.

Pantev, C., Dinnesen, A., Ross, B., Wollbrink, A., and Knief, A. (2006). Dynamics of auditory plasticity after cochlear implantation: a longitudinal study. *Cerebral Cortex*, 16(1):31–36.

Pascual-Leone, A., Amedi, A., Fregni, F., and Merabet, L. B. (2005). The plastic human brain cortex. *Annual Review of Neuroscience*, 28(1):377–401.

Paxinos, G. and Mai, J. (2004). *The Human Nervous System*. Elsevier Science.

Peelle, J. E., Gross, J., and Davis, M. H. (2013). Phase-locked responses to speech in human auditory cortex are enhanced during comprehension. *Cerebral Cortex*, 23(6):1378–1387.

Peng, W., Hu, L., Zhang, Z., and Hu, Y. (2012). Causality in the association between P300 and alpha event-related desynchronization. *PLoS ONE*, 7(4):e34163.

Peters, B., Litovsky, R., Lake, J., and Parkinson, A. (2004). Sequential bilateral cochlear implantation in children. *International Congress Series*, 1273:462–465.

Pfurtscheller, G. and da Silva, F. L. (1999). Event-related EEG/MEG synchronization and desynchronization: basic principles. *Clinical Neurophysiology*, 110(11):1842 – 1857.

Philiastides, M. G. and Sajda, P. (2006). Causal influences in the human brain during face discrimination: a short-window directed transfer function approach. *IEEE Transactions on Biomedical Engineering*, 53(12):2602–2605.

Picton, T., Hillyard, S., Krausz, H., and Galambos, R. (1974). Human auditory evoked potentials. I: Evaluation of components. *Electrophysiology and Clinical Neurophysiology*, 36:179–190.

Ponton, C. W., Vasama, J. P., Tremblay, K., Khosla, D., Kwong, B., and Don, M. (2001). Plasticity in the adult human central auditory system: evidence from late-onset profound unilateral deafness. *Hearing Research*, 154(1-2):32–44.

Porcaro, C., Zappasodi, F., Rossini, P. M., and Tecchio, F. (2009). Choice of multivariate autoregressive model order affecting real network functional connectivity estimate. *Clinical Neurophysiology*, 120(2):436 – 448.

Purves, D., Fitzpatrick, D., Katz, L. C., Lamantia, A. S., McNamara, J. O., Williams, S. M., and Augustine, G. J. (2001). *Neuroscience*. Sunderland (MA): Sinauer Associates.

Rauschecker, J. P. and Tian, B. (2004). Processing of band-passed noise in the lateral auditory belt cortex of the rhesus monkey. *Journal of Neurophysiology*, 91(6):2578–2589.

Rehme, A. K., Eickhoff, S. B., Wang, L. E., Fink, G. R., and Grefkes, C. (2011). Dynamic causal modeling of cortical activity from the acute to the chronic stage after stroke. *NeuroImage*, 55(3):1147–1158.

Reiterer, S., Berger, M. L., Hemmelmann, C., and Rappelsberger, P. (2005). Decreased EEG coherence between prefrontal electrodes: a correlate of high language proficiency? *Experimental Brain Research*, 163(1):109–113.

Repovš, G. (2010). Dealing with noise in EEG recording and data analysis. *Informatica Medica Slovenica*, 15(1):18–25.

Romanski, L. M., Tian, B., Fritz, J., Mishkin, M., Goldman-Rakic, P. S., and Rauschecker, J. P. (1999). Dual streams of auditory afferents target multiple domains in the primate prefrontal cortex. *Nature Neuroscience*, 2(12):1131–1136.

Sakkalis, V. (2011). Review of advanced techniques for the estimation of brain connectivity measured with EEG/MEG. *Computers in Biology and Medicine*, 41(12):1110 – 1117.

Sakkalis, V., Giurcaneanu, C., Xanthopoulos, P., Zervakis, M., Tsiaras, V., Yang, Y., Karakonstantaki, E., and Micheloyannis, S. (2009). Assessment of linear and nonlinear synchronization measures for analyzing eeg in a mild epileptic paradigm. *Information Technology in Biomedicine, IEEE Transactions on*, 13(4):433–441.

Sanderson, A. (2010). Cortical representation of coded speech. Master's dissertation, University of Southampton.

Sandmann, P., Eichele, T., Buechler, M., Debener, S., Jäncke, L., Dillier, N., Hugdahl, K., and Meyer, M. (2009). Evaluation of evoked potentials to dyadic tones after cochlear implantation. *Brain*, 132(Pt 7):1967–1979.

Sasaki, T., Yamamoto, K., Iwaki, T., and Kubo, T. (2009). Assessing binaural/bimodal advantages using auditory event-related potentials in subjects with cochlear implants. *Auris Nasus Larynx*, 36(5):541–546.

Schack, B. and Weiss, S. (2005). Quantification of phase synchronization phenomena and their importance for verbal memory processes. *Biological Cybernetics*, 92(4):275–287.

Schlögl, A. (2006). A comparison of multivariate autoregressive estimators. *Signal Processing*, 86(9):2426 – 2429.

Schlögl, A. and Supp, G. (2006). Analyzing event-related EEG data with multivariate autoregressive parameters. In Neuper, C. and Klimesch, W., editors, *Event-Related Dynamics of Brain Oscillations*, volume 159 of *Progress in Brain Research*, pages 135 – 147. Elsevier.

Seikel, J., King, D., and Drumright, D. (1997). *Anatomy and Physiology for Speech, Language, and Hearing*. Singulalr Publishing Group Incorporated.

Sharma, A., Dorman, M. F., and Kral, A. (2005a). The influence of a sensitive period on central auditory development in children with unilateral and bilateral cochlear implants. *Hearing Research*, 203(12):134 – 143.

Sharma, A., Dorman, M. F., and Spahr, A. J. (2002). A sensitive period for the development of the central auditory system in children with cochlear implants: implications for age of implantation. *Ear & Hearing*, 23(6):532–539.

Sharma, A., Martin, K., Roland, P., Bauer, P., Sweeney, M. H., Gilley, P., and Dorman, M. (2005b). P1 latency as a biomarker for central auditory development in children with hearing impairment. *Journal of the American Academy of Audiology*, 16(8):564–573.

Sharma, A., Nash, A. A., and Dorman, M. (2009). Cortical development, plasticity and re-organization in children with cochlear implants. *Journal of Communication Disorders*, 42(4):272 – 279.

Shim, M., Kim, D.-W., Lee, S.-H., and Im, C.-H. (2014). Disruptions in small-world cortical functional connectivity network during an auditory oddball paradigm task in patients with schizophrenia. *Schizophrenia Research*, 156(23):197 – 203.

Simpson, D., Tierra-Criollo, C., Leite, R., Zayen, E., and Infantosi, A. (2000). Objective response detection in an electroencephalogram during somatosensory stimulation. *Annals of Biomedical Engineering*, 28(6):691–698.

Smulders, Y. E., Rinia, A. B., Rovers, M. M., van Zanten, G. A., and Grolman, W. (2011). What is the effect of time between sequential cochlear implantations on hearing in adults and children? A systematic review of the literature. *Laryngoscope*, 121(9):1942–1949.

Song, J.-J., Punte, A. K., Ridder, D. D., Vanneste, S., and de Heyning, P. V. (2013). Neural substrates predicting improvement of tinnitus after cochlear implantation in patients with single-sided deafness. *Hearing Research*, 299(0):1 – 9.

Sparreboom, M., Snik, A. F., and Mylanus, E. A. (2011). Sequential bilateral cochlear implantation in children: development of the primary auditory abilities of bilateral stimulation. *Audiology Neurotology*, 16(4):203–213.

Stephan, D. F., Levine, D. M., Berenson, M. L., and Krehbiel, T. C. (2012). *Basic business statistics: Concepts And application*. Pearson, Boston, Massachusetts.

Strelnikov, K., Rouger, J., Demonet, J. F., Lagleyre, S., Fraysse, B., Deguine, O., and Barone, P. (2010). Does brain activity at rest reflect adaptive strategies? Evidence from speech processing after cochlear implantation. *Cerebral Cortex*, 20(5):1217–1222.

Striem-Amit, E., Hertz, U., and Amedi, A. (2011). Extensive cochleotopic mapping of human auditory cortical fields obtained with phase-encoding fMRI. *PLoS ONE*, 6(3):e17832.

Strom-Roum, H., Laurent, C., and Wie, O. B. (2012). Comparison of bilateral and unilateral cochlear implants in children with sequential surgery. *International Journal of Pediatric Otorhinolaryngology*, 76(1):95–99.

Sun, F. T., Miller, L. M., and D'Esposito, M. (2004). Measuring interregional functional connectivity using coherence and partial coherence analyses of fMRI data. *NeuroImage*, 21(2):647–658.

Sun, Y., Zhang, H., Feng, T., Qiu, Y., Zhu, Y., and Tong, S. (2009). Early cortical connective network relating to audiovisual stimulation by partial directed coherence analysis. *IEEE Transactions on Biomedical Engineering*, 56(11 Pt 2):2721–2724.

Tallon-Baudry, C. and Bertrand, O. (1999). Oscillatory gamma activity in humans and its role in object representation. *Trends in Cognitive Sciences*, 3(4):151–162.

Tatum, W. (2007). *Handbook of EEG Interpretation*. Demos Medical Publishing, LLC.

Telenczuk, B., Baker, S. N., Herz, A. V. M., and Curio, G. (2011). High-frequency EEG covaries with spike burst patterns detected in cortical neurons. *Journal of Neurophysiology*, 105(6):2951–2959.

Thiel, C. M., Friston, K. J., and Dolan, R. J. (2002). Cholinergic modulation of experience-dependent plasticity in human auditory cortex. *Neuron*, 35(3):567–574.

Thompson, R. (1979). Coherence significance levels. *Journal of the Atmospheric Sciences*, 36:2020–2021.

TjeerdB (2011a). Additive response [cc-by-sa-3.0 http://creativecommons.org/licenses/by-sa/3.0], via wikimedia commons. http://commons.wikimedia.org/wiki/File:Additive_response.png. [Online; accessed 8-September-2014].

TjeerdB (2011b). Amp response [cc-by-sa-3.0 http://creativecommons.org/licenses/by-sa/3.0], via wikimedia commons. http://commons.wikimedia.org/wiki/File:Amp_response.png. [Online; accessed 8-September-2014].

TjeerdB (2011c). Phase resetting [cc-by-sa-3.0 http://creativecommons.org/licenses/by-sa/3.0], via wikimedia commons. http://commons.wikimedia.org/wiki/File:Phase_resetting.png. [Online; accessed 8-September-2014].

Trautner, P., Rosburg, T., Dietl, T., Fell, J., Korzyukov, O., Kurthen, M., Schaller, C., Elger, C., and Boutros, N. (2006). Sensory gating of auditory evoked and induced gamma band activity in intracranial recordings. *NeuroImage*, 32(2):790 – 798.

Tyler, R. and Tye-Murray, N. (1986). The relationship between speech perception and psychoacoustical measurements in noise-induced hearing loss subjects. In Salvi, R., Henderson, D., Hamernik, R., and Colletti, V., editors, *Basic and Applied Aspects of Noise-Induced Hearing Loss*, volume 111 of *NATO ASI Series*, pages 323–333. Springer US.

Tyler, R. S., Dunn, C. C., Witt, S. A., and Noble, W. G. (2007). Speech perception and localization with adults with bilateral sequential cochlear implants. *Ear & Hearing*, 28(2 Suppl):86S–90S.

Van Hoesel, R., Ramsden, R., and Odriscoll, M. (2002). Sound-direction identification, interaural time delay discrimination, and speech intelligibility advantages in noise for a bilateral cochlear implant user. *Ear & Hearing*, 23(2):137–149.

Van Hoesel, R. J. and Tyler, R. S. (2003). Speech perception, localization, and lateralization with bilateral cochlear implants. *Journal of the Acoustical Society of America*, 113(3):1617–1630.

Vaseghi, S. (2008). *Advanced Digital Signal Processing and Noise Reduction*. Wiley.

Vialatte, F.-B., Maurice, M., Dauwels, J., and Cichocki, A. (2009). Steady state visual evoked potentials in the delta range (0.5-5 Hz). In Köppen, M., Kasabov, N., and Coghill, G., editors, *Advances in Neuro-Information Processing*, volume 5506 of *Lecture Notes in Computer Science*, pages 400–407. Springer Berlin Heidelberg.

Viola, F. C., Thorne, J. D., Bleeck, S., Eyles, J., and Debener, S. (2011). Uncovering auditory evoked potentials from cochlear implant users with independent component analysis. *Psychophysiology*, 48(11):1470–1480.

Viola, F. C., Vos, M. D., Hine, J., Sandmann, P., Bleeck, S., Eyles, J., and Debener, S. (2012). Semi-automatic attenuation of cochlear implant artifacts for the evaluation of late auditory evoked potentials. *Hearing Research*, 284(12):6 – 15.

Webster, D. (1995). *Neuroscience of Communication*. Singular textbook series. Singular Publishing Group Incorporated.

Weiss, S. and Mueller, H. M. (2003). The contribution of EEG coherence to the investigation of language. *Brain and Language*, 85(2):325–343.

Weiss, S. and Mueller, H. M. (2012). "Too many betas do not spoil the broth": The role of beta brain oscillations in language processing. *Frontiers in Psychology*, 3:201.

Weiss, S. and Muller, H. M. (2013). The non-stop road from concrete to abstract: high concreteness causes the activation of long-range networks. *Frontiers in Human Neuroscience*, 7:526.

Weiss, S. and Rappelsberger, P. (2000). Long-range EEG synchronization during word encoding correlates with successful memory performance. *Brain Research Cognitive Brain Research*, 9(3):299–312.

Wessinger, C. M., VanMeter, J., Tian, B., Van Lare, J., Pekar, J., and Rauschecker, J. P. (2001). Hierarchical organization of the human auditory cortex revealed by functional magnetic resonance imaging. *Journal of Cognitive Neuroscience*, 13(1):1–7.

Wie, O. B. (2010). Language development in children after receiving bilateral cochlear implants between 5 and 18 months. *International Journal of Pediatric Otorhinolaryngology*, 74(11):1258–1266.

Winterhalder, M., Schelter, B., Hesse, W., Schwab, K., Leistritz, L., Klan, D., Bauer, R., Timmer, J., and Witte, H. (2005). Comparison of linear signal processing techniques to infer directed interactions in multivariate neural systems. *Signal Processing*, 85(11):2137 – 2160.

Wu, J., Zhang, J., Liu, C., Liu, D., Ding, X., and Zhou, C. (2012). Graph theoretical analysis of EEG functional connectivity during music perception. *Brain Research*, 1483(0):71 – 81.

Wu, T., Wang, L., Hallett, M., Chen, Y., Li, K., and Chan, P. (2011). Effective connectivity of brain networks during self-initiated movement in Parkinson's disease. *NeuroImage*, 55(1):204–215.

Wunderlich, J. L., Cone-Wesson, B. K., and Shepherd, R. (2006). Maturation of the cortical auditory evoked potential in infants and young children. *Hearing Research*, 212(12):185 – 202.

Zanto, T. P., Large, E. W., Fuchs, A., and Kelso, J. S. (2005). Gamma-band responses to perturbed auditory sequences: Evidence for synchronization of perceptual processes. *Music Perception*, 22(3):535–552.

Zeitler, D. M., Kessler, M. A., Terushkin, V., Roland, T. J., Svirsky, M. A., Lalwani, A. K., and Waltzman, S. B. (2008). Speech perception benefits of sequential bilateral cochlear implantation in children and adults: a retrospective analysis. *Otology & Neurotology*, 29(3):314–325.

Zervakis, M., Michalopoulos, K., Iordanidou, V., and Sakkalis, V. (2011). Intertrial coherence and causal interaction among independent EEG components. *Journal of Neuroscience Methods*, 197(2):302 – 314.